The development of new qualitative and quantitative metal speciation approaches for low molecular weight metals complexes in plants

Ghaya Alchoubassi

THÈSE

UNIVERSITE DE PAU ET DES PAYS DE L'ADOUR
École doctorale sciences exactes et leurs applications ED211

Présentée et soutenue le 13 décembre 2019

Par **Ghaya ALCHOUBASSI**

Pour obtenir le grade de docteur
De l'Université de Pau et des Pays de l'Adour
Spécialité: chimie analytique de l'environnement

Développement de nouvelles approches qualitatives et quantitatives de spéciation des métaux impliqués dans les complexes de faibles poids moléculaires circulant dans les plantes

The development of new qualitative and quantitative metal speciation approaches for low molecular weight metals complexes in plants

MEMBRES DU JURY

RAPPORTEURS
- Beata GODLEWSKA-ZYLKIEWICZ — Professeur / Université de Białystok-Pologne
- Eduardo BOLEA MORALES — Professeur / Université de Saragosse- Espagne

EXAMINATEURS
- Ryszard LOBINSKI — Directeur de recherche / CNRS-IPREM-Pau
- Rochele SOGARI PICOLOTO — Maitre de conférence / Université fédérale Santa Maria Brésil

DIRECTEURS
- Joanna SZPUNAR — Ingénieur de recherche / CNRS-IPREM-Pau
- Katarzyna BIERLA — Ingénieur de recherche / CNRS-IPREM-Pau

UNIVERSITÉ DE PAU ET DES PAYS DE L'ADOUR

DEVELOPPEMENT DE NOUVELLES APPROCHES QUALITATIVES ET QUANTITATIVES DE SPECIATION DES METAUX IMPLIQUES DANS LES COMPLEXES DE FAIBLES POIDS MOLECULAIRES CIRCULANT DANS LES PLANTES

Ghaya ALCHOUBASSI – 13 Décembre 2019

Introduction:

Des métaux tels que Fe, Mn, Ni, Zn et Cu sont essentiels dans le cycle de vie des plantes pour maintenir les fonctions cellulaires, l'activation enzymatique, l'expression des gènes et le métabolisme des acides aminés, des lipides et des glucides. Leur quantité doit être contrôlée, car des concentrations plus élevées peuvent les rendre toxiques. En conséquence, les usines ont mis au point des mécanismes leur permettant de contrôler et de réguler l'absorption, le transport et le stockage de métaux essentiels mais également non essentiels; et un rôle important dans ces processus est joué par des ligands spécifiques sécrétés par les plantes afin d'améliorer le transport du métal.

Les fluides végétaux contiennent une grande quantité de ligands se complexant avec les métaux et un quantité considérable présente en forme libre, ce qui ouvre la possibilité de formation in situ d'espèces de fer marquées de manière isotopique à la suite de l'ajout d'isotope ionique de Fe à un échantillon permettant la quantification de l'élément d'intérêt présent dans l'échantillon.

Résumé:

L'objectif principal de cette thèse était de développer et de valider des protocoles de méthodes de spectrométrie de masse, qui pourraient être appliqués à la détermination et à la quantification de composés métalliques de faible poids moléculaire dans des liquides végétaux. Malheureusement, la quantité de liquide végétal (par exemple, le xylème), qui peut généralement être échantillonnée après plusieurs semaines de culture fastidieuse, se situe dans la plage des microlitres (ou inférieure), ce qui rend difficile le développement de la méthode. Ainsi, comme compromis, l'eau de coco (Cocos nucifera) a été choisie comme modèle pour les études de développement de méthodes d'endospermes de plantes, car la quantité d'échantillon disponible pour les expériences est beaucoup plus importante.

Sur la base des informations disponibles dans la littérature, les complexes de fer les plus communément identifiés étaient ceux de citrate de Fe et de complexes mixtes de fer avec citrate et malate. L'étude détaillée de la formation de différents complexes a été réalisée pour évaluer leur stabilité et leur équilibre. En outre, différentes colonnes chromatographiques ont été testées et les conditions d'élution ont été optimisées pour une utilisation ultérieure sur les échantillons réels. Les conditions MS ESI ont été ajustées (ionisation en mode positif ou négatif) en fonction des conditions chromatographiques utilisées.

La partie principale de la thèse concerne le développement de méthodes de caractérisation de l'échantillon du modèle. L'influence de différentes étapes de traitement des échantillons (filtration, centrifugation) et des conditions de stockage a été étudiée. La préparation des échantillons avant la séparation HILIC a également été évaluée et les conditions de séparation optimisées sur les complexes modèles ont été testées.

La recherche d'une stratégie analytique générique pour la quantification sans standard de différents complexes métalliques de faible poids moléculaire par spectrométrie de masse moléculaire est poursuivie à l'aide de l'analyse de dilution isotopique (IDA) avec l'ajout d'un pic isotopique 58Fe sous forme ionique et HILIC-ICP-MS. Le protocole a été soigneusement étudié afin de conserver les complexes métalliques d'origine de manière non dégradée et d'obtenir la formation de complexes métalliques avec l'excès de ligands présents dans l'échantillon.

Enfin, les procédures développées ont été appliquées à la caractérisation et à la quantification des composés du fer dans des échantillons de xylème de plusieurs plantes. Les plantes choisies (Pisum sativum, Paspalum urvilleli et Setaria parviflora) étaient hypertolérantes ou hyperaccumulatrices.

Conclusion:

Ce projet de thèse a permis de développer de nouveaux protocoles basés sur la spectrométrie de masse pour la détermination et la quantification de composés métalliques de faible poids moléculaire dans les liquides des végétaux. Les principaux défis étaient la quantité extrêmement faible d'échantillons (par exemple, le xylème est échantillonné dans une plage de microlitres), la faible stabilité des analytes et le manque d'étalons analytiques.

La première partie du travail a été centrée sur la caractérisation des espèces pouvant être potentiellement présentes dans les plantes liquides en étudiant leur équilibre, leur stabilité et leur comportement chromatographique. L'étape suivante a consisté à caractériser complètement l'échantillon modèle: l'eau de coco (Cocos nucifera) utilisée comme modèle pour le métallome de l'endosperme de la plante et disponible en quantités relativement élevées. Différentes conditions chromatographiques ont été testées et optimisées. Les conditions ESI MS ont été ajustées (ionisation en mode positif ou négatif) en fonction de la nature des analytes et des conditions chromatographiques utilisées. De plus, l'influence de différentes étapes de prétraitement des échantillons (filtration, centrifugation) et des conditions de stockage ont été étudiée.

Une stratégie analytique générique pour la quantification sans standard d'un large spectre de complexes métalliques de faible poids moléculaire par spectrométrie de masse moléculaire a été développée à l'aide de l'analyse par dilution isotopique (IDA) avec l'ajout d'un isotope sous forme ionique et de HILIC-ICP-MS. Le protocole a été soigneusement étudié afin de préserver les complexes métalliques d'origine et d'obtenir la formation de complexes métalliques avec l'excès de ligands présents dans l'échantillon.

Enfin, les procédures développées ont été appliquées à la caractérisation et à la quantification de complexes de fer de faible poids moléculaire dans des échantillons réels de xylèmes de plantes hypertolérantes et suraccumulables, notamment *Pisum sativum*, *Paspalum urvilleli* et *Setaria parviflora*.

Acknowledgment:

This dissertation is the culmination of a work carried out at the Institute of Analytical Sciences and Physico-Chemistry for the Environment and Materials (IPREM), under the direction of Professor Joanna SZPUNAR and the co-direction of Katarzyna BIERLA, who shared their experience with me and supported me during the preparation of my defense.

I would like to express my gratitude to Ryszard LOBINSKI, Director of IPREM, for allowing me to carry out this work within the team of environmental analytical chemistry and for being the chairman of the jury assisting to my PhD defence. Professor Beata GODLEWSKA- ZYLKIEWICZ at university of Bialystok and Professor Eduardo BOLEA MORALES at the University of Saragosa, are warmly thanked for having accepted to be the reviewers of this work as well as Dr Veronique VACCHINA for taking part of the Jury.

This work was initiated as part of a collaboration between IPREM and INRA – Montpellier: Thank you to Stephane MARI for the trust they have placed in me throughout the duration of this work and the samples they have collected and entrusted to my care for analysis. Many thanks for Katarzyna KINSKA, researcher at the University of Warsaw, and post Doctorate at IPREM who helped to advance the work of this thesis and in the edition of this manuscript. May she be assured of all my gratitude for her faithful collaboration and all my friendship.

My thanks to my colleagues for their work with me in the 3 recent years, and their know-how in ESI MS and in one form or another to the good realization of the works. Thanks to every person who helped in coconut deliveries. I would like to thank also Paulina PISAREK who did her master's internship in IPREM on this subject and contributes in the first part of this work....

All my gratitude and sympathy to my colleagues from the "coffee break" (they will recognize themselves) for the laughter, the good mood and the good times spent during these moments of decompression.

May my friends (Zaid & Ahmed ALMAYAHI, Ahmed SIALITI) be thanked for their unwavering support, especially recently. Know that your great "bowls of energy" and your "positive thoughts" brought me to the end.

Finally, to my family, my parents Ghazi & Samar ALCHOUBASSI forgive me for my lack of availability, my absences, my moments of fatigue or doubt, thank you for all those moments where a simple smile, a little word from you, gave me the courage and the desire to continue.

Table of content:

List of abbreviations:

AA – ascorbic acid
AC – alternating current
ACN – acetonitrile
AmmAc – ammonium acetate
Asp – aspartate
Asn – asparagine
APCI – atmospheric pressure chemical ionization
APPI – atmospheric Pressure Photoionization
ATP – adenosine-5'-triphosphate
CCS – collision cross section
CI – Ivory Coast coconut
CID – collision induced dissociation
Cit – citrate
COPT – copper transporter family
CR – Costa Rican coconut
CRC – collision/reaction cell
CE – capillary zone electrophoresis/capillary electrophoresis
DC – direct current
DMA – 2'-deoxy- mugineic acid
DNA – deoxyribonucleic acid
EDTA – ethylenediaminetetraacetic acid
Epi-HDMA – 3-epihydroxy 2'deoxy mugineic acid
Epi-HMA – 3-epihydroxy mugineic acid
ESI – electrospray ionization
ESL – embryo sac liquid
ES MS – electrospray mass spectrometry
EXAFS – X-ray absorption fine structure
FIA – flow injection analysis
FT-MS – Fourier Transform mass spectrometry
FRD3 – Ferric reductase defective 3
FRO2 – ferric chelate reductases
Gln – glutamine
Glu – glutamate
HCD – higher- energy collisional dissociation
HILIC – hydrophilic interaction liquid chromatography
His – histidine
HMW – high molecular weight
HR – high resolution
HMA– heavy metal ATPase
HPLC – high performance liquid chromatography
HvIRT1 – *Hordeum vulgare* iron-regulated transporter 1
ICP MS – inductively coupled plasma mass spectrometry
ICR – ion cyclotron resonance
IDA – isotope dilution analysis
ID – isotopic dilution
IFS – isotopic fine structure
IEC – ion-exchange chromatography
IMS – ion mobility spectrometry
IRT (1/2) – iron-regulated transporter (1/2)
LK – Sri Lanka coconut
LMW – low molecular weight
LTQ – linear trap quadrupole
MA – mugineic acid
Mal – malate
MMW – medium molecular weight
MS – mass spectrometer

MS^n – multistage mass spectrometer/spectrometry
MS/MS – tandem mass spectrometer/spectrometry
NA – nicotianamine
NADPH – reduced form of nicotinamide adenine dinucleotide phosphate
RP-LC – reversed phase liquid chromatography
OA – organic acid
PC – phosphatidylcholine
Phe – phenylalanine
ppm – parts per million
PS – phytosiderophores
PSII – photosystem II
PsbO – extrinsic protein for photosystem II
Q – Quadrupole (analyzer)
RF – radio frequency
RNA – ribonucleic acid
SEC – size exclusion chromatography
SS-IDA – Species-Specific isotope dilution analysis
SRM – Single reaction monitoring
TH – Thailand coconut
TOF – time of flight (analyzer)
Trp – tryptophan
UPLC – ultra performance liquid chromatography
VIT1 – vacuolar iron transporter 1
XANES – X-ray absorption near-edge structure
XAS – X-ray absorption spectrometry
YSL – Yellow Stripe proteins family
ZIC-HILIC – zwitterionic–hydrophilic interaction liquid chromatography
ZIP – zinc-regulated transporter, iron-regulated transporter -like protein
ZRT – zinc-regulated transporter

I. Literature part:

1 Role of metals and their species in plants:

There are different sources, either natural or anthropogenic, that may lead to the accumulation of metals in the environment [1]: the metals are derived from natural components accumulated from soil or coming from geological phenomena such as volcanic eruption or from anthropogenic activities such as the use of fertilisers and pesticides. The latter which complicate the remediation process- the presence of metals particularly cadmium (Cd), lead (Pb), and arsenic (As) in the soil is due to either their addition along with pesticides or originate from the long-term application of wastewater and animal manures to agricultural soils- or emissions from, among others, power stations and transportation. The metals, dispersed into air, soil and water, are stable and tend to accumulate in soils and sediments to be later absorbed by plants and may be transferred to humans and animals which can cause damaging effects on health [2]. There are about 45 different metals used in industrial processes that may end up to be accumulated in soils water and air and they can be roughly classified as essential and non-essential elements[3].

Essential elements as chromium (Cr), cobalt (Co), copper (Cu), iron (Fe), manganese (Mn), molibdenium (Mo), nickel (Ni), selenium (Se) and zinc (Zn) play important role in plants at some level but they can be toxic at higher levels by leading to an oxidative stress [2]. Non-essential elements are not important for organisms and are toxic at any level. **Figure 1** shows the effect of the different levels of trace elements in biota (including plants): when the amount of the element of interest is lower than the critical concentration the plant is deficient in this element, when it is higher - it is the phase of toxicity and between those two - it is the element that plays its role at its best. **Table 1** shows the classification of elements in the periodic table between essential and non-essential.

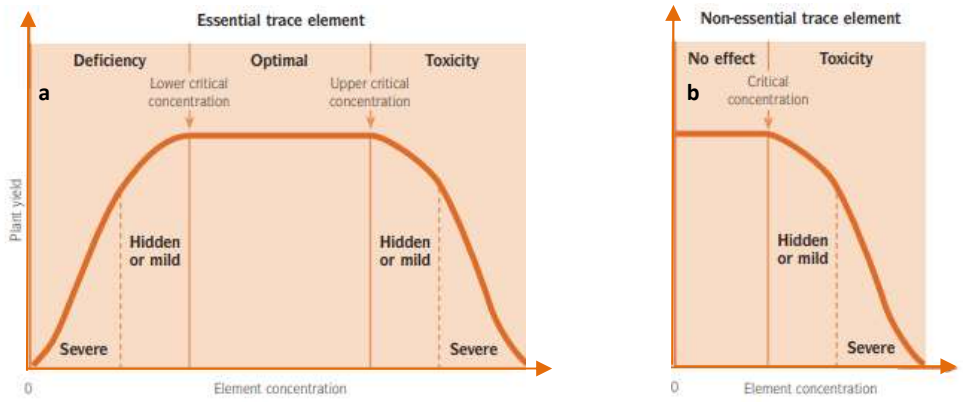

Figure 1. The dose-response curve for a)essential and b) non-essential trace elements modified from Alloway et al. 2008 [4]

Some plants such as lettuce, carrot, radish and zucchini - so called fast growing plants - can accumulate metals more efficiently than slow growing plants [2]: some of metals are more mobile and easily absorbed by the plant [5–8], others are strongly adsorbed to soil particles and hardly available.

At the same time, metals are present in different fractions in the soil which are in a dynamic equilibrium with each other. They include: soluble metal species, metal-containing precipitates, metals sorbed to clays, hydrous oxides and organic matter and metals within the matrix of soil minerals. Metals absorbed by plants can be considered as nutrients although plants are not perfectly selective so they may take up minerals that are non-essential or toxic. The fraction of the metal which plant can absorb is defined as the bioavailable fraction.

Table 1. Elements essential and non-essential for life in the periodic table of the elements.[9]

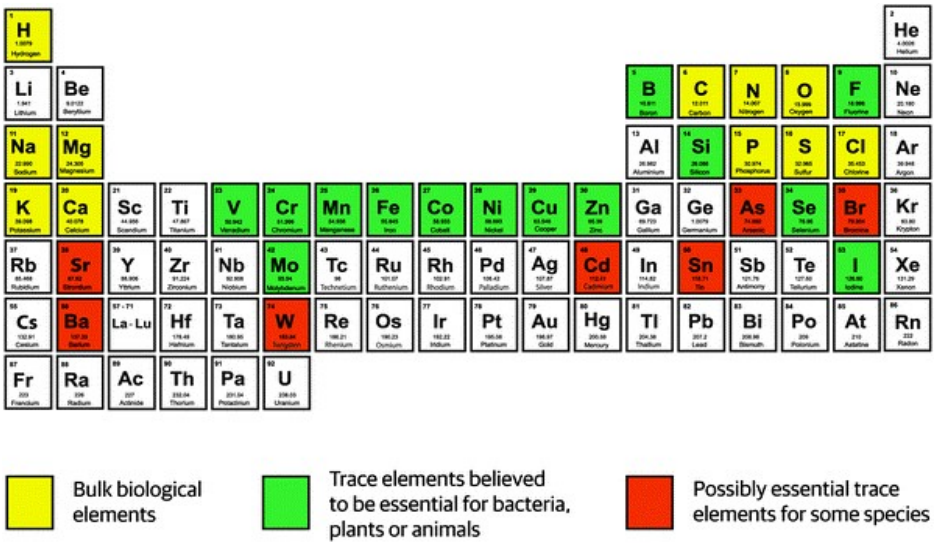

The total metal concentration of soil includes all forms of the metals present. Different soils factors such as pH, organic matter, clay and redox conditions which can determine how much of the metals will be available to plants. Hence, as the amount of organic matter present in soil increases the opportunity for forming stable metal-organic matter complexes increases as well. In general, plants are unable to absorb the large metal-complexes and so - if they predominate - the bioavailability of metals decreases [1].

To reach their final destination within the plant, micronutrients taken up from the growth medium, including metals such as Fe, Mn, Zn, and Cu, must follow a complex path through a number of different plant compartments and membrane systems; thereby, the vascular system, including the xylem and phloem conduits, is an essential segment for long distance translocation of micronutrients within this path [10].

Plant scientists have realized that knowing the total concentration of metals does not provide information about mobility, bioavailability and the biological role of metals; they always interact according to their oxidation state as part of biomolecules.

2 Biological functions of selected elements in plants:

Numerous elements play vital role in life cycle of plants. The most important ones are present in high amounts in plant tissues and thus they are regarded as essential macronutrients, others are present in parts per million and are known as micronutrients. The biological functions of selected elements in plants are presented below.

2.1 Iron

Iron is one of the essential micronutrients for many plant functions because of its ability to accept and donate electrons. It is taken up by plants as either Fe^{2+} (ferrous cation) or Fe^{3+} (ferric cation) to take part in photosynthesis as a red-ox active element, mitochondrial breathing, nitrogen assimilation, DNA synthesis, hormonal biosynthesis as well as defense against pathogens. There is 80% of the iron in chloroplasts, where it participates in photosynthesis.

Iron is present in proteins in various coordination forms - depending on the type of iron ligand, such as proteins with iron-sulfur clusters (Fe-S), proteins with heme part, and others; however, Fe-S clusters are made of inorganic iron and sulfur either spontaneously while in aerobic in vitro conditions, or due to a

specific mechanism in the plant when both components are in low concentrations in the cellular mitochondria [11]; they are involved in the regulation of transcription and translation processes, and control the spatial structure of the protein in the cluster's environment [12].

Concerning enzymes, iron can be either metal component, crucial to maintain their stability and activity or a bridging element between enzyme and substrate. Hemoglobin proteins are produced in mitochondria and chloroplasts, and are present in all cell organelles and are involved in photosynthesis and respiration process, electron transfer and oxygen binding. The heme-containing enzymes are catalase, peroxidase, NADPH oxidase and cytochrome enzymes [11]. It also participates in the synthesis of phytosterols and metabolites. Proteins that do not have a heme group or Fe-S cluster such as ferritin can bind around 4500 iron ion directly helping in maintaining homeostasis and making it non-toxic to cells. Ferritin is mainly found in plastids: etioplasts and amyloplasts, but not in chloroplasts [12]. The facility of iron to form different complexes allows the modulation of its redox potential that may vary broadly depending on the ligand. This changeability is responsible for an important role played by iron in biological redox systems.

An excess of iron is observed as browning of leaves and leads to inhibition of protein synthesis. On the other hand, iron deficiency leads to a decrease in chlorophyll concentration in leaves which leads to a decrease in photosynthesis responsible for the cultures yield [13].

2.2 Copper

Copper is an essential element for photosynthesis because of its presence in chloroplast and mitochondrial respiration, assimilated by the plant in the two oxidation states Cu^{1+} and Cu^{2+} and involved in different functions such as in protein like plastocyanin for electron transport, carbohydrates production, N_2 fixation, saturation and hydroxylation of fatty acids, as cofactor in many enzymes like ascorbate oxidase, cytochrome C oxidase playing role in cellular respiration, defense against free radicals and Fe metabolism as well as it is included in amino acid complexes [2]. The utility of Cu in biochemical reactions results from its ability to cycle between oxidized Cu(II) and reduced Cu(I) states in enzymes and electron carriers [14–16]. After uptake by plant, Cu ions are bound to scavenging proteins to prevent their toxicity, and the part of copper that bypass this system is bound to other small proteins called copper chaperon which guide this element to its target sites in the cell [12].

Cu(II) ion has a relatively low toxicity compared to other elements because Cu requirements by plant are very low; this toxicity is variable between species of plants and affects tissues differently depending on the metabolic requirements [16]. The symptoms of toxicity in plants are chlorosis, and Cu has a high affinity for sulfur and nitrogen containing groups of biological molecules so it can replace other essential elements in enzymes or change the form of the function of macromolecules due to binding. It may also lead to oxidative stress which disturbs metabolic pathways and damage the membranes [17].

2.3 Zinc

Zinc plays an important role in the development of seeds. Plants with zinc deficiency show a delay in reaching maturity because of the lower activity of hydrogenase and carbonic anhydrase, stabilizing the ribosomal fraction and cytochrome synthesis.

There are over 1200 proteins that contain, bind or are involved in the transport of Zn^{2+} ions in plants; they include zinc finger proteins and transcription factors, oxidoreductases and hydrolytic enzymes, such as metalloproteases, involved in the regulation of DNA and RNA transcription and translation [12]. In addition, the activity of all types of DNA and RNA polymerase, enzymes involved in the editing of RNA in chloroplasts and mitochondria, as well as splicing depends on the presence of zinc. Zn-activated enzymes are involved in the metabolism of carbohydrates, the regulation of auxin synthesis and the formation of

pollen and affect the ability to absorb and transport water in plants, and also reduce the negative effects of short periods of thermal and salt stress [18]. By interacting with phospholipids and thiol groups of the membrane proteins, Zn contributes to maintaining the structural continuity of cell membranes. Also, in the cytoplasm, lysosomes and apoplasm having a zinc activity are associated to hydrolytic processes, in which participate other enzymes such as nucleases, aminopeptidases, and metalloproteinases. Furthermore, zinc fingers are transcription factors involved in protein-protein interactions [12].
Zinc deficiency results in the development of many abnormalities in the functioning of the body, which result in stunted growth, chlorosis and reduced leaf size [2][18]. Zinc deficiency also causes deterioration of the quality of crops - sensitivity to irradiation and temperature, and susceptibility to fungal infections.

2.4 Nickel

Nickel is essential for higher plants and its deficiency may have severe effects on plant growth, ageing, disease resistance, nitrogen metabolism, iron uptake and also the normal grain development. In plants, nickel usually occurs on the oxidation stage II, but it also can be found on the first and third oxidation stage [19]. The main symptom of its deficiency is the accumulation of toxic urea caused by the disappearance of urease activity, whose role is to catalyze the decomposition of urea into carbon dioxide and ammonia; Ni^{2+}-binding protein identified as Ni metallochaperone including HypB CooJ and UreE are essential for urease activity [12][20]. Ni plays a very important role in the activation of enzymes such as dehydrogenase, hydrogenase, and methyl reductase. Excessive amount of nickel in soils and waters, is toxic and can induce an inhibition of mitotic activities and reductions in plant growth [20].

2.5 Manganese

Manganese is an essential element for plant metabolism and development; it is present in 35 enzymes of the plant cell in states of oxidation II, III and IV; it has a catalytic role due to manganese containing superoxide dismutase helping in the protection of cells from damage by free radicals [21]. It is also included in enzymes responsible for nitrogen metabolism, RNA polymerase activation and fatty acids biosynthesis. It is responsible for the activation of some enzymes including decarboxylases and dehydrogenases in the krebs cycle and several glycosyltransferases in the golgi apparatus [22]. In addition, Mn can be bound to proteins such as PsbO manganese-stabilizing protein and $(Mn)_4$ cluster, which plays a role in the photosystem II present in the thylakoid membranes of plants and helping in the splitting of water into dioxygen and reducing equivalents [21]. Manganese deficiency leads to a decrease in leaf net photosynthesis and in the quantum yield of PSII. Manganese can be found in green vegetables, nuts, tea and cereals [23].

3 Role and classes of low molecular weight (LMW) metal ligands in plants

The pool of free metal cations in plants is considered to be very limited and metals not involved in protein binding are expected to be bound to low molecular-weight (less than 1 KDa) ligands. Low molecular weight metal complexes in plants are frequently abundant and play a crucial role both in the plant's metabolism and animal/human nutrition. These ligands are small, organic molecules playing a role in metal ion homeostasis by facilitating uptake and transport of poorly soluble cations from the soil and translocate them through the different plant’s compartments [24]. They can also act as chelators implicated in sequestration of metal resulting in the tolerance to metal excess and metal storage. However, these low molecular weight forms are easily degraded which helps in their accessibility to transfer metals to

macromolecular sites in cells. In some cases, complexation of the metal with the low molecular weight ligand may provide a buffer system to absorb other trace metals and may have catalytic activities [25].

Very little cellular metal ion content is expected to exist as free ions. Metal ions not occupying sites in proteins are expected to be bound to low molecular-weight (LMW, less than 1 kDa) metal ligands. These metal ligands work as intracellular chelators for sequestering metal ions in the cytosol or in subcellular compartments, for mobilization from the soil and for translocation within the plant. In order to fulfil these roles, transport mechanisms are required for the secretion or uptake of metal ion ligands by cells or for the movement of ligands between subcellular compartments.
The metals in plants interact with different strengths with organic ligands. In 1953, H. Irving and R.Williams [26] presented a relationship comparing the forces with which transition metal cations interact with sulfur containing ligands S-, nitrogen N-, oxygen O-: these metals forces are classified as follow $Mn^{2+} < Fe^{2+} < Co^{2+} < Ni^{2+} < Cu^{2+} > Zn^{2+}$. Metal homeostasis is composed of a controlled network helping in maintaining the metal amount in the appropriate range because its excess may cause toxic effects, and its availability for interaction with proteins and other organic molecules should be controlled in order to enable binding to the right target sites and to avoid harmful side reactions.
The homeostasis is assured by the formation of complexes between metal and ligands secreted by plants; metals such as mercury Hg, lead Pb(IV), and Cu(I), seek out sulfur (S) and nitrogen (N) centers in biological systems, and may become irreversibly bound, also Cu(II), cadmium Cd, Ni, and Zn, form stable complexes with S, N, and oxygen (O) present in groups such as –SH, -NH as the donor atom [27]. For example, Singh et al. showed that P and S and O are major constituents of iron-binding compounds in grains and that most of the Fe (III) was associated with O and P and about 19% was in coordination of O and S [28][29].

Metal transport is associated with the occurrence of different classes of metal ligands in plant fluids, including:

(i) Compounds with just only O atoms as electron-donors, such as different carboxylates (mainly citrate and malate which structures are shown in **Figure 2** but also some less known ones such as methylated aldaric acid and *ortho*-dihydroxy phenolic compounds such as protocatechuic acid.
(ii) Compounds with O and N atoms as electron donors, such as amino acids (proteinogenic ones such as histidine and non-proteinogenic ones such as nicotianamine (NA) and other phytosiderophores (e.g., MA and DMA); and
(iii) Compounds containing S atoms in which at least one of them acts as an electron donor, such as cysteine, S-containing peptides (e.g., glutathione and its derivatives, PCs) and proteins rich in cysteine (e.g., metallothioneins) [10][30].

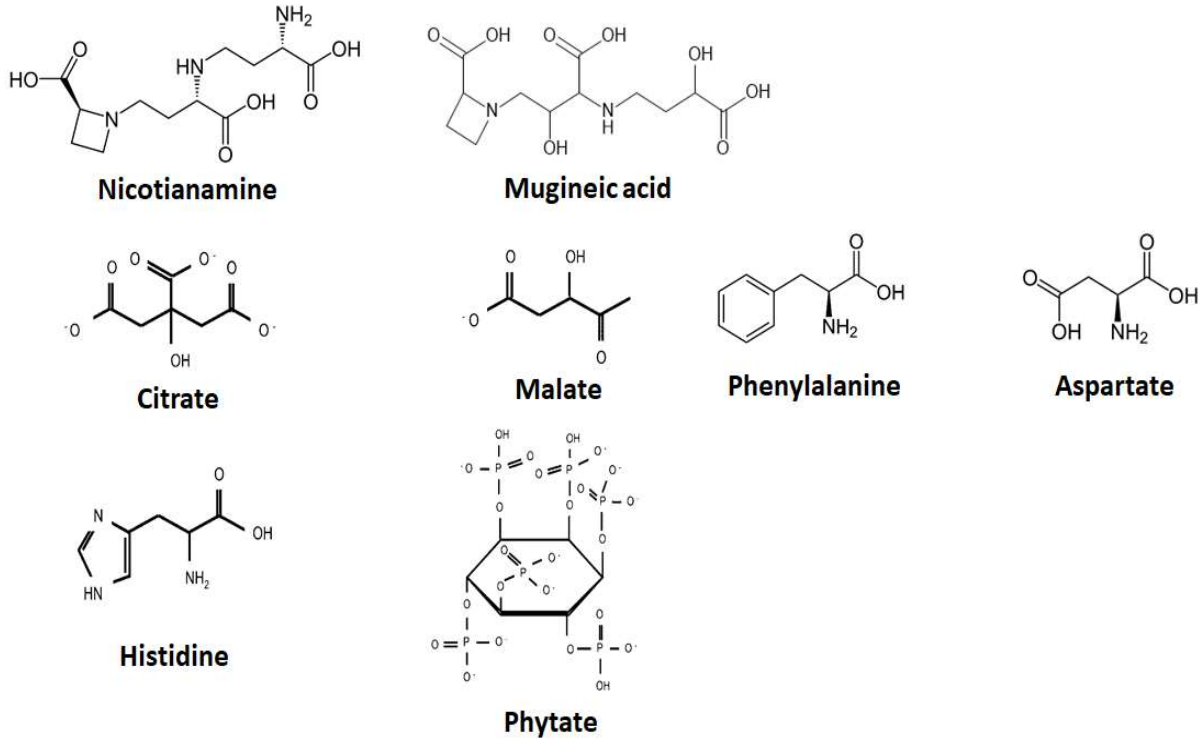

Figure 2. Selected metal ion ligands for iron (Fe), zinc (Zn), copper (Cu), manganese (Mn) and nickel (Ni) in plants [31][32]

3.1 Carboxylic and amino acids

Carboxylic acids, such as citric, malic, fumaric, succinic, malonic, oxalic, formic and piscidic, are found in the root exudates of different plants where they can react with various metal cations because of their negative charge. Their presence is linked to the low nutrient supply in the soil. An example was given in nutrient-deficient maize plants and barley plants where there was a release of higher amounts of citric and malic acids, respectively due to Fe deficiency [33]. Secretion of these organic acid can also be a mechanism of detoxification[34]. Rellan Alvarez et al. [35] and Alvarez-Fernandez et al [10] studied different Fe citrate/malate ratios in plant saps samples; the lowest Fe:citrate ratio ~0.001 was found in sugar beet representing a high amount of citrate present in the sample followed by beans such as faba and soybean at around 0.005. Concerning Fe:malate ratio, *H. vulgare* species represents the lowest ratio ~0.0001 which means the sap of this species contains the highest amount of malate [31].

Several proteinaceous amino acids were found to bind metal ions; they include glutamine, asparagine and aspartate containing a $–CONH_2$ (amide) or a –COOH (carboxylic acid) group in their side chain; they are involved in binding metals in xylem and phloem where tyrosine is one of the principal ligands present in it. Several studies mentioned the role of glutamate (Glu) in complexation of metal ions as well as uncharged aromatic amino acids such as phenylalanine (Phe) and tryptophan (Trp) but identified them as minor ligands in overall metal speciation [36]. In addition, histidine (His) is found to be secreted to increase the mobility of Ni; it acts either as a free amino acid or as a metal-coordination residue in protein. An increase in the amount of Ni in xylem of plants leads to an increase in histidine content [32]. From the organic acids which account for the majority of zinc, Zn-histidine was the second most abundant ligand in leaves and can complex to 70% of Zn in roots [37].

3.2 Metallophores

Metallophores are low molecular weight chelators derived of mugineic acid which are able to solubilise metallic compounds from root environment. The mugineic acid (MA) family of metallophores includes

mugineic acid, 2'-deoxy- mugineic acid (DMA), 3- epihydroxy mugineic acid (epi-HMA) and 3-epihydroxy 2'-deoxy- mugineic acid (epi- HDMA). Metallophores are not involved in the mobilization of Mn because of their low affinity to this metal compared to Fe, Zn and Cu. For every metal a group of ligands that are binding to it helping in its transport, translocation as well as detoxification of the soil. Some of these ligands are presented in **Figure 3**, where those chelating Fe(III) are presented in a dotted semicircle and those Ni in dashed semicircle; the most relevant ligands for each element are circled such as citrate (Cit), malate (Mal), phytate for Fe(III) and nicotianamine (NA) for Ni.
Mugineic acid is synthesized enzymatically from a precursor which is nicotianamine a nonproteinogenic amino acid in graminaceous plant species; this precursor is present in plants and plays a crucial role in maintain solubility and homeostasis of Fe specifically. Each graminaceous plant secretes its own set of MA [38]. Previous work shows a role for NA in Zn and Cu homeostasis [32]. Phytosiderophores are particular metallophores that are specific for the solubilisation of ferric compounds and transport of iron from root to shoot in plants.

In summary, the affinity for NA or for citrate is shared by several metals, which implies a competition for the binding. The metal speciation depends then on the relative amounts of the different ligands and metals (in addition to pH and ion strength).

3.3 Phytate

Myo-inositol hexakisphosphate known as phytate is a storage molecule for phosphorus that is implicated in binding and storage of metals such as Zn. This molecule is synthetized in the cytosol and was found accumulated in vacuoles of the embryo and endosperm in *A. thaliana* [39]. According to the literature, phytate plays also a role in binding Mn ; Mn-phytate was identified in the endoplasmic reticulum [32][40]. Additionally, the studies on *A. thaliana* showed that in seed vacuoles iron seems to be complexed with phytate which represent the main storage form of iron in *A. thaliana* seeds[39].
In addition, Fe-phytate complexes were found in the majority in an insoluble form which may limit iron bioavailability; but there is evidence that some of the soluble Fe in cereal grains for example is bound to inositol pentaphosphate (IP_5) which is a partially dephosphorylated soluble form of phytate and this complex is considered as a medium molecular weight (MMW) Fe−phytate. This soluble Fe−phytate accounted for 2% of the total Fe present in wheat cultivars [41].

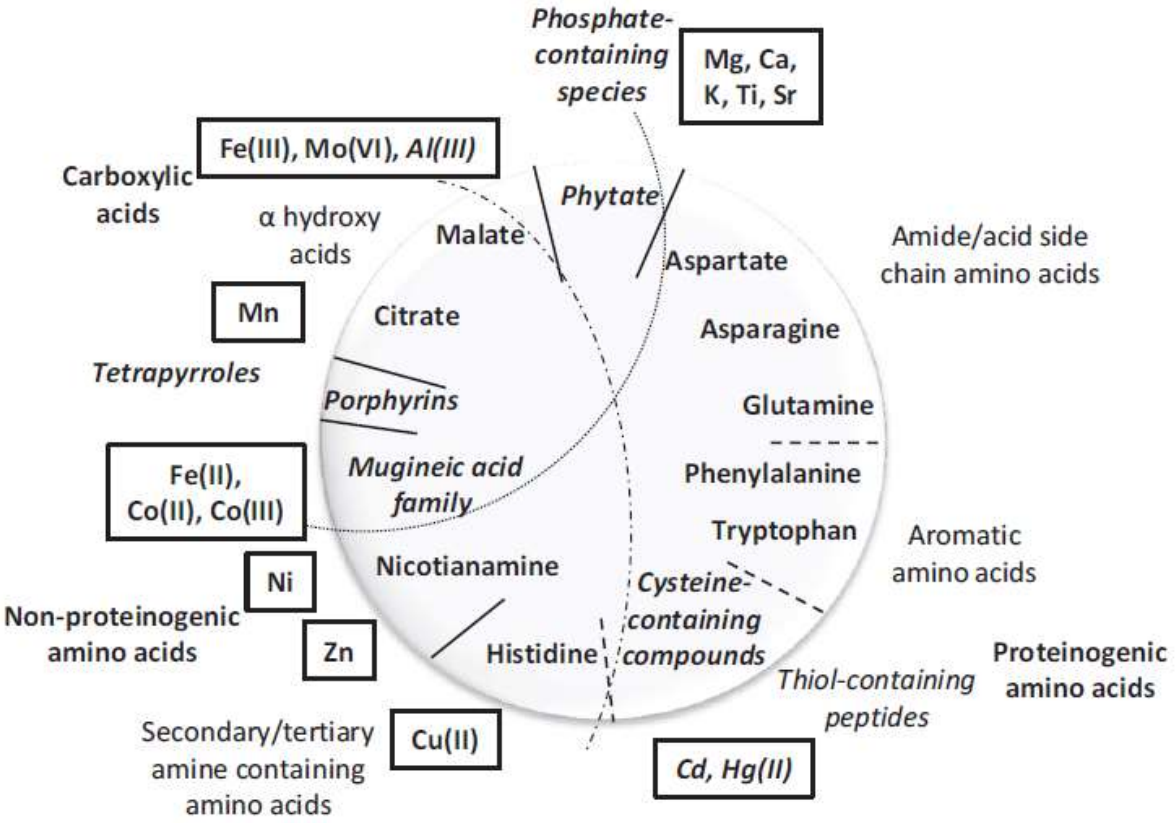

Figure 3. Scheme representing the main low molecular weight ligands (in the central circle) involved in metal binding in pea (pisum sativum). Metal ions (in boxes) are represented close to the ligands to which they are binding. Key ligands are therefore the ones present in the closest vicinity for each metal. As examples, for Fe (III) (dotted semicircle) and for Ni (dashed semicircle), the most relevant ligands for each element are circled. [36]

4 Low molecular weight (LMW) metal complexes in plants:

Metals are found to be transported within plants either in the form of hydrated ions, and this represent only a small amount of the metal, or in combination with ligands [34]. The reactivity and non-selectivity of metals of their bonds to ligands are a challenge for maintaining balance in plant tissues in order to avoid toxicity due to metal excess [32]. However, the toxicity depends not only on the type of element, but also on the solubility of its chemical form and the stability of the complex, as well as its quantity [42]. So, these ligands allow uptake and distribution of metals to tissues maintaining its homeostasis by buffering substances in the cytosol, facilitating the transport of metals inside and outside the cell and allowing long-distance transport to other plant organs.

The importance of LMW complexes in metal transport and homeostasis made them a centre of interest for studies and necessitate the development of analytical approaches in order to identify their structures and quantify the metal involved in their formation in plants. Recently, significant progress has been made in the identification and characterization of some of these transporters and has provided insight into the role of a number of metal ion ligands in metal homeostasis [32].

4.1 Copper complexes

It was shown that a large fraction of Cu in the xylem fluid might bind to asparagine (Asn), histidine (His) and glutamine (Gln) [40],[41]. These results were confirmed and complemented by Liao et al.[45] who reported that NA is the most important Cu ligand in tomato and chicory xylem exudates. However, the transport of Cu in these two plants exudates was efficient even in the absence of NA because it was

assured by His [46][14]. Thus, Cu has a high affinity to NA considered the principal carrier of Cu in xylem and embryo sac liquid as well as in phloem sap of some plants such as rice [47]- it is important to mention that Cu is bound to NA in phloem but to DMA in xylem in rice plants and tomato. Once the Cu-ligand is formed, there are different transporters helping in the integration and transport of these complexes through the plant such as COPT a CTR-like transporters which transport Cu (I) [48], ZIP a Zrt, Irt-like protein transporters and HMA a Heavy Metal transporting ATPase transporters which can transport Cu (II) identified by Burkhead et al (2009)[16], Pilon et al (2011) [49]; these transporters can cooperate together for copper transport such as ZIP2 and ZIP4 which are members of the ATP independent ZIP family and may function in addition to COPT transporters for Cu uptake in plant cells. Additionally, Copper transporters may have functions in opposite directions and this mechanism was studied by Sancenon et al 2003 [48] for COPT1 and HMA5 which are members from COPT and HMA copper transporters. It is important to mention that not all HMA transporters can transport Cu in its second oxidation state: HMA1 was found to have a role in Cu(II) and HMA5 played the same role for Cu(I)[16].

More interestingly, Zheng et al (2012)[50] showed that YSL transporters can transport Cu (II)-NA complex. However, NA is an intermediate in the metabolism of DMA [51] but unlike DMA, which is released to the rhizosphere from the roots, NA is involved in the internal homeostasis of metals in plants [14]. In literature, some data can be found showing affinity of Cu to some aromatic (Tryptophan and Phenylalanine) amino acids [36][45].

The ligands that might bind Cu are collected in **Table 2** showing the amount of every amino acid secreted due to excess or deficiency of Cu [52].

Table 2. Amino acids concentrations (µmol/l xylem) in xylem sap of B. carinata grown under control (0.12 µM CuSO4), excess (2.5 and 5 µM CuSO4) and deficiency (0 µM CuSO4) of copper.

	0	0.12	2.5	5.0
Aspartic acid (Asp)	2.85±1.20	2.85±0.30	4.73±1.58	3.60±1.65
Glutamic acid (Glu)	8.83±3.40	7.81±0.61	9.38±1.15	7.07±0.54
Asparagine (Asn)	1.13±0.60	1.06±0.30	0.75±0.007	1.21±0.60
Glutamine (Gln)	9.72±2.19*	2.33±0.55	5.06±0.41*	7.39±0.68*
Serine (Ser)	8.09±2.95	11.98±3.80	7.71±0.67	5.23±0.47*
Glycine (Gly)	7.46±0.27*	12.12±1.46	22.11±1.46*	22.91±3.73*
γ-Aminobutyric acid (Gaba)	1.55±0.10	1.74±0.38	2.13±0.04	2.04±0.29
Threonine (Thr)	17.54±0.50*	4.36±0.67	17.12±0.92*	21.74±2.94*
Histidine (His)	13.08±4.19	18.63±3.22	102.87±8.64*	139.99±16.43*
Arginine (Arg)	12.92±1.61	14.87±3.50	15.15±2.47	14.18±2.98
Alanine (Ala)	48.04±6.73	43.66±4.26	15.83±1.23*	26.26±6.28*
Proline (Pro)	3.56±0.61	2.69±0.61	5.82±0.17*	6.34±0.78*
Tyrosine (Tyr)	9.27±2.26	6.57±1.04	8.22±1.10	8.77±1.82
Valine (Val)	10.84±1.19*	16.55±2.56	13.23±4.09	11.27±3.19
Methionine (Met)	29.55±0.73*	6.03±0.47	10.99±0.13*	12.53±2.08*
Cysteine (Cys)	ND	5.61±0.49	7.59±1.24	5.53±0.25
Isoleucine (Ile)	14.56±3.05	11.13±3.28	12.27±3.20	13.49±2.21
Leucine (Leu)	17.00±3.81*	22.18±0.61	13.95±2.97*	12.89±1.30*
Phenylalanine (Phe)	5.81±2.00	6.96±0.85	8.71±1.03	8.05±0.24
Lysine (Lys)	63.41±8.00	51.71±3.28	56.98±5.20	58.35±1.16
Nicotianamine (NA)	271.60±37.35*	64.62±10.45	76.22±6.36	58.45±6.30

According to the data in **Table 2**, histidine content increased linearly with increasing external Cu concentration. On the other hand, proline only showed a significant increase with the 2.5 µM $CuSO_4$ treatments but there was no significant difference between the content of this amino acid at the 2.5 µM and 5 µM $CuSO_4$ treatments. Furthermore, under copper deficiency conditions, methionine, nicotianamine, glutamine, and threonine were detected at high levels which can be explained by the fact that these amino acids are secreted in response to different stress conditions and not specifically to copper. In addition, the increase in nicotianamine detected in conditions of copper starvation but not in

copper excess shows that NA is not involved in the response to excess of copper but participates in Cu transport to the shoots in deficiency conditions [52].

4.2 Zinc complexes

Zn (II) is bound by NA when the amount of this ligand is as high as or higher than the Zn amount [36][41]; however, in the case of hyperaccumulating Zn plants, where the amount of Zn can be higher than the amount of NA organic acids such as citrate and malate plays the role of Zn complexation [29] [53]: Zn-malate was found in high concentration in the aerial parts, weheras Zn-citrate was more concentrated in the roots of the *Arabidopsis halleri* studied by Sarret et al 2002 [54]. In addition, Yoneyama et al. [55] showed that The Zn chemical forms in xylem sap are free ions or partially bound to unidentified chelators [39], while the Zn in phloem sap was dominantly bound to NA [55]. In some samples, other ligands such as histidine [37] and glutamine were also observed. LMW complexes such as Zn-NA and Zn-DMA were detected in rice endosperm [53]. In compost amendment conditions, Terzano et al [54] presented Zn as a metal bound to phytate partly blocked just outside the stele and, for a lower fraction, Zn bound to citrate in order to be transported by xylem in *Eruca vesicaria* L. *Cavalieri* [54].

Recently , studies done on goji berries led to the identification of other Zn ligands such as glycine, galacturonic acid, methionine, pterostilbene, caffeic acid, zeaxanthin glucoside, piceatannol, isorhamnetin, linolenic acid and resveratrol [56][57].

4.3 Manganese complexes

Manganese is a major transition element in plants bound mainly to citrate as Mn-$(citrate)_2$ and, at a much lower level, in the Mn-$(malate)_2$ complex. Mn complexes such as Mn(II)-$(malonate)_2$, Mn(II)-oxalate, Mn(II)-$(oxalate)_2$, Mn(II)-succinate, Mn(II)-histidine as well as Mn(III)-acetylacetonate were also identified [58]. Small amounts of Mn-NA were also detected, which is consistent with a possible role of NA for Mn transport via YSL transporters in rice [59][60]. In addition, studies were done on *Morinda citrifolia* (known as noni, a bush grown in tropical Asia and Polynesia) showing that manganese can be complexed by salicylic acid, alizarin, myricetin (a phenolic compound), asperulosidic acid and rutin [61].

4.4 Nickel complexes

Similarly to other metals, nickel transport in plants depends on various factors like form of Ni, plant species, Ni concentration in the substratum, soil pH, metabolism of plant and organic contents in the soil; at first Ni was absorbed by roots as free hydrated cations which bind to amino acids complexes inside the roots to be directed via xylem to the aerial parts, so it was found that Ni is a minor micronutrient bound mainly by NA and histidine. Moreover, Ni-$(histidine)_2$ and Ni-NA have been observed by MS as minor ligands in hyperaccumulating plants for the movement of Ni from the cytoplasm into the vacuole [62]. The Ni-NA complex could also be observed transported by YSL transporters [63–65]. Furthermore, Ni–malate is identified already in the xylem sap of hyperaccumulating plant *Thlaspi caerulescens* together with Ni–NA, Ni–citrate, and Ni–histidine [66]. In addition, citrate was suspected to bind Ni according to 2 ratios 1:1 and 1:2 [67] ; these organic acids, such as citric and malic acids, provide both a source of protons for solubilization and anions for Ni chelation. However, since Ni complexation is dependant of pH of medium where it is present it was mentioned that Ni is mainly chelated by citrate at pH 5.0, but by histidine at pH 6.5 [20][64][68].

4.5 Iron complexes

Iron in plants occurs in two principal oxidation states Fe (II) and Fe (III) forming a variety of complexes of different stability. There are several challenges driving research in iron speciation in plants that include

the understanding of the mechanisms governing the uptake of iron from soil, its transport to aboveground plant tissues and storage, as well as the mechanisms of the bioavailability of Fe from staple food, such as wheat, beans, barley, or maize [41][53].

In plant xylem, iron is solubilised in order to be bound to citrate in acidic, apoplastic conditions; this solubilisation is assured by a citrate effluxer so called FRD3. Moreover, malate was also found to be secreted as a response to iron deficiency [69]. Thus, Fe can be present in mixed-ligand complexes formed of citrate and/or malate identified in the xylem of tomato plants [35]. Fe LMW complexes (including Fe-DMA and Fe-NA) were found in extracts of wholemeal and rice accompanied by HMW forms of Fe predicted to be soluble proteins [53].

Concerning Fe (II), it was found to bind citrate, malate and aspartate but only at trace levels compared to Fe (III). Beside citrate, NA plays a role also in Fe chelation in cytoplasm and phloem loading [70][71] in neutral, cytosolic conditions. Thus, in embryo sac liquid (ESL) iron-NA is present at lower level than the iron bound to organic acids and this complex is transported to the seed by YSL transporter. However, NA has a higher affinity for iron(II) than for iron(III) that is the preponderant iron form in the sample [66].

Recently 2'-deoxymugineic acid (DMA), which is biosynthesized from NA, has also been shown to play a role in the phloem transport of Fe and is thought to be the predominant Fe chelator in the phloem sap of rice [41][72]. Some studies showed that in the extract of rice endosperm both Fe−DMA and Fe−NA can be found [41][73]. In addition, most of the Fe in cereal grain are complexed by phytates, which may be insoluble or soluble depending on the degree of metal bonding to phosphate groups. Thus, the highest concentrations of soluble Fe−phytate were found in the offal and bran flour fractions of plants[41][53][74].

Amino acids such as aspartic acid, serine, glutamic acid, glutamine, proline, alanine, valine, and ɤ-amino-n-butyric acid play role in Fe transport as well; their concentrations in apoplastic fluid are in the micromolar range; iron deficiency caused increases in the apoplastic concentration of total amino acids of approximately 40%. **Table 3** represents the concentrations of amino acid in response to iron deficiency and excess; it shows that the concentration of aspartate in apoplastic fluid decreased with iron deficiency, those of glutamine, alanine, and serine did not change significantly and those of glutamate, valine, proline, and ɤ-amino-n-butyric acid increased. Among the minor amino acids in apoplastic fluid, the concentration of lysine and asparagine decreased with iron deficiency, whereas those of threonine, glycine, and Isoleucine did not change significantly and those of leucine and histidine increased [75].

Table 3. Concentrations of amino acids in µM in sugar beets apoplastic fluid after iron deficiency and iron excess.

Amino Acid	Iron-Sufficient	Iron-Deficient	
	(+Iron)	(−Iron)	−Iron/+Iron
Asp	262 ± 20	177 ± 28	0.7
Ser	121 ± 42	182 ± 56	1.5
Glu	320 ± 3	538 ± 83	1.7
Gln	450 ± 180	396 ± 90	0.9
Pro	<1	77 ± 43	–
Ala	303 ± 130	243 ± 52	0.8
Val	60 ± 55	510 ± 50	8.5
GABA	56 ± 11	166 ± 12	3.0
Thr	44 ± 15	39 ± 8	0.9
Asn	59 ± 10	33 ± 3	0.5
Gly	56 ± 8	48 ± 12	0.8
Ile	16 ± 16	9 ± 4	0.6
Leu	<1	14 ± 7	–
Lys	31 ± 0.5	12 ± 0.1	0.4
His	<1	4 ± 2	–
Total amino acids	1,778	2,448	1.4

Higher plants have developed two distinct strategies to acquire iron, which is only slightly soluble in soil, from the rhizosphere: (i) the reduction strategy where Fe(III) is reduced to Fe(II) and then it can be transported into the root epidermal cells by the divalent metal transporters and (ii) the chelation strategy where Fe(III) is complexed by soluble phytosiderophores (PS) released from the root epidermis [39]. Coumarins were also discovered to play an important role in Fe acquisition from soil by plants [76][77]: its Chelating ability was found in an in vitro model study for the coumarins with 2- hydroxyl groups in ortho position, but not for those with single hydroxyl groups [78]. Thus, there are other compounds playing crucial role in iron speciation studies such as mentioned before in 4.5 section (i) organic acids (ii) siderophores high-affinity Fe(III) (iii) phytate both soluble and insoluble, and (iv) iron-binding proteins, especially ferritin due to its putative role in iron bioavailability from food plants [79].

However, the understanding of the iron metabolism which is critically dependent on the fine knowledge of its speciation may facilitate genetic engineering in order to increase the iron content in the required chemical form (and in a specific plant organ) in the context of human nutrition or environmental clean-up by phytoremediation [80] (cf. the case of the recent red mud flooding in Brazil [81]). Furthermore, hyperaccumulation of iron is achieved through coordination of several processes, including enhanced metal uptake (assisted by secretion of siderophores), efficient root-to-shoot translocation and effective detoxification in leaves due to the use of specific species of plants that are able to take and accumulate high amounts of iron without risk of toxicity [82].

As it is known, iron is an essential micronutrient for plants because it plays a role as an enzymatic cofactor in different metabolic processes, such as photosynthetic and respiratory electron transfer reactions, reduction of nitrate and sulfate, synthesis of fatty acids, and branched amino acids. But excess of iron is also responsible for its potential toxicity because ferrous ions can promote, in the presence of oxygen, the generation of reactive oxygen species and oxidative stress. To date, the number of organic molecules shown to form complexes with iron *in vivo* is extremely limited. Beside citrate which binds iron in acidic, apoplastic conditions, nicotianamine (NA) has a binding capacity for iron in neutral, cytosolic conditions [66]. By increasing the amount of Fe supplied to the plants such as sunflower tomato and cucumber that were analyzed by L.O. Tiffin 1965 [71], there was a doubling and tripling of the citrate amount released by these plants in the exudates. The high amount of Fe given to plants lead to exaggerated uptake of this element but, in the exudates the amount of iron was always proportionally greater than the amount of

released citrate which it would require an uptake of iron by other ligands. So there is a correlation between the amount of Fe and citrate in the plant's exudates; apparently a certain minimum content of iron is required in the roots to maintain a high rate of citrate release in the exudates: This could have an important role in the translocation not only of iron but of other trace metals that can be uptaken by citrate [71].

5 Metabolic pathways of metals in plants – strategies of metal acquisition and homeostasis in plants:

To reach their final destination within the plant (e.g., organelles such as chloroplast or mitochondria) micronutrients taken up from the growth medium, including metals must follow a complex path through a number of different plant compartments and membrane systems [10][83][84]. The vascular system, including the xylem and phloem conduits, is an essential segment for long distance translocation of micronutrients within this path [10]. The molecular mechanisms involved in metals uptake, transport, distribution and storage consists of several stages that are presented in details in **Figure 4** include:

1 - Mobilization: the metals are mobilized by the acidification of the rhizosphere and secretion of the molecules that are able to take them from soil,
2 - Uptake and sequestration: these molecules use transporters that forms various systems placed in the plasma membrane of the cells,
3 - Xylem transport: metals get to the xylem by the processes of compartmentation and sequestration within the root in order to get to the shoots,
4 - Unloading and tissue distribution: in leaves metals are unloaded to different leaf cell types and then moved through plasmodesmata form one cell to another,
5 - Storage: the last stage is metal distribution inside the cell and storage [34].

The efficiency of metal acquisition can be affected at every stage by the concentration and affinities of chelating molecules as well as by different selectivity of the transport systems in the plasma membrane.

5.1 Strategies of metal mobilization and uptake

The bioavailability of metals and their absorption by the roots can be limited by several factors such as soil type, aeration, pH, cation exchange capacity and redox potential as well as metal concentration, the presence of competing ions...etc [27]. There are different mechanisms developed by plants to enhance metal availability and uptake from soil; they include acidification of the rhizosphere, exudation of carboxylates, the reduction-based strategy commonly used by nongraminaceous plants or the chelation-based strategy developed by graminaceous plants[83][85].

5.1.1 Rhizosphere acidification:

Some species of plants diverse protons to the rhizosphere in order to make metals more soluble and more available for plants. These protons decrease the soil's pH which leads to the release of free metals (Fe, Zn and Ni) from the insoluble oxides and insoluble chelates with soil particles. The release of protons may be caused by activation of ATPase proton pump expressed in the root epidermis in case of low iron supply but it has not been yet confirmed[85]. The acidification of rhizosphere can be caused also by roots exudate of organic acid instead of protons release [85].

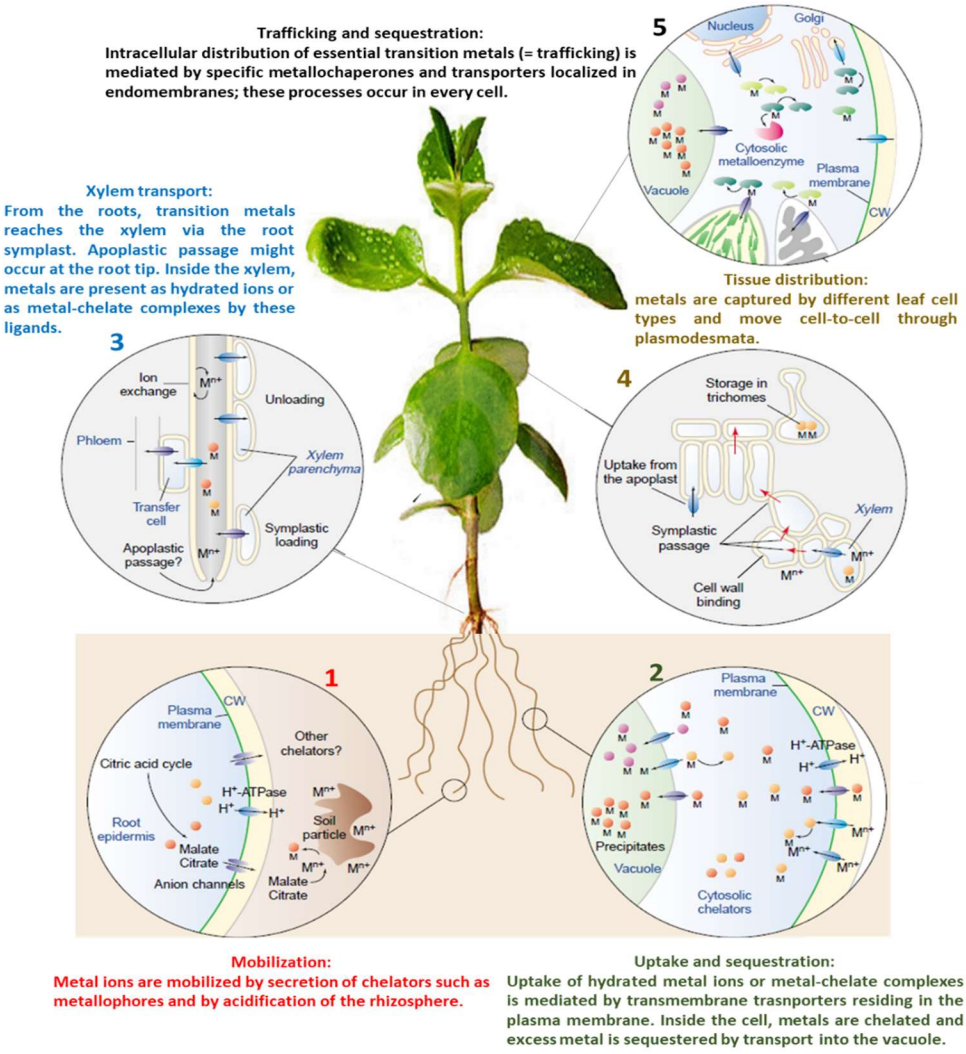

Figure 4. Molecular mechanisms proposed to be involved in metal uptake, transport and accumulation by plants. This figure is a combination of figures from Clemens et al.[83] *and Gupta et al.*[86] *Abbreviations and symbols: CW, cell wall; M, metal; filled circles, chelators; filled ovals, transporters; bean-shaped structures, metallochaperones.*

5.1.2 Reduction and chelation based strategies (strategies I and II):

Strategy I (reduction based strategy) is used for metal uptake by dicots and nongraminaceous monocots because the transporters present in the membrane helping with the transport of metals complexes have a specific affinity for a lower oxidation state of the metal. In order to take the metals such as iron and copper, the secretion of organic acids and phenolic compounds is a must to increase the concentration of metals in the soil which are transported via several transporters present in the plasma membrane inside root cells.

If we consider an example of iron, although it is present in soil in trivalent form, it is transported to cell in divalent form, after being released from insoluble compounds. In plants using this strategy I, Fe (III) is reduced by membrane-bound ferric chelate reductase (FRO2) to more soluble form – Fe (II) which is easily transported into the plant root cells via Fe (II) transporter – IRT1 (iron-regulated transporter. The whole process takes place in plasma membrane of root epidermal cells[39][85].

Strategy II (chelation based strategy) is used by grasses and cereals by the secretion of metallophores into the rhizosphere such as phytosiderophores (PS) for the chelation of Fe (III): in the root cells there is a specific transporter system for Fe-PS[39][85][87].

Both mechanisms of iron uptake are illustrated in **Figure 5** showing reduction of iron and its transport via IRT1 referring to strategy I as well as chelation of Fe(III) by PS to be transported through the plasma membrane (strategy II).

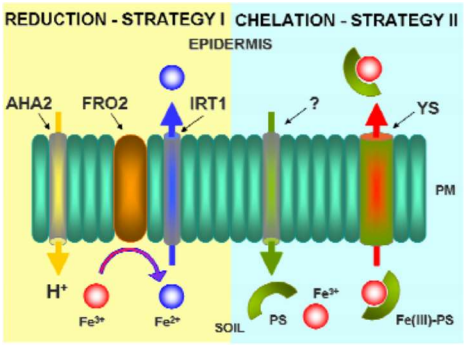

Figure 5. Reduction- and chelation-based strategies used by plants in order to mobilize and uptake metals from the soil. Modified after Guerinot and Yi, 1994. [88]

Some graminaceous plants, such as rice, have the ability to combine both strategies I and II.
In these plants there is a transport of Fe (III) – PS chelates as well as Fe (II). It is possible because rice has the orthologues of IRT1 – transporters of Fe (II) and also putative ferric chelate reductases that are responsible for reduction of Fe (III) to Fe (II) [39].

5.2 Uptake and sequestration

Once the metal is mobilized in soils, it has to be captured by root cells so first metal is bound by the cell wall where transport systems and intracellular high-affinity binding sites mediate and drive uptake across the plasma membrane: the uptake of metal ions is done through dedicated carrier proteins and it is induced by the membrane potential which is negative providing a strong driving force for the uptake of cations through these transporters. However, the sequestration capacity is enhanced by increasing the number of intracellular high-affinity binding sites or the rates of transport into organelles [83].

5.3 Xylem transport

Three processes govern the movement of metals from the root into the xylem: (i) sequestration of metals inside root cells, (ii) symplastic transport into the stele and (iii) release into the xylem. Inside the root, the presence of elevated amounts of a metal specific ligand results in an increase in the rate of its transport into the xylem; chelation with certain ligands can take metals primarily to the xylem but chelation with other ligands, such as phytochelatins or metallothioneins, might route them predominantly to root sequestration. In addition, inside the xylem, low-molecular weight chelators, free hydrated metal cations and metal chelates in the mobile transpiration stream are pH-dependent to maintain species as stable as possible. In conclusion, xylem-unloading processes are primordial in controlled distribution and detoxification of metals in the shoot, as well as delivering the species to phloem for re-distribution [83].

5.4 Unloading, trafficking and storage

Metals have to be scavenged by leaf cells once they reach the apoplast by the xylem sap, this trafficking inside every cell helps in maintaining the concentrations within the specific physiological ranges needed in each organelle and ensuring delivery of metals to metal-requiring proteins: these processes are assured by metallochaperones and pumps. All metals are sequestered in leaf cell vacuoles where they are stored, in a way that every leaf cell type shows pronounced differential accumulation that varies with plant species and element, for example in *T. caerulescens* Zn accumulates more in leaves than in epidermis cells and in

mesophyll cells, whereas in metal-treated *A. halleri*, Zn is more present in the mesophyll cells more than the epidermal cells [83].

5.5 Mechanism of detoxification

More than 30 metals are considered as potentially dangerous for environmental health and they are popularly called "heavy metals". The group of heavy elements includes, among others, antimony (Sb), arsenic (As), bismuth (Bi), cadmium (Cd), cerium (Ce), chromium (Cr), gallium (Ga), lead (Pb), manganese (Mn), mercury (Hg), platinum (Pt), silver (Ag), tellurium (Te), thallium (Tl), tin (Sn), uranium (U), and vanadium (V). Many of these metals are nonessential, however, can accumulate in elevated concentration in plants and this is due to human activity which contributes to the presence of these elements in water and soil and their transmission to plants: the metal amount in these plants depend on the plant species, environment in which plants are cultivated as well as the organ's age where it can be present.

Once the metal is absorbed by a plant it can induce toxicity symptoms such as growth reduction, changes in cell structure, changes in the native conformational structure of protein and thus in its impaired function, blocking the SH-group in enzyme structure and masking its active site leading to inactivation and at the end to disruption of many metabolic processes.

In addition, heavy metals are involved in production of reactive oxygen species inducing oxidative stress in plants as well as in genotoxicity resulting in modification of DNA base, inter- and intramolecular crosslinking of DNA and proteins, breaks in DNA strand, rearrangements and depuration.

Furthermore, some metals can disturb the uptake of the essential ones; for example excess of zinc may cause manganese and copper deficiency in plant shoots or copper and manganese toxicity that may induce iron and magnesium deficiency, respectively [34].

Many plant species have the ability to grow on soil contaminated with heavy metals without any toxicity symptoms. These plants possess extracellular and intracellular mechanisms that allow them to avoid accumulation of metal at toxic concentrations at sensitive sites within the cell. In extracellularly level they have mycorrhizas, for binding metals to the cell wall and for secretion of different compounds to the soil and on the plasma membrane level, they reduce the uptake of metals or, in case the metal have already entered the cytosol, they simulate the efflux pumping of metals.
In addition, there are also several detoxification mechanisms that consist of the chelation of metal ions in the cytosol by various ligands, such as phytochelatins, metallothioneins, metal-binding proteins as well as amino and organic acids to be transported to the vacuole where they are stored away from metabolic processes in non-toxic form [34].

6 Analytical techniques used for speciation analysis of LMW metal complexes in plants

6.1 Sampling

Sampling and sample preparation are one of the most important, time-consuming and labor-intensive parts of the analytical procedure and mistakes at this step may lead to important bias in the whole measurement process. The next step is the sample preservation and storage in order to prevent the physical, chemical and biological processes that may change the sample's composition. Between sample

collection and analysis a lot of processes may take place leading into changes in composition: these processes include volatilization, diffusion, precipitation, and biodegradation….etc

6.1.1 Liquid samples

The most popular liquid samples in plant analysis include fruit juices - analyzed mainly for their nutritional value - and xylem of hyperaccumulating and hypertolerant plants - investigated in frame of physiological and environmental studies.

Sampling of xylem is particularly challenging due to very low volumes available. The methodologies reported in the literature for xylem sap collection can be divided into (i) destructive ones (ending the plant's life) and (ii) non-destructive ones helping the plant to continue growing and living. They include : (1) root pressure exudation, (2) Scholander-Hammel pressure chamber, (3) root system pressurizing chamber according to Passioura (1980)[89], (4) hand- or battery-operated vacuum pump [90] and (5) the use of the xylem-feeding insect meadow spittlebug illustrated in **Figure 6**.(*Philaenus spumarius* L.) that are from cicadomorph family and they have the ability to feed on xylem sap due to their massively developed cibarial dilator muscles, with a large and heavily reinforced precibarium which help them to suck against the strong tensions created by xylem [91–93].

Figure 6. The meadow spittlebug, Philaenus spumarius. Photographs Showing the extensibility of the abdomen of a P. spumarius spittlebug (A, contracted; B, extended) [94]

As mentioned before, xylem sap can also be collected using a modification of the "pressure vessel technique" of Scholander et al. [95] .This was the technique that was used in this project. According to this method, gas pressure was applied to the root which cause xylem sap flow in the opposite direction. This device is composed principally of a vertical metal cylinder on a bank with its upper end open and its lower part tightly fixed on the bank. The cylinder is supplied with N_2. The cylinder can be tightly sealed with a special cup, in the middle of which the root is appropriately placed for the sampling purposes[91].

6.1.2 Solid samples

The plant material such as roots and leaves were cut into small pieces with scissors. Leaf samples were either used as freshly cut material, frozen in liquid nitrogen directly after cutting and lyophilized overnight, or fresh leaves put in paper bags and air-dried for 24 h at room temperature [96].

6.2 Sample preparation for analysis:

Preparation of samples should be optimized before analysis taking into account the sample concentration, its state of matter as well as the matrix complexity. Ideally, the speciation analysis should be carried out with a minimum of sample preparation which is possible for plant fluids, such as xylem, phloem or root exudates. Otherwise, during the sample preparation, the two major risks concern (i) dissociation of complexes and (ii) change of oxidation state of the metal ion of interest. Freeze-drying samples may lead to iron precipitation and destruction of complexes so lyophilisation should be avoided.

6.2.1 Liquid samples

Liquid samples were stored frozen down to -80 °C until analysis. A dilution is often used to reduce the matrix effect and limit physical interferences; however, a risk of dilution below the LOD of elements of interest present in a sample exists. Samples are usually diluted in mobile phases used for chromatographic separation; this dilution helps in the stabilization of pH if the buffer used as a mobile phase has a specific pH.

6.2.2 Solid samples

Solid samples, such as plant leaves are frozen in liquid N_2, then homogenized in a ball mill or in a mortar where the plant tissues and the cell walls are destroyed while the different chemical forms of metals stay unchanged. After homogenization, an extraction step is needed to get species of interest in the soluble form where the extractant used should be chosen carefully: in this case the use of the extractant which pH is adjusted to pH of the sample may not work in the case of leaves and root because pH vary between the different cell compartments. After extraction, centrifugation and filtration are applied. However, it should be kept in mind that solubilization of metals species from solid samples bears a risk of their degradation and transformation (ligand exchange). Ideally, various sample preparations should be tested to see if consistent speciation analysis results are obtained. It is better not to mix the sample with any compound that would affect the speciation. However, if there is such a need, some reagents altering species (example enzymes) can be used to transform species in a controlled way.

6.3 Direct analysis by x-ray spectroscopy

X-ray spectroscopy (XAS) provides information on the oxidation state and immediate coordination environment of metals present and it indicates the relative amount of major species in the sample. However, these techniques present limitation in the detection limit because the identification of a metal complex requires a concentration at the ppm levels but in the other hand, X-ray elemental mapping techniques can play a key role in answering questions at every level of metal (loid) homeostasis in plants, from the rhizosphere interface, to uptake pathways in the roots and shoots.

In a typical XAS spectrum two regions can be recognized, as reported in **Figure 7**. The region in the energy range of -50 to +200 eV with respect to the edge position provides information about geometry and oxidation state of the element and its analysis is defined as X-ray absorption near edge structure spectroscopy (XANES). A second region in the energy range of +200 to +1000 eV represent the extended X-ray absorption fine structure spectroscopy (EXAFS) with respect to the edge position provides information about metal site ligation and bond distances [97].

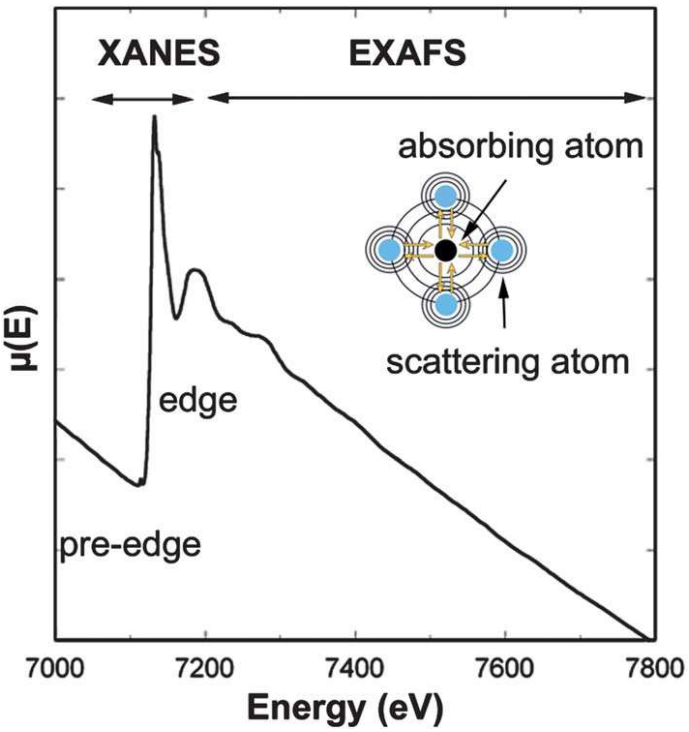

Figure 7. X-ray absorption spectroscopy. Schematic representation of a XAS spectrum showing the characteristic variation of the absorption coefficient μ(E) in function of the X-ray incident energy [97].

XAS technique does not allow the detection of unknown species. With improved detectors and optics and coherent X-ray sources, these techniques are likely to become increasingly useful for the study of trace metals in soil–plant systems.

6.4 Metals speciation by hyphenated techniques HPLC coupled to ICP-MS and ESI-MS:

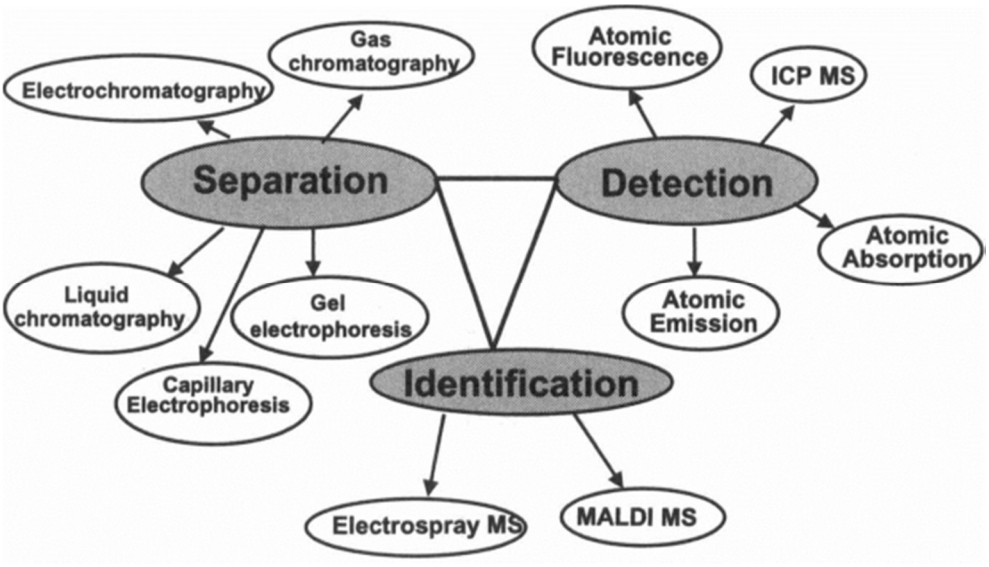

Figure 8. Hyphenated techniques for speciation analysis [98]

Hyphenated techniques based on coupling of chromatographic separation techniques with ICP-MS and ESI-MS detection (**Figure 8**) are now established as the standard analytical tool available for real-life speciation analysis [98][99]**.** Both detection techniques provide complementary information as detailed in **Table 4**: ESI MS is used for molecular and structural identification of species using ionization of the

molecule at low energy, in contrary to ICP MS which is an elemental technique allowing detection of the element and its isotopes in precision without any structure definition and with ionizing it at high energy. Moreover, on one hand ICP MS requires a step of sample digestion before analysis which destroys the covalent and non-covalent bonds, on the other hand ESI MS does not require this step which preserves the bonds maintaining the molecules. In addition, samples matrix present important effects on the ESI MS results but has less impact on ICP MS results because of the digestion step required. These two techniques are used in coupling with HPLC systems for species separation before identification and detection and together are efficient in both quantification and identification of species of interests based on isotopical signal in ICP MS and complementarity of information provided by ESI MS.

Table 4. ESI MS and ICP MS mass spectrometry [100]

ESI MS	ICP MS
Molecular and structural information	Elemental information
Possible isotopic information	Precise isotopic information
Ionization at low energy	Ionization at high energy
Covalent and non-covalent bonds preserved	Covalent and non-covalent bonds destroyed
Important matrix effects	Less important matrix effects
Quantification dependent of ionization	Quantification based on isotopical signal
Identification of new species	No identification of species
Possible coupling to HPLC	Possible coupling to HPLC

ICP-MS is usually coupled to size exclusion (SEC), ion exchange (IE), reverse phase chromatography (RP) and capillary electrophoresis (CE). The hyphenation requires an acceptance by the plasma of the sample transmitted from the separation system. The parameters to be taken into account include the eluent flow rate and its composition. The key to a successful HPLC and ICP-MS coupling is the interface so the column flow should be the matched with the optimum nebulizer flow in the aim to get an effective separation, so the typically selected nebulizer is the one that assures the presence of the highest proportion of fine droplets in the aerosol: for typical HPLC flows of 100 µL/min to 1 mL/min. In some chromatographic separations, organic solvents must be used which causes a problem when coming to plasma because the solvent will be burnt resulting in the deposition of carbon inside the instrument which limits its performance. Thus, several precaution should be taken in order to protect the instrument and make sure to get the best performance: the use of oxygen mixed in the argon stream of the atomizer is a must in order to dissolve this carbonic deposit by transforming it into carbon dioxide removed with the exhaust gas, as well as cooling the spray the chamber helps in reducing the amount of organic matter reaching the plasma [101][102].

The coupling of ESI-MS to liquid chromatography allows the separation of sample components and reduces matrix complexity which facilitates the analysis. The parameters to be adjusted include: capillary temperature, carrier gas temperature, shielding gas pressure and spray voltage.

At present, the methodologies used in metallometabolomics are based mainly on liquid chromatographic methods combined with mass spectrometric (MS) detection. LC-MS-based methodologies have been used for the analysis of both non-polar and polar compounds. For both target analysis and non-target profiling. Ultra-high performance liquid chromatography (UHPLC) presents a huge interest since it allows an increase in chromatographic resolution via capillary LC applications, enabling a reduction of sample

consumption especially when available sample volume is low. Results have shown further advantages such as the detection of higher numbers of ions and an increase in sensitivity compared to ordinary LC–MS analysis [103].

6.4.1 Chromatographic techniques

Different chromatographic techniques are used for purification and separation of the metal species present in plant liquids and extracts and their introduction to the detectors for qualitative and quantitative analysis. The selection of a suitable chromatographic technique depends on physical and chemical properties, such as volatility, polarity and charge of analytes of interests. **Figure 9** represent the application areas of liquid chromatography where there is an important role for HILIC in coupling to mass spectrometry (MS) with medium and high sensitivity as well as its application for relatively high polarity compounds. The application of gas chromatography for metal speciation in plants is limited because metal species present in plant samples are generally non-volatile and they usually cannot be converted in volatile species either. The techniques used for separation of metal complexes in plant samples are high performance liquid chromatography (HPLC) and capillary electrophoresis (CE).

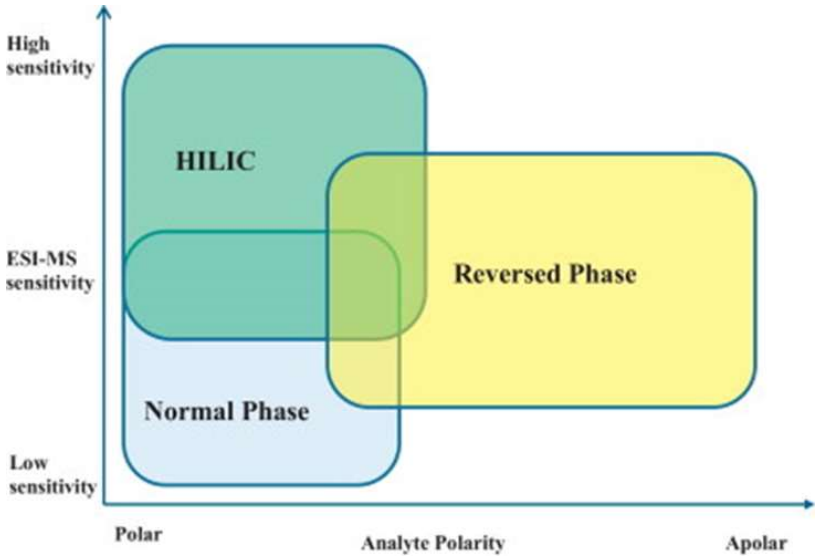

Figure 9.application areas of different liquid chromatography [104].

The choice of a proper mobile phase, its pH and ionic strength as well as elution gradient and time of analysis are critical not only to obtain a good separation but also to preserve the chemical forms of the compounds of interest in case they were unstable [99].

HPLC is a robust, reliable and reproducible separation technique that provides high resolution, especially when used in gradient mode. It can be applied for a large variety of samples including plant saps and extracts[105]. The separation process takes place on the column stationary phase - the substances interact with the filling grains. Over the years, the size, shape, porosity and grain composition were optimized in order to obtain the best efficiency of the columns. In order to protect the stationary phase from impurities present in the sample and damage related to the reaction of the substance introduced into the column bed, pre-columns are used which act as a filter. Furthermore, the proper mobile phase must also be chosen for the best separation of the components in the analyzed sample. This eluent is chosen according to its polarity relative to the sample and the stationary phase. This solvent used may also be changed during separation in order to change the polarity and therefore elute the various components separately. A list

of eluents is given below with their polarity index from the less polar to the most molar. The major HPLC separation mechanisms applied in environmental speciation vary requiring the use of different types of stationary and mobile phases; we can distinguish size-exclusion (SEC), hydrophilic interaction (HILIC), reversed phase (RP) and ion-exchange (IEC) chromatography. Many chromatographic parameters have to be optimized during the development of a chromatographic method, such as the type of stationary phase, the possible use and proportion of organic solvent, the nature and the concentration of salts, the pH of the mobile phase and its temperature. The flow-rate can be changed for increasing resolution or decreasing run time, with observing the pressure as the limiting factor; but these parameters have secondary impact on HPLC separations and can be less considered.

Size exclusion chromatography (SEC)

Unlike most other chromatographic techniques, the separation principle in size exclusion chromatography is not based on the chemical or electrostatic interaction of the sample mixture with the stationary phase. Differences in the size and shape of molecules present in the sample are the factor allowing the separation of compounds: smaller molecules are retained longer in the pores of the stationary phase, which is usually built of densely cross-linked polymers. The species of the largest size are washed out the fastest from the column, because they do not penetrate into the pores of the stationary phase; **Figure 10** shows an example of separation of compounds by SEC columns showing the elution of high molecular weight compounds at first followed by intermediate and finally low molecular weight compounds. The degree of crosslinking and pore size of the bed is selected according to the mass range in order to protect the column from destruction or obstruction. There are two types of packing used in SEC, polymeric gels or modified silica particles. In SEC columns the number of theoretical plates is relatively small and the separation efficiency is measured as the number of theoretical plates which can be improved by using stationary phase with a smaller particle size and adapting the chromatographic conditions to this choice such as low flow rates and long run time because smaller particle size leads to an increase in back pressure. Moreover, the success of SEC depends primarily on choosing conditions that give sufficient selectivity and counteract peak broadening effects during the separation; so, the selectivity of a SEC medium depends on its pore size distribution. **Figure 11** shows the selectivity curve of different SEC columns differing by the particle size of their stationary phase; it is clear that by increasing the particle size the partition coefficient increase which improve the column selectivity [106].

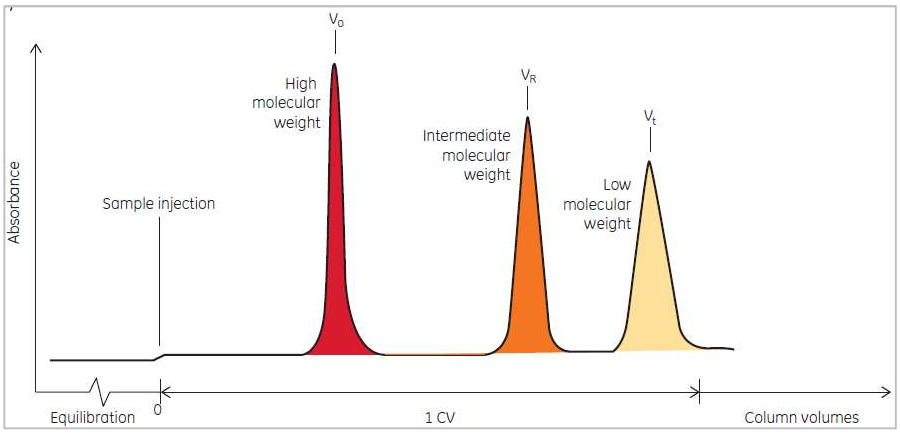

Figure 10. Separation mechanism by SEC columns.

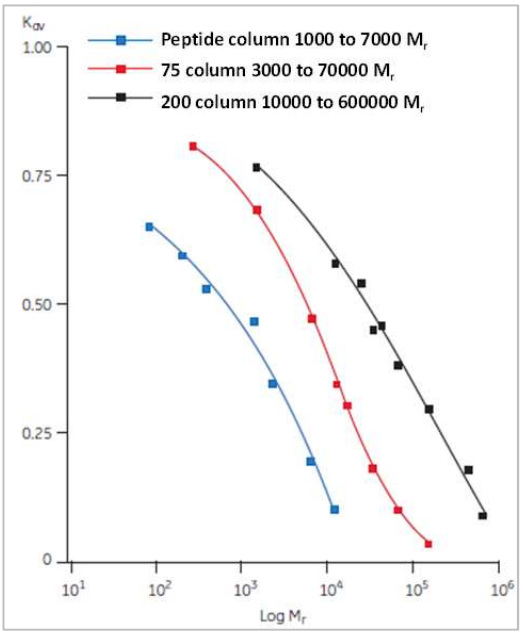

Figure 11. Selectivity curve of superdex SEC columns. [106]

Furthermore, in speciation studies SEC columns are used for sample purification by removing low molecular weight contaminants such as salts, for buffer exchange before and after different chromatography techniques as well as for fractionation to isolate one or more components, to separate monomers from aggregates. However, there is no clear information given about retention time of compounds of interest separated by these type of columns [107].

Reversed - phase chromatography

Reversed-phase chromatography RP-LC is the most commonly used type of liquid chromatography. It is based on the distribution of the solute between the two phases according to the binding properties of the medium, the hydrophobicity of the solute and the composition of the mobile phase: this technique uses gradient elution, so initially, experimental conditions are optimized to favor adsorption of the solute from the mobile phase to the stationary phase then, the mobile phase composition is modified to favor desorption of the solute from the stationary phase back into the mobile phase for elution [108]. However, in the case of strongly hydrophilic and high-polar compounds, it is often impossible to achieve their complete separation - analytes do not interact with the column bed and are non-selectively eluted.

Reversed-phase chromatography was used in limited application for metals speciation: the recent example is speciation of copper complexed to phenolic compounds such as phenylalanine, tyrosine…etc; the main novelty of the study was the application of µRPLC ESI-MS/MS to obtain the copper polyphenols complexes via enzymatic hydrolysis by hemicellulase and pectinase [109][110].

Hydrophilic interaction liquid chromatography (HILIC)

This separation mechanism was the main LC technique used in this work hence it is described in more details.

Contrary to the previously described RP, the stationary phase at HILIC is polar, made of modified silica or polymer and can contain neutral (e.g, amide groups, diol groups), positively charged (amines and triazoles), negatively charged (PSI - polysuccoimides, -OH groups of silica), positively and negatively charged, with a solid core and a porous shell (angular-shell) and monolithic [67][111][112]. HILIC is a combination of a hydrophilic stationary phase with a hydrophobic, mostly organic, mobile phase which the principle is based on the partitioning of analytes between a water-enriched liquid layer at the

stationary phase and the mobile phase. This layer of water is an integral part of the surface of the stationary phase, that's why the primary mechanism of retention in HILIC is a solute sharing between the mobile phase and the water layer.[113]

Optimization of the operation conditions in HILIC separation:

Stationary phase is the first parameter to take into consideration because it provides retention and selectivity differences. The choice of the appropriate stationary phase as HILIC is based on potential interactions between this phase and polar analytes.

Stationary phases are divided into different groups such as unbounded bare silica gels and bonded phases, and these ones are classified in neutral, charged, and zwitterionic phases according to functional groups present on the surface and their charged state.

Silica gels present silanol groups that at mobile phase pH above 4–5 are deprotonated and can work also as cation-exchangers, retaining positively charged basic analytes.

Polar chemically-bonded phases were developed for specific applications by derivatization of the support surface (silica or polymer) with polar functional groups and they are conveniently classified in neutral, charged and zwitterionic phases on the basis of the charged state of the groups:

- Neutral stationary phases contain polar functional groups that are in neutral form in the range of pH 3–8, which retain analytes according to hydrophilic interactions. Many HILIC stationary phases belong to this category such as the amide (TSK gel Amide-80), aspartamide (PolyHYDROXYETHYL A), diol (YMC-pack Diol), cross-linked diol (Luna HILIC), cyano (Alltima Cyano) and cyclodextrin (Nucleodex ß-OH) groups. These columns are used for the separation of oligosaccharides, peptides, proteins, and oligonucleotides.

- Amino phases contain an aminopropyl ligand with a primary amino group positively charged showing high affinity for anionic acid compounds that can be occasionally irreversibly adsorbed.

- Zwitterionic HILIC stationary phases are considered as the HILIC all-purpose phases. Some of the zwitterionic phases are commercialized under the trademarks ZIC-HILIC, ZIC-cHILIC, KS-polyMPC, Obelisc R and Obelisc N. Zwitterionic ligands comprise a permanent positive charged group and a permanent negative charged group. These phases can retain according to hydrophobicity but at the same time according to ion-exchange properties. These columns can be employed for the separation of neutral, acid and basic analytes, as well as for the separation of inorganic ions.

The mobile phase buffer is chosen to maintain original conditions such as (buffer pH, buffer salts, gradient...) also to minimize competition with the endogenous metal complexes in the sample in order to improve species detection and minimize degradations and artifacts [36].

The mobile phases used in HILIC contain from 5 to 40% water or buffer; the elution depends on the percentage of the aqueous buffer (usually volatile ammonium formate or ammonium acetate if used in combination with MS) in the organic solvent, such as acetonitrile. At the beginning of analysis, at high concentration of organic solvent the analytes are retained on the stationary phase, when a gradient is applied by increasing the concentration of aqueous buffer the elution of the compounds occurs: these two steps are presented in **Figure 12** showing the behavior of polar compounds in HILIC. As it was mentioned the retention in the HILIC mode depends on the selection of the organic solvent; the elution strength of the organic solvent depends on its polarity and ability to participate in proton-donor/proton-acceptor

interactions so we can classify the organic solvent as follows methanol > ethanol > 2-propanol > tetrahydrofuran > acetonitrile with acetonitrile the strongest used organic solvent in HILIC applications since the % of the organic solvent in the mobile phase is the principal factor controlling the result of separation. A list of eluents with their polarity index is given in **Table 5** below.

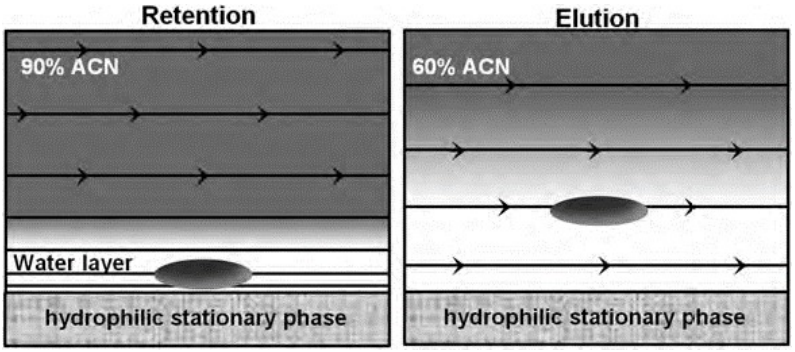

Figure 12.General behavior of a polar compound in HILIC: a) high retention with high Percentage of acetonitrile, b) elution when the eluting force of the mobile phase increases (60% ACN).[114]

The most commonly salts used in mobile phase are ammonium acetate and formate because they can be used with the detection conditions in molecular MS regarding their volatility. The increase in the concentration of the salts in the mobile phase has effect of decreasing the electrostatic interactions between charged analytes and stationary phase and can lead to antagonistic consequences on the retention of the compounds. If the electrostatic interactions between the solute and the stationary phase are repulsive: the interactions between the salts and the phase can reduce the phenomena of electrostatic repulsions between the solute and the stationary phase so the retention time increases. If the electrostatic interactions between the solute and the stationary phase are attractive: increasing the concentration of the salt will increase the volume of the water layer on the surface of the stationary phase salts and solutes will be in competition so the retention time decreases.

The pH of the mobile phase influences the state of charge of the analyte in the case of acid or basic compounds. The pH also modifies the charge of the stationary phase at level of the functional groups but also at the level of the residual silanols present on the surface of the grafting support [100][115]. Buffer at specific pH is also used to avoid degradation of the compounds which especially important in the analysis of LMW metal complexes.

Table 5. The polarity of the different eluents used in HPLC separation.

Eluents	Polarity index
cyclohexane	0.04
n-hexane	0.1
carbon tetrachloride	1.6
i-propyl ether	2.4
toluene	2.4
diethyl ether	2.8
tetrahydrofuran	4.0
ethanol	4.3
ethyl acetate	4.4
dioxane	4.8
methanol	5.1
acetonitrile	5.8
water	10.2

Addition of organic solvent (usually acetonitrile or methanol) to the eluent (so to the sample) can change metal speciation because of the lower solubility of some compounds potentially associated to metals. In particular, an addition of acetonitrile to aqueous samples leads to the precipitation of most proteins (>10 kDa). Therefore, the use of HILIC should be limited to studies of small (<10 kDa) metal complexes. Samples should be analyzed as soon as they are mixed with the solvent to limit potential loss of metal species[31]. The temperature primarily modifies the viscosity of the mobile phase, diffusion of the analytes and their enthalpy of transfer between the mobile phase and the stationary phase [100]. Otherwise analytical techniques such as mass spectrometry (MS)[62][70] usually involve ionization step based on high temperatures and voltages and this could be tough for relatively labile compounds such as LMW metal complexes and may lead to their destabilization .

6.4.2 Mass spectrometry:

The basic step in mass spectrometry is to convert the neutral molecule into a charged form - an ion. This takes place in the ionization source, where, depending on its type, the molecule may further fragment. A mass spectrometer consists of the following elements: a sample introduction system, an ion source, one or more mass analyzers, a detector and a data collection and processing system. In the analyzer, the ions are separated on the basis of the ratio of ion mass to its charge - m / z. Individual ions are counted by the detector. The measurement results are presented as a mass spectrum showing dependence of the analytical signal intensity on the m/z ratio. In mass spectrometry, four terms should be taken into account and worked on to get the best of it: mass resolving power, mass resolution, mass accuracy and mass precision because they characterize the performance of mass spectrometers. it is essential to define these parameters so mass resolving power ($m/\Delta m_{50\%}$) refers to the observed mass divided by the mass peak width at 50% height for a well-isolated single mass spectral peak and mass resolution (either $m_2 - m_1$ in Da or $(m_2 - m_1)/m_1$ in ppm) is the smallest difference between equal-magnitude peaks such that the valley between them is a specified fraction of either peak height [116][117].

Choosing the source of ionization is a fundamental issue before proceeding with the analysis. The conditions to be taken into consideration include polarity, sample type (solution, solid) and the possibility of combination with chromatographic / electrophoretic method: flow rate, type and polarity of the eluent.

The most common forms of ionisation modes coupled with LC in small-molecule research are electrospray ionisation (ESI); atmospheric pressure chemical ionisation (APCI); and atmospheric pressure photoionisation (APPI). As illustrated in **Figure 13** ESI is better suited to higher-molecular-weight and polar compounds [118]. The ionization sources used in studies of LMW metal complexes are inductively coupled plasma (ICP) for elemental detection and electrospray (ESI) for molecular one.

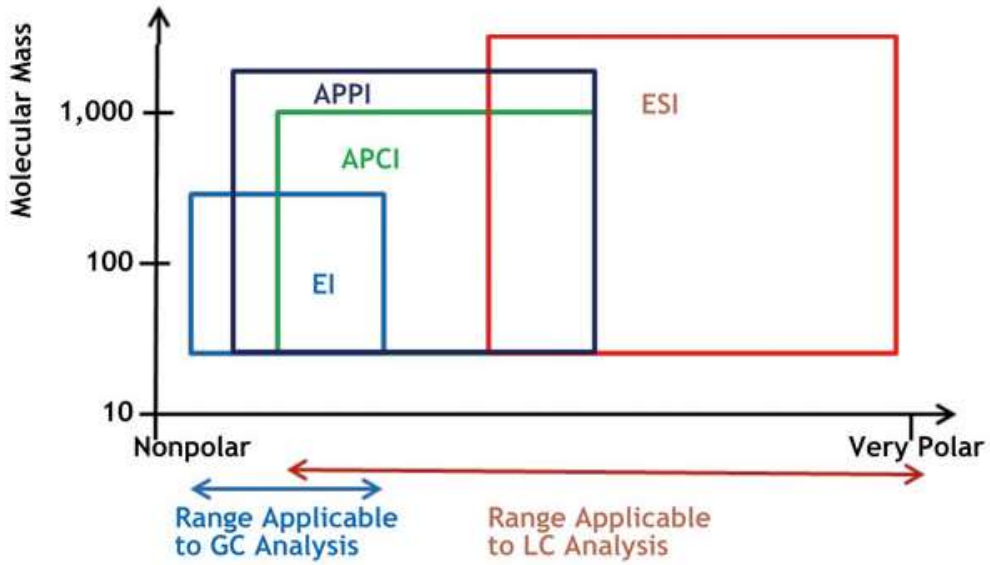

Figure 13.Common ionization methods in molecular MS and application areas.

Inductively coupled plasma ionization

ICP-MS is a reference techniques used for inorganic analysis because of its performance for both elemental and isotopic analysis [34][100]. ICP MS gives information about the total metal content of a sample but not about the oxidation state of the metal and its interaction with molecules present in the sample [63]. Argon plasma used in ICP MS has a very high ionization power which makes possible the analysis of a very large number of elements; 90% of the elements from the periodic table are totally ionized as monocharged positive ions by this technique.

In a standard configuration liquid samples are delivered to the nebulizer by a peristaltic pump where they are converted into aerosols in presence of a carrier argon gas; then fine droplets of aerosols are separated from the large ones in a spray chamber. Concerning solid samples, laser ablation coupled to ICP MS is used to determine elements directly with minimal sample preparation. The principle of ICP MS is presented in **Figure 14**.

The droplets are transported into the horizontal plasma torch: The plasma torch consists of three concentric tubes: outer tube, middle tube and sample injector. The outer tube and the middle tube are responsible for plasma cooling and adjusting its position while the sample injector is responsible for transport of the aerosol into the plasma. Argon flow is supplied to the internal tube at the stage of nebulization of the sample - it acts as a carrier gas and transports the sample inside the injector. Its flow is controlled by speed of sample introduction. Argon flowing through the central tube - the auxiliary gas - separates the sample stream leaving the injector from the plasma flame and prevents extinction of the plasma.

Plasma is formed by RF oscillation of the current applied to the load coil creates an electromagnetic field at the top of the torch and the high-voltage spark applied to argon gas causes a loss of electrons for some argon atom that are caught and accelerated in the magnetic field. Collisions of argon atoms with electrons leads to the formation of high temperature plasma discharge at around 10000 K.

The aerosols entering the plasma pass in different heating zones that cause vaporization of solvent and creation of small particles which are changed into charged atom then into ions due to the collision with energetic argon electrons. Once monocharged positive ions are formed in the plasma, they are moved to the mass spectrometer via the interface region consisted of two metallic cones called sampler and skimmer helping in the transition between the ICP ionization chamber at atmospheric pressure and the analyzers under high vacuum. Ion pass through the cones and the optics to reach the analyzer; the important parameters to be optimized include: the position of the plasma according to the interface region and the argon flow rates in order to obtain an aerosol transport and optimal plasma stability.

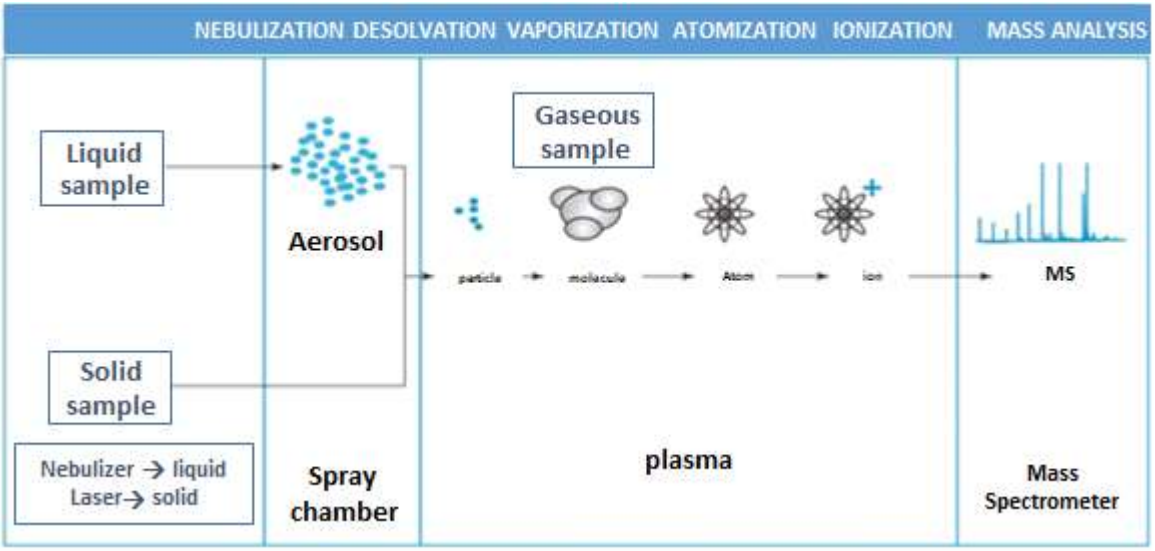

Figure 14. Principle of ICP MS [119]

The ICP-MS technique is characterized by high selectivity, however it suffers from some interference. Two main groups of interference can be distinguished:

- Matrix interferences - suppression or increase of the analyte signal, which leads to an incorrect determination result. They are related to differences in the physical properties of the matrix components.
- Spectral interferences - by applying peaks, they can mask the presence of a peak or, on the contrary, increase its height. They may originate from the ions of other elements (isobaric interferences) that are part of the matrix, formed as a result of the combination of atoms (polyathomic interferences) or multiple ionizations.

Table 6. presents the elements analyzed during this study with their detection limit by ICP MS, isotopes as well as polyatomic interferences that may affect the signal obtained for each metal, yellow boxes represent isobaric interferences among metals studied in this work.

Table 6. Isotopes, polyatomic interferences and detection limit of Fe, Mn, Cu, Ni and Zn [120].

element	number of isotopes	polyatomic interferences	detection limit in ppt
Mn	^{55}Mn	$^{40}Ar^{14}N^{1}H^{+}$, $^{39}K^{16}O^{+}$, $^{37}Cl^{18}O^{+}$, $^{40}Ar^{15}N^{+}$, $^{38}Ar^{17}O^{+}$, $^{36}Ar^{18}O^{1}H^{+}$, $^{38}Ar^{16}O^{1}H^{+}$, $^{37}Cl^{17}O^{1}H^{+}$, $^{23}Na^{32}S^{+}$, $^{36}Ar^{19}F^{+}$	1-10 ppt
Fe	^{54}Fe	$^{37}Cl^{16}O^{1}H^{+}$, $^{40}Ar^{14}N$, $^{38}Ar^{15}N^{1}H^{+}$, $^{36}Ar^{18}O^{+}$, $^{38}Ar^{16}O^{+}$, $^{36}Ar^{17}O^{1}H^{+}$, $^{36}S^{18}O^{+}$, $^{35}Cl^{18}O^{1}H^{+}$, $^{37}Cl^{17}O$	
	^{56}Fe	$^{40}Ar^{16}O^{+}$, $^{40}Ca^{16}O^{+}$, $^{40}Ar^{15}N^{1}H^{+}$, $^{38}Ar^{18}O^{+}$, $^{38}Ar^{17}O^{1}H^{+}$, $^{37}Cl^{18}O^{1}H^{+}$	
	^{57}Fe	$^{40}Ar^{16}O^{1}H+$, $^{40}Ca^{16}O^{1}H^{+}$, $^{40}Ar^{17}O^{+}$, $^{38}Ar^{18}O^{1}H^{+}$, $^{38}Ar^{19}F^{+}$	
	^{58}Fe	$^{40}Ar^{18}O^{+}$, $^{40}Ar^{17}O^{1}H^{+}$	
Ni	^{58}Ni	$^{23}Na^{35}Cl^{+}$, $^{40}Ar^{18}O^{+}$, $^{40}Ca^{18}O^{+}$, $^{40}Ca^{17}O^{1}H^{+}$, $^{42}Ca^{16}O^{+}$, $^{29}Si^{2+}$, $^{40}Ar^{17}O^{1}H^{+}$, $^{23}Na^{35}Cl^{+}$	
	^{60}Ni	$^{44}Ca^{16}O^{+}$, $^{23}Na^{37}Cl^{+}$, $^{43}Ca^{16}O^{1}H^{+}$	
	^{61}Ni	$^{44}Ca^{16}O^{1}H^{+}$, $^{45}Sc^{16}O^{+}$	
	^{62}Ni	$^{46}Ti^{16}O^{+}$, $^{23}Na^{39}K^{+}$, $^{46}Ca^{16}O^{+}$	
	^{64}Ni	$^{32}S^{16}O_2^{+}$, $^{32}S_2^{+}$	
Cu	^{63}Cu	$^{31}P^{16}O2^{+}$, $^{40}Ar^{23}Na^{+}$, $^{47}Ti^{16}O^{+}$, $^{23}Na^{40}Ca^{+}$, $^{46}Ca^{16}O^{1}H^{+}$, $^{36}Ar^{12}C^{14}N^{1}H^{+}$, $^{14}N^{12}C^{37}Cl^{+}$, $^{16}O^{12}C^{35}Cl^{+}$	
	^{65}Cu	$^{49}Ti^{16}O^{+}$, $^{32}S^{16}O_2\ ^{1}H^{+}$, $^{40}Ar^{25}Mg^{+}$, $^{40}Ca^{16}O^{1}H^{+}$, $^{36}Ar^{14}N_2\ ^{1}H^{+}$, $^{32}S^{33}S^{+}$, $^{32}S^{16}O^{17}O^{+}$, $^{33}S^{16}O_2^{+}$, $^{12}C^{16}O^{37}Cl^{+}$, $^{12}C^{18}O^{35}Cl^{+}$	
Zn	^{64}Zn	$^{32}S^{16}O_2^{+}$, $^{48}Ti^{16}O^{+}$, $^{31}P^{16}O_2\ ^{1}H^{+}$, $^{48}Ca^{16}O^{+}$, $^{32}S_2^{+}$, $^{31}P^{16}O^{17}O^{+}$, $^{34}S^{16}O_2^{+}$, $^{36}Ar^{14}N_2^{+}$	
	^{66}Zn	$^{50}Ti^{16}O^{+}$, $^{34}S^{16}O_2^{+}$, $^{33}S^{16}O_2\ ^{1}H^{+}$, $^{32}S^{16}O^{18}O^{+}$, $^{32}S^{17}O_2^{+}$, $^{33}S^{16}O^{17}O^{+}$, $^{32}S^{34}S^{+}$, $^{33}S_2^{+}$	
	^{67}Zn	$^{35}Cl^{16}O_2^{+}$, $^{33}S^{34}S^{+}$, $^{34}S^{16}O_2\ ^{1}H^{+}$, $^{32}S^{16}O^{18}O^{1}H^{+}$, $^{33}S^{34}S^{+}$, $^{34}S^{16}O^{17}O^{+}$, $^{33}S^{16}O^{18}O^{+}$, $^{32}S^{17}O^{18}O^{+}$, $^{33}S^{17}O_2^{+}$, $^{35}Cl^{16}O_2^{+}$	
	^{68}Zn	$^{36}S^{16}O_2^{+}$, $^{34}S^{16}O^{18}O^{+}$, $^{40}Ar^{14}N_2^{+}$, $^{35}Cl^{16}O^{17}O^{+}$, $^{34}S_2^{+}$, $^{36}Ar^{32}S^{+}$, $^{34}S^{17}O_2^{+}$, $^{33}S^{17}O^{18}O^{+}$, $^{32}S^{18}O_2^{+}$, $^{32}S^{36}S^{+}$	
	^{70}Zn	$^{35}Cl^{35}Cl^{+}$, $^{40}Ar^{14}N^{16}O^{+}$, $^{35}Cl^{17}O^{18}O^{+}$, $^{37}Cl^{16}O^{17}O^{+}$, $^{34}S^{18}O_2^{+}$, $^{36}S^{16}O^{18}O^{+}$, $^{36}S^{17}O_2^{+}$, $^{34}S^{36}S^{+}$, $^{36}Ar^{34}S^{+}$, $^{38}Ar^{32}S^{+}$	

Electrospray ionization (ESI MS)

The use of techniques that allow molecular specific detection and the identification of the structure of compounds at the trace level in complex matrixes is a must in the analytical field of speciation. Electrospray MS is the most popular of them used for studies of biological samples. Electrospray ionization preserves the integrity of species without fragmenting them; it can be used for both low- and high mass ions such as proteins.

ESI MS can give information about relatively stable metallo-species that metal forms with amino acids, peptides, proteins and carbohydrates: there is a possibility to work in positive or negative ion mode since ESI provides protonated apparent molecular ions $[M + zH]^{z+}$ with a charge of ≥ 1 (positive ion mode) and deprotonated ones $[M\text{-}zH]^{z-}$ (negative ion mode) that enables to find the ideal conditions to ionize different types of metal species[36][103].

The electrospray ionization consists of a number of stages**: ion formation, nebulization and desolvation, which provides transfer of ions from the liquid to the gas phase and their introduction into the MS vacuum.** These stages are discussed below illustrated in **Figure 15**. showing processes taking place from the ion formation until the mass analyzer**:**

i. The aqueous analytes are passing through the electrospray needle which causes the generation of the spray of small, highly charged droplets as a result of contact of the sample stream with a high-value electric field.
ii. From the droplets, the neutral solvent molecules are evaporated leading to decrease of the droplet size and at the end to formation of molecular ions. When the charge exceeds the Rayleigh limit the droplet explosively dissociates, leaving a stream of charged ions.
iii. The molecular ions are often multiple charged and in the next step they are transported from the atmospheric pressure to the high vacuum area where they explode generating the analyte ions.
iv. Then, in the mass analyzer, the ions are separated according to their mass-to-charge ratio.

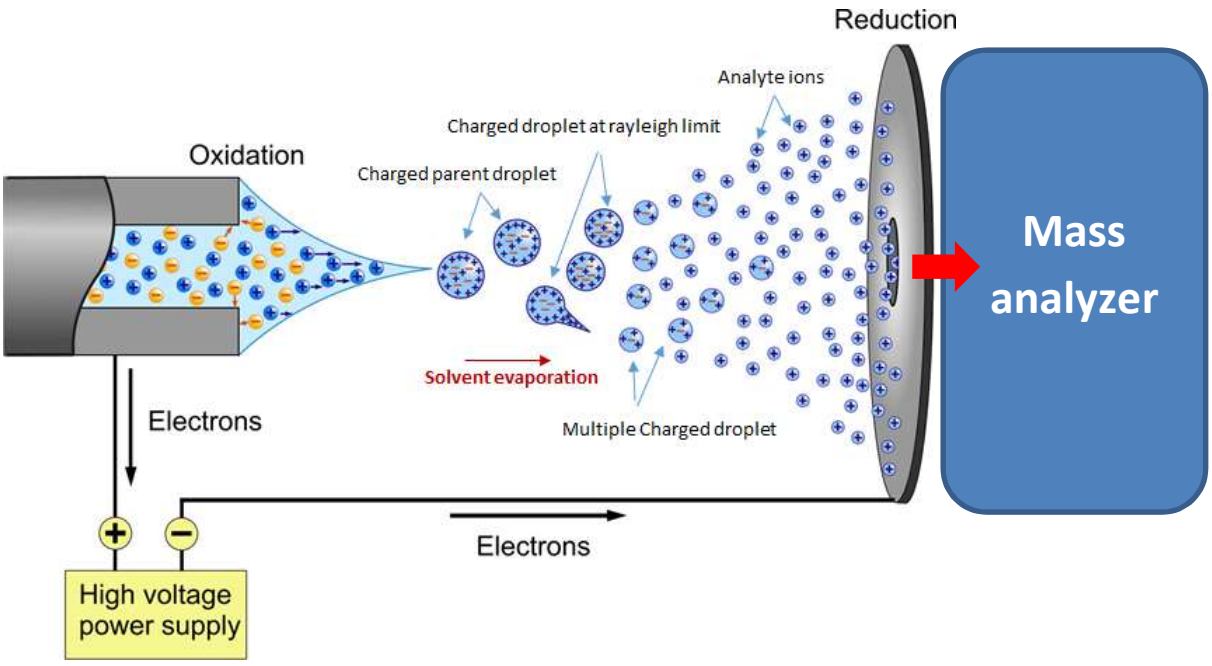

Figure 15. Principle of electrospray ionization.

The ESI-MS mass spectrometry can be used as an independent source of information or in combination with various separation techniques, such as liquid chromatography and capillary electrophoresis: volatile solvents should be used to avoid source contamination and the presence of salts should be limited as much as possible in the sample because they can crystallize inside the system.in ESI MS if the salts are non-volatile they may deposit on lens elements leading to ionization suppression and coating of the ion optics which may lead to a significant sensitivity reduction.

The parameters to be optimized [100][118][121] in order to obtain optimal detection conditions such as high sensitivity and signal stability are:

- position of the probe: to maximize the introduction of analytes into the analyzer
- drying gas flow and auxiliary: to optimize desolvation (vaporization temperature can be used to facilitate desolvation) and to better focus the spray
- capillary tension applied to Ionize the analytes: to maximize the generation of ions through the spray
- temperature of transfer through capillary: to complete desolvation and help transport of ions to the analyzer
- voltage applied to the different poles of ions optics: to focus the ions towards the analyzer

Mass analyzers

The role of a mass analyzer is to allow the analyte ions of a particular mass-to charge ratio reach the detector. The mass analyzer is also responsible for filtering out all the non-analyte, interfering and matrix ions. The choice of the analyzer is influenced by the size of the species. Mass range of the analyzer, the maximum value of the m/z ratio that can be measured by it, is important especially for large molecules. In addition to the range of masses, important parameters of the analyzers include: operating mode (continuous, pulsed), mass accuracy, analysis speed, ion permeation mode and resolution. There are different mass analyzers, including quadrupole, time-of-flight (TOF), ion trap, magnetic sector, cyclotron ion resonance and Orbitrap. A comparison between FT ICR MS and Orbitrap MS and TOF MS are grouped in **Figure 16.**

Quadrupole (Q) mass analyzer is widely used as detectors in ICP and molecular ESI mass spectrometers (85% of all ICP mass spectrometers used for trace element analysis) because it is cheap, light-weight, use low ion acceleration and has an absolute detection limits in subpicogram range [118]. Quadrupole mass analyzer consists of four cylindrical or hyperbolic rods made of metal (stainless steel or molybdenum) that have the same length and diameter: these rods are set in parallel to each other and arranged in the way that the direct current (DC) field and alternating current (AC) of radio frequency are placed on opposite pairs of rods. When a particular potential is applied to the rods, the analyte ion of interest oscillate down the middle of the four rods to the end, where it will emerge and be converted to an electrical pulse by the detector. The other ions of different mass to charge will be unstable, pass through the spaces between the rods, and be ejected from the quadrupole [122].

Different configurations of quadrupole analyzers are available such as the simple linear to triple quadrupoles. In triple quadrupole, the first and third quadrupoles are used for mass selection and second quadrupole works as collision cell. The collision cell is important for the elements that suffer from different spectral interferences (e.g. argon, solvent and/or sample based interferences). Thus, the ability of the quadrupole mass analyzer to separate different masses depends on the shape, diameter and length of the rods, applied RF/DC voltages, frequency of quadrupole power supply and operating vacuum [122].

Time-of-flight mass analyzer measures the flight time of an ion from source to detector in a vacuum; this time is dependent on m/z [118]. At the beginning, all ions have the same position at the same time and are accelerated by the electric field according to their masses and velocities. As ions have different masses their velocities are also different: So, the lightest ion that has the highest velocity is able to reach the detector first, followed by an ion of medium mass-to-charge ratio and, ultimately, the heaviest ion with the lowest velocity.
The main advantage of TOF mass analyzer is that it allows the simultaneous extraction of all mass-to-charge ions and collection of multielement data sets without any significant losses in quality. Also, it is faster than the sequential scanning mode of quadrupole mass analyzer and allows fast scanning (500 scans per second) over a mass range of 1000 Da with reasonable mass resolution.
In addition, this mass analyzer is suitable to detect transient signals produced by high speed chromatographic techniques and is ideal for high precision isotope ratio analysis.

Fourrier Transform mass spectrometry:
Ion Cyclotron Resonance (ICR) MS is a mass analyzer offering the highest resolution and the highest mass accuracy. Ions are moved to the ICR cell in the middle of superconducting magnet where they are trapped; this phenomenon causes that the ions motions are confined to circular orbits that have characteristic frequency which is called ion cyclotron frequency. The orbital frequency, dependent on m/z, is detected as an image current and is converted from time to frequency domains than to mass spectra with a Fourier transform. The measurement of ion cyclotron frequency provides the information about ion masses. The main disadvantages of ICR MS instruments are their high purchase and running costs[34][123].

Orbitrap confines ions in an electrostatic potential well created between carefully shaped coaxial central and outer electrodes .Ions are pulsed into the device so that they rotate around the central electrode and oscillate along it. The outer electrode is split into two halves to allow differential image-current detection. Unlike ICR, ion excitation is not necessary to induce large amplitude and coherent oscillations. Instead, ions are injected with the requisite coherent motion -by the use of C trap- to accumulate, store and thermalize the ions by a low pressure of nitrogen prior to injection [118], and detection occurs immediately after all ions have been injected into the trap and after voltage on the central electrode has stabilized [34][123]. The image current from the trapped ions is detected and converted to a mass spectrum using the Fourier transform of the frequency signal.

The FT ICR and orbitrap analyzers surpass other mass spectrometers with respect to the maximum mass resolution and accuracy obtained even for small numbers of ions: It is important to define that the mass accuracy is the ratio of the m/z measurement error to the true m/z, usually presented in parts per million (ppm) and it acts as a powerful “filter” helping in the identity confirmation or identification of a new compound.
ICR MS and Orbitrap MS share certain features, such as an image current detection system and the application of Fourier transform mathematical operations for generating mass spectra from time domain transients produced by the image current. Consequently, they are often referred to as Fourier transform-based mass spectrometers (FTMS) [124].
FT MS allows very high resolving power, mass accuracy, and dynamic range to be achieved because of fidelity in frequency determination. Since FT MS is based on a magnetic field, mass resolving power will increase linearly with increasing magnetic field which increases the mass accuracy and it influences the data acquisition speed which can lead to gain in time [124].

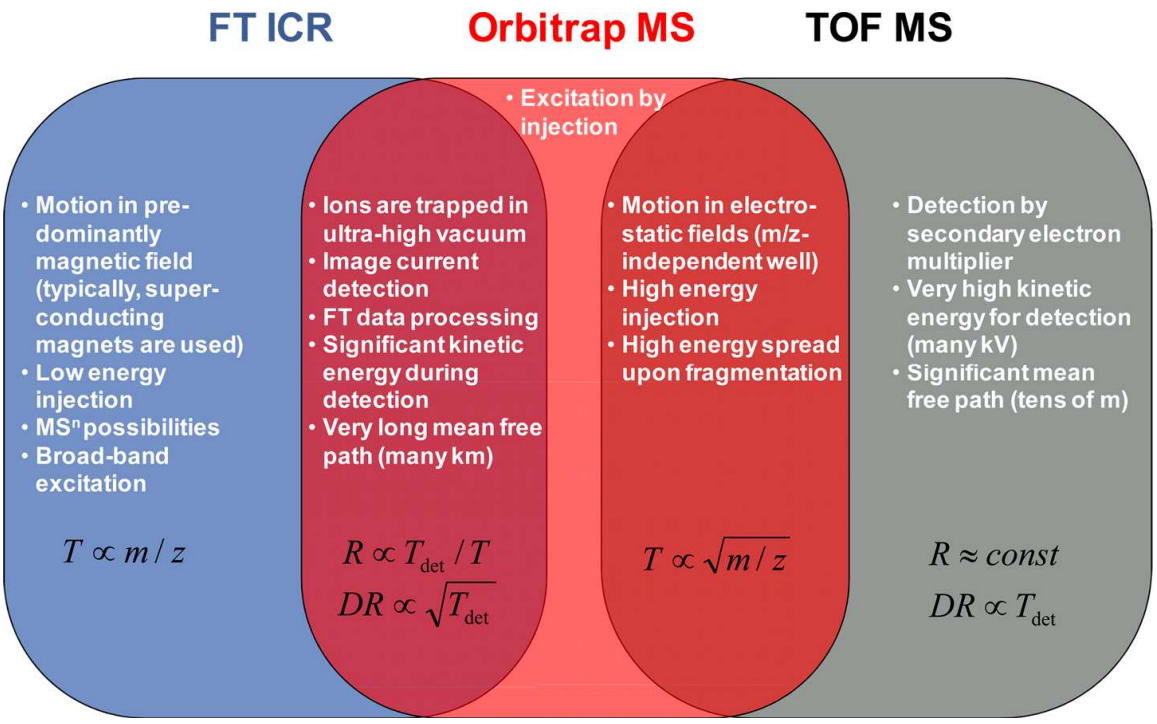

Figure 16. Comparison of physical and analytical features for high-resolution, full mass range techniques in mass spectrometry (T is period of oscillation, R is resolving power, DR is in-spectrum dynamic range, T_{det} is duration of detection per one spectrum) [125].

Tandem mass spectrometry:

In tandem mass spectrometers two mass analyzers are combined in one instrument linked with a collision cell, the first mass analyzer is used to select ions for further fragmentation and subsequent analysis of the product ions in a second mass analyzer; it permits to elucidate the molecule structure and confirm of its identity. Different analyzers can be combined to create "hybrid" instruments, e.g., QToF. Tandem mass spectrometers can work in several measurement modes presented in **Figure 17** [126]: these measurement modes differs by the way how the parent ions from which the analyte ion was selected. Thus, there is the precursor ion scan, product ion scan, neutral loss scan and the SRM - Single Reaction Monitoring.

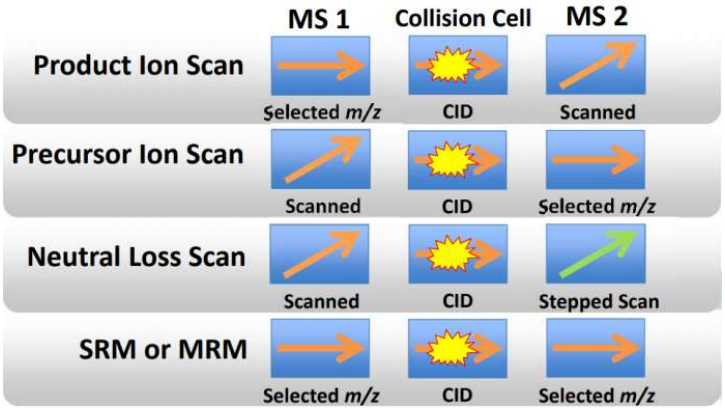

Figure 17. Different measurement modes in tandem mass spectrometry [126]

CID is the most propular fragmentation technique in MS/MS: it allows the fragmentation of gaseous ions by passing an ion beam through a collision cell where the collision gas (He, N_2, Ar) is set to a pressure considerably above of the pressure of surrounding high vacuum. A CID cell can be, for example, an RF only quadrupole, hexapole, octopole or a travelling wave ion guide. In tandem mass spectrometer configurations, such as in Q-TOF and LTQ-orbitrap, special modes utilizing full-scan and fragment

information can be used: In the LTQ-orbitrap, a C-trap can be used as a collision cell by raising the RF voltage. The nitrogen present in the C-trap works as the collision gas. After several oscillations, precursor ions have undergone dissociating fragmentation and all ions have accumulated in the middle of the C-trap. This kind of collision cell is termed higher-energy C-trap dissociation (HCD) [34][118]. So Typical MS/MS modes for the orbitrap are CID and electron transfer dissociation. Orthogonal TOF mass spectrometers typically employ quadrupole mass filters (Qq) before the TOF for CID [123].

MS^n is used for different purposes such as the elucidation of structure, determination of fragmentation mechanisms, determination of elementary compositions, applications to high-selectivity and high-sensitivity analysis, observation of ion–molecule reactions and thermochemical data determination (kinetic method); this technique allows more structural information to be obtained on a particular ionic species and may help as an identity proof of the species [116]. In this case tandem mass spectrometry involves the activation of a precursor ion formed in the source and the mass analysis of its fragmentation products in order to understand more the environment in which the element of interest (e.g. metal) is involved [127]: Rellan alvarez et al. [35] proposed that Fe_3Cit_3 complex is a mixture of $[Fe(III)_3Cit_3H]^{2-}$ and $[Fe(III)_3OCit_3H_3]^{2-}$ ion and to prove this hypothesis ESI-TOF MS was used to identify the composition of this complex by searching isotopic patterns of Fe_3; Spectrums obtained showed a difference of 9 m/z from $[Fe(III)_3Cit_3H]^{2-}$ to $[Fe(III)_3OCit_3H_3]^{2-}$ assigned to correspond to a labile ligand such as aquo OH_2, hydroxo OH^- or oxo O^{2-}.

Ion mobility mass spectrometry/ion mobility QTOF MS

The ion mobility spectrometry (IMS) technique is based on ions drift going through a buffer gas, under the influence of an electric field. The measured drift times are exclusively dependent of experimental parameters such as drift tube length, buffer gas pressure, temperature, electric field strength, the drift gas species and mass and shape of the analyte ion. IMS is often presented as an additional dimension of separation to MS since it gives information about the compound's chemical structure and three-dimensional conformation which help in differentiating isomers[128]. So, this is what makes the combination of LC–IM–MS an extremely attractive technique that increases separation power and improves compound identity confirmation for metabolomics by allowing the separation in 3-dimensions: LC (polarity), IMS (structure and size) and MS (mass to charge ratio) [129][130][131]. Drift times can be directly converted into a collision cross section (CCS) which represents a physicochemical property of an ion [129] and it depends on the mass and charge, as well as on the shape of the analyzed complex. Thus, larger ions are the slowest because they collide more frequently with the neutral gas which increases their drift time relative to more compact ions; this offers a way to distinguish between conformational states of the same complex [132].

Furthermore, ion mobility can be coupled to (time-of-flight) mass spectrometry [IM (TOF) MS] where both mobility and mass of ions are recorded exhibiting a mass-mobility correlation for classes of ions so, ions having high mass-mobility correlation are more 'dense' since they are more tightly folded so they are slower and, conversely, ions having lower mass-mobility are faster since they are less compacted [133].

7 QUANTIFICATION APPROACHES

In many studies, qualitative information is not enough and quantification become a must in order to better understand the role of species in a sample. The lack of homogeneous standard protocols and suitable reference materials for the analytical procedures often constitutes an obstacle for comparing results among laboratories and for reproducing experiments [134].

Quantification of LMW metal complexes can't be done by molecular MS due to strong matrix effects so the use of ICP MS was ideal for quantitative analysis and the principle relies on the use of stable isotopes as tags, applying isotope dilution analysis (IDA) approaches which can be species specific IDA or species unspecific IDA. The validity of the measurement is critically dependent on the quantitative recovery of the analyte from the column. In many cases, isotope dilution MS is recommended as a solution for quantification approaches without the need of commercial standards.

7.1 Isotope dilution MS

Isotope dilution analysis is a well-established analytical technique based on the measurement of the isotopic ratio of an element in a sample which isotopic composition has been modified by the addition of a known quantity of a spike isotope, normally in solution form, which is enriched in the isotope with minor natural abundance. Isotopes whose ratios are measured using the IDMS technique should be characterized by adequate purity determined along with uncertainty, long half-life time and durability during the analytical procedure. In addition, isotopes selected for quantification should be free from spectral interference [100][135]. It is clear that the abundance of the two isotopes (the element of interest and the added spike) and the isotopic ratio in the mixture will be intermediate between those in the sample and the added spike (**Figure 18**) and it will depend both on the amount of spike added and on the initial amount of the element in the sample.

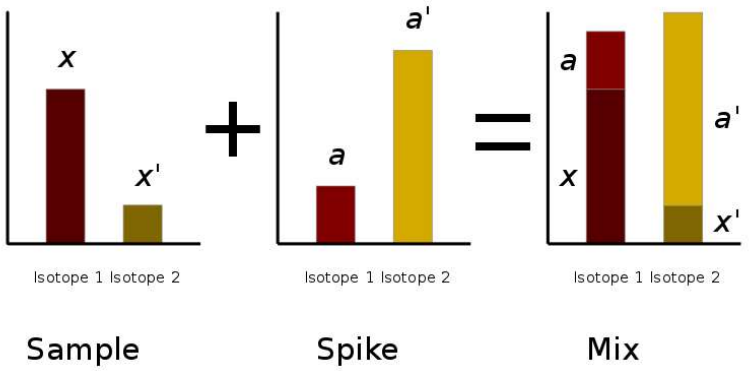

Figure 18.principle of ID MS

This technique has several advantages such as no influence of the matrix on the final value of the element concentration and if there are losses in the isotopic diluted sample there will be no influence on the final result once complete isotope equilibration between the sample and the spike has been achieved [136][137].

7.1.1 *ID MS technique in speciation analysis*

Two types of the isotope dilution method can be distinguished according to the time of addition and the chemical form of the added isotopic standard: specific and non-specific to a given metal speciation. [138]

Non-specific isotope dilution method

In the non-specific method, an isotope is added after the chromatographic step of separating the components of the sample - post column spiking. In this case, the spike may be in a different speciation form since the only conditions to be optimized are the absence of analyte loss before spiking and the complete mixing of the analyte with the added spike before the ionization ensuring the measurement of the isotopic ratio. This type is used when the type and structure of the species in which the metal is present

is not known, and when there are no commercially available or when it is difficult to synthetize the isotopically labelled compounds.

The method does not offer all the advantages of ID MS because adding the standard after the chromatographic separation stage causes that the analyte losses generated in this stage are not corrected. However, the ability to quantify species with unknown structures without the need to perform a calibration curves using standards makes this method a versatile tool for determining proteins and speciation of metals in complex biological samples. In addition, the method can only be used if the ionization efficiency is independent of the chemical form of the element. The only source of ionization that provides these conditions is ICP-MS [139].

Specific isotope dilution method

In the 'Species-Specific Isotope Dilution Analysis' method (SS-IDA), the spike is added to the sample before the chromatographic separation of its components. The composition and structure of the species of interest must be exactly known in order to either synthetize the corresponding enriched species or acquire the proper spike solution if it is commercially available. It is assumed that there should be a balance between the isotopic spike mixed with the analyte and it is important to make sure that there is no isotope exchange between the different species. The possible losses occurring during the passage through the column bed are the same, therefore knowing the amount of the added spike and measuring its content after the chromatographic step, the quantitative result of the analyte can be corrected. In this way, the result includes the matrix effects and incomplete recovery of the analyte, which significantly improves the accuracy of the determination and makes them independent of the conditions for the determination [140].

The method requires the availability of an isotopic spike of the analyzed substance. Large biomolecules with a complicated structure are particularly problematic. Before synthesizing an isotopically labeled particle, its structure should be accurately characterized and accurately reproduced in the synthesis process together with the spatial and near-spatial structure, so that it does not differ from the analyte. The smallest differences may lead to different behavior of the pattern during the subsequent stages of the analytical procedure, which is contrary to the basic conditions for using the ID.

8 Metallometabolomic studies in plants: state-of-the-art and perspectives.

8.1 Metallometabolomics: definition

The word “metabolism” comes from a Greek word that means “change”. The different metabolites (molecules < 1 kDa) are either endogenous when they are under the host genome control and cellular function-dependent or exogenous when they are being introduced via environmental exposure or via diet and medication. Metabolites are the intermediate products of metabolic reactions naturally occurring within cells. It refers to small molecules participating in important metabolic functions and fulfilling critical roles such as signaling molecules or secondary metabolites. There are two categories of metabolites: primary metabolites synthesized by the cell because they are indispensable for their growth and secondary metabolites produced by an organism but they are not required for primary metabolic processes, and may have important ecologic and other functions.

Metabolomics, understood as a comprehensive study of the entirety of metabolites, has been developed following advances in hardware for the separation and detection of analytes, to the software used for data storage and analysis in the field of the biochemical analysis of biological complex materials: this developed

combination of techniques gives us comprehensive information about metabolites present in cells, tissues, biological fluids or entire organism [141].

The challenge of metabolomics studies lies on the chemical complexity of the different classes of small molecules defined as metabolites either endogenous or exogenous. The metabolites range between 50 Da and 1500 Da of mass, from low picomolar concentration to molar and they range also from the most polar compounds to the most non-polar ones which may lead to different biological functions. It is this diversity which made the detection of the whole set of metabolites present in a biological sample challenging and an ambitious goal [103].

Metallometabolomics is an emerging field from metabolomics helping to the comprehensive analysis of metallometabolites (metal containing metabolites) in a sample requiring high throughput and targeted analysis of the transformation, speciation, localization and structural characteristics of metallometabolites. Metallometabolite is a metal complexed with endogenous organic non-proteinous ligand formed due to exposure of organism to stress because of high metal concentration. In plant related studies, it gives information about the mechanism of uptake of metals, how the homeostasis is maintained in cells and about metal detoxification process.

Regulation of the assimilation of metals by organism is necessary to assure a suitable function or organs and tissues. Therefore, in this case the chemistry of a cell needs to be characterized by the distribution of the metals and metalloids among the different species and cell compartments, this is what we call 'metallome' given by Williams [142] who referred to it as an element distribution, equilibrium concentrations of free metal ions or as a free element content in a cellular compartment, cell or organism: it refers to all metals species present in organism compartments complexed to biomolecules such as organic acids or especially with proteins referring to metalloproteome. However, this work is focused on low molecular weight complexes of metals with ligands present in plants saps and not on metals bound to proteins since these LMW might have an important environmental and phytoremediating role. This definition of metallome should be seen in the context of speciation of an element, defined by IUPAC as the distribution of an element under defined chemical species in a system: Speciation analysis refers to the analytical activities of identification and quantification of one or more individual chemical species in a sample: this study is known as metallomics, per similarity to genomics and proteomics. Species of interest for metallomics will include complexes of trace elements and their compounds (e.g. metal probes) with organic acids, proteins, sugars or DNA fragments [105][143–145].

Similarly to classical metabolomics, metallometabolomic studies can be achieved with two strategies:

(a) Untargeted approaches: measurement of the widest possible range of the small molecules present in the sample analyzed from sample extraction to data evaluation. These approaches can help uncover new metabolites and new hypotheses,

(b) Targeted approaches: detection and measurement of a specific set of metabolites. These approaches support well-defined hypotheses.

However, in recent years, these two strategies have been applied simultaneously or in sequence because the results are complementary.

8.2 Metallometabolomics: tools

For metabolomics analytical techniques were used either separately or in various combinations for compound or element separation and detection. Combination of analytical techniques is necessary because single methodology is not sufficient for the analysis of the global metabolic profile and has its own limitations [134][146].

At present, the methodologies used in metallometabolomics are based mainly on liquid chromatography (LC) combined with mass spectrometric (MS) detection. The selection of the suitable methodology depends on:

- The physicochemical characteristics of the analytes
- The target of the analysis (target versus non-target profiling)
- The type of the matrix
- The amount of sample available
- The expected concentration of the analytes.

A well-planned analytical protocol with a careful quality control includes a proper design of experiment, optimization of sample preparation and final analysis, data storage and manipulation, and data processing and validation. Ultra-high performance liquid chromatography (UHPLC) presents a huge interest since it allowed the use of high pressure level instruments which leads to an increase in chromatographic resolution via capillary LC applications, enabling a reduction of sample utilization especially when available sample volume is relatively low. Results have shown further advantages such as the detection of higher numbers of ions and an increase in sensitivity compared to ordinary LC–MS analysis [103].

Inductively coupled plasma mass spectrometry (ICP-MS) detection coupled to separation techniques (LC) has proved a valuable tool for the qualitative and quantitative detection of metallometabolites. This technique is element specific and, in principle, it doesn't provide information about the molecular structure of the analyte. However, with the development of "soft" electrospray ionization (ESI) technique, mass spectrometry was able to provide information about the molecular structure of metabolites; so the combination of ICP-MS with ESI-MS can be deployed to one single HPLC system for simultaneous quantification and structural identification of the formed complexes[147][148].

The high polarity and low hydrophobicity of metallometabolites make aqueous normal phase chromatography, also called hydrophilic interaction chromatography (HILIC), an ideal sample introduction technique for metallometabolomics by electrospray MS: this technique uses water as the strong eluent solvent and allows the retention of polar analytes by using a polar stationary phase and a mixture of water and a less polar solvent (mostly acetonitrile, acetone or methanol).the composition of the mobile phase in HILIC makes it ideal for coupling with ESI MS and acceptable for ICP under certain conditions [146][143–145].

In addition, in recent experiments molecular MS (ESI-MS) was used in combination with species fragmentation by high-energy collisional dissociation (HCD) to obtain element specific information after fragmentation of metal complexes.

There are several steps to pass by before analyzing the samples in order to preserve to the maximum the analytes especially when there is a mixture of polar and non-polar compounds in the sample. The first step needed to preserve the integrity of metabolites is suitable sample collection: the control of the temperature before, during, and after sample collection and storage (freezing, freeze drying, thawing) and control of the materials used for storage such as tubes in order to avoid contamination.

Sample preparation is the second step and it is a process that widely changes depending on the metabolites and the matrix constituting the sample to be analyzed: Optimal sample preparation for non-targeted analysis requires special care in order to minimize possible sources of contamination and systematic errors. Extraction of species of interest is required in order to simplify as much as possible the matrix where the analytes reside [103][144].

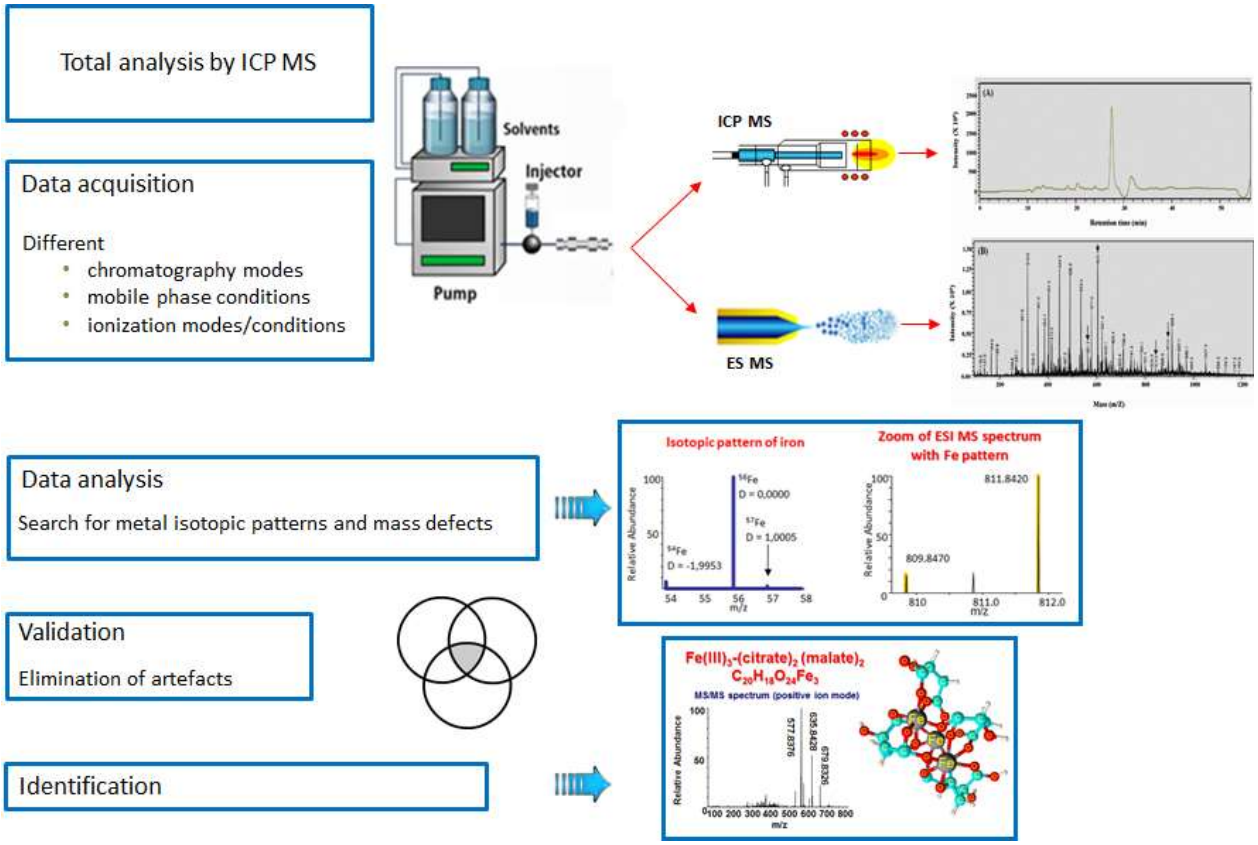

Figure 19.detailed steps to study metabolomics of metal complexes. Example given for iron.

The state-of-the-art analytical approach to metallometabolomics illustrated in **Figure 19** involves (after sample preparation):

1- Determination of the total concentration of the metal present in species of interest by ICP MS.
2- ICP MS and ESI MS detection coupled to HPLC for elemental and molecular identification; it is important to follow continuously the species recovery and their stability on the column. HILIC ICP MS and HILIC ESI MS was used for the separation of the compounds according to their hydrophobicity since the species of interest in samples analyzed are polar.
3- Data analysis of a HPLC-FTMS chromatogram in order to identify the species known to be present by searching for the metal isotopic patterns (as it is shown in **Figure 19** for iron as an example) and mass defect.
4- Data validation by removing artefacts and identity proof by fragmentation step by MS^n for each of the compounds detected [144].

8.3 Metallometabolomics: application fields

Metallometabolomics in all its branches is a transdisciplinary research area which has an impact on different fields such as geochemistry, clinical biology and pharmacology, plant and animal physiology and nutrition. Its ultimate goal is to provide a global and systematic understanding of the metal uptake, trafficking, role and excretion in biological systems.

Plant biochemistry and physiology: [141][144][149]

Metallometabolomics approaches are used for the identification and quantification of low molecular metal-containing metabolites present in plants in order to understand their mobilization from soil, translocation in plant and sequestration in its compartments since the chemical composition of plant tissues varies according to internal (genetic) factors as well as external (environmental) factors. All of these information help in the studies of:

(i) Uptake and bioavailability of essential elements, mainly Fe and Zn. The related research aims at the follow up of these elements pathways to get into grains and/or other edible plant tissues: once these plant tissues are eaten, it provides a rich nutritional intake in order to limit the micronutrient malnutrition that affects more than half of the world population.

(ii) Metal hyperaccumulation in specific plants that can accumulate metal ions at high levels without being intoxicated which helps in phytoremediation and detoxification of soil. The use of fungi and bacteria could also be possible to remediate contaminated sites.

(iii) Plant defense mechanisms against heavy metal stress provide information about the implied genes and enzymes. Metabolomics phenotype studies of different genotype plants of the same species helps to compare and identify their different genotypes. In literature data was found for major food crops such as rice ([150]) , wheat ([151]) , tomato ([152]) , melon ([153]), Brassica ([154]) , coffee ([155]) , and potato ([156]).

Nutrition and essential element supplementation:

Element speciation in the aim to characterize the chemical forms and develop objective biomarkers of dietary intake as well as to measure the quantity of metal implied in the species of interest is an important approach giving information that can help in many fields related to nutrition such as prevention of diseases and malnutrition by increasing interest in the supplementation of food and feed with mineral elements: perturbations in the gut microbiota for example leads to the production of co-metabolites which can influence metabolic phenotype and possibly induce different disorders such as intestinal disease, obesity or cancer [103][157][158].

The metallomics studies focus also on the validation that some elements are present in some products in quantities and forms that are suitable with the one required by the regulations of governmental agencies issuing sales authorizations: this gives also precious tracer of the origin of the product and its control allows a better optimization of the biotechnological production process [144].

The **Tables 7 a-b-c-d-e** below represent studies achieved by different scientific researchers on the speciation of different metals such as iron on which the methodology used in this thesis was developed, followed by table representing articles about zinc speciation as well as copper nickel and manganese.

Tables 7. Sample preparation, Methodology used for metal speciation and complexes identified in different plants species. (a) Fe speciation, (b) Zn speciation, (c) Ni speciation, (d) Cu speciation and (e) Mn speciation

(a)

Plant	Aim of the study	Sample preparation	Methods	Fe complexes	Ref
Grain samples of 6 wheat cultivars: high [Fe] in 3 cultivars (Rialto, San Pastore, Tiger) low [Fe] in the other 3 cultivars (Crousty, Rialto, Riband)	1. Establishment relation between [Fe] and [Zn] in whole grain and white flour of wheat. 2. Determination of Fe and Zn speciation in the soluble extracts of wheat flour and their difference between a high-Fe (Rialto) and a low Fe (Riband) cultivar	Grain samples stored at 4 °C prior to analysis. Sample dried, milled and divided on milling fraction. **Total Mineral Analysis**: 500 mg portion (oven-dried at 80 °C for 4 h) of sample digested in ultrapure HNO3 and HClO4 (87:13% v/v) in triplicate using digestion blocks (200 °C, 12 h)	SEC-OES SEC-ICP-MS	Fe-DMA Fe-NA soluble Fe-phytate	[41]
Beans (*Phaseolus vulgaris*) with different genotypes	Determination of the proportion of ferritin and nonferritin iron in low and high iron bean genotypes and ascertain the potential of increasing ferritin iron by plant breeding	Beans ground under liquid nitrogen with a rotor mill using a titanium sieve (0.25 mm mesh). The ground samples were kept at 4 °C in airtight and lightproof vessels and were used for quantification of iron, zinc, phytate, polyphenols, and ferritin bound iron.	Ferritin specific IDMS [Phytic acid] measured by modification of Makower Method Statistical analysis of correlation of total Fe and phytate, ferritin iron, and polyphenol contents	ferritin iron 13 to 35% 10-25 ug/g, Fe-phytate (correlation between amount of non-ferritin iron and phytatic acid content)	[159]
2 wheat cultivars (*Triticum aestivum cv*. Hereward and Paragon	Investigation how the N supply (100 and 350 kg of N ha−1,) affects the chemical speciation of Fe and Zn in the soluble extracts of whole wheat grain and fractions prepared by sequential pearling of the grain	The grain was air-dried to 12% moisture content, pearling mill Total analysis: sample digested with HNO3/HClO4 (87/13, v/v) in a heating block Speciation analysis: extraction with 50mM Tris−HCl buffer (pH 7.5), incubation at 37 °C for 18 h with shaking at 120 rpm. Extracts	ICP-OES ICP-MS SEC-ICP-MS	LMW: Fe-NA, Fe-DMA MMW: soluble iron-phytate	[53]

		were centrifuged (21000g, 13 °C, 10 min) and the supernatant was filtered		HMW: soluble proteins (probably)	
xylem sap of Fe-deficient tomato (*Solanum lycopersicum* Mill. cv. 'Tres Cantos')	naturally occurring Fe complexes in xylem sap	Xylem sap was sampled using the detopping technique. Shoots were cut below the first leaf using a razor blade, and xylem sap was left to exude. The sap of the first 5 min was discarded to avoid contamination, the surface was washed with distilled water and blotted dry, and sap was then directly collected for 20 min using a micro-pipet. pH of the samples was measured with microelectrode. Samples frozen at −80°C until analysis	HPLC–ESI-TOFMS HPLC–ICP-MS Total analysis: IDA-ICP-MS	tri-citrate complex (Fe_3Cit_3) in the xylem sap binuclear Fe(III)–Cit species Fe_2Cit_2 , was only detected in Fe–Cit standard solutions	[35]
Barley	comparison of different column types for the HILIC separation of iron citrate and copper histidine species; results are discussed with respect to retention mechanisms and chromatographic stability of these metal species	Speciation analysis: extraction with doubly distilled water and centrifugation. The extracts were stored at −18 ◦C. before analysis the samples were thawed, diluted with 50% solvent B and filtered before analysis	ZIC-HILIC-FTICR-MS ZIC-HILIC-ESI-MS	Fe:Cit species of 3:4, 1:2, 2:2 stoichiometry (+3:3 in standard solution)	[160]
tomato seedlings (*Solanum lycopersicum L.*, cv. 'Marmande superprecoce'	Different organic Fe-complexes and xylem sap of Fe deficient plants were analyzed with XANES under a cryo-stream of liquid nitrogen vapors to explore possible radiation damage likely to affect Fe speciation.	Frozen xylem sap samples were shipped in dry ice; for XAS analyses xylem sap samples, placed in special capillaries were mounted on a magnetic sample holder and analyzed under a stream of liquid nitrogen vapor.	Total: ICP-AES Organic acid determination: HPLC-UV/Vis XANES	Fe(III)-acetate, Fe(III)-citrate, Fe(0)	[161]
3 lines of wheat (*Triticum aestivum L.*)	Establishment of metal distribution and complexation in mature wheat grains. Determining the bioavailability of minerals in cereal diets to determine the precise molecular form of these essential	grain samples were prepared with a steel blade; the sections were embedded in Epocure cold curing resin, a working surface was prepared on each grain section with a Reichert Ultracut microtome using a freshly prepared glass knife	XRF and EXAFS	Iron phytate, ferritin	[162]

	micronutrients in the grain and particularly in the mineral-rich aleurone cells.				
Barley (*Hordeum vulgare L.* cv Himalaya)	Simultaneous identification of PSs and PS–Fe complexes in plant samples with LC-ESI-Q-TOF-MS	Freeze-dried roots, dried in vacuum freeze-dryer (60 ton80C for 8–10 h), were extracted with methanol for 30 min under sonication at room temperature (25 °C). Root extracts were microfiltered and used directly for LC-ESI-Q-TOF-MS analysis.	UPLC-ESI-Q TOF-MS (positive and negative mode)	in Fe-deficient roots: DMA–Fe (III), epi-HMA–Fe (III) MA–Fe(III), NA–Fe (II), AVA–Fe (III) and HAVA–Fe (III)	[163]
Xylem exudates of wheat plants (iron deficient and non-deficient	prove the suitability of IEF for the separation and enrichment of non-covalent metal species in preparative mode as well as in analytical mode (CIEF)	Samples were adjusted to pH 7 and mixed with the CA solution directly before starting the focusing process. When the focusing was finished; the fractions were collected along the pH gradient	IEF (fraction.) : UV/Vis, AAS, MS, or zic-HILIC-ESI/MS Multi-dimensional separations by combining IEF with subsequent HPLC-MS analysis.	Fe(III)-DMA	[164]
Wheat grains (cv. Akteur , E-type winter wheat exhibiting excellent bread making properties, moisture content 14.8%)	The speciation of Fe by using the newly available method of XANES imaging. The spatially resolved XANES imaging analyses focused on the aleurone cells, the main storage tissue of nutrient elements and the crease region.	Longitudinal and transverse cross sections (80 µm thick) of the middle part of the wheat grains glued to a plastic support and sliced using a vibrating diamond blade microtome. A piece of Kapton polyimide film was pressed on the surface of the residual grain, with the diamond blade of the microtome cutting underneath. In this way, sections were directly obtained on the Kapton tape without the need for embedding.	synchrotron X-ray fluorescence microscopy mapping XANES and co-localization of Fe with its possible ligands	Iron with ligand: phytate/citrate, phytate, protein, Fe-NA/FeO(OH)	[165]
barley grains (*Hordeum vulgare* cv. Golden Promise) were	Phosphorus and sulfur were determined since these elements are major constituents	The grains were rinsed 3 times in Milli-Q water and subsequently freeze dried for 24 h. The awns and embryo of each grain were	Total: ICP-OES	Fe co-eluted with P. phytic acid	[166]

fractionated into awns, embryo, bran and endosperm	of phytic acid and proteins, respectively, involved in Fe and Zn binding.	removed and separated by hand using a Teflon-coated scalpel. The rest of the grain was transferred to a Zr tube, where the inner walls were coated with sand paper (P-120). The Zr tube was agitated at 30 shakes/s for 2x 20 min in order to polish off the bran (The fused testa and aleurone tissue layers) from the endosperm (the main constituent of white flour). +Elemental mass balance analysis of tissue fractions+ Extraction procedure	SEC-ICP-MS (with O2 reaction gas)	(IP6) was the main Fe binding ligand, with the Stochiometry $\mathbf{Fe_4(IP_6)_{18}}$.	

(b)

Zn complex	plant	Sample preparation	method	Ref
Zn-phosphate Zn-phytate Zn-citrate Zn-malate	*Arabidopsis Halleri* *Arabidopsis lyrate*	Roots and aerial parts were frozen In liquid nitrogen then ground and Pressed pellets from the powder Were prepared	EXAFS µEXAFS µSXRF	[167]
Zn-$(Gln)_2$ Zn-$(His)_2$ Zn-NA Zn-$(Cit)_2$	*Pisum* *Sativum*	Direct analysis of xylem and embryo sac liquid diluted in ACN and water	SEC/HILIC-ICP-MS SEC/HILIC-HR FT-ESI-MS	[36]
Zn-NA Zn-DMA	*Arabidopsis Thaliana* Wheat plants	Roots and shoots squeezed in a Hydraulic press then direct analysis Of obtained press sap and xylem Sap after filtration and dilution	ZIC-cHILIC-ESI-MS	[70] [67]
	Rice seeds	Seeds were homogenized then ground and extracted in ice-cold Tris with acid-washed quartz sand under N_2 flow, followed by centrifugation	SEC-ICP MS HILIC –ESI-TOF -MS	[168]
Zn-phosphate Zn-oxalate Zn-phytate Zn-citrate Zn-malate	*Nicotiana Tabacum* (roots)	Different sequential extractions: -10mM CuSO4, then 100mM HCl -10mM CuSO4 (3 times), then 100mM HCl -water, then 10mM $CaCl_2$ -10mM EDTA	EXAFS	[169]
Zn-GSH Zn-cysteine	*Agropyron elongatum*	Sample washed and frozen in liquid nitrogen, then mixed with quartz sand and Tris-HCl buffer and ground until a homogeneus paste was formed. Supernatant filtered and stored in liquid nitrogen until analysis.	SEC-ICP-MS	[170]
Zn-Histidine	*Thlaspi caerulescens*	Frozen hydrated samples were ground to powder and filled into EXAFS cuvettes (-80°C)	EXAFS	[171]
Zn-malate Zn-citrate Zn-cell wall	*Sedum alfredii*	Fresh plant tissues were ground under liquid nitrogen and pressed prior to EXAFS analysis	EXAFS µXRF	[172]

Zn-citrate Zn-malate Zn-phytate Zn-histidine	*Noccaea caerulescens*	Xylem samples loaded into a perspex sample holder intact roots and leaves enclosed in mylar film and mounted onto a sample holder	XANES	[173]
Zn-phosphate Dihydrate Zn-phytate	*Phaseolus vulgaris*	TEM-EDX; fixation of samples in glutaraldehyde , dehydration in ethanol , samples embedded in spurr's resin EXAFS: samples were freeze-dried, ground and pressed as 2mm thick pellets	EXAFS TEM-EDX	[167]
Zn-histidine Zn-citrate Zn-oxalate	*Thlaspi caerulescens*	Frozen plant tissues were ground under liquid nitrogen and compacted into Lucite sample holders with Mylar windows	EXAFS XAS	[37]
Zn-NA	*Arabidopsis halleri*	Fresh root samples extracted in ice-cold Tris, following grinding in liquid N2 with acid-washed quartz sand. After centrifugation ultrafiltration with a cutoff < 100KDa	SEC-ICP-MS HILIC-ESI TOF MS	[174]
	Oryza sativa L	Phloem sap obtained by insect/laser method	SEC-ICP-MS/ESI TOF MS	[72]
	Ricinus communis	Direct analysis of xylem and phloem sap	SEC- ESI TOF MS	[175]
Zn-phosphate Zn-oxalate	*E.vesicaria* *L.cavalieri* (soil without compost)	Fresh living plant , washed with dionized water	SR-XRF-µCT µ-XANES	[54]
Zn-phosphate Zn-cysteine Zn-histidine	*E.vesicaria* *L.cavalieri* (soil with compost)			
Zn-NA Zn-malate Zn-citrate	*Noccaea caerulescens*	Cell sap of fresh material extracted by mortar and pestle, with acid washed sand and tri/HCl, under N_2 and ice-cold conditions	SEC-ICP MS HILIC-ESI TOF MS	[176]
	Arabidopsis halleri	Direct analysis of xylem exudates	SEC-ICP MS	[29]
Zn-PS	*Zea mays L.*	Purified root exudates prior to direct scintillation counting	Scintillation counting	[177]
Zn-citrate	Glycine max	Plant were cut , frozen in liquid N2 axially sectioned with a cryomicrotome and next mounted onto kapton and ultralene film	µXANES µXRF	[178]
Zn-nitrate	*P.juliflora-velutina*	Roots were washed with HNO3 , leaves and roots were cut and frozen and next mounted onto kapton tape	µXANES µXRF	[179]
Zn-Gly Zn-Galacturonic acid Zn-methionine Zn-pterostilbene	Gogi berries	Dry goji berries grounded and homogenized using liquid N_2 and agate mortar. Goji berry powder was extracted by vortexing with tris-HCl for 2h then centrifugation of the sample for 15 mins through 10 KDa cut off filter	CE ICP MS CE ESI MS	[57]

Zn-caffeic acid Zn-zeaxanthin glucoside Zn-piceatannol Zn-isorhamnetin				
Zn-zeaxanthin Zn-caffeic acid Zn-resveratrol Zn-ɤ linolenic acid	Goji berries	Total analysis : digestion of goji berries : Dry goji berries grounded and homogenized using liquid N_2 and agate mortar then digested in microwave with a mixture of HNO_3 and H_2O_2	ICP MS XRF SEC ICP MS µHPLC ESI MS/MS	[56]

(c)

Ni complex	plant	Sample preparation	method	Ref
Ni-malate Ni-citrate Ni-NA Ni-histidine	*Thlaspi caerulescens*	Leaves were harvested and sterilized then rinsed with deionized water and feathered every 1 mm with a razor blade in a plasmolysis medium (9% mannitol and salts). The leaves were digested with cellulase 1% (w/v) and macerozyme 0.5% (w/v) and filtered through 300 and 80 mm nylon mesh and centrifuged at 55 g for 5 min. The pellet was resuspended in the plasmolysis medium and centrifuged again under the same conditions. The pellet re-suspended in a Percoll solution (75% Percoll, 526 mM sucrose). Intact protoplasts recovered using a sucrose density gradient centrifugation (55 g for 10 min), washed and re-suspended in the plasmolysis medium.	ICP MS SEC ICP MS HILIC ICP MS HILIC QTOF MS/MS	[62]
Ni-NA	*Thlaspi caerulescens*	Total analysis: Leaves and roots rinsed in distilled water or 15 mM EDTA, and dried at 80°C for 48 h. digestion with HNO_3 for 30 min at 250 °C and then diluted with ultra-pure water to 1% HNO_3. Xylem sap was collected by inserting a capillary tube in decapitated plant stems.	ICP MS SEC-ICP-MS HILIC ICP MS/ESI-QTOFMS	[64]
Ni-NA Ni-DMA Ni-(aspartate)$_2$ Ni-(malate)$_2$ Ni-(histidine)$_2$	*Arabidopsis thaliana* wheat plants cv Bezostaya	Xylem sap exuded into the tube for 30 min was collected with a Pasteur pipette and stored at –20°C. Shoot and roots of wheat plants were harvested separately, rinsed with ultrapure water, blotted dry between paper towels, and squeezed in a hydraulic press centrifuged at 25000xg for 30 min stored at –20°C.	HILIC-HR-ESI MS	[67]
Ni with carboxylic acids	*A. serpyllifolium ssp. lusitanicum*	Xylem sap was extracted from the largest stems of the plants, within 72 h after harvesting, using a Scholander pressure chamber from Manofrígido (Amadora, Portugal) pressurized with nitrogen Before storage in Eppendorf caps at −20 ◦C, the pH of the xylem sap composite sample was measured	Total Ni by FAAS voltammetric titrations for nickel speciation	[180]
Ni-Citrate Ni-Citrate$_2$ Ni-Malate Ni-Malonate Ni-Acetate Ni-Oxalate	*Alyssum murale/ Odontarrhena muralis* *R. bengalensis*	Total: Solid samples (0.1 g) were digested with 8.5 mL of HNO_3 and 1.5 mL of H_2O_2 in a microwave oven. Liquid samples (2 mL) were digested with 1 mL of HNO3. Digestates were diluted to 50 mL with ultra-pure water and filtered.	Total by ICP-AES Ni speciation investigated at thermodynamic equilibrium,	[181]

Ni-Acetate$_2$			using Chess computer software	
Ni-Citrate Ni-glutamine Ni-Histidine	Thlaspi arvense L. Thlaspi goesingense Ha´la´csy	Total: Plant samples were dried at 60°C for 3 d, and then digested at 180°C for 105 min in 5 mL of HNO_3. Samples were cooled to room temperature, 1 mL of 30% (w/v) H_2O_2 was added, the mixture was heated at 180°C for 20 min, cooled, and deionized water added to a final volume of 12.5 mL Speciation: Samples mounted in 1-mm pathlength lucite sample holders with mylar windows. Frozen plant tissues were ground under liquid nitrogen and compacted into liquid nitrogen- cooled cells. Aqueous models were diluted by 30% to 50% (v/v) with glycerol before being pipetted into holders and frozen in liquid nitrogen.	ICP MS X-ray absorption spectroscopy	[182]
Ni-histidine Ni–succinate Ni-glutamate Ni–malate Ni–citrate Ni–oxalate	*T.caerulescens* *L. emarginata* *A. murale*	Analysis directly on the samples, without preliminary extraction or preparation	XANES/EXAFS	[183]
Ni-gluconate Ni-citrate	Naturata cocoa powder	Total: microwave assisted digestion of cocoa samples. Cocoa infusions were prepared by adding 0.5 g of sample into 50 mL of boiling Milli-Q water, the contents kept to boil for next 5 min and after cooling to room temperature, the samples were filtered. Speciation: 0.5 mL of cocoa infusion was injected onto a CIM DEAE monolithic column. An aqueous 0.6 mol L^{-1} NH_4NO_3 linear gradient elution was applied for 10 min at a flow rate of 1.0 mL min^{-1}	ICP MS. CIM DEAE monolithic column coupled to ESI MS, HR MS and MS/MS for Ni speciation. Quantification of Ni species by CIM DEAE ICP-MS.	[184]

Ni-citrate	*Glochidion cf. sericeum*	Total: samples were dried at 70 °C for 5 days in an oven; the dehydrated plant tissues were ground and digested using 1:1 (v/v) HNO_3 (70%) - H_2O_2 (30%) in a microwave oven for a 45-min and diluted with ultrapure water. Tissue samples for synchrotron XAS analysis were excised with a razor blade, placed in polycarbonate cuvettes, covered with Kapton tape and rapidly frozen by immersion in liquid N_2 in the field. Tissue samples for XFM analysis were excised and immediately shock-frozen using a metal mirror technique. The samples were then wrapped in aluminium (Al) foil stored in a cryogenic container (at least −190 °C) The tissue samples for XFM analysis were cryo-transferred on dry ice (−80 °C) into the cryo-chamber of the microtome (maintained at −30 °C) and mounted on a plate by application of freezing (−8 °C) polypropylene glycol for physical support. The leaves were then cut to 30 µm sections using a cooled stainless-steel blade (−20 °C), transferred to pre-cooled 1 mL cryo-containers and stored in a liquid N_2 (at −196 °C). vapour-Dewar	ICP AES Scanning electron microscopy with X-ray microanalysis (SEM-EDS) X-ray fluorescence microscopy (XFM) X-ray absorption spectroscopy (XAS)	[185]
Ni-succinate Ni-His Ni-Cystein	*Clethra barbinervis*	Total Approximately 50 mg of each powdered sample was digested with 5 mL of HNO_3 in a microwave. The digest was then filtered through a 0.45-µm membrane filter. Each leaf sample was wrapped in polypropylene thin film. Ventilation holes were then made in the film to allow He gas to circulate and 10–30 µl of ultrapure water was dropped on the side opposite	ICP AES Synchrotron radiation micro XRF (SR-µ-XRF) K-edges µ-XANES	[186]

(d)

Cu complex	plant	Sample preparation	method	Ref
Cu-cystein Cu-polygalacturonic acid Cu-citrate Cu-histidine	*Vigna unguiculata*	hydrated (and preferably, fresh) plant tissues collected at the time of harvest, filtered to 0.22 mm, acidified using 20 mL of concentrated HCl (10 M), and refrigerated at 4°C	ICP MS Synchrotron Analysis (m-XRF) Synchrotron Analysis (XAS)	[187]
CuO NPs CuS NPs	*Triticum aestivum*	Roots were briefly rinsed in Cu-free hydroponic medium, and with shoots were separated, weighed, and lyophilized. Plant tissue was digested in a 1:1 solution of DI water: concentrated HNO3 at 95°C for 30 minutes. Solution was then brought to a 2:1 ratio of concentrated HNO3: H2O2, heated to 95°C for 2 h, then allowed to return to room T	ICP MS µ-XRF and bulk XANES analysis on	[188]
Cu-NA Cu-Histidine	*Cichorium intybus L.* cv. Grasslands Puna) tomato (*Lycopersicon esculentum* Mill. cv. Rondy)	Roots and shoots samples were collected washed in deionised water and a solution of 0.1 mM Ca(NO3)2 and 0.1 mM NaEDTA were added and finally deionized water added, each for 30 min. Root and shoot samples were oven dried at 65 °C for 48 h and digested in nitric acid The chicory stems were severed using a stainless-steel razor blade at about 1 cm above media surface. Xylem sap was collected with a micropipette	FAAS for total analysis pH titration of free Cu^{2+}	[189]
Cu-NA Cu-histidine Cu-proline	*Brassica carinata*	Stems were cut using a stainless steel razor blade at about 2 cm above the media surface perpendicular to the stem axis. The decapitated stumps were wiped gently and fitted with Tygon tubing. The saps were filtered (0.45 lm) and frozen at –80 °C until needed	AAS for total Cu amino acids detection by RP-HPLC- UV pH titration of free Cu^{2+}	[52]
Cu-NA Cu-DMA	*Oryza sativa*	The phloem was collected by the insect-laser Nilaparavata lugens Stal. (brown planthopper), cultured with young rice seedlings in insect boxes installed in a room (temperature 25°C, RH 60%, 12-h light and 12-h dark cycle). shoots were cut with a knife at 2 cm from the root–shoot interface. The exudates (xylem sap)	ICP MS CE MS Collection fraction by SEC	[14]

		from the cut surfaces were collected into micro capillary tubes and then mixed with 0.05M HNO_3 and stored at -20°C The tissue samples were dried at 60°C for 3 days. The dried tissues were cut into small segments, transferred into a Teflon tube and mixed with 69% HNO_3 and kept for 2 h at room temperature. The tubes were then heated first at 100°C for 30 min and then at 130°C for 3 h on a hot plate. The extracts were dried at 80°C and then mixed with 0.1M HNO_3 protease digestion of phloem sap	ESI TOF MS in direct infusion GF AAS	
Cu-quercetin 3-O-(6”-acetyl)galactoside Cu-cyanidine 3-O-(6”-malonyl)glucoside Cu-daidzein-7-O-glucoside Cu-tryptophan Cu-ornithine Cu-resveratrol Cu-ferrulic acid	*Lycium Barbarum L.*	The dried goji berries were grounded in liquid nitrogen using agate mortar and pestle until a homogenous powder was formed. Ground dry goji berries were extracted using vortexing for 1 h with 2 mL of each solvent. The obtained solutions were centrifuged for 15 min at 15 000 rpm at 21 ◦C. The final supernatant was filtered with 0.45 m syringe filter. A portion of the filtrate (1.0 mL) was digested by microwave with a mixture of 4 mL of HNO_3 and 1.5 mL of H_2O_2. The digests were diluted with MQ water to the volume of 10 mL and further with 2% HNO3. The second portion was injected on SEC column.	ICP MS X-ray fluorescence spectrometry SEC ICP MS µ-HPLC-ESI–MS/MS	[56]

(e)

Mn complex	plant	Sample preparation	method	Ref
Mn-salicylic acid Mn-alzarin Mn-myricetin Mn-asperulosidic acid Mn-Malate Mn-rutin	*Morinda citrifolia*	Total: sample (0.2 g dry mass after lyophilization) was digested by microwave with a mixture of 5 mL of HNO_3 and 2 mL of H_2O_2. Collection of the peaks from SEC representing Mn for ESI MS	SEC ICP MS ESI MS	[61]
Mn(II)-malate Mn(II)-$(malonate)_2$ Mn(II)-oxalate Mn(II)-$(oxalate)_2$ Mn(II)-citrate Mn(II)-succinate Mn(II)-histidine Mn(III)-acetylacetonate	(hyper)accumulating species	Mature leaves from wild plants were harvested directly into humid packaging to maintain field-freshness and to avoid dehydration. Tissues were stored cool, and cryo-fixed within 24 h of collection before freeze-drying. As it was imperative that cell contents be retained in situ, a rapid freezing method was employed. Small leaf samples were excised immediately before being contact-frozen under vacuum in melting nitrogen. Cryo-fixed frozen leaf tissues were then freeze-dried (FD) for 48 h at -40°C and 0.2 mbar.	K-edge X-ray absorption near-edge spectroscopy (XANES)/EXAFS	[58]

8.4 Metallometabolomics: future perspectives

Metallometabolomics is an emerging field, and thus the analytical technologies, data processing and informatics are still being developed in response to the demands of this area.

The possible development can be achieved at three different levels:

- Miniaturization of separation system allowing analysis of extremely low volumes of the samples. In this case the first choice would be the use of nano flow LC but the nanoHPLC systems available nowadays on the market don't allow to deal with precision (inject) with nL volumes of samples (less than 20nL). A possible solution would be development of chip based separation (with separation mechanisms based on different chromatographic mechanism or capillary electrophoresis) which would require in addition development of interface in order to be coupled to mass spectrometer.
- Use of Isotopic Fine Structure (IFS) which is the unique mass spectral signature arising from naturally occurring isotopes within the molecule being measured. It's possible to be achieved when using the ultrahigh mass-resolving power. The highest resolution registered till now was when 21T ICR MS was used ($m/\Delta m_{50\%}$ > 2 700 000 at m/z 400) and mass accuracy (80 ppb rms) which enabled resolution and confident identification of tens of thousands of unique elemental compositions. There is possibility to accelerate the Extreme Resolution Isotope Fine with Launch of New solariX™ 2XR FTMS System which the principle is illustrated in **Figure 20** presenting faster and easier analysis with mass resolving power of 1.2 million in one second which can now routinely determine the molecular sum formulae of unknown small molecules with an affordable 7 Tesla magnet. The solariX 2XR allows the user to routinely view isotopic fine structure, eliminating ambiguity for elemental formula determination.

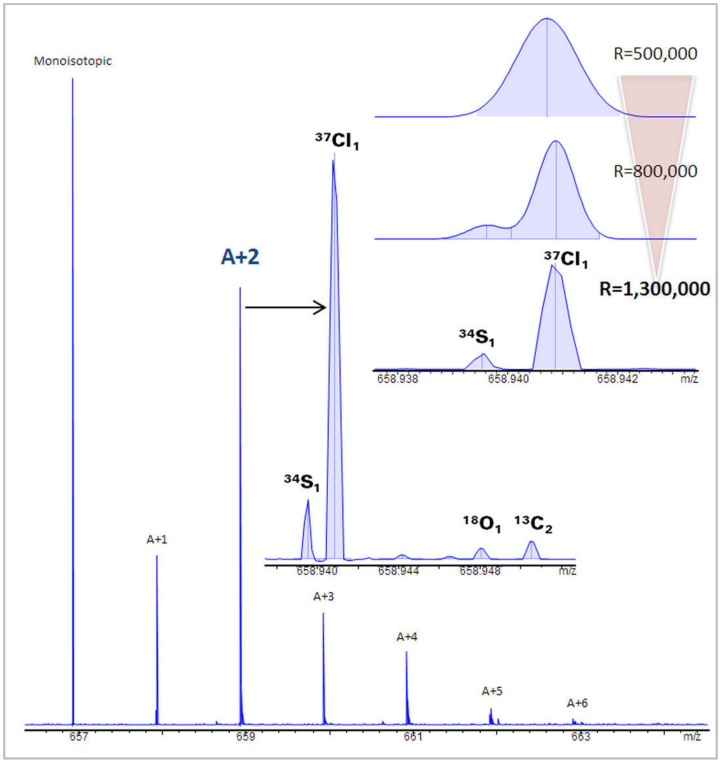

Figure 20. Principle SolariX™ 2XR FTMS System

Nevertheless, long transients of ICR technology are not compatible with narrow peaks obtained with UPLC separation and direct infusion is not possible due to complexity of the sample matrix. A possible solution would be the use of still developing high field orbitrap technology and the

newest instruments allowing to get $m/\Delta m_{50\%}$ 1 000 000 at m/z 200. In addition, improved results can be obtained when using dedicated softwares "cleaning" the signal. Further, software development should be also carried out to "fish out" the desired IFS patterns from obtained spectrums.

- Development of reliable quantification strategies based on isotopic spikes. Until now majority of data obtained for metal complexes in plants were just qualitative. No quantitative information was available due to the absence of standards, which could be used for quantification or attempts of post column isotope spiking were undertaken. In contrary to the classical post-column isotope spiking, the proposed method will compensate for possible on-column dissociation of metal complexes allowing for truly quantitative analysis based on the supposition that the added isotopes will create exactly the same species with the excess of ligands present in the sample like. This strategy could also be used in order to facilitate the detection and identification of Fe-compounds by ESI MS. The method of multiple enriched isotopes addition could be developed allowing the creation of "new" iron isotopic pattern, which will be much easier to detect in ESI MS spectrum.

9 Goal of the PhD project:

The main goal of this thesis was to develop and validate protocols of mass spectrometry methods, which could be applied for determination and quantitation of low molecular weight metal compounds in plant liquids. Unfortunately, the amount of plant liquid (eg. xylem), which usually can be sampled after several weeks of fastidious plant cultivation, is in low microliters range (or lower), which make the method development difficult task. Thus, as a compromise, coconut (*Cocos nucifera*) water was chosen as a model for method development studies of plant endosperm metallome, as the amount of sample available for experiments is much higher.

Based on the information available in literature the most commonly identified iron complexes were Fe-citrate ones and mixed complexes of iron with citrate and malate. The detailed study of formation of different complexes was carried out to evaluate their stability and equilibrium between them. Additionally different chromatographic columns were tested and elution condition were optimized to be used later on to the real samples. ESI MS condition were adjusted (positive or negative mode ionization) depending on chromatographic conditions used.

The principal part of the thesis concerns the development of methods for characterization of the model sample. Influence of different sample treatment steps (filtration, centrifugation) and storage condition was studied. Also, sample preparation before HILIC separation was evaluated, and the separation conditions optimized on model complexes was tested.

The quest of a generic analytical strategy for the standardless quantification of different low-molecular weight metal complexes by molecular mass spectrometry is pursued using the Isotope Dilution Analysis (IDA) with the addition of an isotope spike ^{58}Fe in ionic form and HILIC-ICP-MS. The protocol was carefully studied in order to keep the original metal complexes in non-degraded way and achieve the formation of metal complexes with the excess of ligands present in the sample.

Finally, the developed procedures were applied for characterisation and quantification of iron compounds in xylem samples of several plants. The plants chosen (*Pisum sativum, Paspalum urvilleli, and Setaria parviflora)* were hypertolerant or overaccumulating ones.

II. Experimental Part:

1 Outline:

The **first part** of the experimental work was focused on the analysis of model species and the development of chromatographic methods for the separation of LMW metal complexes. Because of its importance for plant nutrition, the investigations were focused on iron.

The development of analytical strategy required the availability of large volumes of real world sample to carry out the optimization and validation. The choice was coconut water showing all the characteristics of embryo sac liquid ESL. The **second part** of the study was devoted to detailed characterization of this material. The final and main goal was the development of the method for iron quantitation involved in LMW complexes which is presented in the **third part** followed by the application to real world low volume xylem samples reported in the final **fourth part** of the experimental report.

2 Reagents and instrumentation:

2.1 Reagents

The following reagents were used for digestions, dilutions and the preparation of HPLC mobile phases: ammonium acetate (≥98% for molecular biology, *Sigma-Aldrich St. Louis, USA*), nitric acid (V) (70%, *Fisher Chemical, Loughborough, UK*), acetonitrile (≥99.9%, *Sigma-Aldrich St. Louis, USA*) hydrogen peroxide (30%, *Sigma-Aldrich St. Louis, USA*), formic acid (*Lichropur*, 98%-100% *MERCK* for LC-MS) hydrochloric acid (37%, *Fluka, Steinheim, Germany*). Standard solutions (1000 ppm, *Plasmacal, SCP sciences*) of Fe, Mn, Ni, Cu, Zn, Rh, Sc were used to prepare specific metal standards for the calibration of the instrument and as internal standards (Sc and Rh). The results of the total amount determinations were validated by the analysis of standard reference materials: Mixed Food Diet (*high purity standard, Greyhound chromatography, UK)*.

^{58}Fe metallic iron (93%+) was purchased from *STB Isotope Germany GmbH*, Germany and dissolved in aqua regia (HNO_3:3HCl) to produce a stock solution mg/ml which was then diluted. EDTA (ethylenediaminetetraacetic acid) was used for column cleaning. Milli-Q® Type 1 Ultrapure Water Systems (*Millipore, Bedford, Ma*) was used throughout.

2.2 Instrumentation

2.2.1 Reagents:

All powder reagents were weighed by an analytical balance *(XT 220A Precisa, Bruges, Sweden)*. The adjustments of pH of mobile phase used for chromatographic separation were done using a five-easy pH meter, *Mettler Toledo, FiveEasy, Szwerzenbach, Switzerland*. For samples centrifugation Eppendorf MiniSpin centrifuge by (*Eppendorf AG, German)* was used. The digestion of samples was carried out in Digi Prep MS (*SCP Science, Quebec, Canada)* system.

2.2.2 HPLC pumps and columns:

Two chromatographic systems were used**:**

- Agilent 1200 Series *(Tokyo, Japan)* used for size-exclusion separation using a Superdex 75 10/300 GL column (*GE Healthcare*) that was calibrated before use in order to get the mass ranges and be able to show the retention times of the peaks representing metals species of interest according to these ranges and

- *Dionex Ultimate 3000 RS (Thermo Scientific*, *UHPLC, Germany)* used for HILIC separations using a Phenomenex Kinetex HILIC column *(Kinetex chromatographic column, with the pre-Column Security Guard ULTRA, USA)* and a zwitterionic type HILIC column SeQuant Zic-cHILIC (*Merckmillipore)*

Typical operating conditions are given in **Table 8**.

2.2.3 Mass spectrometers:

ICP MS:

The ICP MS instruments used and illustrated in **Figure 21** were Agilent Model 7500 equipped with an integrated autosampler *(I-AS)* and 7700s (both from agilent, Tokyo, Japan) equipped with a collision cell with hydrogen/Helium as a collision gas. The ICP system consists of a 50 mL/min micromist U nebulizer *(Glass Expansion, Australia)*, a Scott type spray chamber, a 1 mm ID. injector torch (agilent Technologies, Japan), and a set of nickel cones (sampler and skimmer cones from agilent technologies, USA) for total analysis and platinum cones in case of coupling with HPLC where organic solvents can be used.

The experimental parameters such as plasma power, torch position, voltage on extraction and focusing lenses were optimized before every day by using a tune solution containing 1 µg/L each of Li, Mg, Y, Ce, Tl and Co in a matrix of 2% HNO_3. To reduce the spectral interferences hydrogen was used as a reaction gas. Typical operating conditions are given in **Table 9.**

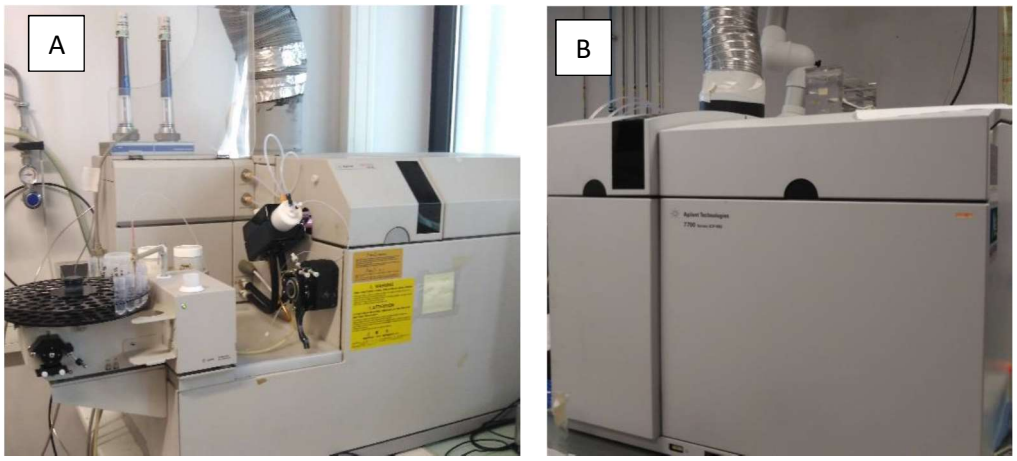

Figure 21. Representing (A) Agilent Model 7500 (B) Agilent Model 7700s

ESI MS

Electrospray ionization mass spectrometer used was Q Exactive plus Quadrupole-Orbitrap Hybrid Mass Spectrometer *(Thermo Scientific, Bremen, Germany)* in positive and negative ionization modes. The following parameters were adjusted: capillary temperature, carrier gas temperature, shielding gas pressure and spray voltage. Data processing was carried out in the Thermo XCalibur program used for the generation of theoretical masses and their comparison with experimental ones.

Optimized ESI conditions used during analysis are grouped in **Table 10**.

Tables 8. Chromatographic conditions used.

HILIC		
Column	**Phenomenex Kinetex HILIC** column (Kinetex chromatographic column (150 x 2.1 mm), 2.6 µm, with the pre-Column security guard ULTRA, USA)	**SeQuant®Zic®-cHILIC** (150x2.1mm),3µm 100 A
Mobile Phase	A: 25 mM ammonium acetate at pH=5.5; B: ACN	A: 10% 5mM ammonium acetate pH 5.5+ 80% H_2O + 10% ACN B: 10% 5mM ammonium acetate pH 5.5 + 90% ACN
Flow rate	0.5 ml/min	0.2 ml/min
Injection volume	10 µL	2 µL
Gradient elution	0-1 min 95% B ; 1-10 min 80% ; 10-13.5 min 80% B ; 13.5-17 min 60% B ; 17-21 min 60% B ; 21.01-30 min 95% B.	0-2.5 min 100% B ; 2.5-27 min 65% B ; 27-35 min 60% B ; 35-36 min 100% B ; 36-46 min 100% B.

Size –exclusion chromatography	
Column	Superdex 75 10/300 GL SEC column GE Healthcare
Mobile Phase	100 mM ammonium acetate at pH=7.5
Flow rate	0.7 mL/min
Injection volume	100 µL
elution	isocratic

*Table 9. ICP MS conditions (*when coupled to HILIC)*

cones	platinum
plasma generator power	1550 W
Plasma gas flow rate	0.64 L / min
Reaction gas flow rate H2	4.5 mL / min
Oxygen optional gas*	7.5%
Extract 1: Voltage on extraction lenses	-7.3 V
Extract 2: Voltage on focusing lenses	-162.5 V
Deflect	-0.3
OctP Bias	-18 V (-6 in no gas mode)
QP Bias	-15 V (-3 in no gas mode)

Table 10. ESI MS conditions

Polarization mode	Positive	Negative
Resolution	140000	70000
AGC	$1e^6$	$3e^6$
Max injection time in ms	500	500
Capillary temperature °C	350	280
Carrier gas temperature °C	400	300
Lens voltage V	40	40
Spraying voltage KV	3.2	2.5
Shielding gas flow rate	60	35
Carrier gas flow	20	10

3 Procedures:

3.1 Total element analysis:

Samples were treated with mixture of nitric acid and hydrogen peroxide in ratio (3:1) and digested at 65°C temperature until the observation of a clear solution. The maximum temperature of the process did not exceed 65°C. After approx. 2h 30 the digests were cooled down to the room temperature. After an appropriate dilution and addition of internal standards, the total content of selected elements was measured. The analytical blanks were run in parallel.

Metals of interest such as Mn, Fe, Cu, Ni and Zn were analyzed using ICP-MS 7500; the following isotopes ^{55}Mn, ^{56}Fe, ^{58}Ni, ^{63}Cu, ^{64}Zn were monitored. Specific metal standards in the linear range of each metal of interest were prepared to get a calibration curve giving equation to calculate the concentration of the metal of interest. The accuracy of the applied method used for analysis was determined by using a standard reference material, Mixed Food Diet SRM-MFD-250with the matrix most similar to that analyzed [190][191].

3.2 Sampling and sample preparation for speciation analysis

Specific sampling and sample preparation methodologies for speciation analysis are given in respective sections **(sections 4.1, 4.2, 4.3, 4.4).**

3.3 Preparation of chromatographic eluents:

Two concentrations 5mM and 25mM of ammonium acetate are prepared for chromatographic separation: ammonium acetate is weighed and dissolved in H_2O. Once the salt is dissolved the pH is adjusted at 5.5 because it is the pH of the real samples that will be analyzed. Acetonitrile and ammonium acetate are mixed together in adequate proportions.

4 Results and Discussion:

4.1 Method optimization for the study of standard Fe-malate-citrate and Fe-citrate complexes:

On the basis of the literature (please see section **8.3 Metallometabolomics: application fields**) the most popular LMW ligands complexing Fe in plant liquid are citrate and malate. Thus, the study focused on the complex equilibria and HPLC behavior of these particular class of species. The aim was to study the formation of the possible complexes that can be formed, and develop an analytical method for their detection and identification by HILIC chromatography coupled to either ICP MS or ESI MS.

4.1.1 Sample preparation:

Iron citrate (Fe-Cit) and iron citrate-malate (Fe-Cit-Mal) standard solutions at different Fe: malate: citrate ratios were prepared by adding the appropriate amounts of iron trichloride to citric and malic acid solutions prepared in 100 mM ammonium acetate at pH 5.5. The solutions were gently vortexed, diluted and immediately analyzed. They were prepared according to the Table below (**Table 11**) following the literature procedure of Silva et al [192] discussing iron citrate speciation in aqueous solution:

a) Preparation of 100mM ammonium acetate buffer in H_20, pH=5.5
b) Preparation of 100mM $FeCl_3$ in H_20 at pH=2
c) Preparation of 100mM citric acid in 100mM ammonium acetate buffer in H_20, pH=5.5
d) Preparation of 100mM malic acid in 100mM ammonium acetate buffer in H_20, pH=5.5
e) Just before analysis, addition of appropiate amount of citric acid and/or malic acid (as listed in the Table below) to buffer and vortexing (30s) then addition 25 µl of solution 100 mM $FeCl_3$ in H_20 at pH=2 and vortexing (30s).

Solution were prepared ca. 30 minutes before analysis to let enough time for complexes to be formed:

Table 11.Preparation of standard solution of iron, malate and citrate mixed at different ratios to obtain the complexes of interest

Lp.	^{56}Fe Cit/FeCit Mal standard solution	Final volume: 10 ml			
		V 100mM Fe (100mM FeCl3) [ml]	V 100mM malic acid [ml]	V 100mM citric acid [ml]	V 100mM ammonium acetate buffer pH 5.5 [ml]
1	^{56}Fe:Mal:Cit (1:25:5)	0,025	0,625	0,125	9,225
2	^{56}Fe:Cit (1:1)	0,025	-	0,025	9,950
3	^{56}Fe:Cit (1:10)	0,025	-	0,250	9,725
4	^{56}Fe:Cit (1:50)	0,025	-	1,250	8,725
5	^{56}Fe:Cit (1:100)	0,025	-	2,5	7,475

Concentration of Fe in the complex = 14 ppm

4.1.2 Optimization of the chromatographic separation

The speciation procedure was based on the coupling of high performance liquid chromatography - to separate species according to either size by using a size exclusion column or hydrophobicity by using a HILIC column - to mass spectrometric detection. According to literature [160], the optimal separation of Fe-citrate (and also Cu-histidine) complexes was achieved using three columns with the diol-, amide-, and zwitterionic stationary phases: the possible structures of zwitterionic HILIC stationary phase that we can use are gathered in **Figure 22**. In this project, 2 types of stationnary phase: zwitterionic phase ZIC-cHILIC, carrying phosphorylcholine type functionality and kinetex phase formed of unbonded silica phase used under hydrophilic interaction chromatography conditions were used.

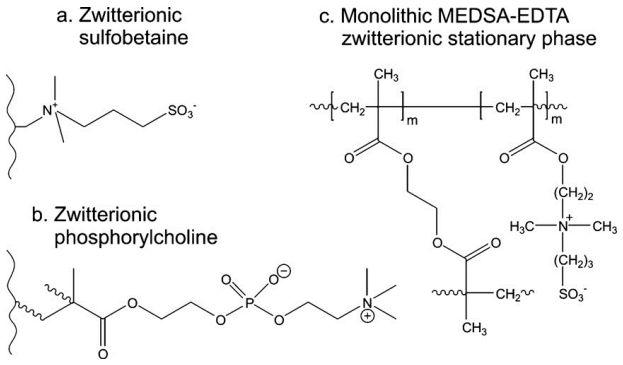

Figure 22. Structures of some zwitterionic HILIC stationary phases.[111]

Kinetex ultra high performance HPLC columns are based on the fused core technology; the stationary phase contains hard, non-porous center particles coated by a thick film of totally porous silica which constitutes a significant fraction of the total particle diameter. Berger (2011) [193] compared the Kinetex Hilic column with a totally porous silica gel column: The superficially porous column was better as it required half the time with almost 50% higher efficiency related to the diffusion path length, which is the porous shell thickness, not the total particle diameter with relatively low pressure drops[193]. In addition, these columns showed better resolution than conventional totally porous columns[194–196]. The optimal HPLC separation conditions used for further analysis were given in **section 2.2.2** , **Table 8**.

Two results obtained for both columns studied are shown below:

4.1.2.1 *Iron citrate complexes:*

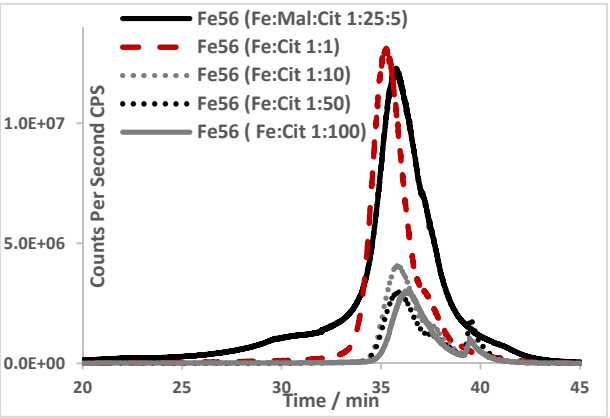

Figure 23.Chromatograms representing counts per second of Fe^{56} in different standard solutions of iron citrate and malate at different ratios. Conditions: 0-2.5min 100%B (10% 5mM ammonium acetate pH 5.5 in H_20+ 90%ACN) B) , 0% A(10% 5mM ammonium acetate pH 5.5 in H_20+ 80 % H_20+ 10%ACN), 2.5-27 min 65 %B, 27-35 min 60 %B, 35-36 min 100%B, 36-46 min 100 %B, flow rate: 0.2 ml/min, injection volume: 2µl , column SeQuant® ZIC®-cHILIC (150 x 2.1 mm), silica 3 µm, column temperature: 20 °C, buffer concentration used in mobile phase: 5 mM and 100mM.

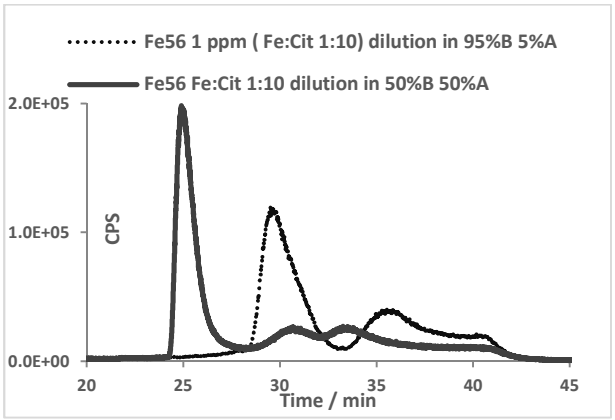

Figure 24. Chromatograms representing counts per second of Fe^{56} in different standard solutions of iron citrate at ratio 1:10. Same Conditions as figure 23. The differences in the elution times was due to sample preparation where samples were diluted either in initial conditions of mobile phase such as 95%B 5%A or in 50%B 50%A.

Blue box represent principal axis and Red box secondary axis.

Figure 23 shows no clear separation of the complexes formed in the standard solution prepared; a small peak appeared at around 39 minutes in standard solutions formed by Fe and citrate only at high ratios such as Fe: Cit at 1:50 and 1:100. However, regarding Fe: Mal: Cit mixture there is only one wide peak at around 35.5 minutes representing non-separated complexes.

In the next step, the chromatographic separation was reassessed for standard mixtures of Fe and citrate at ratios 1:1 , 1:10, 1:50 and 1:100 using two different sample preparations for analysis : (i) with dilution in 95% B and (ii diluted in 50% B. **Figure 24** shows the example of standard mixture of Fe citrate at ratio 1:10 where the compounds diluted in 50% B eluted earlier because of the high concentration of aqueous phase helping the release of the compounds from the stationary phase. The both ways of sample preparation were found suitable; finally dilution in initial conditions of mobile phase was chosen.
In the subsequent step, another HILIC column (Phenomenex Kinetex) with unbonded silica phase used under to provide the selectivity needed for the retention and separation of polar compounds was tested to see if separation can be improved. As can be seen in **Figure 25**, at around 8 minutes a wide peak appeared corresponding to compounds formed in the mixture of Fe malate and citrate at ratio 1:25:5 which expanded the scope of speciation analysis Fe complexes with malates and citrates and necessited an optimization of the separation of these compounds for further studies. As a conclusion, HILIC columns of unbounded silica stationary phase (kinetex type) are suitable for iron malate citrate complexes and zwitterionic type columns are suitable for iron citrate ones.

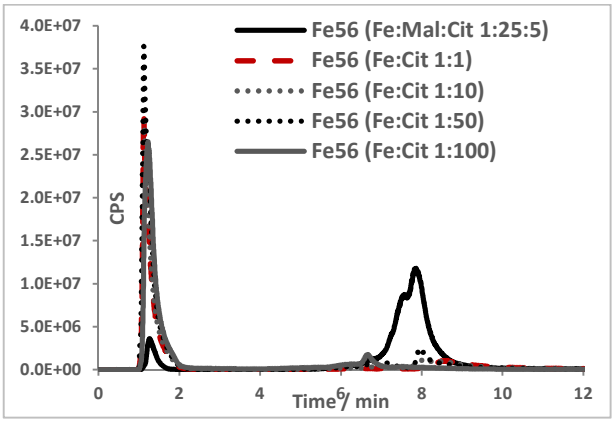

Figure 25. Chromatograms representing counts per second of ^{56}Fe in different standard solutions of iron citrate and malate at different ratios. Conditions: 0-1min 100%B (ACN), 0% A (25mM ammonium acetate pH 5.5 in H_2O), 1-8 min 60 %B, 8-12min 60 %B, 12.01-17min 100%B flow rate: 0.5 ml/min, injection volume: 20µl , column Phenomenex Kinetex (150 x 2.1 mm), 2.6 µm, column temperature: 20°C. Standard solutions were prepared 2 weeks before analysis.

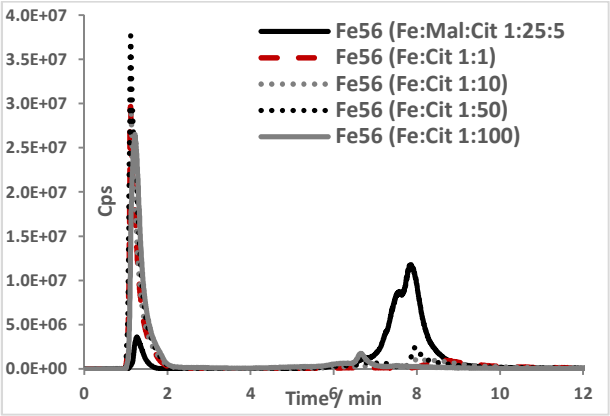

Figure 26. Chromatograms representing counts per second of ^{56}Fe in different standard solutions of iron citrate and malate at different ratios. Conditions: 0-1min 100%B (ACN), 0% A (25mM ammonium acetate pH 5.5 in H_2O), 1-8 min 60 %B, 8-12min 60 %B, 12.01-17min 100%B flow rate: 0.5 ml/min, injection volume: 20µl , column Phenomenex Kinetex (150 x 2.1 mm), 2.6 µm, column temperature: 20°C. Standard solutions were freshly prepared.

In addition, it is essential to know if the compounds of interest are stable; it is known that the stability of these complexes is pH and temperature dependent. To maintain the pH of the the mobile phase, it was prepared from ammonium acetate and the pH was adjusted pH to 5.5: it is important to mention that this pH was chosen according to literature [35][197][198] as the most suitable for metals complexes in plants since it is the pH of xylem saps where metals complexes can be found transported inside the plant. **Figure 25** presents chromatograms obtained for standard solutions prepared 2 weeks before analysis and **Figure 26** presents the same analysis with the same conditions but the only difference is that the standard mixtures were freshly prepared directly before analysis. As a conclusion, it is obvious that the compounds of interest are stable with time since there was no change in the elution time, number of peaks obtained or signals intensity.

In order to confirm the presence of Fe-Cit and Fe-Mal-Cit complexes, DI-ESI-MS (DI - Direct Infusion) analyses were performed. The stock solutions were diluted in 95% of eluent B and 5% of eluent A.

Theoretical masses of molecular ions were generated in the Thermo XCalibur program. The masses observed in the spectral spectrum were plotted in Tables 12 A B C D and E. The mass accuracy was calculated according to the formula:

$$\Delta[ppm] = \frac{m/z_{measured} - m/z_{calculated}}{m/z_{calculated}} \cdot 10^6$$

The spectra obtained has been analyzed for the presence of molecular ions resulting from the ionization of iron complexes with different stoichiometry. The occurrence of a characteristic isotopic profile was verified, the presence of which indicates the presence of iron atoms in the molecular ion.

The identification of these complexes is in agreement with some previous literature studies , such as Silva et al [192], Koster et al [164] and Flis et al [36].
The results obtained by FIA ESI MS are given in the Tables below (**Table 12 A B C D E**). For every ratio of iron citrate and or malate a set of m/z were detected in both negative and positive modes. 2 complexes $FeCit_2$ m/z 435.96 and $Fe_3(Cit)_4$ m/z 462.414 were identified in negative ionization mode in all the samples of Fe:Cit at all ratios studied. Only $FeCit_2$ m/z 435.96 was found in the mixture of Fe:Mal:Cit when analyzed in negative ionization mode; this is because Fe is less available for citrate since with presence of malate there is formation of complexes identified in positive ionization mode.

Table 12.Complexes detected in both negative and positive mode by FIA ESI MS

A- Fe:Cit 1:1 at concentration 200ppb of ^{56}Fe analyzed in negative ionization mode :

Molecular ion	Molecular formula	Calcutated m/z	Measured m/z	Mass accuracy m/z [ppm]
$[Fe_3Cit_3H]^{2-}$	$C_{18}H_{13}O_{21}Fe_3$	366.40043	366.40189	4.0
$[FeCit_2H_4]^-$	$C_{12}H_{12}O_{14}Fe$	435.95820	435.95987	3.8
$[Fe_2Cit_2H]^-$	$C_{12}H_9O_{14}Fe_2$	488.86966	488.87170	4.2
$[Fe_3O(Cit)_3H_3]^{2-}$	$C_{18}H_{13}O_{22}Fe_3$	375.40571	375.40723	4.04
$[Fe_3(Cit)_4H_5]^{2-}$	$C_{24}H_{21}O_{28}Fe_3$	462.41393	462.41492	2.14

B- Fe:Cit 1:10 at concentration 200ppb analysed in negative ionization mode :

Molecular ion	Molecular formula	Calcutated m/z	Measured m/z	Mass accuracy m/z [ppm]
$[Fe_3Cit_3H]^{2-}$	$C_{18}H_{13}O_{21}Fe_3$	366.4004	366.40089	1.3
$[FeCit_2H_4]^-$	$C_{12}H_{12}O_{14}Fe$	435.9582	435.95861	0.9
$[Fe_2Cit_2H]^-$	$C_{12}H_9O_{14}Fe_2$	488.8696	488.87067	2.2
$[Fe_3Cit_4H_5]^{2-}$	$C_{24}H_{21}O_{28}Fe_3$	462.4139	462.41486	2.1

C- Fe:Cit 1:50 at concentration 200ppb:

Molecular ion	Molecular formula	Calcutated m/z	Measured m/z	Mass accuracy m/z [ppm]
$[Fe_3(Cit)_3H]^{2-}$	$C_{12}H_{13}O_{21}Fe_3$	366.40043	366.40024	-0.51
$[Fe(Cit)_2H_4]^-$	$C_{12}H_{12}O_{14}Fe$	435.95820	435.95807	-0.29
$[Fe_3(Cit)_4H_5]^{2-}$	$C_{24}H_{21}O_{28}Fe_3$	462.41393	462.41394	0.02
$Fe_2Cit_2H]^{-1}$	$C_{12}H_9O_{14}Fe_2$	488.86966	488.86960	-0.122

D- Fe:Cit 1:100 at concentration 200ppb:

Molecular ion	Molecular formula	Calcutated m/z	Measured m/z	Mass accuracy m/z [ppm]
$[Fe(Cit)_2H_4]^-$	$C_{12}H_{12}O_{14}Fe$	435.95820	435.95769	-1.16
$[Fe_3(Cit)_4H_5]^{2-}$	$C_{24}H_{21}O_{28}Fe_3$	462.41393	462.41382	-0.23

E- Fe:Mal:Cit 1:25:5 at concentration 200ppb in positive ionization mode :

Proposed structure	Molecular ion	Molecular formula	Calcutated m/z	Measured m/z	Mass accuracy m/z [ppm]
$FeCit_2$	$[FeCit_2H_6]^+$	$C_{12}H_{14}O_{14}Fe$	437.9738	437.9734	-0.9
$Fe_3Cit_1Mal_3H_6$	$[Fe_3Cit_1Mal_3H_5]^+$	$C_{18}H_{18}O_{22}Fe_3$	753.8338	753.8347	1.2
$Fe_3Cit_2Mal_2$	$[Fe_3Cit_2Mal_2]^+$	$C_{20}H_{20}O_{24}Fe_3$	811.8393	811.8404	1.4
$Fe_3Cit_3Mal_1$	$[Fe_3Cit_3Mal_1]^+$	$C_{22}H_{22}O_{26}Fe_3$	869.8448	869.8458	1.1

In negative mode:

Proposed structure	Molecular ion	Molecular formula	Calcutated m/z	Measured m/z	Mass accuracy m/z [ppm]
$FeCit_2$	$[FeCit_2H_6]^-$	$C_{12}H_{12}O_{14}Fe$	435.9571	435.95780	1.6

An example of spectrums obtained is presented in **Figure 27** showing the 4 complexes identified in a mixture of Fe: citrate at ratio 1:10:

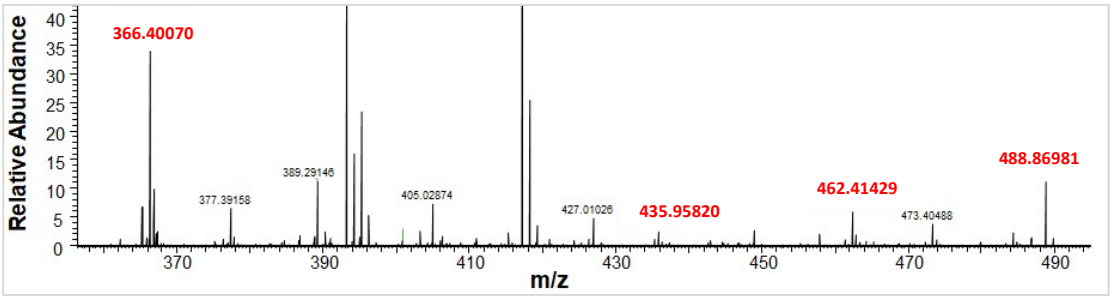

Figure 27. Mass spectrum of standard solution Fe: Cit (1:10).

These complexes were identified also after chromatographic separation on Zic-cHILIC column. The exemple of complexes identified in standard solution of Fe:Cit at ratio 1:10 is given by **Figure 28**. It is necessary to mention that the retention time shift is due to the changement of pumping system used for chromatographic separation where for ICP MS studies Agilent pump was used and Dionex pump was used for ESI MS.

Thus, in **Figure 28** four complexes were identified in the mixture of iron-citrate 1:10:

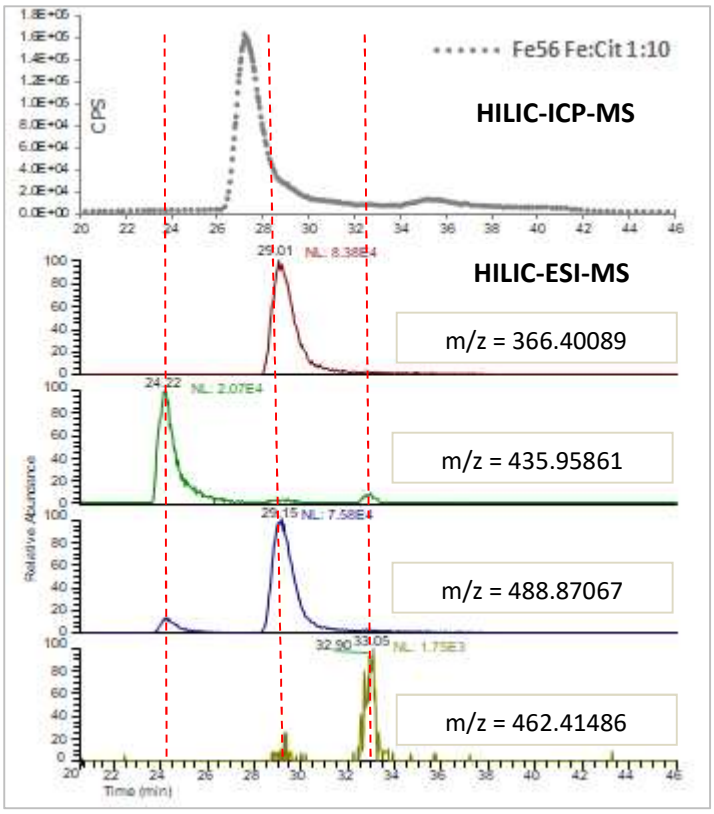

Figure 28. HILIC-ESI-MS chromatograms of a ^{56}Fe–Cit standard solution (Fe: Cit ratio 1:10), 2 ppm ^{56}Fe.Chromatograms obtained in SIM mode are presented for species $[Fe_3Cit_3H]^{2-}$ (366 m/z), $[FeCit_2H_4]^{-}$(436 m/z), $[Fe_3Cit_4H_5]^{2-}$ (462 m/z), $[Fe_2Cit_2H]^{2-}$ (489 m/z).Conditions: 0-2,5min 100%B (10% 5mM ammonium acetate pH 5.5 in H_20 + 90% ACN) , 0% A (10% 5mM ammonium acetate pH 5.5 in H_20 +80% H_2O + 10%ACN) 2,5-27 min 65 %B, 27-35 min 60 %B, 35-36 min 100%B, 36-46 min 100 %B, flow rate: 0,2 ml/min, injection volume: 2µl , column SeQuant® ZIC®-Chilic (150 x2.1 mm), silica 3 µm, column temperature: 20 °C.

4.1.2.2 *Mixed citrate- malate iron complexes:*

To study the formation of different iron complexes with malates and citrates and their separation using HILIC, model solutions with different citric acid concentration were prepared. The values were selected based on the concentration of different organic acids in coconut water, described by Zhang et al (2018) (1.23mg/mL for malic acid, 0.03mg/mL for citric acid) and assuming iron concentration around 5ppm, molar ratio of Fe: Mal: Cit was calculated as 1: 100: 2. Based on that, model solutions with different citric acid concentration were prepared, from 100: 1 up to 100: 100, with constant iron concentration. Detailed information concerning their preparation were gathered in **Table 13**.

Table 13. The volumes of individual 100mM solutions used for the preparation of specific Fe: Mal: Cit model complex mixtures.

Fe: Mal: Cit	100mM $FeCl_3$/ µL	100mM Mal/ µL	100mM Cit/ µL	100mM AmAc / µL
1: 100: 1	10	1000	10	3980
1: 100: 2.5	10	1000	25	3965
1: 100: 5	10	1000	50	3940
1: 100: 10	10	1000	100	3890
1: 100: 25	10	1000	250	3740
1: 100: 50	10	1000	500	3490
1: 100: 100	10	1000	1000	2990

Figure 29A shows distinctions in the chromatograms recorded for each model solution depending on iron: citrate ratio. To identify all $Fe_xMal_yCit_z$ complexes created in model solution and in order to assign them to the corresponding retention times HILIC ESI MS method was applied. Mass spectrometry made possible to identify 3 different complexes of iron with studied organic acids, which retention times coincided with main three peaks recorded by ICP MS detection. At low citric acid concentration, the main peak belongs to the compound of m/z 811.84 (11.7 min) and other for compound of m/z 753.83 (around 16.7 min). The above mentioned masses correspond to $FeMal_2Cit_2$ and $FeMal_3Cit_1$ respectively. With increasing citrate concentration $FeMal_3Cit_1$ gives way to $FeMal_1Cit_3$ with m/z 869.84 (13.5 min). When the ratio of Mal: Cit is 100: 100, compound of m/z 869.84 is the dominant one. Peaks corresponding to each molecular mass are marked on the **Figure 29B**.

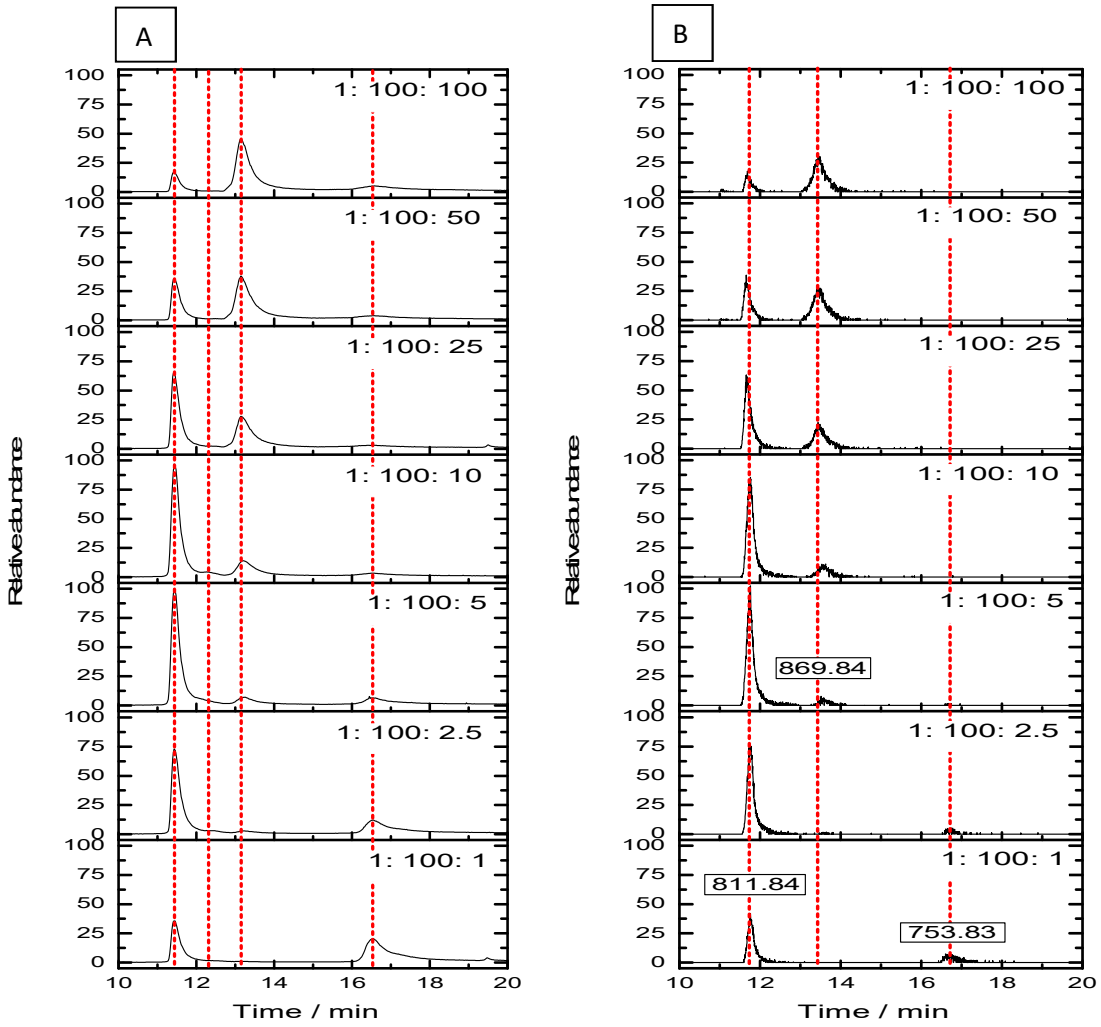

Figure 29. A HILIC ICP MS chromatograms of iron complexes with malate and citrate - different Fe: Mal: Cit ratios, B HILIC ESI MS chromatograms of iron complexes with malate and citrate - different Fe: Mal: Cit ratios. Column used: Column Phenomenex Kinetex (150 x 2.1 mm), 2.6 µm, column temperature: 20°C

To check the stability of the prepared complexes HILIC ICP MS chromatograms were recorded after different durations of time after the preparation of model complexes, to see if any changes take place in iron speciation. **Figure 30** shows no significant changes observed between 24h and 90h after mixture preparation when the experiment was conduct which means that once the complexes are formed in the mixture they are maintained stable with time.

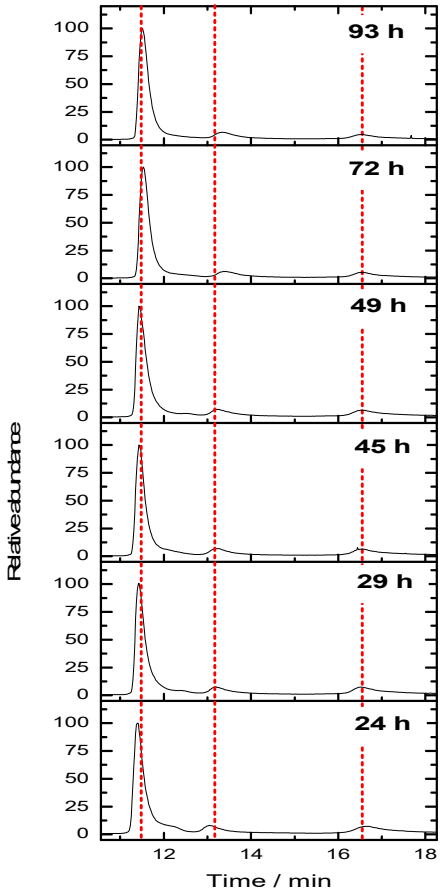

Figure 30. HILIC ICP MS chromatograms of Fe: Mal: Cit complex (1: 100: 5) as a function of time elapsed since sample preparation. Column Phenomenex Kinetex (150 x 2.1 mm), 2.6 µm, column temperature: 20°C

In the aim of getting the best separation of compounds the method used for chromatographic separation should be optimized. The study was done on a phenomenex kinetex column (150 x 2.1 mm), 2.6 µm by the use of acetonitrile and 25 mM ammonium acetate in H_2O at pH 5.5 as eluents. The methods tested are shown in **Table 14** where each method can differ from the other either by the amount of acetonitrile during gradient elution, the time, during which, compounds are exposed to the mobile phases or the curve used to smoothen the peaks obtained. Methods 1 and 2 differ by the curve used for peak establishment but they present the same gradient for elution. Method 3 and 4 were slowed down of 5 minutes at 85% of acetonitrile and method 5 was the slowest between the 5 methods tested. The results obtained are shown in the chromatograms of **Figure 31**.

Table 14.The optimization of the gradient used for the elution of compounds of interest.

Method 1			Method 2			Method 3			Method 4			Method 5		
Gradient		**curve**	**Gradient**		**curve**	**Gradient**		**curve**	**Gradient**		**curve**	**Gradient**		**curve**
Time min	% ACN		Time min	% ACN		Time min	% ACN		Time min	% ACN		Time min	% ACN	
0-1	95		0-1	95		0-1	95		0-1	95		0-1	95	
												1-5	85	
												5-6	82	
												6-7	81	
		5			7	1-5	85	5	1-5	83	7	7-10	81	5
1-10	80		1-10	80		5-10	80		5-11	80		10-11	80	
10-13.5	80		10-13.5	80		10-13.5	80		11-14.5	80		11-13.5	80	
13.5-17	60		13.5-17	60		13.5-17	60		14.5-17	60		13.5-17	60	
17-21	60		17-21	60		17-21	60		17-21	60		17-21	60	
21.01-30	95		21.01-30	95		21.01-30	95		21.01-30	95		21.01-30	95	

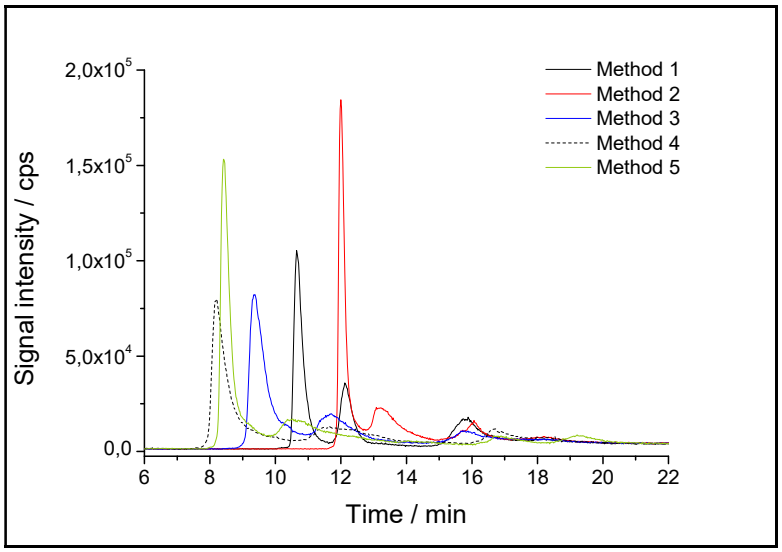

Figure 31. Chromatograms HILIC ICP MS representing counts per second of ^{56}Fe in standard solution of iron citrate and malate at 1:25:5. Conditions were changed from method to another to choose the most suitable method for the compounds separation. Column Phenomenex Kinetex (150 x 2.1 mm), 2.6 µm, column temperature: 20°C.

Figure 31 illustrates different separation methods of mixed iron: malate: citrate complex. Although any of the applied methods gives complete separation of the analyzed mixture of iron complexes with malates and citrates, method 1 was used at a later stage of the study, as it gave the most satisfactory chromatographic results. The first peak is eluted at the retention time 10.6 minutes followed by compounds eluted at 12.1 and 15.8 minutes. This method is shown in the **Table 15** and it was used for further analysis.

Table 15.The optimized conditions for iron citrate malate complexes separation.

Time / min	ACN / %	Curve
0 – 1	95	5
1 – 10	80	5
10 – 13.5	80	5
13.5 – 17	60	5
17 – 21	60	5
21 – 21.01	95	5
21.01 – 30	95	5

The optimized conditions for gradient elution by HPLC separation consist of a gradient elution of 30 minutes starting with 95% of acetonitrile for 1 minute then the % of ACN starts to decrease to 80% and 60% giving place to 25mM ammonium acetate at pH 5.5 helping into the elution of compounds fixed by stationary phase.

4.2 Comprehensive speciation analysis of metal complexes in coconut water as a model for method development for studies of plant endosperm metallome

4.2.1 Introduction:

This part of the project presents the development of an analytical methodology for the characterization of chemical forms of Mn, Fe, Zn Ni, Mo and Cu in liquids circulating in plants. Although xylem was the sample of main interest, the amount of xylem which can be sampled is in low microliters range which make the method development difficult task since it provides a volume for one or two injections maximum. In case the methodology developed doesn't work and needs more optimization there is no more xylem sample for analysis. Thus, as a compromise, coconut (*Cocos nucifera*) water was chosen as a model for method development studies of plant endosperm metallome since it is present in big amounts inside the nut going to 300 ml which provides enough sample for doing several injections helping in improving the methodology developed and studying repeatability.

The cocos nucifera belongs to palmaceae family of palm trees that grows well under tropical climates. It is one of the oldest plants families but also the most evolved; it includes 3000 species and more than 200 sorts. There is around 80 coconut trees varieties that were described in literature presenting a variety of colours and morphologies (green dwarf in Brazil , aromatic green dwarf in Thailand, king coconut in Sri Lanka, orange dwarf in India) [199][200].

The coconut tree (Cocos Nucifera) gives the coconut which is the mature fruit consumed by millions of inhabitants of South Asia , pacific islands and many other countries in Asia, America, Oceania and Africa [199][201]. The coconut fruit reach full maturity after 11-12 months. The inner part of the nut is edible and called endosperm and formed of the white kernel and a clear liquid so called coconut water that should not be confused with coconut milk which is obtained from grating the solid endosperm [199,200,202]. This water is a refreshing drink that remains sterile inside the cavity of the nut; once the nut is opened , its biochemical composition and physical appearance change [203]. In the 6th or 8th month the solid albumen is gradually formed during the hardening of the browning shell, this gelatinous albumen solidifies gradually thanks to the progressive formation of cellulosic membranes. The nut reaches its stage of maturity after 9 months of growth when the water volume begins to decrease [204][205].The presence of natural cytokine nucleotides in this water provides it a crucial anti-ageing role and peptides provide it an anti-microbial, antioxidant and anti-cancer activity [200][206–209]. Furthermore, coconut water is traditionally used as a growth agent in plants culture because it contains phytohormones which regulates plant growth [202].

Coconut water is composed of both organic and inorganic compounds. The main components are soluble sugars as sorbitol, glucose, fructose and it contains also proteins, salts and oil. The second constituent are minerals such as potassium which is the main element in this water [190][203][210]. According to literature, there is a difference in mineral composition due to potassium, chloride, iron and sulfur between immature and mature coconut water. Moreover, coconut water contains amino acids and aromatic compounds that contribute to the aroma of the fresh liquid; thus, organic acids such as malic, succinic, citric, acetic and tartaric acid are responsible of coconut water taste. Among organic acids, malic acid has the largest contribution. The composition and quality of coconut water may be influenced by several factors such as variety and maturity stage of the nut: the maturity of the coconut fruit strongly affects its quality (juice and flesh are sour and over soft in immature fruit, sweet and hard in over-mature fruit). From what was found in literature, there was significant difference in the amount of reducing sugars: in

immature coconut water it constituted 57-98% of total sugars, while in mature one only 25-66%. It should be noted that type and origin of coconut also has a huge impact on those values. pH of mature coconut water vary between 5.2-6.1 and it is a little bit higher than in immature ones (4.8-5.2) [208,210–215].
This composition and quality of coconut water may be influenced by several factors such as variety and maturity stage of the nut: the maturity of the coconut fruit strongly affects its quality. However, the properly mature fruit represent a sweet but slightly sour juice [216]. The most significant change was observed in the volume of the coconut water: as the nut becomes mature, there is an increase in the nut water-holding capacity until the formation of the white jelly inside the cavity of the fruit (9 months) then the volume of water decreases, because it is replaced by fully mature cells[203]. Thus, the volume of coconut water in immature (6-7 months) coconuts differs from 240-553mL while in mature nuts 154-385mL. Moreover, at a given stage of maturity, the biochemical composition of coconut water is slightly influenced by the variety and the environment where the palm was cultivated. In this work, judging the maturity of the coconuts studied and the variety/origin sometimes was difficult because the nuts were purchased from suppliers with no clear information about origins and harvest time of the nut.
Several batches of coconut water were used during this work. All of the coconut samples were randomly selected from four different suppliers in France, Spain and Switzerland. One of the coconuts was harvested directly from the coconut tree in Thailand.

4.2.2 Sample preparation:

Coconut husks were opened by doing an orifice with a drilling machine (**Figure 32**.) perforating the fruit mesocarpe without getting to the albumen to avoid contamination. Coconut water was manually extracted by pipette avoiding the use of any metallic equipment. All coconut water were prepared on the same day of analysis ; This water is ultracentrifuged then rapidly distributed in different eppendorf tubes to be either analyzed immediately or frozen at - 80°C for later analysis. The liquid is difficult to preserve, even in the frozen state and the choice has been made to work with fresh or frozen lots with a shelf life of less than 2 weeks [191][201].

Figure 32. Opening coconut with drilling machine

Different coconuts waters with different stages of maturity were analyzed to identify the metabolite present inside which are responsible of the physiological and biochemical changes and quality deterioration during the post-harvest storage, affecting the flavor and the industrial value [217]. Therefore, by using metabolomics analysis, it was possible to conclude that the most suitable storage life for coconut water should be within a storage period of no more than 4 months [149]. Until I started my project there was no studies or data showing metallometabolomics in coconut water. This idea will be developed in the coming chapter.

4.2.3 Total analysis of metals in coconut water from different origins:

The research on the development of the comprehensive procedure of plant fluids analysis has started with determining the total content of biologically relevant elements in fresh and pre-freezed coconut water. During the studies, 16 coconuts, of different origin and from various suppliers, were analyzed. As coconuts were purchased from different providers, its hard to define the stage of maturity of fruits, which affects the biochemical composition of coconut water, together with environmental conditions of palm cultivation. The analysis of the results gathered for all coconuts in **Figure 33** showed that among evaluated elements the highest contents were recorded for manganese. In two of the samples tested, significantly higher concentrations of iron and zinc were also found: LK coconuts represent coconuts from Sri Lanka which 4 coconuts were opened and its water was analyzed, CI represent ivory coast coconuts CR refers to costa rica coconut and TH represent coconuts from Thailand. The highest amount of Fe was obtained in LK4 going to around 7 ppm and ~3 ppm of Zn were found in the CR variety. Ni and Cu were at the level of 1 ppm in CR and CI. One of the reasons for variations in the content of elements in the analyzed matrix is the big difference in the volume of the solution obtained from each coconut/seed. As previously stated, the volume of liquid is dependent not only on the coconut size but also on the level of fruit/seed maturity as well as the nut's origin.

As it was described in the experimental section, part of the liquid collected from the coconut was immediately ultracentrifuged at 80000xg for 30 mins at 4°C. This step made it possible to isolate the suspended fraction from the coconut water. The results obtained by ICP MS indicate, that in most cases, no statistically significant differences in the total content of Mn, Fe and Ni in the ultracentrifuged and non-ultracentrifuged fresh samples were found. Though slightly higher concentrations were noted for non-ultracentrifuged samples, as predicted. Surprising results were obtained when samples beforehand stored at -80°C were subjected to ultracentrifugation (**Figure 34**). For some samples, the increase of elements content was observed after ultracentrifugation of thawed samples. It might be explained by the cells explosion after freezing-unfreezing step and releasing metals that was retained inside the cells constituting suspended fraction.

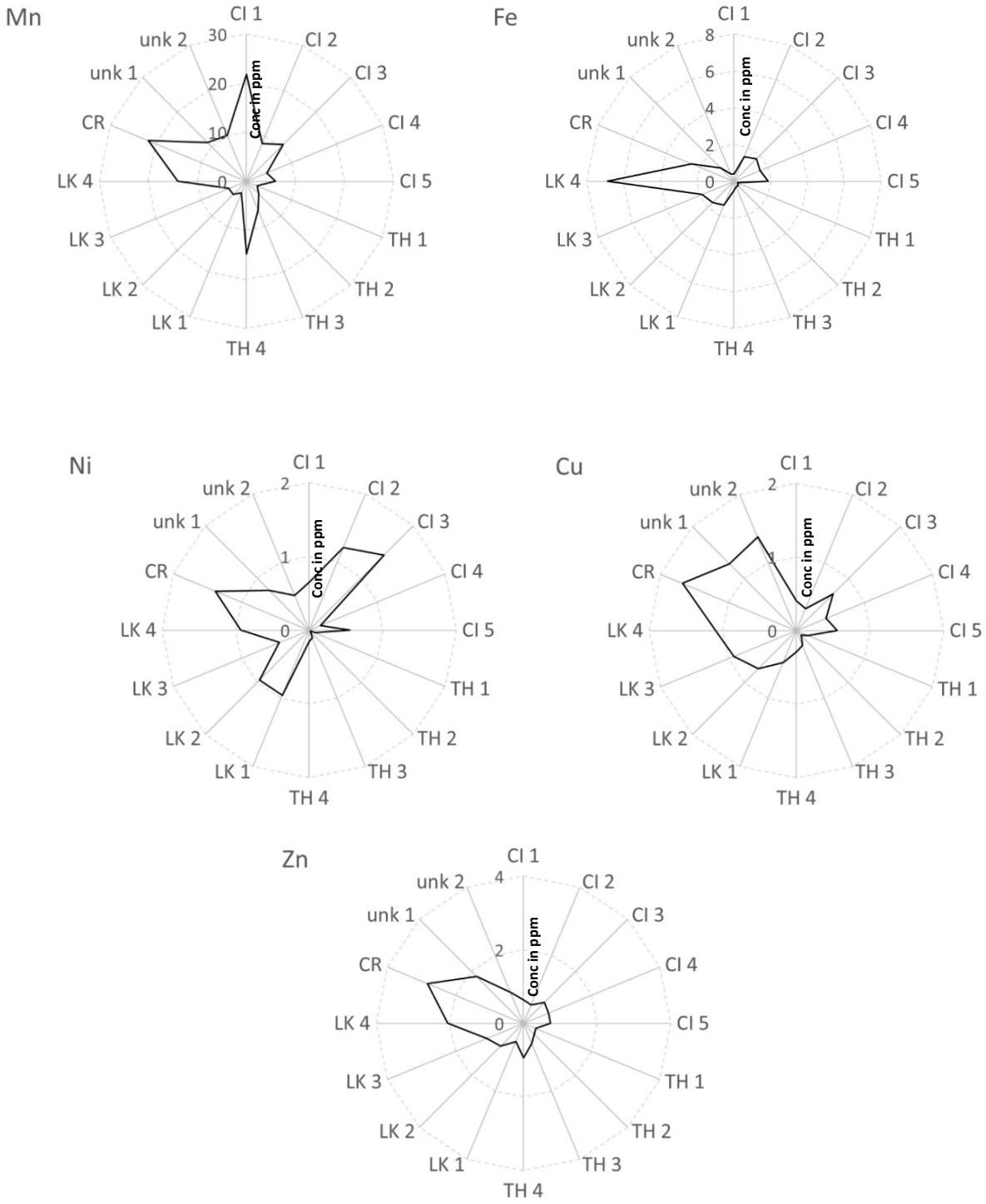

Figure 33. Spider graphs of Fe, Mn, Ni, Cu and Zn in different coconut water samples. CI - Ivory Coast; TH – Thailand; LK – Sri Lanka; CR -Costa Rica; unk – unknown origin.

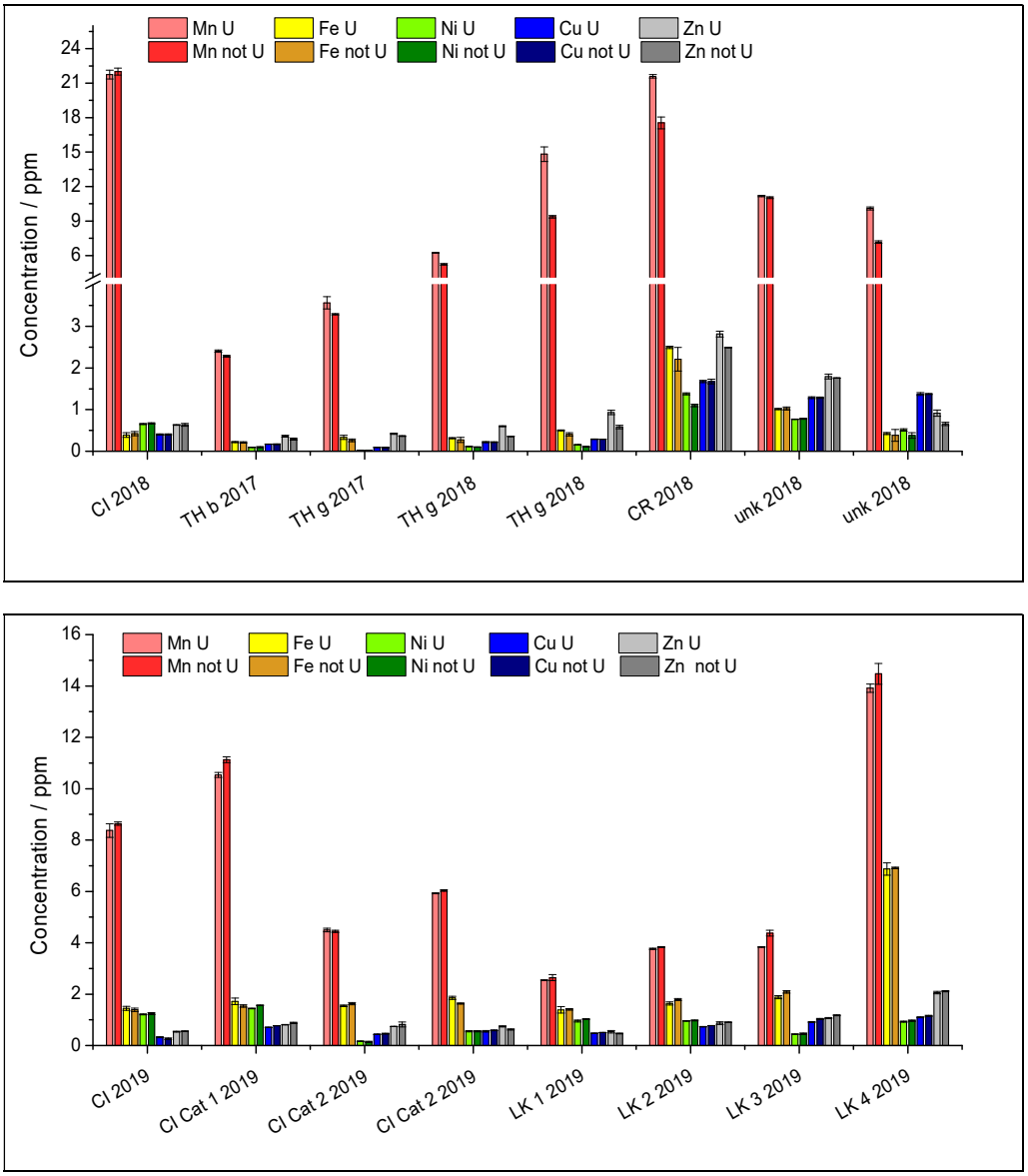

Figure 34. Total contents of metals in samples of coconut water, before and after ultracentrifugation. CI – Ivory Coast; LK – Srilanka; TH -Thailand; CR - Costa Rica; unk – unknown origin.

Ultracentrifugation is a vital step in sample pre-treatment procedure, as it allows the removal of the particles present in the coconut water and purify it as much as possible before further analysis when undigested samples are injected into the chromatographic columns and ionization sources. As ultracentrifugation before sample's storage has a negligible influence on the metals concentration it should be applied on the fresh samples to remove all particles and avoid possible deposits in sample introduction systems.

4.2.4 Metal-Low Molecular Weight complexes separation by SEC coupled to ICP MS:

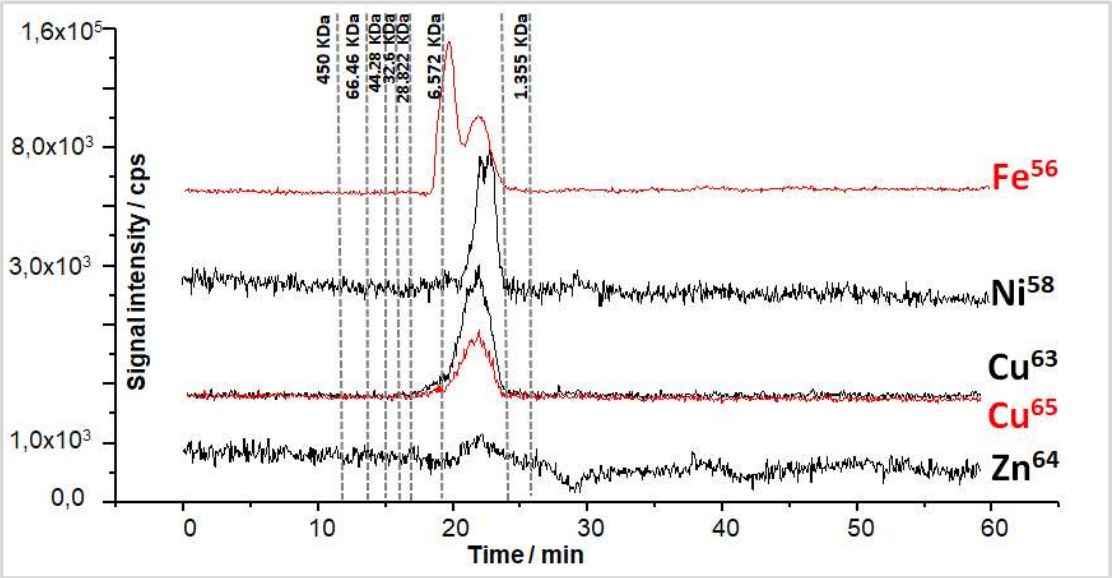

Figure 35. SEC ICP MS Chromatograms showing species of metals of interest. Conditions: isocratic elution mode 0-60 min 100% B (100mM ammonium acetate in H_2O pH 7.5) Vinj 100µl and flow rate 0.7ml/min.

Figure 35 shows chromatograms consisting of 2 peaks for Fe representing two species of different masses, and one peak for the other elements such as Cu Ni and Zn representing one set of species with the same mass range.

- *Effect of ultracentrifugation before sample's storage on the metal speciation by SEC ICP MS in coconut water:*

As it was stated in previous chapter, concerning total elements analysis, carried out after freezing-unfreezing process, a hypothesis was elaborated that the elements might be released due to cell wall cracking. Nevertheless it was proven, that ultracentrifugation of fresh coconut water samples does not affect the total metal content. The next step was to check whether ultracentrifugation is negligible also from the point of view of speciation analysis. In the next step we compared the profiles recorded for one of the coconut waters after separation by SEC for samples prepared with and without ultracentrifugation 80000xg for 30 mins.

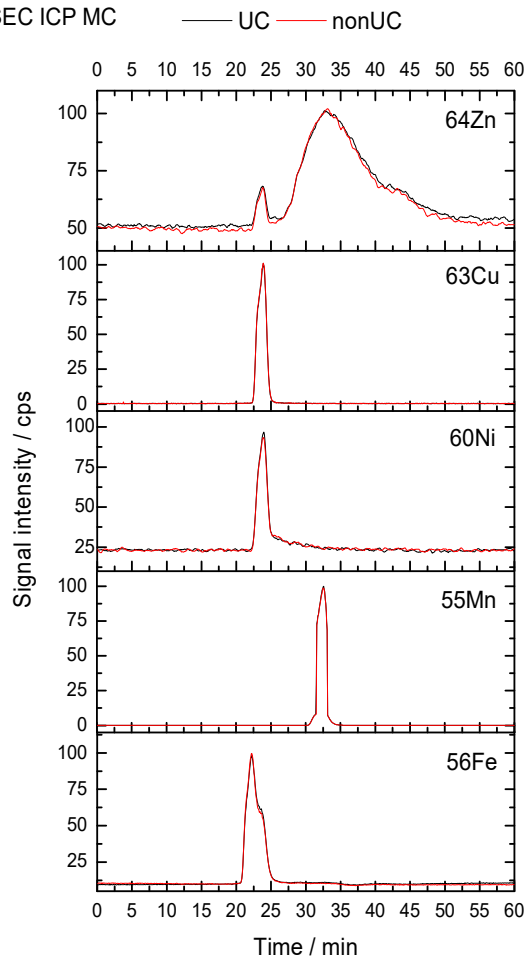

Figure 36. The comparison of SEC chromatograms of samples prepared after or without ultracentrifugation.

Figure 36 shows no significant changes in the peaks intensities of all recorded signals, which allows to apply ultracentrifugation to sample preparation procedure without any restrictions.

- *Effect of storage temperature and ascorbic acid addition on metals speciation by SEC ICP MS:*

Numerous studies show that coconut water remains sterile inside the cavity of the nut but once the nut is opened, its biochemical composition and physical appearance change. To find optimal conditions of sample preservation before speciation analysis we applied different storage temperatures. Additionally the influence of the ascorbic acid presence was evaluated. After a week of storage samples were analyzed by SEC ICP MS. Only slight differences in signal intensities were noted between sample stored in -80°C, +4°C and ambient temperature (**Figure 37**). However, the signal obtained for sample from ambient temperature was the lowest, hence, to maintain speciation, it is necessary to store samples at low temperature.

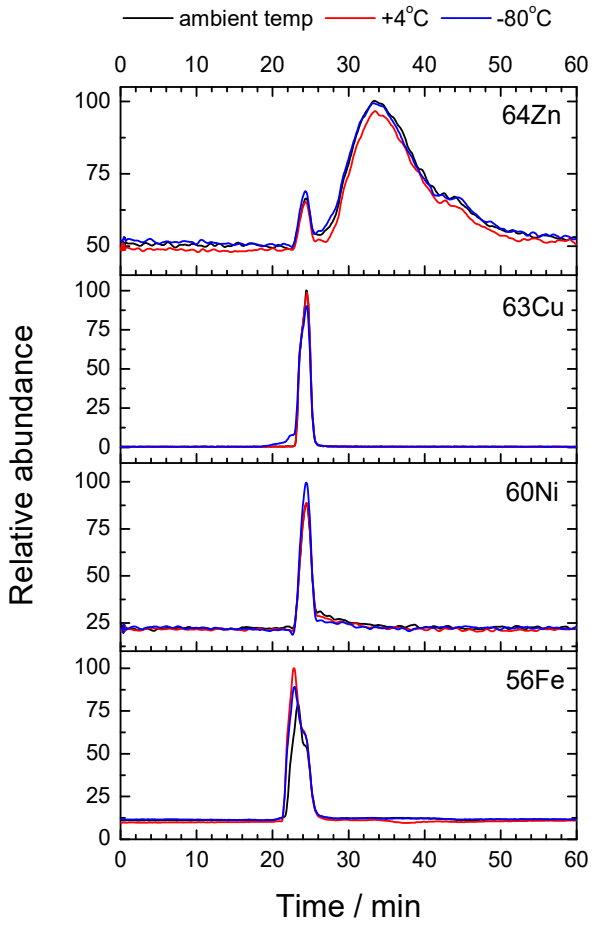

Figure 37. Comparison of SEC separation of samples stored in different temperature conditions.

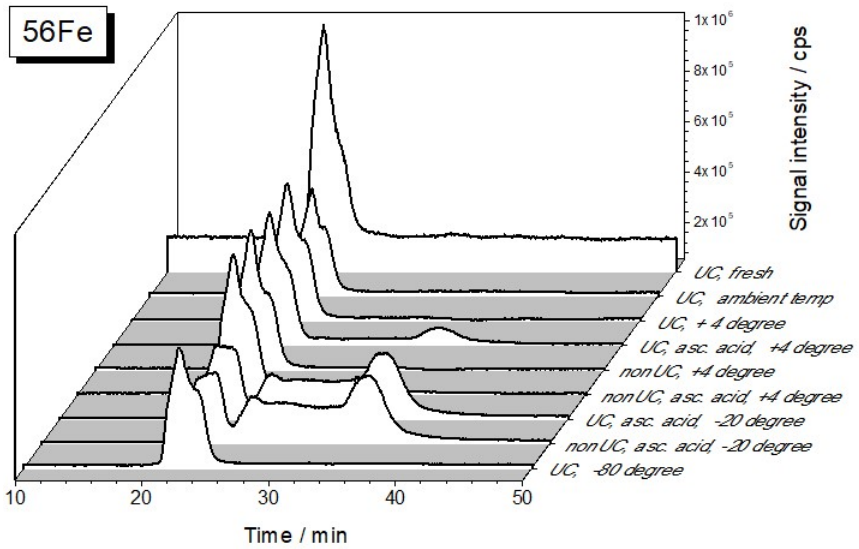

Figure 38. Comparison of SEC separation of samples stored in different temperature conditions and with or without ascorbic acid.

From **Figure 38** it is obvious that the addition of ascorbic acid caused the appearance of new signals at retention times corresponding to the lower masses. This effect was to a much lesser extent observed for samples stored at +4°C, while a number of new signals for ^{56}Fe were recorded at a subzero temperature, with a decrease in the intensity of peak at 22 min. The effect is related to the reducing properties of

ascorbic acid and possible redox reaction between AA and Fe(III), even in pH 5-6, which is typical for coconut water, and formation of ferrous-ascorbate complexes. It was already observed this reducing agent is responsible for the reduction of Fe(III) in mixed citrate-malate complexes by embryos efflux of *Pisum sativum.* Ascorbic acid does not influence the speciation of other metals in the same degree. After comparing HILIC chromatograms for the same samples we can see that for all four elements only differences in peaks intensity were recorded. For ^{56}Fe, the signal reduction of half of the height was observed. For ^{63}Cu, in the presence of ascorbic acid, a signal reduction with a retention time of 15 minutes was observed with a simultaneous increase in the signal around 5 min.

- *Effect of Acetonitrile addition on the separation chromatographic profile:*

Additionally, the addition of ACN was examined to see its influence on the species separation, as this step is required before samples analysis by HILIC and their further analysis by ESI MS. SEC-ICP MS chromatogram in **Figure 39** confirms the removal of the HMW molecules-bound to iron fraction upon the addition of acetonitrile. The addition of ACN removes high molecular weight complexes of iron and allows targeting low molecular Fe species only; the effect of ACN on HMW removal can be seen in the UV spectrum below: when ACN was not added we obtained 2 peaks representing species of iron, but once ACN was added, the first peak obtained at around 20 minutes disappeared and in the UV spectrum the corresponding peak with small intensity representing HMW (proteins) disappeared.

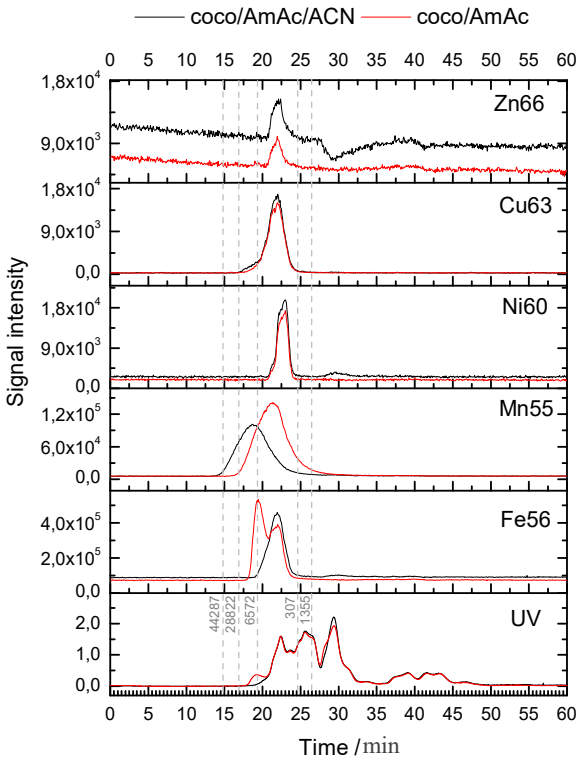

Figure 39. Chromatogram SEC ICP MS showing metals of interest after analysis on superdex 75 10/300 GL column before and after addition of Acetonitrile prior analysis. UV spectrum of proteins present in the sample.

After conducting all the experiments, it was decided that the samples will be stored, after prior ultracentrifugation, at -80°C. Such conditions do not significantly affect the metal's speciation. In the same time, the stability of coconut water is guaranteed for longer period of time. However, if possible, it is recommended to analyze fresh samples.

4.2.5 Separation of metals complexes present in coconut water by HILIC ICP MS

Sample preparation is an important step to avoid sample's loss and to preserve it as much as possible from contamination; it is important also to reduce the matrix effect that may induce formation of interferences that can influences the metals speciation. At the beginning the coconut water was ultracentrifuged then diluted in initial conditions of mobile phase of the gradient used for elution: so coconut water was added to a mixture of 95% B (acetonitrile) and 5% A (25mM ammonium acetate in H_2O at pH 5.5) in the eppendorf tube vortexed for 30 seconds and then centrifuged for 5 minutes at 10000 RPM. To the naked eye, there was formation of two phases other than the pellet formed after centrifugation. Further experiments have shown that to avoid this it is necessary to dilute sample with 25mM ammonium acetate at least two times before mixing it with ACN. Dilution factor depend from the iron complexes concentration and vary from sample to sample.

The conditions of sample preparation were optimized and the final are presented in the **Table 16** below: 25-250 µL of the sample were mixed with ammonium acetate pH 5.5 up to 500 µL and vortexed for 30 seconds. Then 500 µL of acetonitrile was added to the mixture which was vortexed and then centrifuged for 5 minutes at 10000 RPM.

Table 16. The condition of coconut water preparation before HILIC separation

Sample	Sample / µL	25 mM AmAc / µL	ACN / µL
Coconut water	25-250	475-250	500

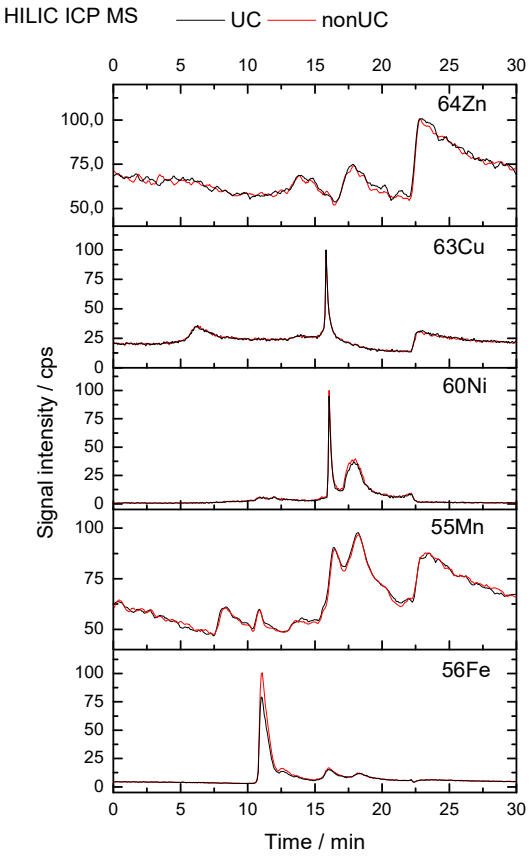

Figure 40. Separation of metal species in samples prepared with and without ultracentrifugation. The chromatograms were obtained using Phenomenex Kinetex column after injection of 10 µL of the sample and gradient elution with 5 mmol L^{-1} ammonium acetate (pH 5.5) and acetonitrile (ACN) mixtures; flow rate of 0.5 mL min^{-1}.

The chromatograms obtained for several elements for one of the coconut waters were presented on **Figure 40**. Once again samples with and without ultracentrifugation were compared. The chromatograms

recorded for ^{56}Fe show an intensive signal at the retention time around 11.1 min and three less intensive peaks at around 12.6, 16.0 and 18.4 min. Sample premixing with ammonium acetate at pH 5.5 not only dilute the matrix but also helps in maintaining pH at around 5.5 to try avoiding complexes degradation.

Final conditions of sample preparation and storage described above were applied to compare the speciation of iron, nickel, manganese and copper in 8 coconut water samples. All samples were opened and analyzed in the same day, after prior ultracentrifugation. It was noticed that all of the samples, irrespectively of the fruit origin and maturity, were characterized by similar chromatographic profiles for all elements (**Figure 41**). According to the total element concentration the signal intensity of registered peaks were different with a maximum intensity observed for one of the coconuts from SriLanka (LK4 coconut 16).

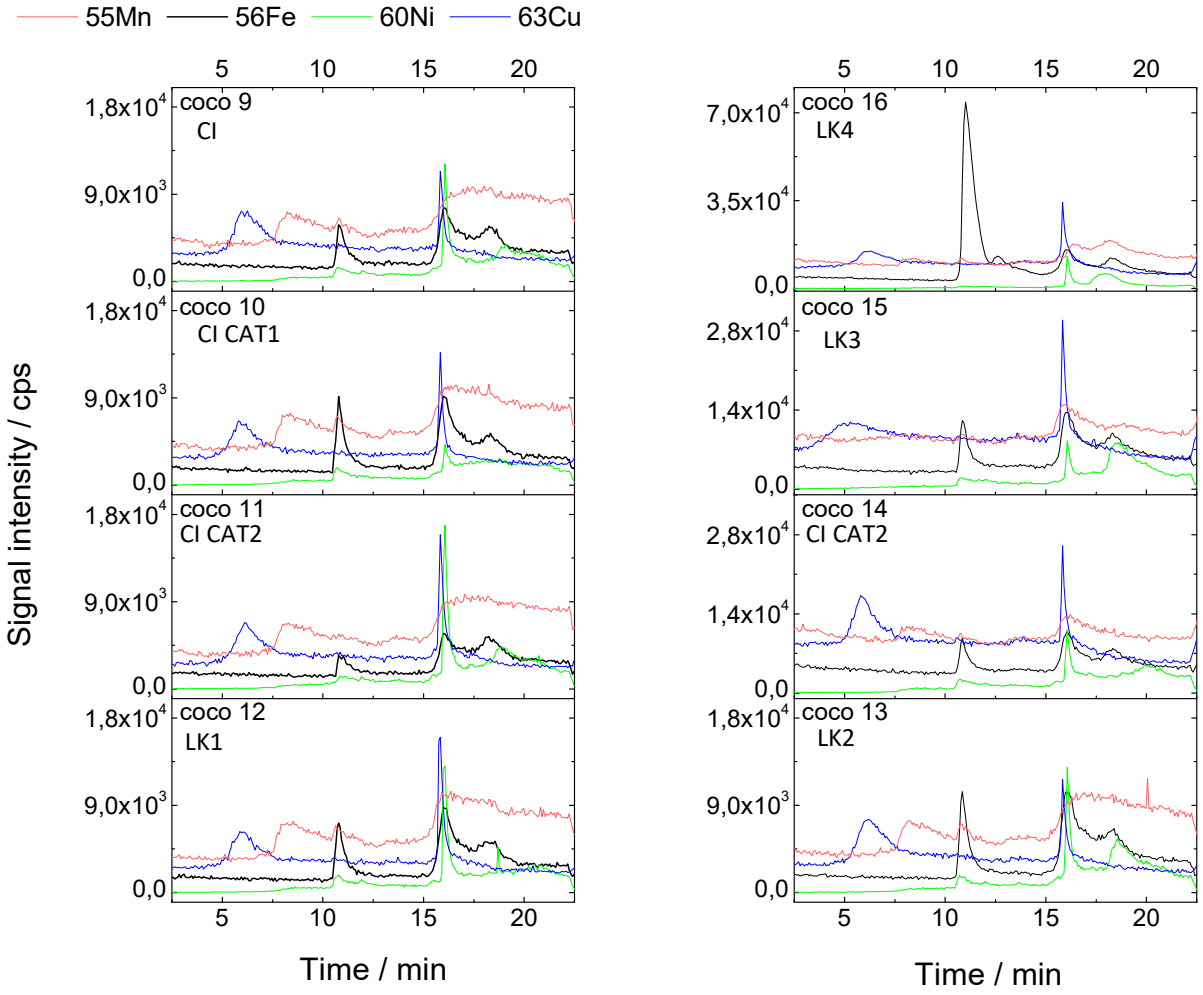

Figure 41. HILIC chromatograms of fresh coconut water samples.

4.2.6 Identification of metals complexes formed in coconut water samples by HILIC ESI MS:

For further analysis, the coconut water used was CI coconut: **Figure 42**. Below shows one intensive peaks and 2 peaks with very low intensity representing Cu complexes at around 16 minutes and 6-11 minutes, 2 peaks representing Ni complexes at 8 and 16 minutes respectively, and 4 peaks representing Fe complexes at 11, 12.5, 16 and 18 minutes. Signal representing Zinc complexes is low compared to signals for other metals.

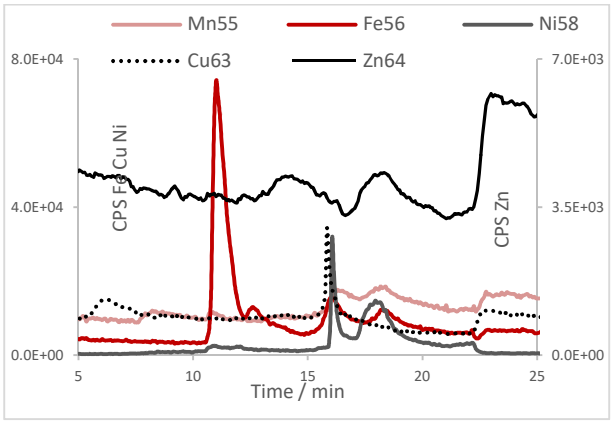

Figure 42. Chromatograms obtained by HILIC ICP MS representing all metals complexes preset in coconut water. Conditions: gradient of method 1, flow rate: 0.5 ml/min, injection volume: 10µl, column Phenomenex Kinetex (150 x 2.1 mm), 2.6 µm, column temperature: 20°C.

These complexes were identified by HILIC coupled to Q-exactive ESI MS. The list of predicted complexes present in xylem and ESL of peas was given by Flis et al [34]: these complexes were predicted to be found in coconut water since it has similar characteristics of plant liquids. Results obtained for the identification of these different peaks are given below; the main iron containing peak was attributed to a complex of a m/z 811.84, which includes in its structure three atoms of iron bound to two molecules of citrate and malate. In addition to above mentioned, in the coconut water there was also a compound of a similar structure, but carrying three molecules of citrate and one malate. Two peaks for iron species, corresponding to $(Fe(III)_3Cit_2Mal_2)$ and $(Fe(III)_3Cit_3Mal_1)$ were already obtained, after separation on TSK gel amide 80 HILIC column by Grillet et al. in a liquid endosperm of pea [66]. Additionally, we identified iron complexes with some amino acids - glutamine and aspartic acid: based on literature study, Fe(III) $(Gln)_2$ was detected also in xylem and ESL of pea plants after separation on zwitterionic hydrophilic interaction stationary phase (ZIC-HILIC)[31]. Additionally, Lopez-Milan et al. studied the effect of iron deficiency on the release of amino acids such as Gln in the apoplastic fluid of sugar beet; it was shown that the amount of Gln doesn't change importantly when there is Fe deficiency but it can play a role in Fe transport [75]. Moreover, Fe (II) NA was identified in the endosperm of coconut; this complex was referred to the literature study where this same complex was identified in the ESL of pea plants but not in its xylem by Flis et al. using TSK gel amide 80 HILIC column [36], in grain samples from wheat cultivars by using SEC column (Superdex 75 10/300 GL size exclusion Column) coupled to ICP MS done by Eagling et al. and Xue et al [41][53]. Thus, Tsednee et al worked on a sensitive LC (HSS T3 column with trifunctional C18 stationary phase) coupled to ESI-QTOF-MS to reveal new phytosiderephores-iron complexes including Fe-NA [163]. Similar complexes were also found for copper and nickel ions with NA: For nickel the most abundant was the complex with nicotianamine recorded by Flis et al in pea xylem and ESL by coupling TSK gel amide 80 as HILIC column to ICP MS [36], Weber et al. in *Arabidopsis Thaliana* by HILIC column such as ZIC-cHILIC–ESI-MS in addition to $Ni(II)(Asp)_2$ [67] and in *Thlaspi caerulescens* by Mari et al by SEC column such as Superdex Peptides HR 10/30 column coupled to ICP MS and ESI MS [64]. In coconut water an intensive peak was recorded also with phenylalanine but in literature there was no detection of this complex in other plants fluids. Similar connections were also important for copper that was found complexed to NA in chicory and tomato detected by Liao et al [189] , in xylem and phloem saps from rice (*Oryza sativa*) detected by CE MS and by Collecting fractions by SEC infused to ESI TOF MS [14] and in *Brassica carinata* by Irtelli et al [52].

The complexes identified for every metal bound to a ligand are grouped in this **Table 17** with their molecular formula, calculated m/z, measured m/z and mass error and presented in chromatograms and spectrum in **Figure 43**:

Table 17. Metal complexes detected by hydrophilic interaction chromatography electrospray ionization mass spectrometry (HILIC-ESI-MS) in liquid endosperm of Cocos nucifera L.

Proposed structure	Molecular formula	Calcutated m/z	Measured m/z	Mass Accuracy m/z [ppm]
$Mal_2Cit_2Fe(III)_3$	$C_{20}H_{20}O_{24}Fe_3$	811,83873	811,83942	0,001
$Gln_2Fe(III)$	$C_{10}H_{18}O_6N_4Fe$	346,05703	346,05743	1,162
$Mal_2Fe(III)$	$C_8H_{10}O_{10}Fe$	321,96179	321,96205	0,808
NAFe	$C_{12}H_{20}O_6N_3Fe$	358,06960	358,07022	1,721
$MalCit_3Fe(III)_3$	$C_{22}H_{22}O_{26}Fe_3$	869,84421	869,84467	0,531
Asp_2Mn	$C_8H_{13}O_8N_2$ Mn	320,00469	320,00461	-0,2
NANi	$C_{12}H_{20}O_6N_3Ni$	360,07001	360,06998	-0,082
Phe_2Ni	$C_{18}H_{21}O_4N_2Ni$	387,08507	387,08475	0,229
Asp_2Ni	$C_8H_{13}O_8N_2Ni$	323,00199	323,00197	-0,061
NACu	$C_{12}H_{20}O_6N_3Cu$	365,06426	365,06430	0,102
Phe_2Cu	$C_{18}H_{21}O_4N_2Cu$	392,07918	392,07862	-1,440
Phe_3Cu	$C_{27}H_{32}O_6N_3Cu$	557,15816	557,15863	0,838

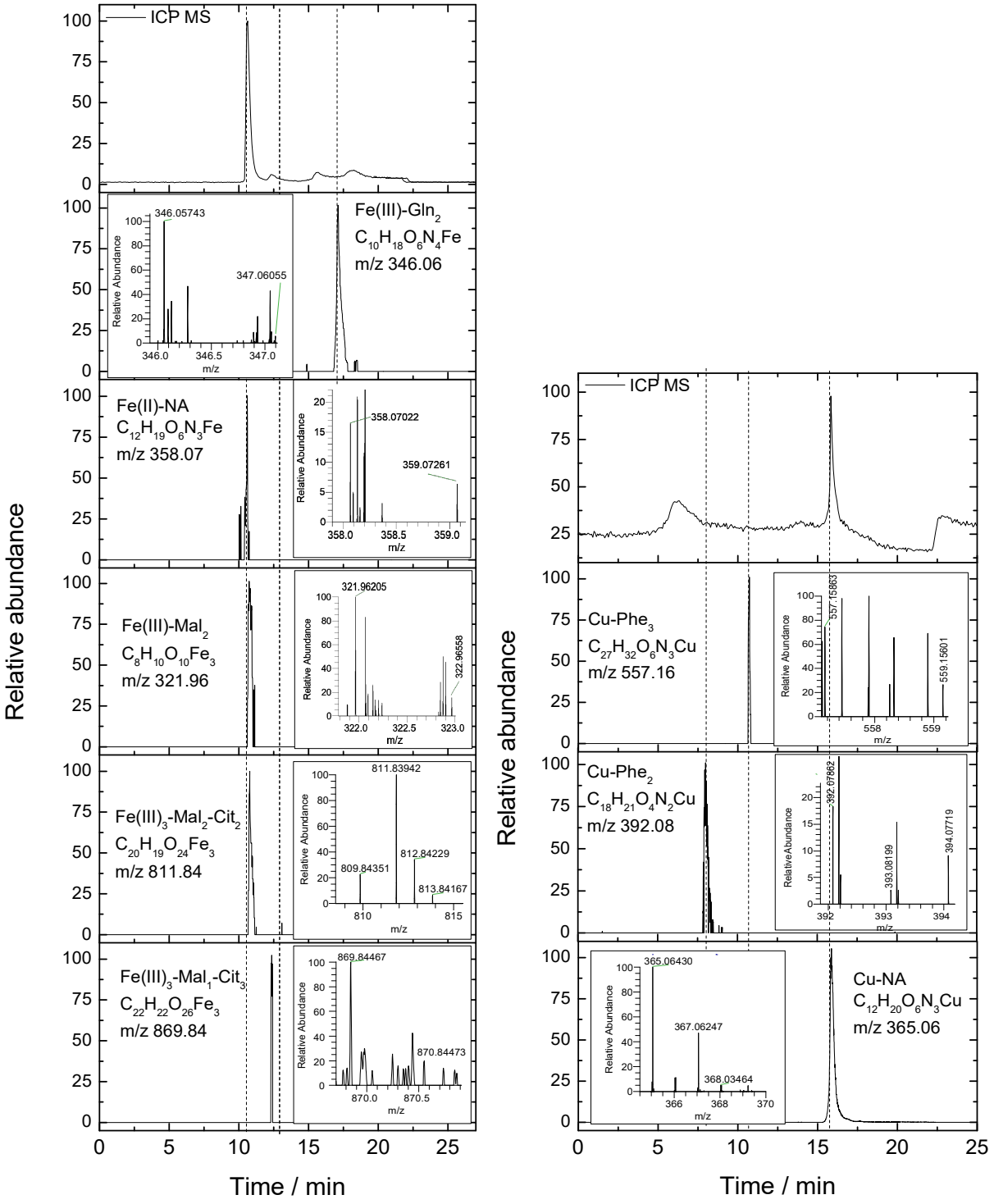
ICP MS
Fe(III)-Gln2
C10H18O6N4Fe
m/z 346.06
346.05743
347.06055
Fe(II)-NA
C12H19O6N3Fe
m/z 358.07
358.07022
359.07261
Fe(III)-Mal2
C8H10O10Fe3
m/z 321.96
321.96205
322.96558
Fe(III)3-Mal2-Cit2
C20H19O24Fe3
m/z 811.84
811.83942
809.84351
812.84229
813.84167
Fe(III)3-Mal1-Cit3
C22H22O26Fe3
m/z 869.84
869.84467
870.84473
Relative abundance
Relative Abundance
m/z
Time / min
ICP MS
Cu-Phe3
C27H32O6N3Cu
m/z 557.16
557.15863
559.15601
Cu-Phe2
C18H21O4N2Cu
m/z 392.08
392.07862
393.08199
394.07719
Cu-NA
C12H20O6N3Cu
m/z 365.06
365.06430
367.06247
368.03464
Relative abundance
Time / min

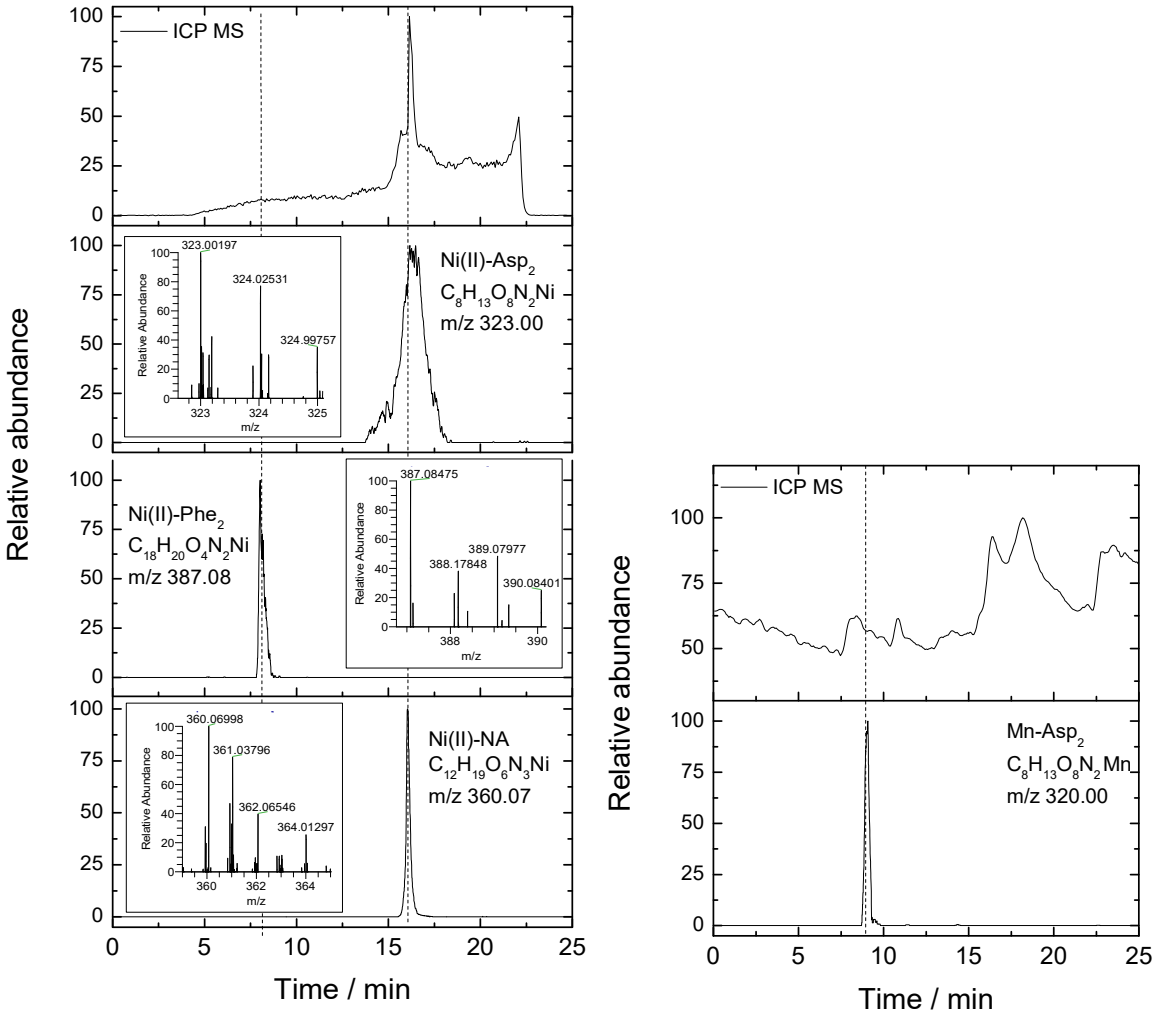

Figure 43. Identification by HILIC-ICP-MS and HILIC-ESI-MS of iron, copper, nickel and manganese species in coconut water. HILIC-ICP-MS chromatogram and extracted ion chromatograms of species identified.

The presence of every metal in these complexes was confirmed by the comparison of the isotopic pattern of this metal in the complex to its theoretical isotopic pattern as well as by MS/MS as proof for identity by identifying the charged molecules obtained after fragmentation. An example of isotopic patterns metals involved in $Fe_3Mal_2Cit_2$, CuNA and NiNA as well as spectrum representing fragmentation of ($Fe(III)_3Cit_1Mal_3$) are presented in **Figures 44** and **45**.

From MS/MS spectra, the fragments $[M\text{-}Cit]^+$ and $[M\text{-}Mal]^+$ were detected and these fragments should contain Fe so as proof of identity the isotopical pattern of Fe_3 involved in these fragments was searched and compared to the theoretical isotopical pattern of Fe_3: the fragment $[M\text{-}Mal]^+$ was shown as example of compatibility between the theoretical isotopical patterns obtained shown in spectra 1 and the experimental isotopical patterns of Fe3 involved in the fragment 616.9583 m/z shown in spectra 2.

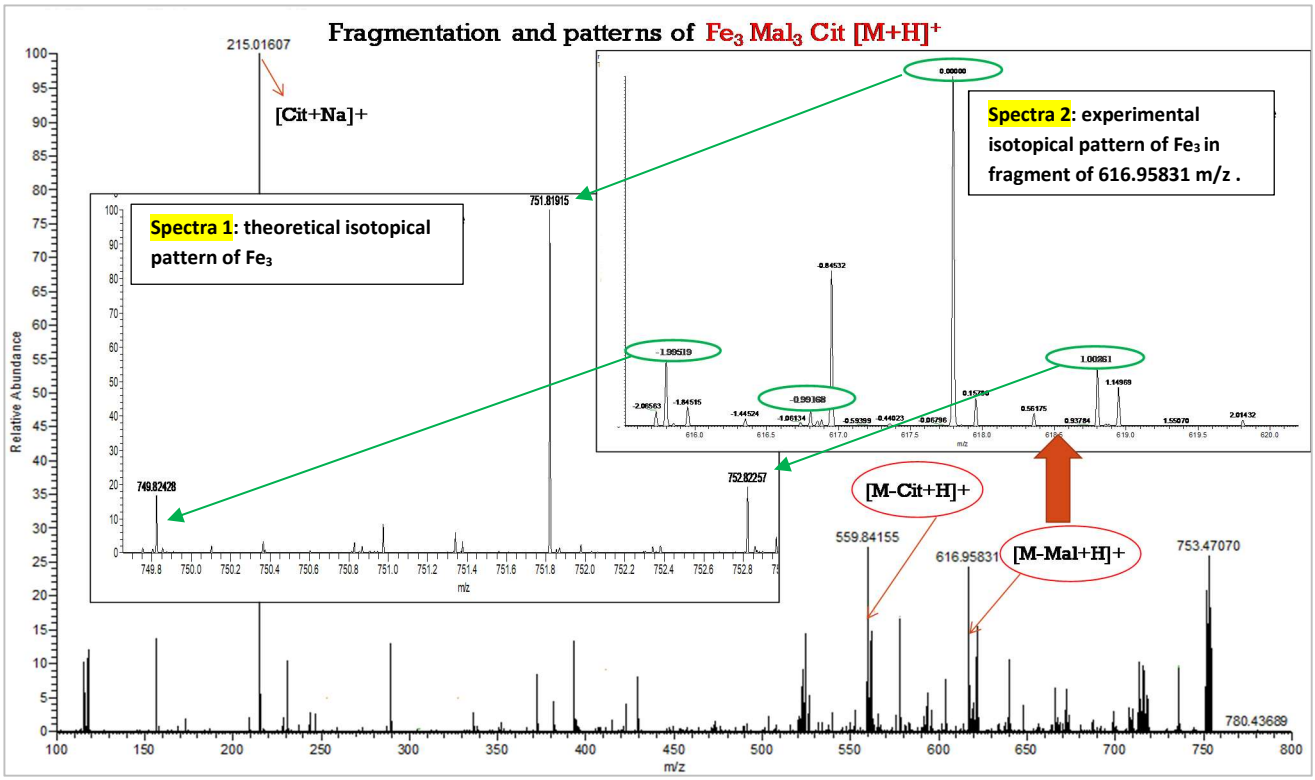

Figure 44. Proof of identity: Identification of complexes of iron by HILIC – MS/MS.

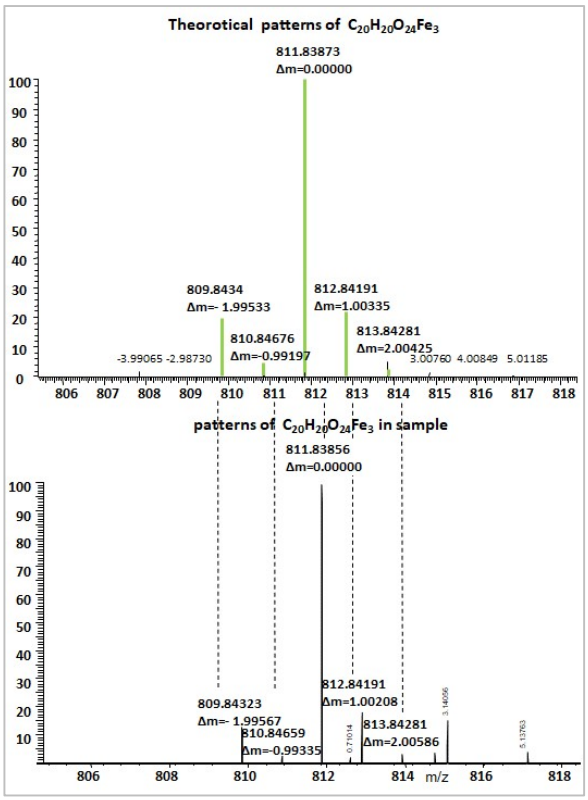

(1)

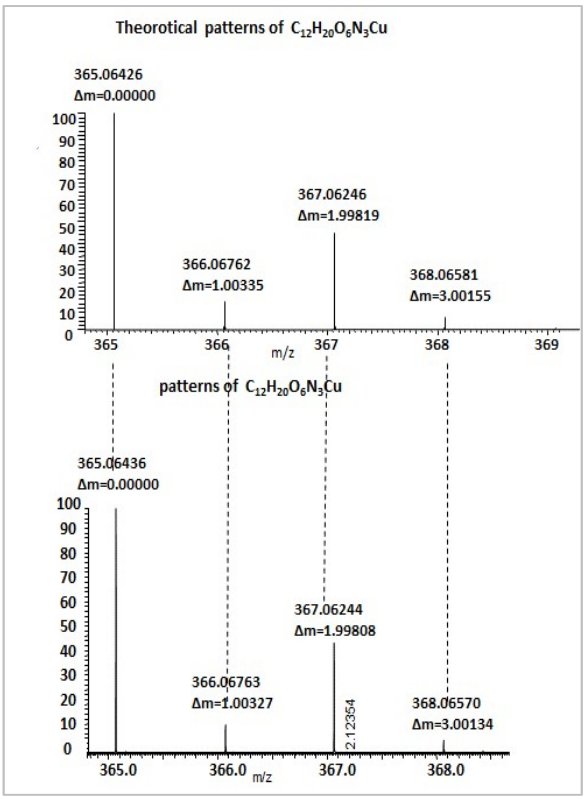

(2)

(3)

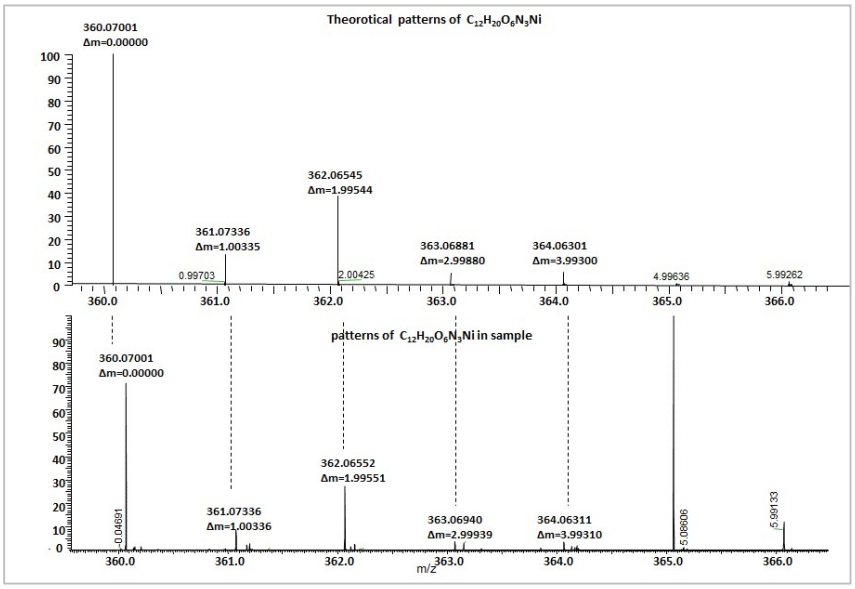

Figure 45. *Experimental isotopical patterns* of metals involved in complexes in *coconut water compared to theoretical isotopical pattern. (1) isotopical pattern for* $C_{20}H_{20}O_{24}Fe_3$, (2) *isotopical pattern for* $C_{12}H_{20}O_6N_3Cu$, *(3) isotopical pattern for* $C_{12}H_{20}O_6N_3Ni$.

4.3 In-situ isotopic dilution for quantitative speciation of iron complexes in coconut water by MS

In the previous chapter, the attention was focus on the identification of different metal species in coconut water and its proper preparation before each step of analysis. It was shown that among all element studied, iron compounds gave the most intensive signals. Also for iron, the greatest variety of complexes were identified by HILIC ESI MS. In this part a quantitative speciation method, developed to determine the amount of iron involved in the complexes formed in the coconut water is described. As it was previously highlighted, coconut water was used as a model research sample because its composition is similar to essential plant fluids but the volume of the sample is much higher. It make coconut water ideal candidate to conduct studies aimed at the development and optimization of new analytical methods. Samples of interest in which the quantitative speciation analysis should be applied, as xylem saps or embryo sac fluid of common plants are extracted in sub microliters volume, so direct method development is not possible. Quantitative speciation analysis face several problems, which may make it very complicated task. First of all, we should take into consideration the variation in the sample matrix and the presence of metal-containing compounds in different biological samples. It was already shown that even between samples belonging to the same family, as *Cocos nucifera* L., different results concerning the presence and ratio of the individual complexes may be obtained. This is due to the concentration and proportion between an element of interest and specific ligands, which is particularly important in mixed complexes. In one of the previous chapters it was shown that special attention should be paid to the equilibria of complex creation in the solution. We cannot forget also about the on-column phenomenas, which may take place. A risk of on-column dissociation and Fe (II) oxidation is possible on column. It may cause column's contamination, poorly reproducible retention times and lead to systematic errors in the analysis of plant samples.

A quite innovated method was found to avoid on-column precipitation and changes in speciation during chromatography when standard is added. The method relies on the in-situ formation of isotopically labelled species of iron, as a result of the addition of ionic Fe isotope to a sample. The prerequisite is the complete reaction of the added spike which can be readily verified by HPLC-ICP MS. Knowing that iron has 4 natural isotopes: ^{54}Fe, ^{56}Fe, ^{57}Fe and ^{58}Fe with natural relative abundance of 5.85, 91.75, 2.12 and 0.28%, respectively, multiple possibilities to isotope dilution quantification of specific Fe-containing molecules are appearing. Nevertheless, it must be assured that enriched iron-labelled standards are available and that iron is not exchanged with other ligands present in the sample. The **Figure 46** shows that different plant fluids contain considerable excess of free ligands such as citrate or malate.

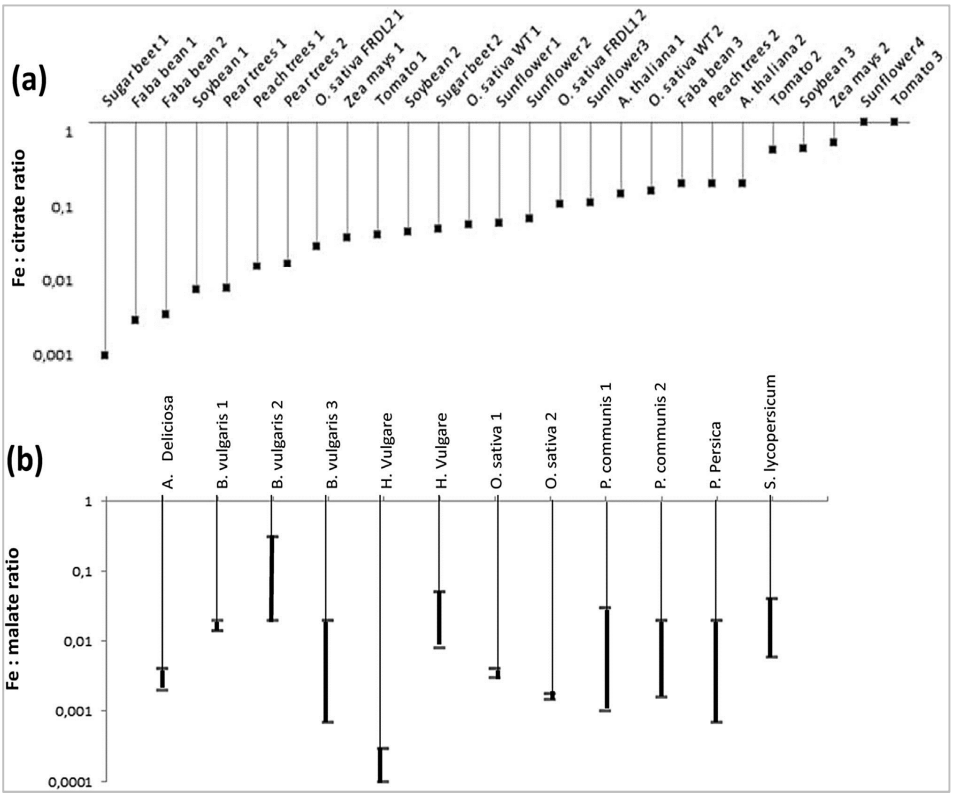

Figure 46. Fe: citrate (a) and Fe: malate (b) ratios in plant sap samples reported in the literature [31].

It has been already shown that coconut water contains mainly mixed iron citrate malate complexes and the check of chromatographic profiles led to an assumtion that malates dominates in the matrix. The purpose of the next step of the study was to see the behaviour of iron species in the medium after addition of a spike. Aside from use for quantification purposes, the enrichment of ^{58}Fe can change the isotopical patterns of Fe to facilitate detection in ESI MS, which is difficult due to the low abundance of its isotopes such as ^{57}Fe and ^{58}Fe. The results obtained were presented in chromatograms showing the influence of such addition to the sample on the peaks intensity and the possibility of apparition of other peaks as well as the identification of these species obtained by ESI MS.

Addition of ^{58}Fe to coconut water

The first attempt to quantify iron complexes in coconut water samples started with spiking of the sample with two concentration of ^{58}Fe. The proportions of sample to other solutions used were collected in **Table 18**. Fresh, ultracentrifuged coconut water sample was mixed with ammonium acetate, then ^{58}Fe was added. All substrates were mixed and finally ACN was introduced. Solution was mixed again and centrifuged. The results obtained for samples prepared in that way were shown on **Figure 47**.

Table 18. Sample preparation with the addition of spike ^{58}Fe at different concentrations.

	Sample	Sample / µL	25 mM AmAc / µL	ACN / µL	^{58}Fe / µL	Initial C ^{58}Fe ppm
Coconut water – Coco A	Coconut - Cl	250	250	500	0	1
+ 20ppb ^{58}Fe		250	230	500	20	
+ 40ppb ^{58}Fe		250	210	500	40	
+ 50ppb ^{58}Fe	Coco A	400			5	10
+ 100ppb ^{58}Fe	Coco A	400			10	

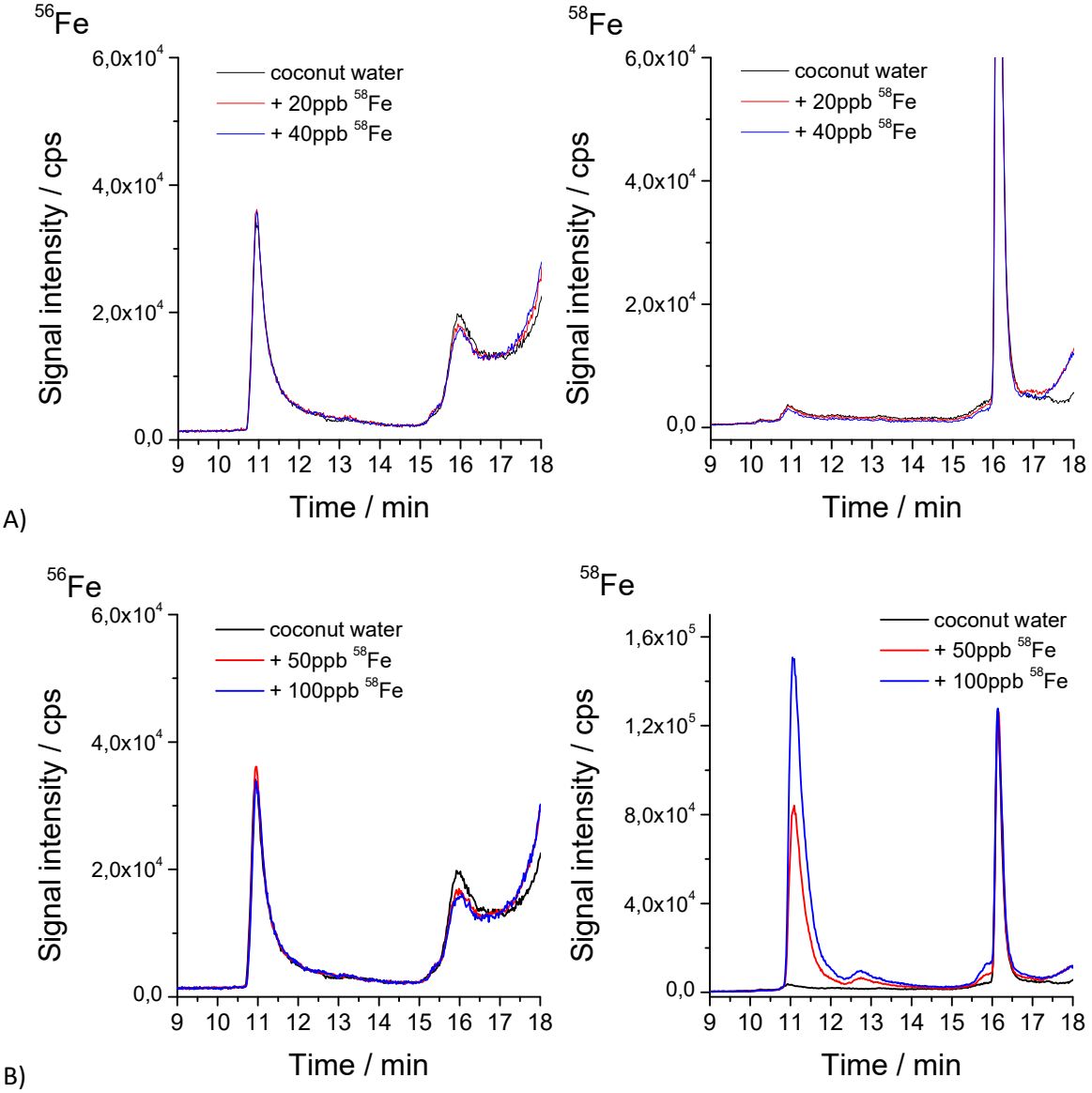

Figure 47. HILIC ICP MS chromatograms for two iron isotopes, ^{56}Fe and ^{58}Fe in coconut water sample with addition of ^{58}Fe. The spikes were made before (A) or after (B) addition of ACN.

After addition of ^{58}Fe to coconut water no significant changes were observed in the signal intensity recorded for ^{56}Fe isotope, occuring naturally in the analysed sample. At the same time no changes were observed also for sample enriched with ^{58}Fe (**Figure 47-A**). According to these results it was concluded that iron added to the sample was bound to high molecular weight compounds present in raw sample. To prove that, spike with ^{58}Fe was done on the sample previously mixed with ACN (coco A). **Figure 47-B** shown increase in the signals of ^{58}Fe, with retension times similar to those recorded to ^{56}Fe. According to these experiments it was clearly shown that ^{58}Fe standard addition need to be carried out after removal of high weight molecular fraction using ACN.

The formation of isotopically labelled complexes has been confirmed by HILIC coupled to ESI MS. **Figure 48** shows the differences in peaks abundance representing the complexes $Fe_3Cit_2Mal_2$ after addition of ^{58}Fe. On the upper spectrum only m/z corresponding to iron complex can be observed – 811.84. On the sample spiked with 100ppb of ^{58}Fe, isotopically labelled species can be also observed at m/z 817.84. With

increasing concentration of ^{58}Fe in coconut water sample, further changes in relative intensity of molecular ions of 811.84 and 817.83 can be noticed. The first m/z corresponds to the molecular ion containing 3 atoms of ^{56}Fe, which is naturally present in the sample. The second one corresponds to the compound subsequently created from the excess of ligands in the sample and the isotopically enriched ^{58}Fe added to reach m/z of 817.83. In conclusion, the results obtained permits to say that coconut water contains free ligands such as citrate and malate in a suffiescient quantity to complexe with ^{58}Fe and form the same but ^{58}Fe labelled complexes as the one formed with ^{56}Fe.

As it was proven, with increasing concentration of ^{58}Fe added to coconut water sample, increasing signal intensity of individual iron species is observed, in the next step special attention was paid to the rate of the formation of particular complexes in the presence of sample matrix. To study that, coconut water samples with 0-200ppb concentration of ^{58}Fe were prepared (**Table 19**). All five samples were injected on HILIC column in five replicates, each with 2.5h difference.

Table 19. Sample preparation with spike addition.

	Sample	Sample / µL	25 mM AmAc / µL	ACN / µL	^{58}Fe / µL	initial C ^{58}Fe ppm
Coco A	Coconut "4" - CI	25	475	500	-	10
Coco B		25	475	500	-	
Coco C		25	475	500	-	
Coco D		25	475	500	-	
50 ppb	Coco ABCD	500	245	250	5	
100 ppb		500	240	250	10	
150 ppb		500	235	250	15	
200 ppb		500	230	250	20	

- all samples A-B were centrifuged for 5 min, 1000rpm after addition of ACN;
- Coco ABCD was obtained by mixing 900 µL of supernatants of samples coco A-D and then ^{58}Fe was added.

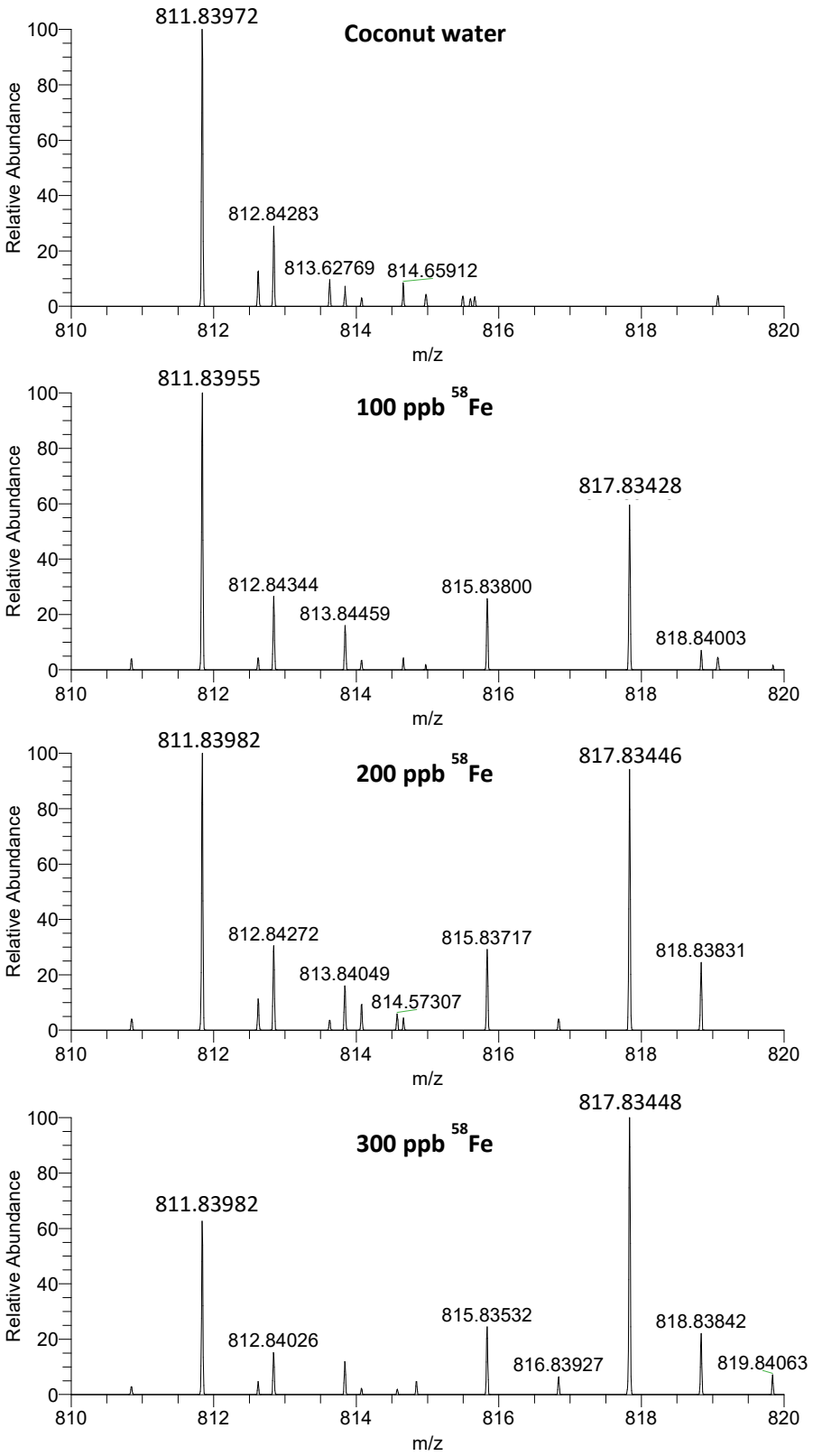

Figure 48. Spectrum showing the abundance of species identified for m/z 811 in positive ionization mode after ^{58}Fe addition at 2 different concentrations.

Figure 49-A show the chromatograms of coconut water sample with addition of 50ppb of ^{58}Fe, recorded within specific time after addition of standard. It's clear that the most significant change in signal intensity was observed between 2 and 4.5h. Regardless of the concentration of ^{58}Fe in the sample, similar correlations of signal surface area versus time elapsed since the preparation of the solutions were obtained. The areas of particular peak were measured: 10.5-12.4 min, 12.4-14.9 min and 14.9-17.6 min. At this stage the signal recorded for blank was not substracted. Though it need to be taken into account that the blank profile influence the area of the last peak in the greatest extent. That's why the values provided for those peaks are relatively high.

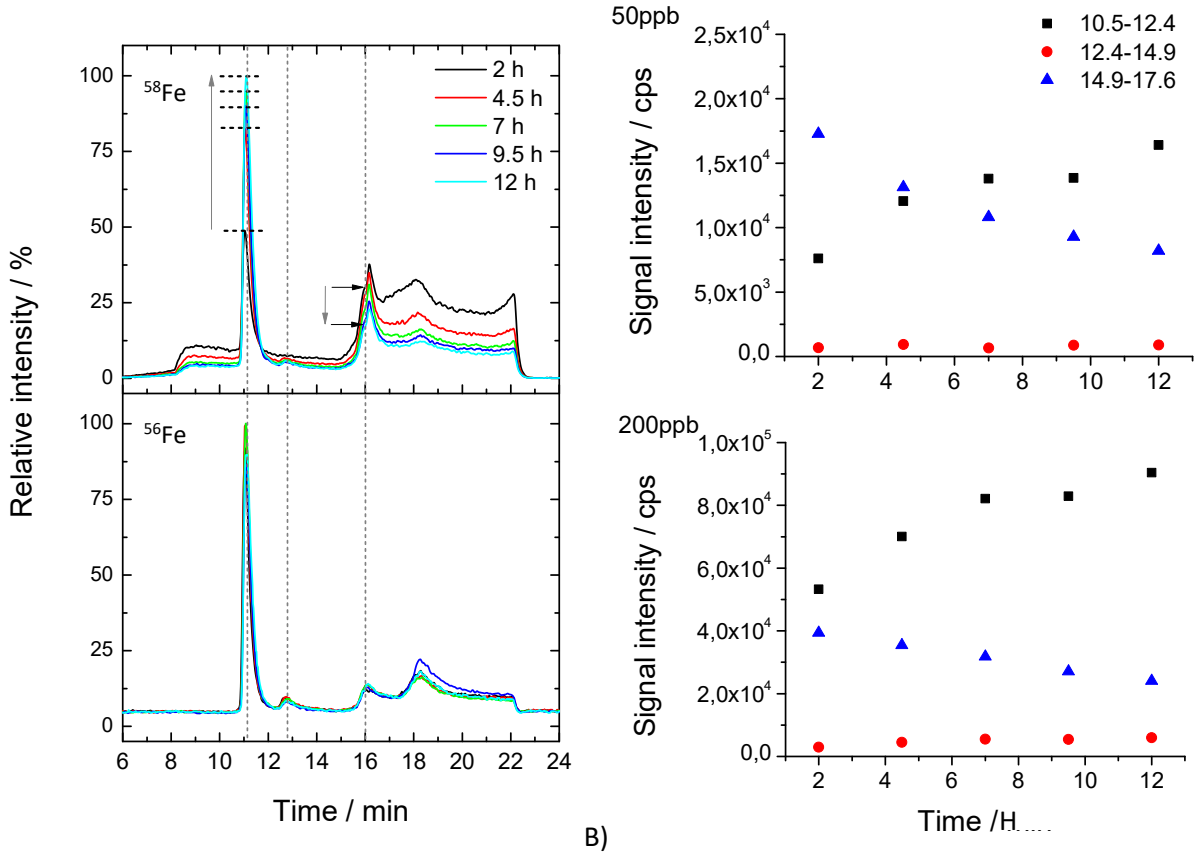

Figure 49. HILIC ICP MS chromatograms for two iron isotopes, ^{56}Fe and ^{58}Fe in coconut water sample with addition of ^{58}Fe (A). Signals recorded within a specified period of time after isotop addition. (B) The Conditions: gradient of method 1, flow rate: 0.5 ml/min, injection volume: 10µl, column Phenomenex Kinetex (150 x 2.1 mm), 2.6 µm, column temperature: 20°C.

Due to the elution position of the last chromatographic peak, at 16 min, its correct quantification was possible only after background subtracting. In the case of ^{56}Fe, the signals of interest were reduced of the signal for the mobile phase (**Figure 50A**). In the case of ^{58}Fe, the signals after spiking were reduced by the signal from the coconut sample alone (**Figure 50B**). This was particularly important, as it allowed to eliminate the contribution of interfering ^{58}Ni. The chromatograms obtained after signal substracting are presented on **Figure 50C-D**. The ranges within which the signals were integrated are marked on the chromatograms and the peak areas taken to quantification of each iron species were highlighted.

The chromatograms show that signals obtained for ^{56}Fe (**A;C**) represent the same signal intensity and profile whatever was the spike's concentration added. The original speciation of ^{56}Fe remained unchanged despite the ^{58}Fe additions. Chromatogram presented on **Figure 50B** shows the formation of species with the same retention times as with ^{56}Fe but labelled with ^{58}Fe and the intensity of the peaks representing these complexes increases proportionally with the concentration of spike added.

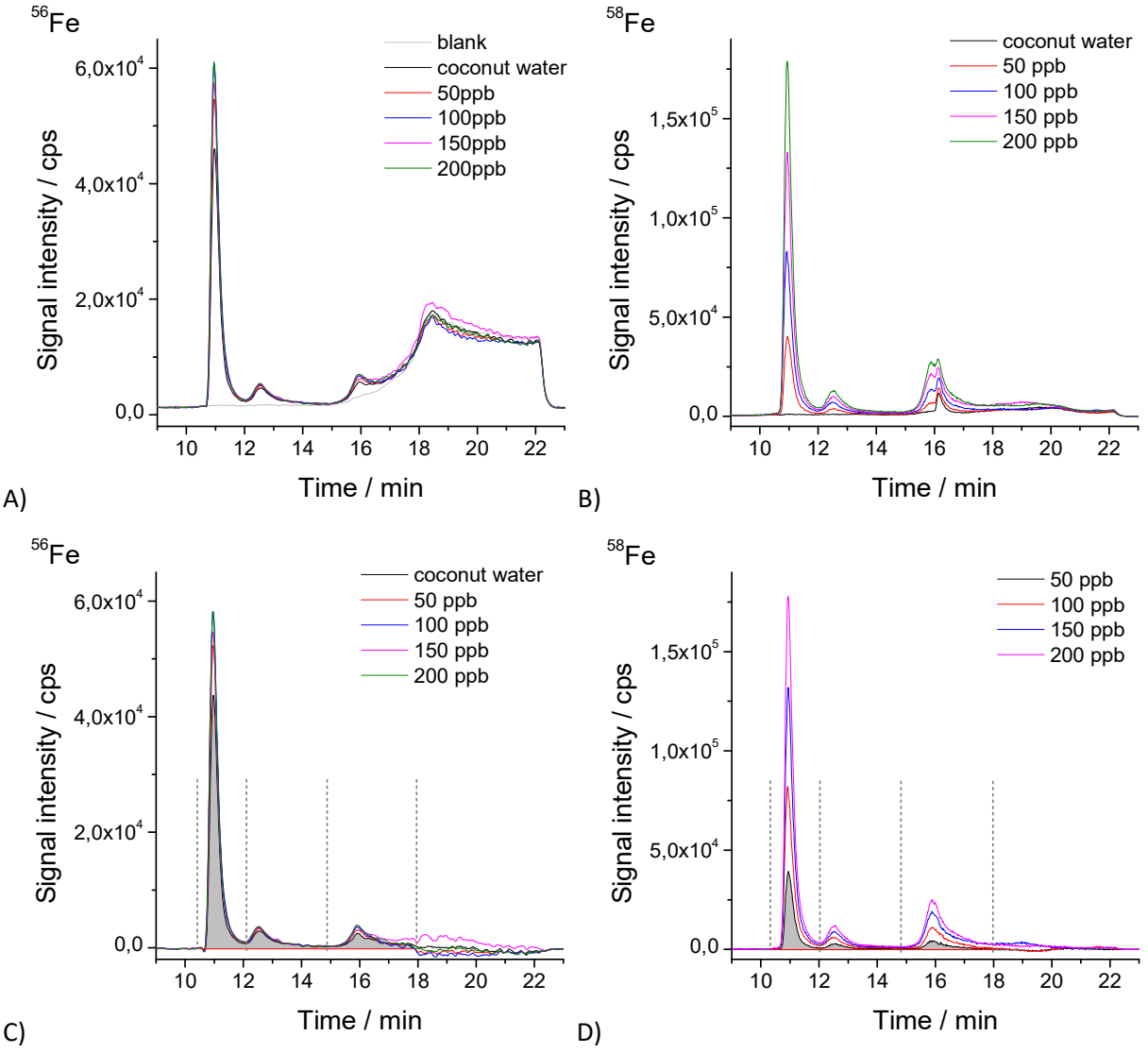

Figure 50. Chromatograms obtained by HILIC ICP MS representing Fe^{56} (A) complexes and Fe^{58} (B) complexes behavior after different concentrations spike addition present in coconut water. Figure (C) present the chromatogram of spiked coconut water for ^{58}Fe, after substraction of raw coconut water. On part (D), the way of signal mesure was shown.

The values of peak areas for the model/exemplary sample of coconut water, for which the chromatograms are shown in **Figure 50C-D**, were gathered in **Table 20**. The percentage of each peak area was calculated compared to the area of all separated iron species. It allowed estimating what part of ^{58}Fe added to the sample participated in the formation of each $Fe_xMal_yCit_z$ complex. The values were 69%, 14% and 17% for $Fe_3Cit_2Mal_2$, $Fe_3Cit_3Mal_1$ and $Fe_3Cit_1Mal_3$ respectively. Based on this data, the calibration curves were plotted and the equations were established.

Table 20. Peak areas of signals recorded after chromatographic separation of coconut water spiked with several concentration of ^{58}Fe, after background substraction.

^{58}Fe	sA	C [ppb]	A1	% of sA	C [ppb]	A2	% of sA	C [ppb]	A3	% of sA
50	21091	34	14350	68	6	2599	12	10	4142	20
100	46898	64	30230	64	12	5838	12	23	10830	23
150	74884	94	46690	62	17	8434	11	40	19760	26
200	100090	127	63340	63	23	11290	11	51	25460	25
^{56}Fe	23524		16210	69		3408	14		3896	17

A – Peak area; sA- summaric area; A1-10.3 – 12.0 min; A2-12.0 – 14.8 min; A3-14.8 – 18.0 min

The data of peak areas of three peaks of interest, corresponding to 3 iron complexes, were obtained from 5 independent measurements. Additionally, based on the equation related to every single calibration curve, points to the same concentration were calculated for each peak. Based on these data, the average of multiple curves was prepared for each peak separately. It was presented on the **Figure 51** as the sets of calibration curves (A) and as linear regression on the average of the points, with standard deviation (B).

The data obtained for all measurements were subsequently used to calculate the amount of ^{56}Fe involved in the formation of the complexes present in the coconut water. The average values of ^{56}Fe compounds concentration, together with its standard deviation, were shown in **Table 21.** Taking into consideration the isotopic distribution of ^{56}Fe is 91.72%, it was calculated that 2.01±0.38 ppm of iron is involved in $Fe_3Cit_2Mal_2$, 0.24±0.09 ppm in $Fe_3Cit_3Mal_1$ and 0.52±0.12 ppm represent ^{56}Fe in $Fe_3Cit_1Mal_3$.

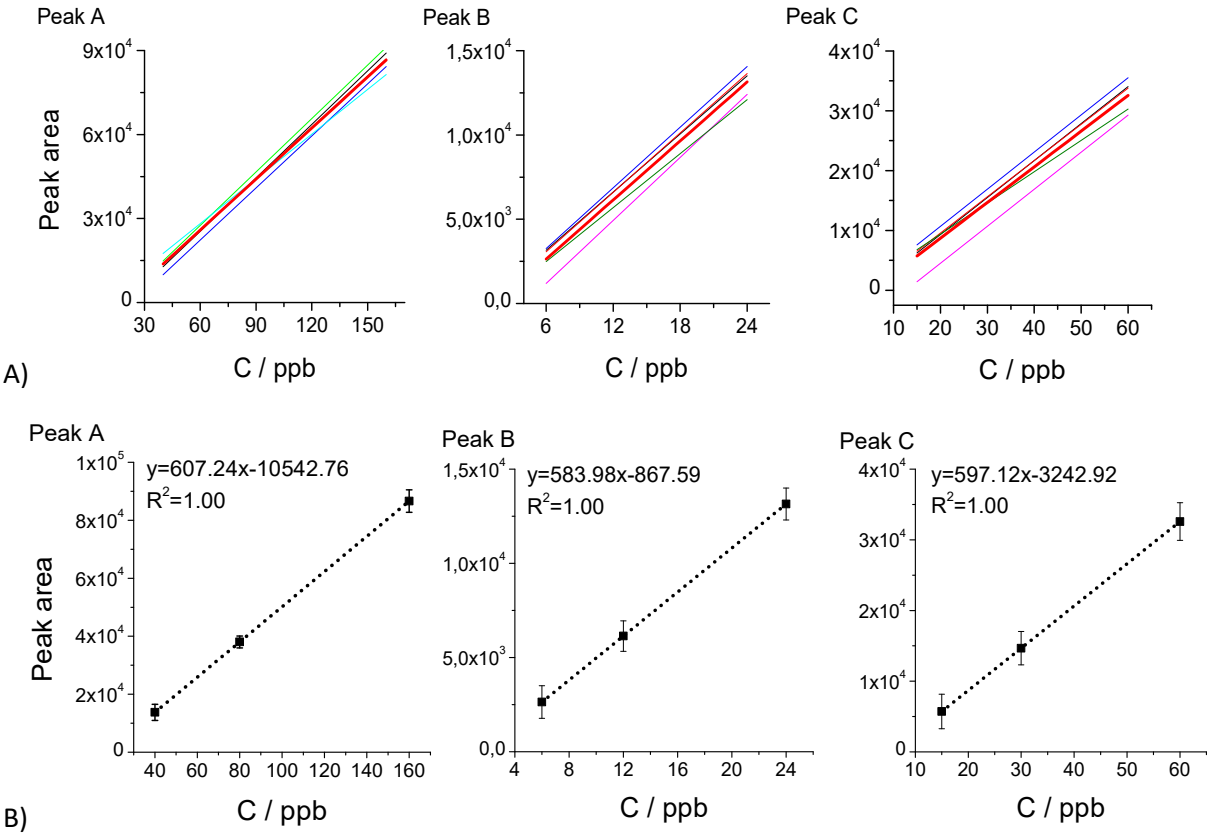

Figure 51. Calibration curves for ^{58}Fe prepared based on area of individual peaks: 10.5-12.0min, 12.0-14.8min and 14.9-18.0min. The bench of calibration curves with the average of multiple curves (A) and linear regression based on the means of five points obtained for each peak, with standard deviation marked (B); n=5.

Table 21. Concentration of ^{56}Fe in the complexes formed including the natural isotopic distribution of ^{56}Fe; n=5.

c of complex [ppm]			**sum**
$Fe_3Cit_2Mal_2$	**$Fe_3Cit_3Mal_1$**	**$Fe_3Cit_1Mal_3$**	
2.20±0.41	0.27±0.10	0.57±0.13	
c of complex [ppm] (including isotopic distribution of ^{56}Fe (91.72%)			
2.01±0.38	0.24±0.09	0.52±0.12	2.78±0.49

In summary, the method of isotopic dilution using ^{58}Fe, developed as part of the studies, permits quantitative determination of low molecular weight iron complexes present in the coconut water. After addition of ^{58}Fe, similar chromatographic profiles were obtained for isotope-labelled and natural iron complexes represented by the most abundant ^{56}Fe. The continuing increase in surface areas of ^{58}Fe signals, associated with low molecular complexes - Fe_3Mal_3Cit, $Fe_3Mal_2Cit_2$ and $Fe_3Mal_1Cit_3$, were obtained after each subsequent spike. Based on the information extracted from chromatographic data, it was possible to define calibration curves with correlation coefficient very close to unity (100%).

It should be remembered, however, that quantitative determination of iron complexes by the isotope-dilution method is possible only using the appropriate protocol, which, among others assumes the removal of high molecular compounds before the addition of enriched isotope. The samples must be prepared within a specified time regime, to give enough time for quantitatively bound ^{58}Fe by an excess of organic ligands. While processing the data, it is necessary to subtract the background chromatograms. Despite some restrictions, however, it is a method that allows quantitative determination of various metal speciation forms in complex matrices.

4.4 Identification and quantification of Fe metabolites in South-American plants (*Setaria parviflora* and *Paspalum urvillei*) tolerant to excess of iron:

4.4.1 Background of the study:

Human activity has always contributed in water and soil contamination due to excess of essential metals such as iron which can be, on one hand, toxic to plants cultivated in this soil: for example, Iron mining does not result only in billions of dollars and "development", but it is filled with dangers, deaths and socioenvironmental destruction like Workers death or illness. In addition, the amount of waste is gigantic, and it is accumulated in dams; the burst of dams because of the mud with different toxicity levels can cause huge tragedies such as deaths and environmental destruction and this is what lately happened in Mariana in Brazil. On the other hand, there is species of plants which present the potential to adapt to extreme environments and can contribute in revitalizing the contaminated areas by colonizing naturally metal enriched soils and to maintain functional heavy metal ecosystems [218]. The success of phytoremediation depend on three factors: (1) the degree of metal contamination of the soil; (2) the degree of metal bioavailability (its chemical and physical aspects); (3) the capacity of the higher plants to accumulate the metal in the shoots. However there is either hypperaccumulating plants or hypertolerant plants which can play the role in soil decontamination.

Iron hyperaccumulation has been much less reported, probably because Fe has a low bioavailability caused by the low solubility of iron oxyhydroxides in natural environments and instead, acts as a limiting factor for plant growth.

The perennial grasses *Paspalum urvillei* Steudel and *Setaria parviflora*, native species from South America, were identified among the few species able to grow spontaneously at the margins of decantation ponds of an Fe ore pelletizing industry located in Brazil, in the Ubu district (municipality of Anchieta, state of Espìrito Santo, South-Eastern Brazil)[219]. These ponds are supplied with water from the mining system and plumbing of the iron ore pelletizing industry, therefore creating an environment rich in iron particles. *Paspalum urvillei* and *Setaria parviflora* were further described as highly tolerant to Fe excess [219,220].

The information about content of Fe and its chemical species is essential to understand the mechanism of hypertolerance of these plants to iron. However, the extremely low volumes of plant liquids make the analysis challenging. The methodology developed in this thesis was used to help to elucidate the molecular mechanism of iron uptake and transport by *Setaria paviflora* and *Paspalum urvillei*.

4.4.2 Growth conditions and plants treatment:

Plants were grown in INRA laboratory in Montpellier **Figure 52**: Seeds of *Paspalum urvillei* Steudel (Poaceae), *Setaria parviflora* and *pisum sativum* were grown in a glasshouse (average temperature 23°C), in 3-liter plastic pots containing 0.5 L of quartz sand and 2.25 L of Humin substrate N_2 Neuhaus (Klasmann-Deilmann, Bremen, Germany) irrigated with tap water for approximately 10 days. Plantlets with 3 leaves were quickly washed in tap water, rinsed and transferred to 2.4 L boxes containing Hoagland nutrient solution, at full ionic strength, with aeration every 4 hour, at pH 5.0. After that, these plants were cultivated in growth chamber with 14 hour light at 28°C and 10 hours dark at 25°C, at 80% humidity, for one week in solution containing 0.5 mM $NH_4H_2PO_4$, 3 mM KNO_3, 2 mM $Ca(NO_3)_2{\cdot}4H_2O$, 1 mM $MgSO_4{\cdot}7H_2O$, 23.13 µM H_3BO_3, 4.57 µM, $MnCl_2{\cdot}4H_2O$, 0.382 µM $ZnSO_4$.$7H_2O$, 0.16 µM, $CuSO_4{\cdot}5H_2O$ and 0.0695 µM MoO_3. The list of samples is given in **Table 22**. The plants were fed with Fe-citrate at concentrations given in **Table 22**.

Xylem sap sample of *pisum sativum* was collected after insertion of a glass capillary in the stem of the decapitated plants. Embryo sac liquid, also called liquid endosperm, was obtained by inserting a capillary glass in pea seed before complete seed maturation. Both type of samples were immediately stored after collection at -20°C. Samples were collected from several plants and pooled until reaching a volume of 200 µL. Peas were grown three times to get replicates and check sample content and analytical method reproducibility.

Table 22. Abbreviation of samples analyzed and conditions under which each specie was cultivated

Sample name	Description of samples
Xylem	*Paspalum urvillei* (control conditions 50 µM of Fe Cit)
DGL1	*Pisum sativum* mutant overaccumulating Fe
DGL2	
DGV	*Pisum sativum* growing in control conditions (100 µM of Fe-citrate)
PC1	*Paspalum urvillei* growing in control conditions (100 µM of Fe-citrate)
PC2	
PT1	*Paspalum urvillei* treated with 7mM of Fe-citrate
SC1	*Setaria parviflora* growing in control conditions (100 µM of Fe-citrate)
SC2	
ST1	*Setaria parviflora* treated with 7mM of Fe-citrate
ST2	
SC3	*Setaria parviflora* growing in control conditions (50 µM of Fe-citrate)
ST3	*Setaria parviflora* treated with 5mM of Fe-citrate

Figure 52. Fe-sufficient plants put in boxes where they were fed with 0.1 mM Fe(III)-citrate and Fe-excess plants fed with 7 mM Fe(III)-citrate during 6 days

4.4.3 Xylem extraction:

Xylem saps are extracted by our collaborators in the INRA laboratory in Montpellier (description of extraction procedure in part of **analytical techniques, sampling**) were collected from two cultures of grass plants *setaria parviflora*: Contrôle samples cultivated with 50µM Fe:Cit and Supplemented samples cultivated with 5mM Fe:Cit.

Fresh liquid samples (plant juices) were usually filtered or centrifuged and then stored by short-term at –4°C in the dark [34]. To avoid sample loss and contaminations, purified reagents were used and proper tools (e.g. containers, Eppendorf etc.) were used for storage.

Plant roots were cut a little bit from the head then the plant is introduced in a 50ml tube sealed into the top of the pots with silicone rubber (**Figure 53**.) the tube was put in the Scholander pressure chamber. The surface was washed with distilled water and sap was collected with a micro-pipette and maintained in eppendorf tubes kept on ice. Immediately after sample collection, the pH of the samples was measured [35][221].

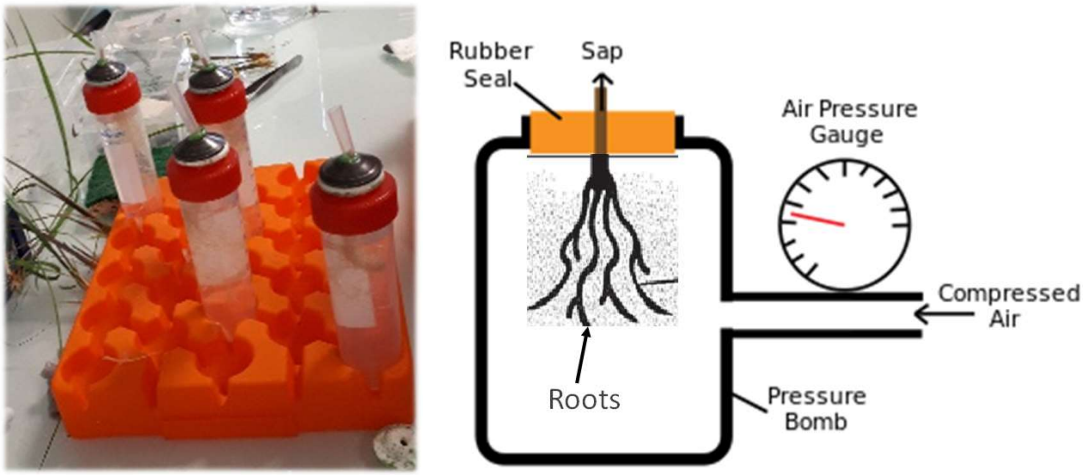

Figure 53. *Presentation of the roots preparation for xylem collection and the device used for scholander pressure exercised on them*

4.4.4 Analysis of Fe tolerance and accumulation:

The analysis of Fe tolerance and accumulation was done by our collaborator in INRA at the University of Montpellier, France where the plants were grown and xylem was collected: the results obtained by them are shown respectively.

Paspalum urvillei and *Setaria parviflora* have been described as being tolerant to Fe excess [219]. To further confirm the Fe tolerant behavior of these two species, the tolerance to high concentrations of Fe-citrate of *Paspalum urvillei* and *Setaria parviflora* young plants with, respectively, rice (*Oryza sativa* cv nipponbare) and *Setaria viridis* was compared, two model species used here as reference [222]. The visual symptoms of standard and excess Fe on *Setaria parviflora* and *Setaria viridis* are illustrated in **Figure 54**. Exposure to high Fe provoked the formation of brow necrotic spots in *S. viridis* leaves, whereas leaves from *S. parviflora* did not show any visible sign of toxicity. Similar symptoms were observed when comparing *Paspalum urvillei* and *Oryza sativa* (data not shown). Roots of *S. parviflora* displayed an intense brown coloration in Fe excess corresponding to the formation of the iron plaque and this phenomenon was almost absent in *S. viridis* (**Figure 54**). The shoot biomass of *P. urvillei* and *S. parviflora* plants was not significantly affected by an exposure to 7 mM Fe, compared to control media, whereas Fe excess provoked a two-fold reduction in biomass for O. *sativa* and *S. viridis* (**Figure 55A**). This result further confirmed the Fe tolerance capacity of *P. urvillei* and *S. parviflora*. In roots, Fe excess induced a reduction of growth that was equivalent for *P. urvillei* and *O. sativa*, whereas the root biomass of both *Setaria* species was not significantly affected by the Fe treatments (**Figure 55B**).

Figure 54. Visual symptoms of Fe toxicity on Setaria parviflora and Setaria viridis plants. Ten day-old seedlings were grown for 6 days in medium supplemented with 0.1 mM or 7 mM Fe-citrate. Bar = 1cm.

Having established that *P. urvillei* and *S. parviflora* are well-suited species to study responses to Fe excess, the Fe content in roots and shoots of plants grown on the two Fe regimes was measured. In control condition (0.1 mM Fe-citrate) no significant difference in Fe concentration was observed in leaves of the four species (**Figure 55C**). Iron excess had a moderate effect on the shoot Fe concentration of *P. urvillei* and *S. parviflora* with a 3 to 4 fold increase in Fe accumulation whereas *O. sativa* and *S. viridis* shoots accumulated massive amounts of Fe, representing ca 50-fold increase, relative to standard Fe treatment (**Figure 55D**). The exposure to Fe excess induced a limited increase in Fe accumulation in roots of *P. urvillei, S. parviflora* and *S. viridis* whereas roots of *O. sativa* overaccumulated Fe, reaching up to 9000 ppm in response to Fe excess (**Figure 55C**). From these results, it was concluded that both *P.urvillei* and *S. parviflora* plants were able to tolerate high concentrations of Fe in the medium with a very moderate effect in growth that could be attributed to their capacity to restrict Fe accumulation in their organs, when compared to the less tolerant species *O. sativa* and *S. viridis*.

Additional investigations were carried out by Marie-Pierre Isaure and Nicolas Trcera at Synchrotron SOLEIL, Gif-sur-Yvette in order to gain further insights in the tolerance mechanisms set up by *P. urvillei* and *S. parviflora*, we studied Fe localization in roots and shoots in control and excess conditions. In standard condition, for all species, Fe was only visible as aggregates around the roots, corresponding to the iron plaque (IP) (**Figure 56**). Upon exposure to 7 mM Fe-citrate, roots of the four species displayed different behavior. *Paspalum urvillei* and *Setaria parviflora* roots had built up a significant iron plaque, compared to *O. sativa and S. viridis* (**Figure 56**, middle row). Within the root tissues of *P. urvillei* and *S. parviflora*, Fe deposits completely filled the entire volume of all cortex cells. Additionally, a strong staining was visible around the epidermal and cortical cells and this staining was attributed to the cell walls. The strong difference in Fe accumulation between epidermal-cortical cells and the central cylinder indicated that the endodermis was playing a central role in the control of Fe loading into the vascular system. To a

lesser extent, rice roots also accumulated high concentrations of Fe inside cells. Strikingly, the iron staining in the central cylinder was as intense as in the cortex, suggesting that, contrarily to *P. urvillei* and *S. parviflora*, the endodermis was not such a barrier for the movement of Fe towards the conductive elements of the stele. Finally, root cells of *S. viridis* did not accumulate Fe in the vacuoles as the other species, instead, Fe-rich dot-shaped deposits were visible within cells. These Fe-rich structures were identical to Fe-ferritin complexes previously described in both roots and leaves of *Arabidopsis thaliana* plants treated with iron excess.

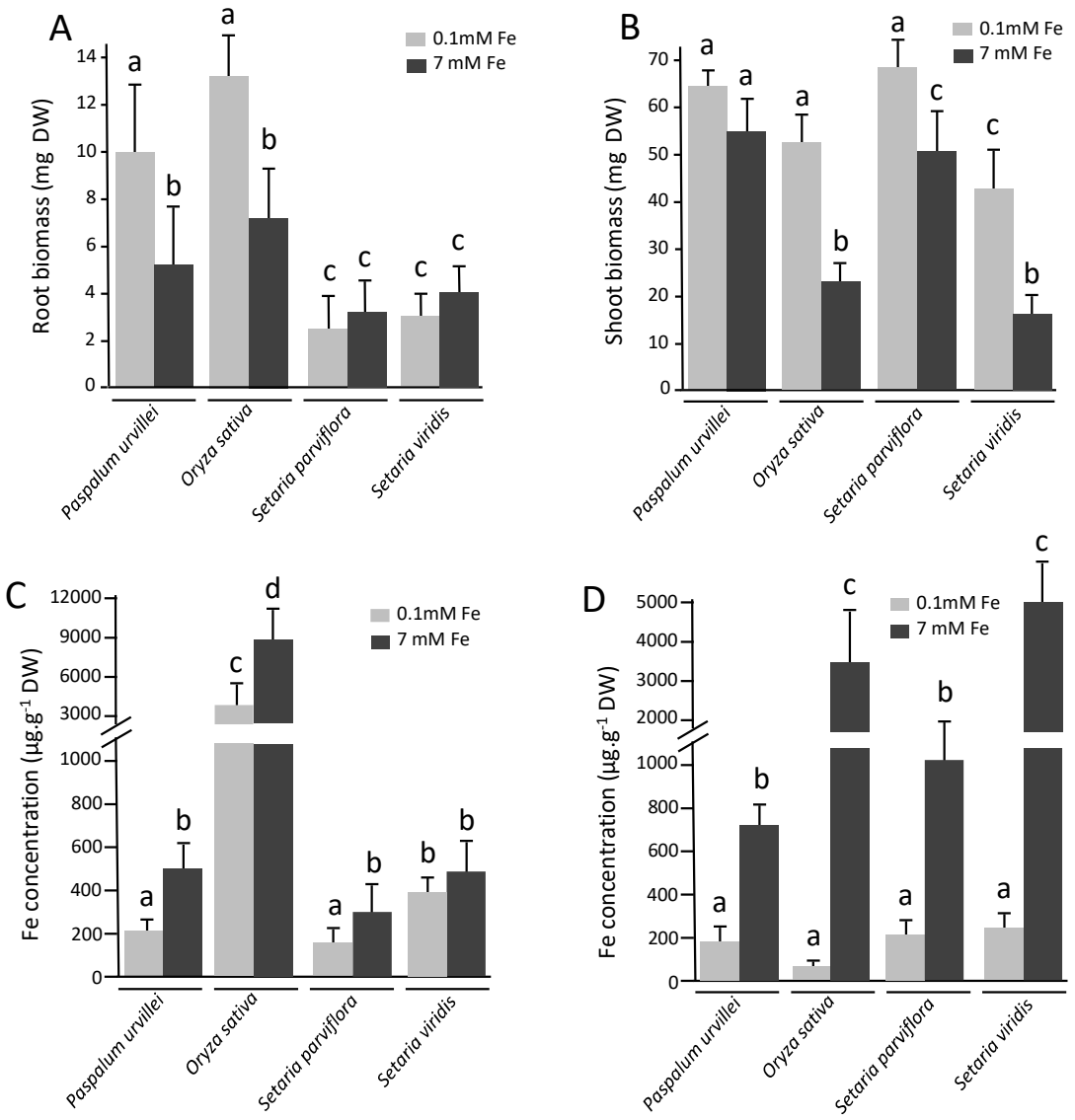

Figure 55. Biomass and Fe concentration of roots and shoots of Paspalum urvillei, Oryza sativa, Setaria parviflora and Setaria viridis plants grown in standard and excess Fe. 10 day-old seedlings were grown for 6 days in medium supplemented with 0.1 mM or 7 mM Fe-citrate. (A) Root biomass, (B) shoot biomass, (C) Fe concentration on roots, (D) Fe concentration in shoots. Values are average ± SD, values followed by the same letter do not differ by Tukey's test at 5% probability [222].

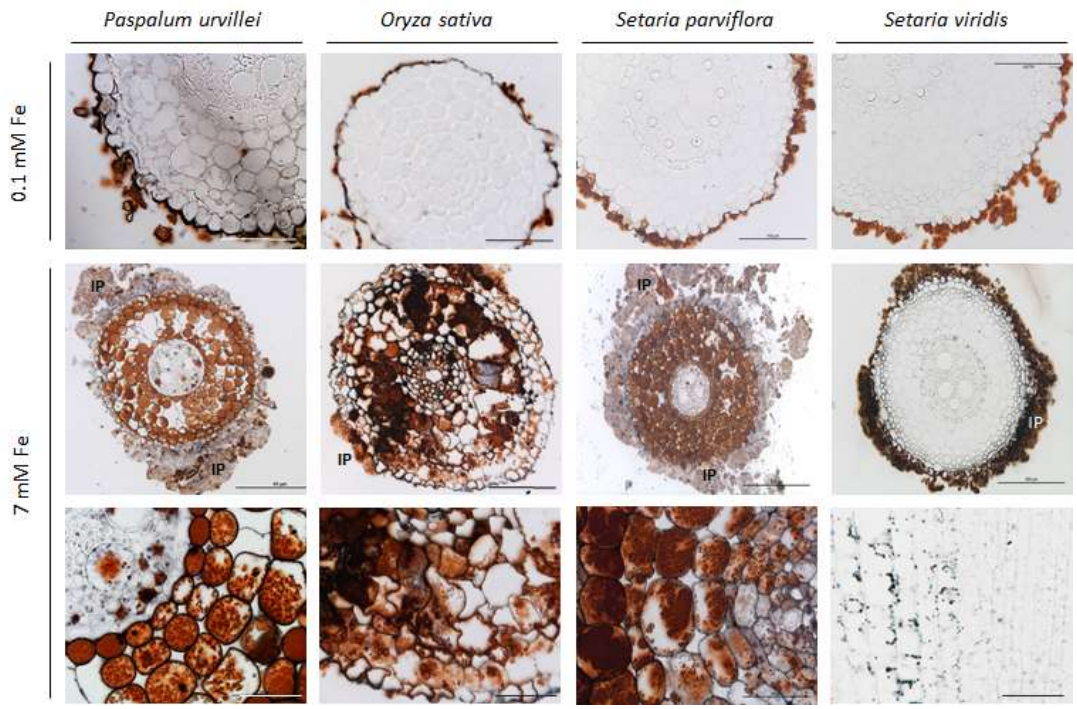

Figure 56. Fe localization in root sections of P. urvillei, O. sativa, S. parviflora and S. viridis. Plants were treated with 0.1 mM or 7 mM Fe-Citrate during 6 days and root samples were further fixed and embedded in resin. Sections were submitted to Perls Dab staining. IP, Iron plaque. Bar = 200 µm unless stated otherwise[222].

4.4.5 Total analysis of iron in xylem of studied plants:

The total analysis was carried for the original samples (as received, done once) and after (done using two different dilutions) short centrifugation (**Table 23**). In the majority of the samples, severe problems due to iron precipitation were encountered and some of the biological replicates had to be discarded. All samples except ST3 and SC3 have recovery of < 50% of iron in supernatant and the analysis was carried out on these two samples ST3 and SC3 only. Total results obtained for replicates of *paspalum urvillei* and *setaria parviflora* grown in control conditions are the same (Fe in **PC**~7.5 ppm and in **SC**~9 ppm). The amount of Fe in samples collected from plants supplemented with Fe is higher than the amount in samples collected from plants grown in control conditions.

Table 23. Total content of Fe in replicates of samples analyzed

	Fe [ppm] in centrifuged solution
SC3	14.06
ST3	170.15
Xylem	8
DGL1	60
DGL2	27.9
DGV	31.4
PC1	7.5
PC2	7.3
PT1	30.9
SC1	9.2
SC2	8.6
ST1	11
ST2	80.3

ST3: [Fe] after spinning = 146.23 ppm; 86% Fe recovered in supernatant
SC3: [Fe] after spinning = 7.05 ppm; 50% Fe recovered in supernatant

4.4.6 Iron speciation analysis in plant xylem:

Qualitative analysis of iron citrate/iron citrate-malate complexes was performed on Orbitrap MS and ICP-MS by the comparison of their retention time with retention time of the complexes obtained in standards solution of Fe:Mal:Cit (1:25:5) (**Figure 57**) and the identity confirmation by searching the characteristic isotopic pattern of iron. Samples analyzed were the one containing the highest amount of iron according to total analysis. In addition, the determination of the concentration of ^{56}FeMalCit complexes in plant samples was performed by adding different amount of solution of ^{58}Fe in water to the plant sample. The presence of free ligands (malate and citrate) in samples allowed the formation of the appropriate ^{58}FeMalCit and ^{58}FeCit complexes.

Figure 58 A-B shows chromatograms obtained for ^{58}Fe-spiked samples by HILIC-ICP-MS. In these conditions, it was possible to separate two Fe complexes in supplemented sample (ST3); in addition, a broad continuum was present between 17 and 25 mins. However, no clear peaks were observed in the control sample (SC3), only the broad continuum (also between 17 and 25 mins) was present. The comparison of the chromatogram shown in **Fig. 58B** with that of the standard Fe malate-citrate and Fe: citrate complexes suggests the identity of the species as $Fe_3Cit_2Mal_2$ (RT 12.23 min) and Fe_3Cit_3Mal (RT 14.21); the final confirmation was carried out by HILIC-ESI MS by searching the specific isotopic pattern (exact inter-isotopic mass differences and isotopic ratios) at the retention times corresponding to the peaks detected by HILIC ICP MS.

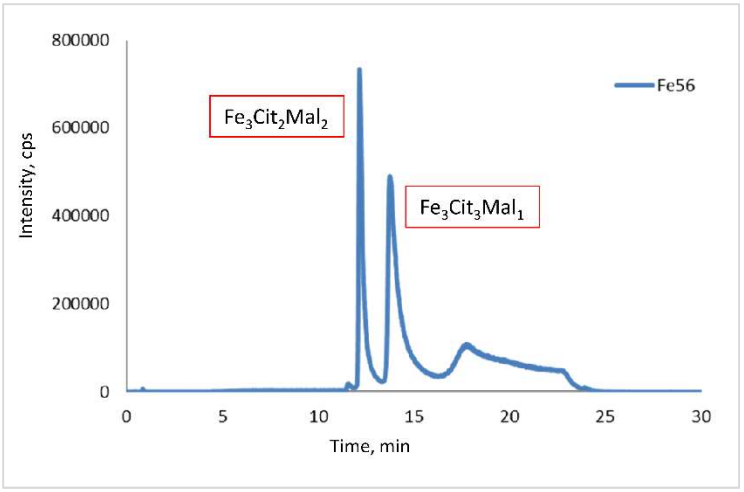

Figure 57. HILIC ICP MS of standard solution of Fe:Malate:Citrate at ratio 1:25:5 on Phenomenex Kinetex column.

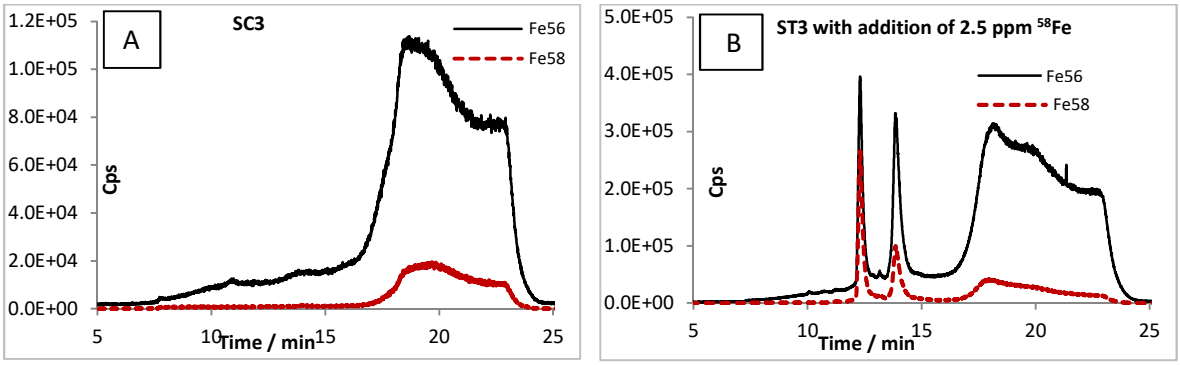

Figure *58*. HILIC ICP MS of control and supplemented spiked samples on Phenomenex Kinetex column.

The identity of the iron complexes was confirmed by the agreement of the chromatographic profiles of HILIC-ICP MS with HILIC-XIC-ESI MS corresponding to masses of the expected species: $Fe_3Cit_2Mal_2$ (m/z 811.8384) and Fe_3Cit_3Mal (m/z 869.8437) as shown in **Figure 59** for ST3 sample. **Figure 60** presents chromatograms obtained by HILIC ESI MS showing two peaks for DGL and ST2 samples; $Fe_3Cit_2Mal_2$ (m/z 811.8384) and Fe_3Cit_3Mal (m/z 869.8437) identified in DGL sample and Fe_3Cit_3Mal (m/z 869.8437) Fe_3Cit_3 (m/z 735.8231) in ST2 supplemented sample. The spectra taken at the peak apexes at RT of each complex in the samples analyzed are presented in **Figures 61** and **62**.

In figure 61, there is identification of Fe complexes labelled with ^{56}Fe and ^{58}Fe, after spike addition in xylem of *Setaria Parviflora* sample, of respectively m/z 811.84 and 817.84 representing the first complex eluted by HILIC ICP MS and m/z 869.84 and 875.84 representing the second eluted complex. Additionally, figure 62 shows Spectrum with isotopic patterns for every m/z identified as Fe complex with citrate and malate in xylem of *Setaria parviflora* cultivated in supplemented medium.

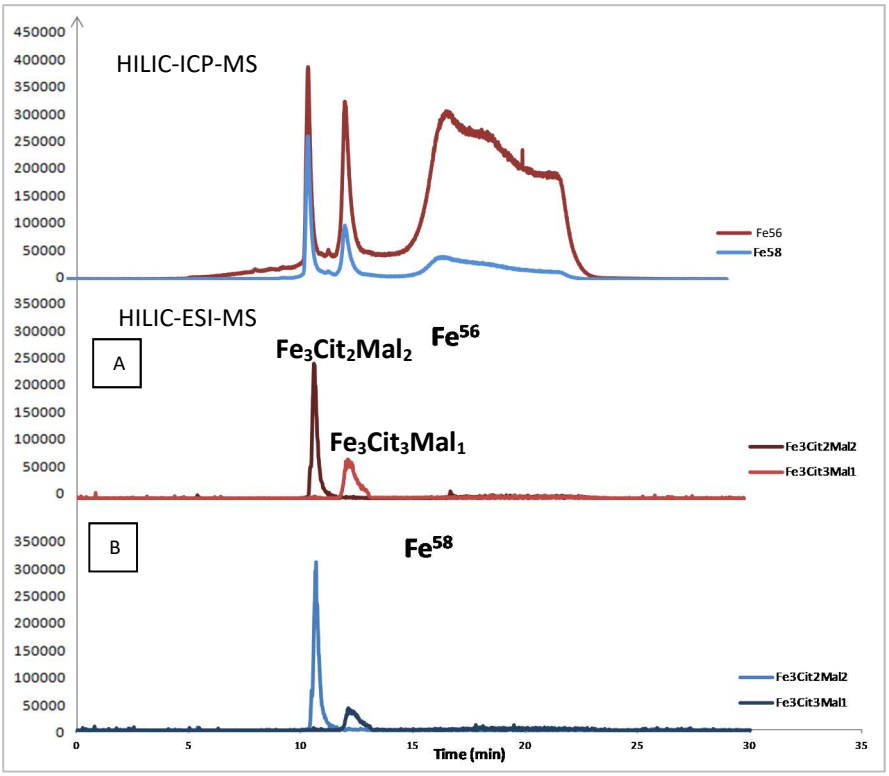

Figure 59. HILIC ICP MS (upper panel) and ESI MS (A - ^{56}Fe complexes and B - ^{58}Fe complexes) of ST3 (supplemented) sample spiked with ^{58}Fe; the complexes were $Fe_3Cit_2Mal_2$ and Fe_3Cit_3Mal.

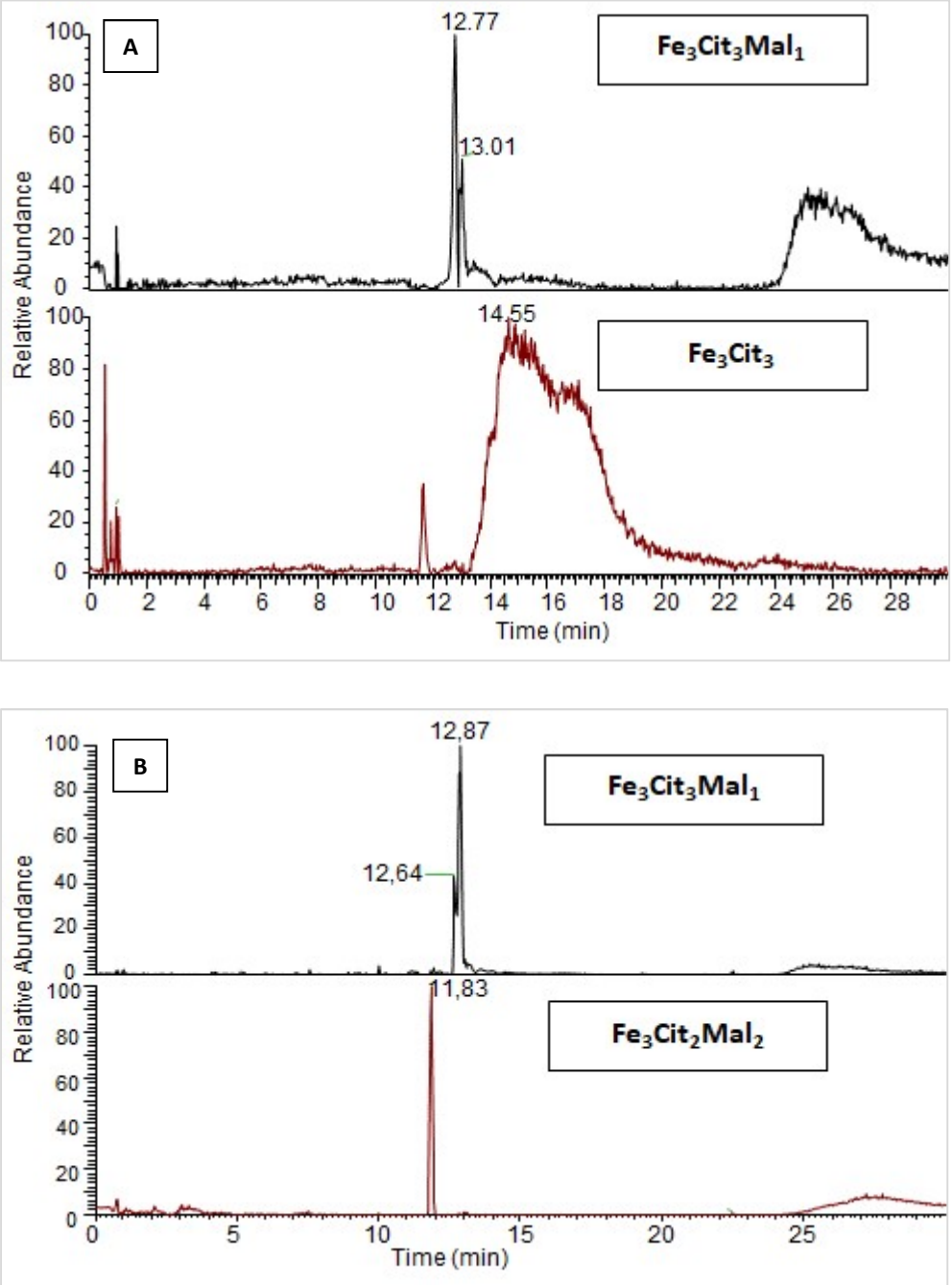

Figure 60. HILIC ESI MS of ST2 (A) and DGL (B) samples showing the identification $Fe_3Cit_2Mal_2$ (m/z 811.8384) and Fe_3Cit_3Mal (m/z 869.8437) identified in DGL sample and Fe_3Cit_3Mal (m/z 869.8437) Fe_3Cit_3 (m/z 735.8231) in ST2 supplemented sample.

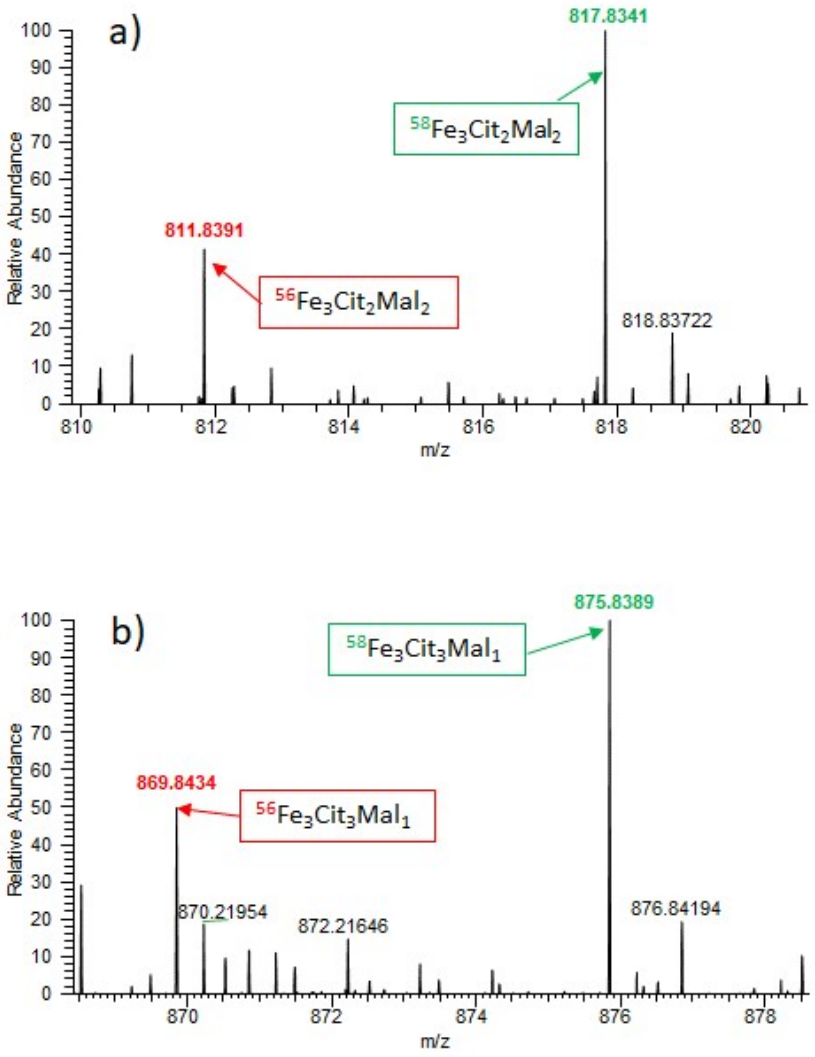

Figure 61. Spectra taken at the peak apexes at RT 12.23 min (upper panel) and RT 14.21 min (bottom panel) showing the presence of $Fe_3Cit_2Mal_2$ and Fe_3Cit_3Mal species in Setaria Parviflora.

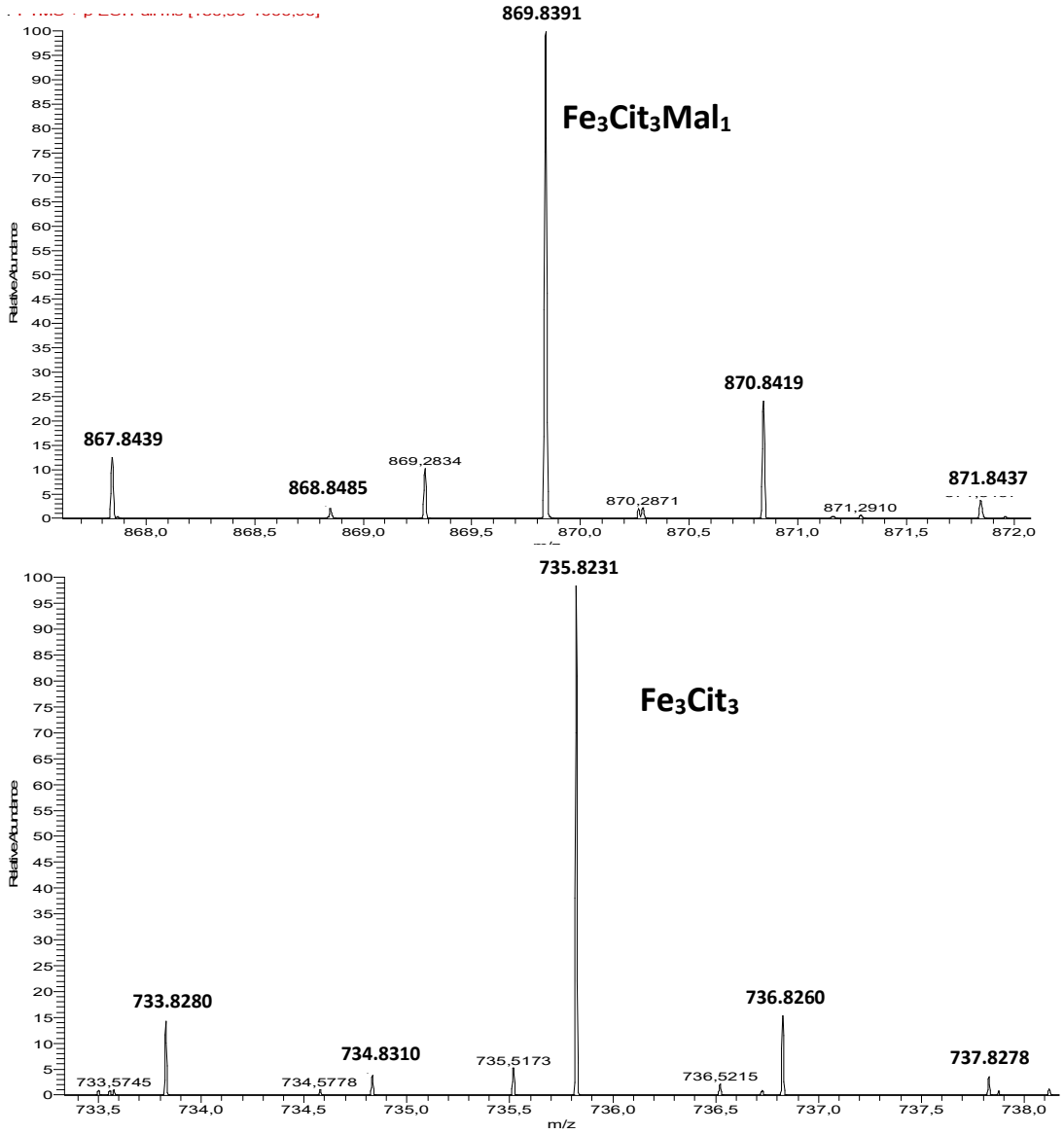

Figure 62. Spectrum showing isotopic patterns for every m/z identified as Fe complex with citrate and malate

4.4.7 Quantitative iron speciation in xylem saps of *Pisum sativum*, *Setaria parviflora* and *Paspalum urvillei*:

Sample preparation for analysis:

Sample preparation scheme is shown in **Figure 63** below: Shortly, samples were diluted with ammonium acetate, divided in aliquots of 5µL to which standard of ^{58}Fe was added in order to create calibration curve. Later on, acetonitrile was added to obtain a 1:2, sample to acetonitrile ratio, vortexed and centrifuged. A 2 µL aliquot of the supernatant was injected into the HILIC column each time.

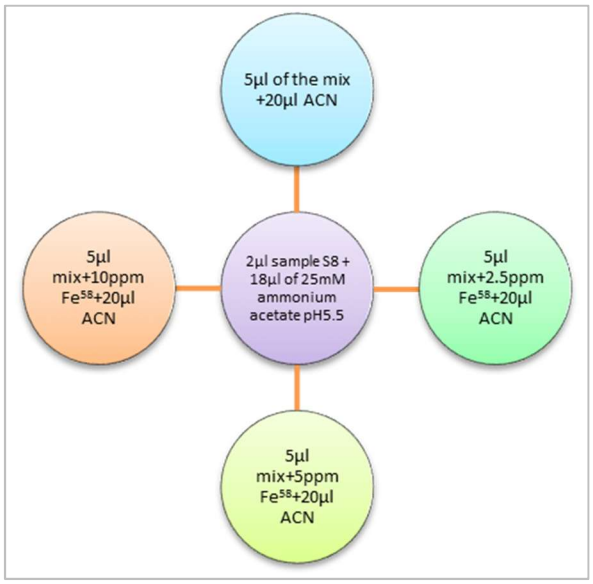

Figure 63. Experimental scheme of the isotope addition to xylem sap.

Sample preparation consist of mixture of the sample with ammonium acetate to stabilize iron species that are pH dependent so ammonium acetate was prepared at pH 5.5 which is the pH of xylem saps analyzed. The steps for spike addition are detailed below:

a) Dilution of samples 1:9 in 25 mM ammonium acetate buffer pH=5.5 (4 µl of sample + 36 µl of buffer)
b) Division of samples into four equal parts (4 x 10 µl)
c) Analysis one part of sample without addition of ^{58}Fe - 10 µl of sample + 20 µl of ACN- vortexing, centrifugation (5000 rpm, 5 min) – injection (10 µl)
d) Addition of 2, 5, 10 ppm of ^{58}Fe prepared in H_2O (pH=2) (when the total amount of ^{56}Fe in sample was in range 10-100 ppm) and 0.2, 0.5 and 1 ppm (when the total amount of ^{56}Fe in sample was in range 1-10 ppm) to the other three parts – wait for the formation of appropriate ^{58} FeMalCit/FeCit complexes before injection.
e) Addition of 20 µl of ACN to samples, vortexing, centrifugation (5000 rpm, 5 min) – injection (10 µl)

Analysis conditions were the same as given in 4.1 and 4.2.

Results

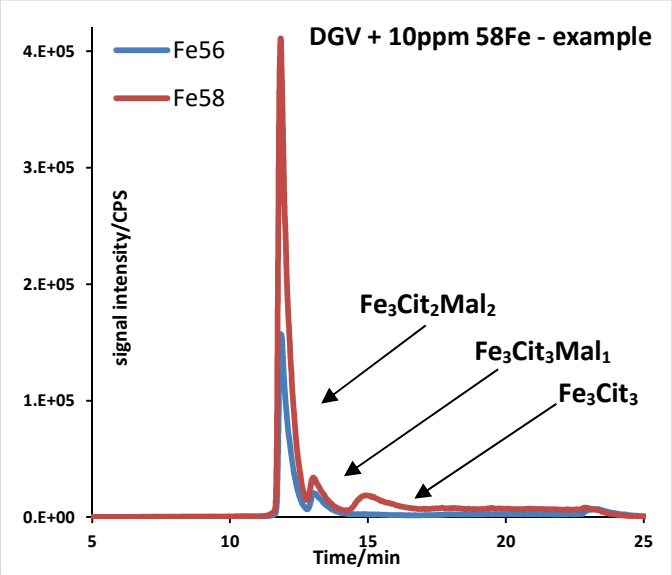

Figure 64. HILIC ICP MS of DGV sample spiked with ^{58}Fe; the complexes were $Fe_3Cit_2Mal_2$ Fe_3Cit_3Mal and Fe_3Cit_3.

The presence of free ligands (malate and citrate) in samples allowed the formation of the appropriate ^{58}FeMalCit and ^{58}FeCit complexes present in **Figure 64** where 3 complexes were separated. Based on ^{58}Fe chromatograms, the area percentage of each formed complex in total area of ^{58}Fe complexes was calculated. It has been assumed that added ^{58}Fe is fully complexed with malate and citrate present in sample (only if their amount is sufficient). The area percentage of each complex allowed to calculate the concentration of each formed ^{58}Fe complex in sample. For example, for sample DGV, addition of 10 ppm of ^{58}Fe to sample, lead to formation of 7.9 ppm of $^{58}Fe_3Mal_2Cit_2$ (the area percentage of this complex is 79 %) – which calculations are grouped in **Table 24** below. Calibration curve for each formed ^{58}Fe complex (**Figure 65**) was constructed by plotting area corresponding to appropriate complex against concentration. Based on the equation of the calibration curve for ^{58}Fe complexes the concentration of ^{56}Fe complexes in sample and including the isotopic distribution of ^{56}Fe (91.72 %) without addition of ^{58}Fe was calculated. It has to be mention, that the area (in fact concentration) of ^{56}Fe complexes is not changing after addition of ^{58}Fe. As it was mentioned before, the addition of ^{58}Fe into sample matrix reduces matrix effect and correct recoveries.

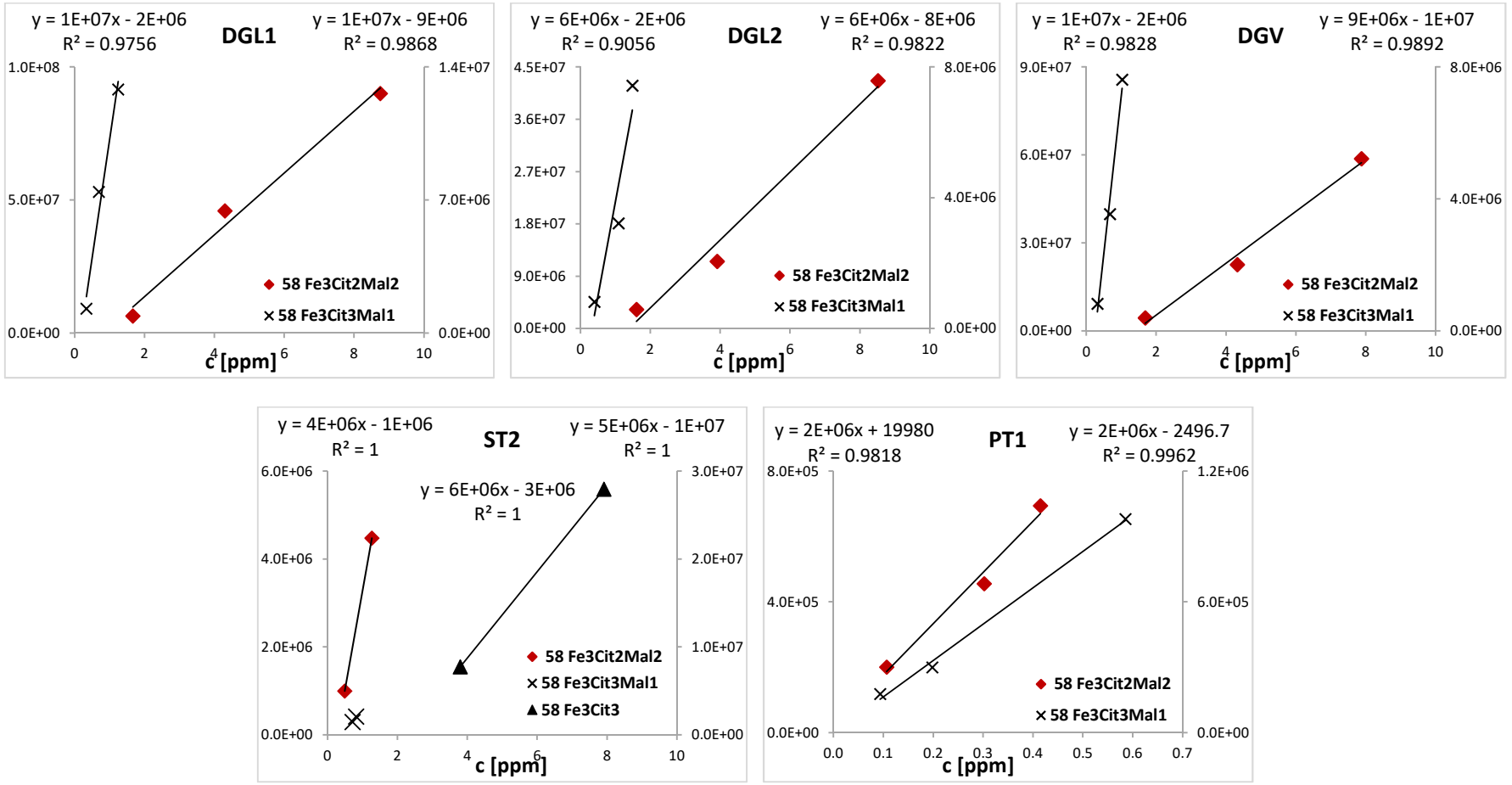

Figure 65. Calibration curves for ^{58}Fe prepared based on area of individual peaks

Table 24. Concentration of ^{56}Fe involved in the formation of FeMalCit complexes in analyzed samples

Sample name	Concentration of ^{56}Fe in sample[ppm]	Concentration of iron in complex form in sample [ppm]				% of ^{56}Fe complex in total amount of Fe			
		$^{56}Fe_3Cit_2Mal_2$	$^{56}Fe_3Cit_3Mal_1$	$^{56}Fe_3Cit_3$	TOTAL	$^{56}Fe_3Cit_2Mal_2$	$^{56}Fe_3Cit_3Mal_1$	$^{56}Fe_3Cit_3$	TOTAL
xylem sap	8.0	<LOD	<LOD	<LOD	<LOD	<LOD	<LOD	<LOD	<LOD
DGL 1	60.0	35.8	9.5	<LOD	45.3	60	16	-	76
DGL 2	27.9	17.6	7.9	<LOD	25.5	63	28	-	91
DGV	31.4	15.7	3.4	<LOD	19.1	50	11	-	61
PC1	7.5	~0.5	~2.0	<LOD	~2.5	6	24	-	30
PC2	7.3	<LOD	<LOD	<LOD	<LOD	-	-	-	-
PT1	30.9	3.0	3.3	x	6.3	10	11	x	21
SC1	9.2	<LOD	<LOD	<LOD	<LOD	-	-	-	-
SC2	8.6	<LOD	<LOD	<LOD	<LOD	-	-	-	-
ST1	11.0	3.1	3.2	x	6.3	28	29	x	57
ST2	80.3	3.9	1.9	31.0	36.8	5	2	39	46

LOD of Fe by ICP MS = 0.002 ppm

X = not quantified

Figure 66 shows the comparison of amount of Fe in ppm obtained from total analysis of real world samples of *pisum sativum*, *paspalum urvillei* and *setaria parviflora* with the calculated amount of Fe involved in the complexation with citrate and malate after separation on HILIC column, we see that there is difference between values obtained. These differences can be due to Fe losses during sample preparation which was discussed before by the effect of acetonitrile addition to the sample after spike addition and centrifugation which can lead to precipitation of HMW molecules present in sample and containing the lost ^{56}Fe.

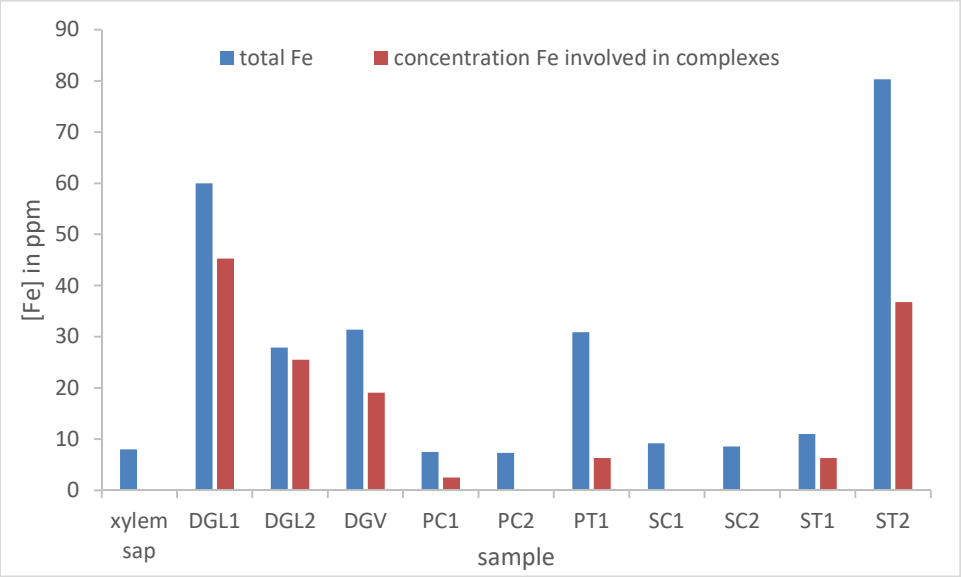

Figure 66. Comparison of total analysis of ^{56}Fe in ppm obtained for the results obtained for real world samples of paspalum urvillei pisum sativum and setaria parviflora with the calculated total amount of ^{56}Fe involved in the complexation with citrate and malate after separation on HILIC column.

4.4.8 Analysis of medium where plants were cultured by HILIC ICP MS

It was considered interesting to analyse the growth media and check for the presence of iron species – the citrates used for plant feeding and/or citrate-malate formed during Fe uptake and metabolism.

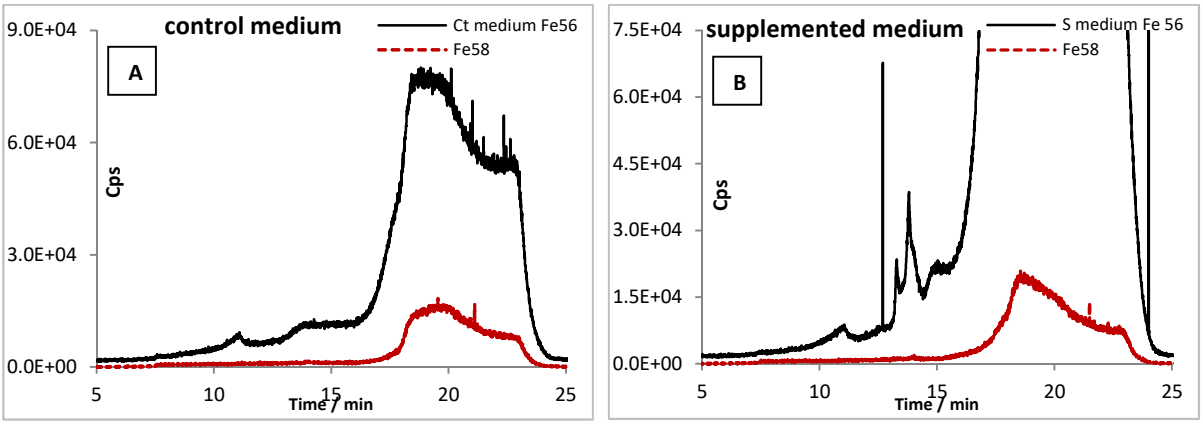

Figure 67. HILIC ICP MS chromatograms of control (A) and supplemented (B) medium compared to HILIC ICP MS chromatogram of standard Fe:Mal:Cit (Figure 57).

By comparing chromatograms A and B of **Figure 67** we see that the peaks observed in supplemented medium (**Figure 67B**) which are not present in **Figure 67A** co-elute with the complexes of Fe ($Fe_3Cit_2Mal_2$ and $Fe_3Cit_3Mal_1$) identified in standard solution of Fe: Mal: Cit (ratio: 1:25:5): these results obtained may suggest a liberation of Fe complexes by plants cultivated in this medium.

In conclusion, until now, nothing is known about the long-distance Fe transport in Fe hyperaccumulating and/or hypertolerant plants, and therefore the identification, speciation and quantification of Fe transport forms in xylem sap are crucial to understand this long-distance transport. This developed methodology allowed the quantitative speciation of Fe in xylem of paspalum *urvillei pisum sativum* and *setaria parviflora.*

5 Conclusion

The PhD project allowed the development of a novel mass spectrometry based protocols for the determination and quantification of low molecular weight metal compounds in plant liquids. The main challenges included the extremely low amount of samples (e.g., xylem is sampled in low microliters range), the low stability of the analytes and lack of analytical standards.

The initial part of the work was focused on the characterization of the species which can be potentially present in plants liquid by studying their equilibria, stability and chromatographic behavior. The next step involved a full characterization of the model sample: coconut (Cocos nucifera) water used as a model for of plant endosperm metallome and available for experiments in relatively high quantities. Different chromatographic conditions were tested and optimized. ESI MS condition were adjusted (positive or negative mode ionization) depending on the nature of the analytes and chromatographic conditions used. In addition, the influence of different sample pre-treatment steps (filtration, centrifugation) and storage condition was studied.

A generic analytical strategy for the standardless quantification of a large spectrum of low-molecular weight metal complexes by molecular mass spectrometry was developed using the Isotope Dilution Analysis (IDA) with the addition of an isotopic spike in ionic form and HILIC-ICP-MS. The protocol was carefully studied in order to preserve the original metal complexes and achieve the formation of metal complexes with the excess of ligands present in the sample.

Finally, the developed procedures were applied for characterization and quantification of low molecular weight iron complexes in real world xylem samples of hypertolerant and overaccumulating plants including *Pisum sativum*, *Paspalum urvilleli*, and *Setaria parviflora*.

6 References

[1] S.M. Reichman, The Responses of Plants to Metal Toxicity : A review focusing on Copper , Manganese and Zinc, Aust. Miner. ENERGY Environ. Found., (2002) 1–54.

[2] I. Valeur, Speciation of heavy metals and nutrient elements in digestate, norwegian university of life science, 2011.

[3] S.P. McGrath, F.J. Zhao, E. Lombi, Plant and rhizosphere processes involved in phytoremediation of metal-contaminated soils, Plant Soil, 232 (2001) 207–214.

[4] B.J. Alloway, Zinc in Soils and crop nutrition, Brussels, Belgium and France, 2008.

[5] M.J.I. Mattina, W. Lannucci-Berger, C. Musante, J.C. White, Concurrent plant uptake of heavy metals and persistent organic pollutants from soil, Environ. Pollut., 124 (2003) 375–378.

[6] G.P. Cobb, K. Sands, M. Waters, B.G. Wixson, E. Dorward-King, Accumulation of heavy metals by vegetables grown in mine wastes, Environ. Toxicol. Chem., 19 (2000) 600–607.

[7] T.E. Bahemuka, E.B. Mubofu, Heavy metals in edible green vegetables grown along the sites of the Sinza and Msimbazi rivers in Dar es Salaam, Tanzania, Food Chem., 66 (1999) 63–66.

[8] R.L. Hough, N. Breward, S.D. Young, N.M.. Crout, A.M. Tye, A.M. Moir, I. Thornton, Assessing potential risk of heavy metal exposure from consumption of home-produced vegetables by urban populations, Environ. Health Perspect., 112 (2004) 215–221.

[9] Metallomics: Whence and whither, Metallomics, 4 (2012) 1017–1019.

[10] A. Alvarez-fernandez, P. Díaz-benito, A. Abadía, A. Lopez-Millan, J. Abadía, Metal species involved in long distance metal transport in plants, Front. Plant Sci., 5 (2014) 1–20.

[11] G.R. Rout, S. Sahoo, Role of Iron in Plant Growth and Metabolism, Rev. Agric. Sci., 3 (2015) 1–24.

[12] R. Hänsch, R.R. Mendel, Physiological functions of mineral micronutrients (Cu, Zn, Mn, Fe, Ni, Mo, B, Cl), Curr. Opin. Plant Biol., 12 (2009) 259–266.

[13] V. Mary, Caractérisation de mutants d ' Arabidopsis thaliana affectés dans le stockage du fer dans leurs graines, paris-sud, 2015.

[14] Y. Ando, S. Nagata, S. Yanagisawa, T. Yoneyama, Copper in xylem and phloem saps from rice (Oryza sativa): The effect of moderate copper concentrations in the growth medium on the accumulation of five essential metals and a speciation analysis of copper-containing compounds, Funct. Plant Biol., 40 (2013) 89–100.

[15] J.F. Artiola, Speciation of Copper: Speciation of Copper in the Environment, in: Handb. Elem. Speciat. II-Species Environ. Food, Med. Occup. Heal., Arizona, 2005: pp. 174–186.

[16] J.L. Burkhead, K.A. Gogolin Reynolds, S.E. Abdel-Ghany, C.M. Cohu, M. Pilon, Copper homeostasis, New Phytol., 182 (2009) 799–816.

[17] D. Nohr, H. Biesalski, speciation of copper in clinical and Occupational Aspects, Handb. Elem. Speciat. II Species Environ. Food, Med. Occup. Heal., 3 (2005).

[18] B. Hafeez, Y.M. Khanif, M. Saleem, Role of Zinc in Plant Nutrition- A Review, Am. J. Exp. Agric., 3 (2013) 374–391.

[19] P.M. Kopittke, P. Wang, E. Lombi, E. Donner, Synchrotron-based X-Ray Approaches for Examining Toxic Trace Metal(loid)s in Soil–Plant Systems, J. Environ. Qual., 46 (2017) 1175–1189.

[20] C. Chen, D. Huang, J. Liu, Functions and toxicity of nickel in plants: Recent advances and future prospects, Clean - Soil, Air, Water, 37 (2009) 304–313.

[21] J. Barber, Photosystem II: The engine of life, Q. Rev. Biophys., 36 (2003) 71–89.

[22] C.A. Hebbern, K. Holst, A.H. Ladegaard, S.B. Schmidt, P. Pedas, Latent manganese deficiency increases transpiration in barley (Hordeum vulgare), Physiol. Plant., 135 (2009) 307–316.

[23] M. Intawongse, uptake of heavy metals by vegetable plants grown on contaminated soils their bioavailability and speciation, 2007.

[24] D.L. Callahan, A.J.M. Baker, S.D. Kolev, A.G. Wedd, Metal ion ligands in hyperaccumulating plants, J. Biol. Inorg. Chem., 11 (2006) 2–12.

[25] C.D. Walker, R.M. Welch, Low Molecular Weight Complexes of Zinc and Other Trace Metals in lettuce leaf, J. Agric. Food Chem., 35 (1987) 721–727.

[26] B.H. Irving, R.J.P. Williams, 3192 637, (1949).

[27] W.E. Rauser, Structure and function of metal chelators produced by plants, Cell Biochem. Biophys., 31 (1999) 19–48.

[28] S.P. Singh, K. Vogel-Mikuš, I. Arčon, P. Vavpetič, L. Jeromel, P. Pelicon, J. Kumar, R. Tuli, Pattern of iron distribution in maternal and filial tissues in wheat grains with contrasting levels of iron, J. Exp. Bot., 64 (2013) 3249–3260.

[29] J.Y. Cornu, U. Deinlein, S. Höreth, M. Braun, H. Schmidt, M. Weber, D.P. Persson, S. Husted, J.K. Schjoerring, S. Clemens, Contrasting effects of nicotianamine synthase knockdown on zinc and nickel tolerance and accumulation in the zinc/cadmium hyperaccumulator Arabidopsis halleri, New Phytol., 206 (2015) 738–750.

[30] D.L. Callahan, U. Roessner, V. Dumontet, N. Perrier, A.G. Wedd, R.A.J. O'Hair, A.J.M. Baker, S.D. Kolev, LC-MS and GC-MS metabolite profiling of nickel(II) complexes in the latex of the nickel-hyperaccumulating tree Sebertia acuminata and identification of methylated aldaric acid as a new nickel(II) ligand, Phytochemistry, 69 (2008) 240–251.

[31] G. AlChoubassi, J. Aszyk, P. Pisarek, K. Bierla, L. Ouerdane, J. Szpunar, R. Lobinski, Advances in mass spectrometry for iron speciation in plants, TrAC - Trends Anal. Chem., 104 (2018) 77–86.

[32] M.J. Haydon, C.S. Cobbett, Transporters of ligands for essential metal ions in plants, New Phytol., (2007) 499–506.

[33] J. Abadía, A. Lopez-Millan, A. Rombola, A. Abadia, Organic acids and Fe deficiency a review, Plant Soil, 241 (2002) 75–86.

[34] P.M. Flis, Développement de méthodes analytiques pour une spéciation à grande échelle des composés métalliques dans les plantes, university of Pau and Adour countries, 2013.

[35] R. Rellán-Álvarez, J. Giner-Martínez-Sierra, J. Orduna, I. Orera, J.Á. Rodríguez-Castrilln, J.I. García-Alonso, J. Abadía, A. Álvarez-Fernández, Identification of a Tri-Iron(III), Tri-Citrate Complex in the Xylem Sap of Iron-Deficient Tomato Resupplied with Iron: New Insights into Plant Iron Long-Distance Transport, Plant Cell Physiol., 51 (2010) 91–102.

[36] P. Flis, L. Ouerdane, L. Grillet, C. Curie, S. Mari, R. Lobinski, Inventory of metal complexes circulating in plant fluids: a reliable method based on HPLC coupled with dual elemental and high-resolution molecular mass spectrometric detection, New Phytol., 211 (2016) 1129–1141.

[37] D.E. Salt, R.C. Prince, A.J.M. Baker, I. Raskin, I.J. Pickering, Zinc Ligands in the Metal Hyperaccumulator Thlaspi caerulescens As Determined Using X-ray Absorption Spectroscopy, Environ. Sci. Technol., 33 (1999) 713–717.

[38] C. Curie, J.-F. Briat, IRON TRANSPORT AND SIGNALING IN PLANTS, Annu. Rev. Plant Biol., 54 (2003) 183–206.

[39] J. Morrissey, M. Guerinot, Iron uptake and transport in plants: The good, the bad, and the ionome, Chem. Rev., 109 (2009) 4553–4567.

[40] M.S. Otegui, R. Capp, L.A. Staehelin, Developing Seeds of Arabidopsis Store Different Minerals in Two Types of Vacuoles and in the Endoplasmic Reticulum, Plant Cell, 14 (2002) 1311–1327.

[41] T. Eagling, A.L. Neal, S.P. McGrath, S. Fairweather-Tait, P.R. Shewry, F.J. Zhao, Distribution and speciation of iron and zinc in grain of two wheat genotypes, J. Agric. Food Chem., 62 (2014) 708–716.

[42] O.A.H. Jones, D.A. Dias, D.L. Callahan, K.A. Kouremenos, D.J. Beale, U. Roessner, The use of metabolomics in the study of metals in biological systems, Metallomics, 7 (2015) 29–38.

[43] M.C. White, R.L. Chaney, A.M. Decker, Metal Complexation in Xylem Fluid, Plant Physiol., 67 (1981) 301–310.

[44] G.L. Mullins, L.E. Sommers, T.L. Housley, Metal speciation in xylem and phloem exudates, Plant Soil, 96 (1986) 377–391.

[45] M.T. Liao, M.J. Hedley, D.J. Woolley, R.R. Brooks, Nichols, Copper uptake and translocation in chicory (Cichorium intybus L cv Grasslands Puna) and tomato (Lycopersicon esculentum Mill cv Rondy) plants grown in NFT system I Copper uptake and distribution in plants, Plant Soil, 221 (n.d.) 135–142.

[46] U. Kramer, janet D. Cotter-howells, J.M. Charnock, A.J.M. Baker, J.A.C. Smith, free histidine as a metal chelator in plants that accumulate nickel, Nature, 379 (1996).

[47] R. Rellan-Alvarez, J. Abadia, A. Alvarez-Fernandez, Formation of metal-nicotianamine complexes as affected by pH, ligand exchange with citrate and metal exchange A study by electrospray ionization time-of-flight mass spectrometry, Rapid Commun. Mass Spectrom., (2008) 511–518.

[48] V. Sancenón, S. Puig, H. Mira, D.J. Thiele, L. Peñarrubia, Identification of a copper transporter family in Arabidopsis thaliana, Plant Mol. Biol., 51 (2003) 577–587.

[49] M. Pilon, Moving copper in plants, New Phytol., 192 (2011) 305–307.

[50] L. Zheng, N. Yamaji, K. Yokosho, J.F. Ma, YSL16 Is a Phloem-Localized Transporter of the Copper-Nicotianamine Complex That Is Responsible for Copper Distribution in Rice, Plant Cell, 24 (2012) 3767–3782.

[51] S. Shojima, N.-K. Nishizawa, S. Fushiya, S. Nozoe, T. Irifune, S. Mori, Biosynthesis of Phytosiderophores, Plant Physiol., 93 (1990) 1497–1503.

[52] B. Irtelli, W.A. Petrucci, F. Navari-Izzo, Nicotianamine and histidine/proline are, respectively, the most

important copper chelators in xylem sap of Brassica carinata under conditions of copper deficiency and excess, J. Exp. Bot., 60 (2009) 269–277.

[53] Y.F. Xue, T. Eagling, J. He, C.Q. Zou, S.P. McGrath, P.R. Shewry, F.J. Zhao, Effects of nitrogen on the distribution and chemical speciation of iron and zinc in pearling fractions of wheat grain, J. Agric. Food Chem., 62 (2014) 4738–4746.

[54] R. Terzano, Z. Al Chami, B. Vekemans, K. Janssens, T. Miano, P. Ruggiero, Zinc distribution and speciation within rocket plants (Eruca vesicaria L Cavalieri) grown on a polluted soil amended with compost as determined by XRF microtomography and Micro-XANES, J. Agric. Food Chem., 56 (2008) 3222–3231.

[55] T. Yoneyama, S. Ishikawa, S. Fujimaki, Route and regulation of zinc, cadmium, and iron transport in rice plants (Oryza sativa L) during vegetative growth and grain filling: Metal transporters, metal speciation, grain Cd reduction and Zn and Fe biofortification, Int. J. Mol. Sci., 16 (2015) 19111–19129.

[56] J. Wojcieszek, P. Kwiatkowski, L. Ruzik, Speciation analysis and bioaccessibility evaluation of trace elements in goji berries (Lycium Barbarum, L), J. Chromatogr. A, 1492 (2017) 70–78.

[57] L. Ruzik, P. Kwiatkowski, Application of CE-ICP-MS and CE-ESI-MS/MS for identification of Zn-binding ligands in Goji berries extracts, Talanta, 183 (2018) 102–107.

[58] D.R. Fernando, T. Mizuno, I.E. Woodrow, A.J.M. Baker, R.N. Collins, Characterization of foliar manganese (Mn) in Mn (hyper)accumulators using X-ray absorption spectroscopy, New Phytol., 188 (2010) 1014–1027.

[59] Y. Ishimaru, H. Masuda, K. Bashir, H. Inoue, T. Tsukamoto, M. Takahashi, H. Nakanishi, N. Aoki, T. Hirose, R. Ohsugi, N.K. Nishizawa, Rice metal-nicotianamine transporter, OsYSL2, is required for the long-distance transport of iron and manganese, Plant J., 62 (2010) 379–390.

[60] A. Sasaki, N. Yamaji, J. Xia, J.F. Ma, OsYSL6 Is Involved in the Detoxification of Excess Manganese in Rice, Plant Physiol., 157 (2011) 1832–1840.

[61] J. Rybak, L. Ruzik, Application of chromatography and mass spectrometry to the characterization of cobalt, copper, manganese and molybdenum in Morinda Citrifolia, J. Chromatogr. A, 1281 (2013) 19–25.

[62] L. Ouerdane, S. Mari, P. Czernic, M. Lebrun, R. Łobiński, Speciation of non-covalent nickel species in plant tissue extracts by electrospray Q-TOFMS/MS after their isolation by 2D size exclusion-hydrophilic interaction LC (SEC-HILIC) monitored by ICP-MS, J. Anal. At. Spectrom., 21 (2006) 676–683.

[63] E.M. Kroukamp, T. Wondimu, P.B.C. Forbes, Metal and metalloid speciation in plants: Overview, instrumentation, approaches and commonly assessed elements, TrAC - Trends Anal. Chem., 77 (2016) 87–99.

[64] S. Mari, D. Gendre, K. Pianelli, L. Ouerdane, R. Lobinski, J.F. Briat, M. Lebrun, P. Czernic, Root-to-shoot long-distance circulation of nicotianamine and nicotianamine-nickel chelates in the metal hyperaccumulator Thlaspi caerulescens, J. Exp. Bot., 57 (2006) 4111–4122.

[65] D. Gendre, P. Czernic, G. Conéjéro, K. Pianelli, J.F. Briat, M. Lebrun, S. Mari, TcYSL3, a member of the YSL gene family from the hyper-accumulator Thlaspi caerulescens, encodes a nicotianamine-Ni/Fe transporter, Plant J., 49 (2006) 1–15.

[66] L. Grillet, L. Ouerdane, P. Flis, M.T.T. Hoang, M.P. Isaure, R. Lobinski, C. Curie, S. Mari, Ascorbate efflux as a new strategy for iron reduction and transport in plants, J. Biol. Chem., 289 (2014) 2515–2525.

[67] G. Weber, N. von Wirén, H. Hayen, Hydrophilic interaction chromatography of small metal species in plants using sulfobetaine- and phosphorylcholine-type zwitterionic stationary phases, J. Sep. Sci., 31 (2008) 1615–1622.

[68] B. Shahzad, M. Tanveer, A. Rehman, S.A. Cheema, S. Fahad, S. Rehman, A. Sharma, Nickel; whether toxic or essential for plants and environment - A review, Plant Physiol. Biochem., 132 (2018) 641–651.

[69] A.F. López-Millán, F. Morales, A. Abadía, J. Abadia, Iron deficiency-associated changes in the composition of the leaf apoplastic fluid from field-grown pear (Pyrus communis L) trees, J. Exp. Bot., 52 (2001) 1489–1498.

[70] Y. Xuan, E.B. Scheuermann, A.R. Meda, H. Hayen, N. von Wirén, G. Weber, Separation and identification of phytosiderophores and their metal complexes in plants by zwitterionic hydrophilic interaction liquid chromatography coupled to electrospray ionization mass spectrometry, J. Chromatogr. A, 1136 (2006) 73–81.

[71] L.O. Tiffin, Iron Translocation II Citrate/Iron Ratios in Plant Stem Exudates, Plant Physiol., 41 (1966) 515–518.

[72] R. Nishiyama, M. Kato, S. Nagata, S. Yanagisawa, At. Yoneyama, Identification of Zn–Nicotianamine and Fe–20-Deoxymugineic Acid in the Phloem Sap from Rice Plants (Oryza sativa L), PCP Plant Cell Physiol., 53 (2012) 381–390.

[73] S. Lee, U.S. Jeon, S.J. Lee, Y.K. Kim, D.P. Persson, S. Husted, J.K. Schjørring, Y. Kakei, H. Masuda, N.K.

Nishizawa, G. An, Iron fortification of rice seeds through activation of the nicotianamine synthase gene, Proc. Natl. Acad. Sci. U. S. A., 106 (2009) 22014–22019.
[74] S.M. Kraemer, D.E. Crowley, R. Kretzschmar, Geochemical Aspects of Phytosiderophore-Promoted Iron Acquisition by Plants, Adv. Agron., 91 (2006) 1–46.
[75] A.F. Lopez-Millan, F. Morales, A. Abadia, J. Abadia, Effects of iron deficiency on the composition of the leaf apoplastic fluid and xylem sap in sugar beet Implications for iron and carbon transport, Plant Physiol., 124 (2000) 873–884.
[76] S. Clemens, M. Weber, The essential role of coumarin secretion for Fe acquisition from alkaline soil, Plant Signal. Behav., 11 (2016) 1–6.
[77] P. Sisó-Terraza, A. Luis-Villarroya, P. Fourcroy, J.-F. Briat, A. Abadía, F. Gaymard, J. Abadía, A. Álvarez-Fernández, Accumulation and Secretion of Coumarinolignans and other Coumarins in Arabidopsis thaliana Roots in Response to Iron Deficiency at High pH, Front. Plant Sci., 7 (2016) 1–22.
[78] P. Mladěnka, K. Macáková, L. Zatloukalová, Z. Řeháková, B.K. Singh, A.K. Prasad, V.S. Parmar, L. Jahodář, R. Hrdina, L. Saso, In vitro interactions of coumarins with iron, Biochimie, 92 (2010) 1108–1114.
[79] C. Krüger, O. Berkowitz, U.W. Stephan, R. Hell, A metal-binding member of the late embryogenesis abundant protein family transports iron in the phloem of Ricinus communis L, J. Biol. Chem., 277 (2002) 25062–25069.
[80] L. Guo, T.J. Cutright, Metal storage in reeds from an acid mine drainage contaminated field, Int. J. Phytoremediation, (2016) 1–26.
[81] F.R. Segura, E.A. Nunes, F.P. Paniz, A.C.C. Paulelli, G.B. Rodrigues, G.Ú.L. Braga, W. dos Reis Pedreira Filho, F. Barbosa, G. Cerchiaro, F.F. Silva, B.L. Batista, Potential risks of the residue from Samarco's mine dam burst (Bento Rodrigues, Brazil), Environ. Pollut., (2016) 1–13.
[82] F.J. Zhao, S.P. McGrath, Biofortification and phytoremediation, Curr. Opin. Plant Biol., 12 (2009) 373–380.
[83] S. Clemens, M.G. Palmgren, U. Kramer, A long way ahead : understanding and engineering plant metal accumulation, Trends Plant Sci., 7 (2002) 309–315.
[84] J.F. Briat, C. Curie, F. Gaymard, Iron utilization and metabolism in plants, Curr. Opin. Plant Biol., 10 (2007) 276–282.
[85] C. Palmer, M. Lou Guerinot, A question of balance: facing the challenges of Cu, Fe and Zn homeostasis, Nat Chem Biol, 5 (2009) 333–340.
[86] N. Gupta, H. Ram, B. Kumar, Mechanism of Zinc absorption in plants: uptake, transport, translocation and accumulation, Rev. Environ. Sci. Biotechnol., 15 (2016) 89–109.
[87] P.J. White, M.R. Broadley, Biofortification of crops with seven mineral elements often lacking in human diets – iron, zinc, copper, calcium, magnesium, selenium and iodine, New Phytol., 182 (2009) 49–84.
[88] M.L. Guerinot, Y. Yi, Iron: Nutritious, Noxious, and Not Readily Available, Plant Physiol., 104 (1994) 815–820.
[89] J.B. Passioura, The transport of water from soil to shoot in wheat seedlings, J. Exp. Bot., 31 (1980) 333–345.
[90] A.G. Netting, J.C. Theobald, I.C. Dodd, Xylem sap collection and extraction methodologies to determine in vivo concentrations of ABA and its bound forms by gas chromatography-mass spectrometry (GC-MS), Plant Methods, 8 (2012) 1–14.
[91] M. Alexou, A.. Peuke, Methods for Xylem Sap Collection, Plant Miner. Nutr. Methods Protoc. Methods Mol. Biol., 953 (2013) 195–207.
[92] K.L. Ponder, R.J. Watson, M. Malone, J. Pritchard, Mineral content of excreta from the spittlebug Philaenus spumarius closely matches that of xylem sap, New Phytol., 153 (2002) 237–241.
[93] M. Malone, R. Watson, J. Pritchard, The spittlebug Philaenus spumarius feeds from mature xylem at the full hydraulic tension of the transpiration stream, New Phytol., 143 (1999) 261–271.
[94] K.I.S. Beckett, A.B. Robertson, P.G.D. Matthews, Studies on gas exchange in the meadow spittlebug, Philaenus spumarius : the metabolic cost of feeding on, and living in, xylem sap, J. Exp. Biol., 222 (2019).
[95] P.F. Scholander, H.T. Hammel, E.D. Bradstreet, E.A. Hemmingsen, Sap pressure in vascular plants, Science (80-.)., 148 (1965) 339–346.
[96] T.S. Maier, J. Kuhn, C. Müller, Proposal for field sampling of plants and processing in the lab for environmental metabolic fingerprinting, Plant Methods, 6 (2010) 1–14.
[97] R. Ortega, A. Carmona, I. Llorens, P.L. Solari, X-ray absorption spectroscopy of biological samples A tutorial, J. Anal. At. Spectrom., 27 (2012) 2054–2065.
[98] J. Szpunar, part I principles and fundamentals, in: Hyphenated Tech. Speciat. Anal., 2003: pp. 2–13.
[99] J. Szpunar, Bio-inorganic speciation analysis by hyphenated techniques, Analyst, 125 (2000) 963–988.
[100] L. Beuvier, Developpement d'une methode de separation chromatographique couplee aux

spectrometries de masse a source d'ionisation a source plasma a couplage inductif (ICP-MS) : application a l'analyse de speciation des lanthanides, 2015.
[101] M. Batsala, B. Chandu, B. Sakala, S. Nama, S. Domatoti, Inductively Coupled Plasma Mass Spectrometry (Icp-Ms), Int. J. Res. Pharm. Chem., 2 (2012) 2231–2781.
[102] T. Wang, Liquid chromatography-inductively coupled plasma mass spectrometry (LC-ICP-MS), J. Liq. Chromatogr. Relat. Technol., 30 (2007) 807–831.
[103] S. Forcisi, F. Moritz, B. Kanawati, D. Tziotis, R. Lehmann, P. Schmitt-Kopplin, Liquid chromatography-mass spectrometry in metabolomics research: Mass analyzers in ultra high pressure liquid chromatography coupling, J. Chromatogr. A, 1292 (2013) 51–65.
[104] G. Kahsay, H. Song, A. Van Schepdael, D. Cabooter, E. Adams, Hydrophilic interaction chromatography (HILIC) in the analysis of antibiotics, J. Pharm. Biomed. Anal., 87 (2014) 142–154.
[105] J. Szpunar, Advances in analytical methodology for bioinorganic speciation analysis : metallomics , metalloproteomics and heteroatom-tagged proteomics and metabolomics, Analyst, 130 (2005) 442–465.
[106] G.H.L. Sciences, Size Exclusion Chromatography princicples and methods, 2000.
[107] Harvard apparatus, Guide to Gel Filtration or size exclusion chromatography, Massachusetts, n.d.
[108] K.O. Eriksson, Reversed Phase Chromatography, Biopharm. Process. Dev. Des. Implement. Manuf. Process., (2018) 433–439.
[109] L. Ruzik, J. Wojcieszek, In vitro digestion method for estimation of copper bioaccessibility in Açaí berry, Monatshefte Fur Chemie, 147 (2016) 1429–1438.
[110] J. Wojcieszek, L. Ruzik, Enzymatic Extraction of Copper Complexes with Phenolic Compounds from Açaí (Euterpe oleracea Mart) and Bilberry (Vaccinium myrtillus L) Fruits, Food Anal. Methods, 9 (2016) 2105–2114.
[111] P. Jandera, Stationary and mobile phases in hydrophilic interaction chromatography : a review, Anal. Chim. Acta, 692 (2011) 1–25.
[112] B. Buszewski, S. Noga, Hydrophilic interaction liquid chromatography (HILIC) — a powerful separation technique, Anal Bioanal Chem, 402 (2012) 231–247.
[113] Y. Kawachi, T. Ikegami, H. Takubo, Y. Ikegami, M. Miyamoto, N. Tanaka, Chromatographic characterization of hydrophilic interaction liquid chromatography stationary phases : Hydrophilicity , charge effects , structural selectivity , and separation efficiency, J. Chromatogr. A, 1218 (2011) 5903–5919.
[114] G. Greco, T. Letzel, Main Interactions and Influences of the Chromatographic Parameters in HILIC Separations, J. Chromatogr. Sci., 51 (2013) 684–693.
[115] D. Xie, J. Mattusch, R. Wennrich, Retention of arsenic species on zwitterionic stationary phase in hydrophilic interaction chromatography, J. Sep. Sci., 33 (2010) 817–825.
[116] E. De Hoffmann, V. Stroobant, Mass spectrometry-principles and applications, 2010.
[117] A.G. Marshall, C.L. Hendrickson, S.D.-H. Shi, High-Resolution FT-ICRMS, Anal. Chem., 74 (2002) 252–259.
[118] P. Poho, T. Hyotylainen, Mass Spectrometric Detection for Chromatography, RSC Chromatogr. Monogr. Chromatogr. Methods Metabolomics, (2013).
[119] D. Banerjee, Inductively Coupled Plasma Mass Spectrometry, Anal. Tech. Sci., (2005).
[120] T.W. May, R.H. Wiedmeyer, U.S.G. Survey, B.R. Division, A Table of Polyatomic Interferences in ICP-MS, At. Spectrosc., 19 (1998) 150–155.
[121] B. Michalke, Element speciation definitions, analytical methodology, and some examples, Ecotoxicol. Environ. Saf., 56 (2003) 122–139.
[122] R. Thomas, practical guide to ICP MS, maryland USA, 2004.
[123] A.G. Marshall, C.L. Hendrickson, High-Resolution Mass Spectrometers, Annu. Rev. Anal. Chem., 1 (2008) 579–599.
[124] M. Scigelova, M. Hornshaw, A. Giannakopulos, A. Makarov, fourier transform mass spectrometry, Mol. Cell. Proteomics, (2011) 1–19.
[125] R.A. Zubarev, A. Makarov, Orbitrap mass spectrometry, Anal. Chem., 85 (2013) 5288–5296.
[126] S. Vasquez, Introduction to Tandem Mass Spectrometry, in: Forensic Anal. Sci. Serv., 2010.
[127] J.K. Prasain, Tandem Mass Spectrometry-applications and principles, 2012.
[128] V. Gabelica, A.A. Shvartsburg, C. Afonso, P. Barran, J.L.P. Benesch, C. Bleiholder, M.T. Bowers, A. Bilbao, M.F. Bush, J.L. Campbell, I.D.G. Campuzano, T. Causon, B.H. Clowers, C.S. Creaser, E. De Pauw, J. Far, F. Fernandez-Lima, J.C. Fjeldsted, K. Giles, M. Groessl, et al., Recommendations for reporting ion mobility Mass Spectrometry measurements, Mass Spectrom. Rev., 38 (2019) 291–320.
[129] T. Mairinger, T.J. Causon, S. Hann, The potential of ion mobility–mass spectrometry for non-targeted metabolomics, Curr. Opin. Chem. Biol., 42 (2018) 9–15.

[130] X. Zhang, K. Quinn, C. Cruickshank-Quinn, R. Reisdorph, N. Reisdorph, The application of ion mobility mass spectrometry to metabolomics, Curr. Opin. Chem. Biol., 42 (2018) 60–66.
[131] J.E. Kyle, X. Zhang, K.K. Weitz, M.E. Monroe, Y.M. Ibrahim, R.J. Moore, J. Cha, X. Sun, E.S. Lovelace, J. Wagoner, S.J. Polyak, T.O. Metz, S.K. Dey, R.D. Smith, K.E. Burnum-Johnson, E.S. Baker, Uncovering biologically significant lipid isomers with liquid chromatography, ion mobility spectrometry and mass spectrometry, Analyst, (2016) 1649–1659.
[132] G. Ben-Nissan, M. Sharon, The application of ion-mobility mass spectrometry for structure/function investigation of protein complexes, Curr. Opin. Chem. Biol., 42 (2018) 25–33.
[133] A.B. Kanu, P. Dwivedi, M. Tam, L. Matz, H.H.H. Jr, Proteomic analysis of metacyclic trypomastigotes undergoing Trypanosoma cruzi metacyclogenesis, J. Mass Spectrom., 42 (2007) 1422–1432.
[134] S.K. Wiedmer, T. Hyötyläinen, Selection of Analytical Methodology for Metabolomics, RSC Chromatogr. Monogr., (2013) 1–10.
[135] P. Rodríguez-González, J.M. Marchante-Gayón, J.I. García Alonso, A. Sanz-Medel, Isotope dilution analysis for elemental speciation: A tutorial review, Spectrochim. Acta - Part B, 60 (2005) 151–207.
[136] M. Hoppler, C. Zeder, T. Walczyk, Quantification of ferritin-bound iron in plant samples by isotope tagging and species-specific isotope dilution mass spectrometry, Anal. Chem., 81 (2009) 7368–7372.
[137] K.G. Heumann, Isotope dilution mass spectrometry, Int. J. Mass Spectrom. Ion Process., 118–119 (1992) 575–592.
[138] P. Rodríguez-González, J.I. García Alonso, Recent advances in isotope dilution analysis for elemental speciation, J. Anal. At. Spectrom., 25 (2010) 239–259.
[139] C. Swart, O. Rienitz, D. Schiel, Impact of pump flow fluctuations on post column online ID-ICP-MS, Anal. Bioanal. Chem., 401 (2011) 2025–2031.
[140] D. Schaumlöffel, R. Łobiński, Isotope dilution technique for quantitative analysis of endogenous trace element species in biological systems, Int. J. Mass Spectrom., 242 (2005) 217–223.
[141] N. Hardy, R. Hall, methods in molecular biology, 2012.
[142] R.J.P. Williams, Chemical selection of elements by cells, Coord. Chem. Rev., 216–217 (2001) 583–595.
[143] M. Montes-Bayón, M. Sharar, M. Corte-Rodriguez, Trends on (elemental and molecular) mass spectrometry based strategies for speciation and metallomics, TrAC - Trends Anal. Chem., 104 (2018) 4–10.
[144] S. Mounicou, J. Szpunar, R. Lobinski, Metallomics: The concept and methodology, Chem. Soc. Rev., 38 (2009) 1119–1138.
[145] J. López-Barea, J.L. Gómez-Ariza, Environmental proteomics and metallomics, Proteomics, 6 Suppl 1 (2006) 51–62.
[146] K. Spagou, H. Tsoukali, N. Raikos, H. Gika, I.D. Wilson, G. Theodoridis, Hydrophilic interaction chromatography coupled to MS for metabonomic/metabolomic studies, J. Sep. Sci., 33 (2010) 716–727.
[147] E. Rathahao-Paris, S. Alves, C. Junot, J.C. Tabet, High resolution mass spectrometry for structural identification of metabolites in metabolomics, Metabolomics, 12 (2016) 1–15.
[148] R. Ge, X. Sun, Q.-Y. He, Overview of the Metallometabolomic Methodology for Metal-Based Drug Metabolism, Curr. Drug Metab., 12 (2011) 287–299.
[149] W. Chen, G. Zhang, W. Chen, Q. Zhong, H. Chen, metabolomic profiling of matured coconut water during post harvest storage revealed discrimination and distinct changes in metabolites, RSC Adv., 8 (2018) 31396–31405.
[150] R.D. Hall, I.D. Brouwer, M.A. Fitzgerald, Plant metabolomics and its potential application for human nutrition, Physiol. Plant., 132 (2008) 162–175.
[151] S.F. Graham, E. Amigues, M. Migaud, R.A. Browne, Application of NMR based metabolomics for mapping metabolite variation in European wheat, Metabolomics, 5 (2009) 302–306.
[152] S. Moco, R.J. Bino, O. Vorst, H.A. Verhoeven, J. De Groot, T.A. Van Beek, J. Vervoort, C.H.R. De Vos, J. de Groot, T. van Beek, R. de Vos, A liquid chromatography-mass spectrometry-based metabolome database for tomato, Plant Physiol., 141 (2006) 1205–1218.
[153] A. Moing, A. Aharoni, B. Biais, I. Rogachev, S. Meir, L. Brodsky, J.W. Allwood, A. Erban, W.B. Dunn, L. Kay, S. de Koning, R.C.H. de Vos, H. Jonker, R. Mumm, C. Deborde, M. Maucourt, S. Bernillon, Y. Gibon, T.H. Hansen, S. Husted, et al., Extensive metabolic cross-talk in melon fruit revealed by spatial and developmental combinatorial metabolomics, New Phytol., 190 (2011) 683–696.
[154] M. Jahangir, H.K. Kim, Y.H. Choi, R. Verpoorte, health-affecting Compounds in Br assicaceae, Compr. Rev. FOOD Sci. FOOD Saf., 8 (2009) 31–43.
[155] C. Lindinger, P. Pollien, R.C.H. De Vos, Y. Tikunov, J.A. Hageman, C. Lambot, R. Fumeaux, E. Voirol-Baliguet, I. Blank, Identification of ethyl formate as a quality marker of the fermented off-note in coffee

by a nontargeted chemometric approach, J. Agric. Food Chem., 57 (2009) 9972–9978.
[156] M. Beckmann, D.P. Enot, D.P. Overy, J. Draper, Representation , Comparison , and Interpretation of Metabolome Fingerprint Data for Total Composition Analysis and Quality Trait Investigation in Potato Cultivars, J. Agric. Food Chem., 55 (2007) 3444–3451.
[157] D. González-Peña, L. Brennan, Recent Advances in the Application of Metabolomics for Nutrition and Health, Annu. Rev. Food Sci. Technol., 10 (2019) 479–519.
[158] E. P. Ryan, A. L. Heuberger, C. D. Broeckling, E. C. Borresen, C. Tillotson, J. E. Prenni, Advances in Nutritional Metabolomics, Curr. Metabolomics, 1 (2013) 109–120.
[159] M. Hoppler, I. Egli, N. Petry, D. Gille, C. Zeder, T. Walczyk, M.W. Blair, R.F. Hurrell, Iron Speciation in Beans (Phaseolus vulgaris) Biofortified by Common Breeding, J. Food Sci., 79 (2014) C1–C6.
[160] J. Köster, R. Shi, N. Von Wirén, G. Weber, Evaluation of different column types for the hydrophilic interaction chromatographic separation of iron-citrate and copper-histidine species from plants, J. Chromatogr. A, 1218 (2011) 4934–4943.
[161] R. Terzano, T. Mimmo, B. Vekemans, L. Vincze, G. Falkenberg, N. Tomasi, M. Schnell Ramos, R. Pinton, S. Cesco, Iron (Fe) speciation in xylem sap by XANES at a high brilliant synchrotron X-ray source: Opportunities and limitations, Anal. Bioanal. Chem., 405 (2013) 5411–5419.
[162] A.L. Neal, K. Geraki, S. Borg, P. Quinn, J.F. Mosselmans, H. Brinch-Pedersen, P.R. Shewry, Iron and zinc complexation in wild-type and ferritin-expressing wheat grain: Implications for mineral transport into developing grain, J. Biol. Inorg. Chem., 18 (2013) 557–570.
[163] M. Tsednee, Y.W. Mak, Y.R. Chen, K.C. Yeh, A sensitive LC-ESI-Q-TOF-MS method reveals novel phytosiderophores and phytosiderophore-iron complexes in barley, New Phytol., 195 (2012) 951–961.
[164] J. Köster, H. Hayen, N. von Wirén, G. Weber, Isoelectric focusing of small non-covalent metal species from plants, Electrophoresis, 32 (2011) 772–781.
[165] N. De Brier, S. V. Gomand, E. Donner, D. Paterson, E. Smolders, J.A. Delcour, E. Lombi, Element distribution and iron speciation in mature wheat grains (Triticum aestivum L) using synchrotron X-ray fluorescence microscopy mapping and X-ray absorption near-edge structure (XANES) imaging, Plant Cell Environ., 39 (2016) 1835–1847.
[166] D.P. Persson, T.H. Hansen, K.H. Laursen, J.K. Schjoerring, S. Husted, Simultaneous iron, zinc, sulfur and phosphorus speciation analysis of barley grain tissues using SEC-ICP-MS and IP-ICP-MS, Metallomics, 1 (2009) 418–426.
[167] G. Sarret, P. Saumitou-laprade, V. Bert, O. Proux, J. Hazemann, A. Traverse, M. Marcus, A. Manceau, G. Sarret, P. Saumitou-laprade, V. Bert, O. Proux, J. Hazemann, Forms of zinc accumulated in the hyperaccumulator Arabidopsis halleri, Plant Physiol. Am. Soc. Plant Biol., 130 (2002) 1815–1826.
[168] S. Lee, D.P. Persson, T.H. Hansen, S. Husted, J.K. Schjoerring, Y.S. Kim, U.S. Jeon, Y.K. Kim, Y. Kakei, H. Masuda, N.K. Nishizawa, G. An, Bio-available zinc in rice seeds is increased by activation tagging of nicotianamine synthase, Plant Biotechnol. J., 9 (2011) 865–873.
[169] A. Straczek, G. Sarret, A. Manceau, P. Hinsinger, N. Geoffroy, B. Jaillard, Zinc distribution and speciation in roots of various genotypes of tobacco exposed to Zn, (2008) 1–21.
[170] Z. Wei, J.W. Wong, D. Chen, Speciation of heavy metal binding non-protein thiols in Agropyron elongatum by size-exclusion HPLC-ICP-MS, Microchem. J., 74 (2003) 207–213.
[171] H. Kupper, A. Mijovilovich, W. Meyer-Klaucke, P.M.H. Kroneck, Tissue- and Age-Dependent Differences in the Complexation of Cadmium and Zinc in the Cadmium Zinc Hyperaccumulator Thlaspi caerulescens (Ganges Ecotype) Revealed by X-Ray absorption spectroscopy, Plant Physiol., 134 (2004) 748–757.
[172] L. Lu, X. Liao, J. Labavitch, X. Yang, E. Nelson, Y. Du, P.H. Brown, S. Tian, Speciation and localization of Zn in the hyperaccumulator Sedum alfredii by extended X-ray absorption fine structure and micro-X-ray fluorescence, Plant Physiol. Biochem., 84 (2014) 224–232.
[173] A.C. Monsant, P. Kappen, Y. Wang, P.J. Pigram, A.J.M. Baker, C. Tang, In vivo speciation of zinc in Noccaea caerulescens in response to nitrogen form and zinc exposure, Plant Soil, 348 (2011) 167–183.
[174] U. Deinlein, M. Weber, H. Schmidt, S. Rensch, A. Trampczynska, T.H. Hansen, S. Husted, J.K. Schjoerring, I.N. Talke, U. Krämer, S. Clemens, Elevated nicotianamine levels in Arabidopsis halleri roots play a key role in zinc hyperaccumulation, Plant Cell, 24 (2012) 708–723.
[175] K. Hazama, S. Nagata, T. Fujimori, S. Yanagisawa, T. Yoneyama, Concentrations of metals and potential metal-binding compounds and speciation of Cd, Zn and Cu in phloem and xylem saps from castor bean plants (Ricinus communis) treated with four levels of cadmium, Physiol. Plant., 154 (2015) 243–255.
[176] T. Schneider, D.P. Persson, S. Husted, M. Schellenberg, P. Gehrig, Y. Lee, E. Martinoia, J.K. Schjoerring, S. Meyer, A proteomics approach to investigate the process of Zn hyperaccumulation in Noccaea caerulescens (J and C Presl) FK Meyer, Plant J., 73 (2013) 131–142.

[177] N. Von Wirén, H. Marschner, V. Römheld, Roots of iron-efficient maize also absorb phytosiderophore-chelated zinc, Plant Physiol., 111 (1996) 1119–1125.
[178] J.A. Hernandez-Viezcas, H. Castillo-Michel, J.C. Andrews, M. Cotte, C. Rico, J.R. Peralta-Videa, Y. Ge, J.H. Priester, P.A. Holden, J.L. Gardea-Torresdey, In situ synchrotron X-ray fluorescence mapping and speciation of CeO 2 and ZnO nanoparticles in soil cultivated soybean (Glycine max), ACS Nano, 7 (2013) 1415–1423.
[179] J.A. Hernandez-Viezcas, H. Castillo-Michel, A.D. Servin, J.R. Peralta-Videa, J.L. Gardea-Torresdey, Spectroscopic verification of zinc absorption and distribution in the desert plant Prosopis juliflora-velutina (velvet mesquite) treated with ZnO nanoparticles, Chem. Eng. J., 170 (2011) 346–352.
[180] S. Alves, C. Nabais, M. de L. Simões Gonçalves, M.M. Correia dos Santos, Nickel speciation in the xylem sap of the hyperaccumulator Alyssum serpyllifolium ssp lusitanicum growing on serpentine soils of northeast Portugal, J. Plant Physiol., 168 (2011) 1715–1722.
[181] M. Guilpain, B. Laubie, X. Zhang, J.L. Morel, M.O. Simonnot, Speciation of nickel extracted from hyperaccumulator plants by water leaching, Hydrometallurgy, 180 (2018) 192–200.
[182] U. Krämer, I.J. Pickering, R.C. Prince, I. Raskin, D.E. Salt, Subcellular localization and speciation of nickel in hyperaccumulator and non-accumulator Thlaspi species, Plant Physiol., 122 (2000) 1343–1353.
[183] E. Montargès-Pelletier, V. Chardot, G. Echevarria, L.J. Michot, A. Bauer, J.L. Morel, Identification of nickel chelators in three hyperaccumulating plants: An X-ray spectroscopic study, Phytochemistry, 69 (2008) 1695–1709.
[184] K. Peeters, T. Zuliani, D. Zigon, R. Milacic, J. Scancar, Nickel speciation in cocoa infusions using monolithic chromatography – Post-column ID-ICP-MS and Q-TOF-MS, Food Chem., 230 (2017) 327–335.
[185] A. Van Der Ent, R. Mak, M.D. De Jonge, H.H. Harris, Simultaneous hyperaccumulation of nickel and cobalt in the tree Glochidion cf sericeum (Phyllanthaceae): Elemental distribution and chemical speciation, Sci. Rep., 8 (2018) 1–15.
[186] T. Yamaguchi, C. Tsukada, K. Takahama, T. Hirotomo, R. Tomioka, C. Takenaka, Localization and speciation of cobalt and nickel in the leaves of the cobalt-hyperaccumulating tree Clethra barbinervis, Trees - Struct. Funct., 33 (2018) 521–532.
[187] P.M. Kopittke, N.W. Menzies, M.D. de Jonge, B.A. Mckenna, E. Donner, R.I. Webb, D.J. Paterson, D.L. Howard, C.G. Ryan, C.J. Glover, K.G. Scheckel, E. Lombi, In situ distribution and speciation of toxic copper, nickel, and zinc in hydrated roots of cowpea, Plant Physiol., 156 (2011) 663–673.
[188] E. Spielman-Sun, E. Lombi, E. Donner, A. Avellan, B. Etschmann, D. Howard, G. V. Lowry, Temporal Evolution of Copper Distribution and Speciation in Roots of Triticum aestivum Exposed to CuO, Cu(OH)2, and CuS Nanoparticles, Environ. Sci. Technol., 52 (2018) 9777–9784.
[189] M.T. Liao, M.J. Hedley, D.J. Woolley, R.R. Brooks, M.A. Nichols, Copper uptake and translocation in chicory (Cichorium intybus L cv Grasslands Puna) and tomato (Lycopersicon esculentum Mill cv Rondy) plants grown in NFT system II The role of nicotianamine and histidine in xylem sap copper transport, Plant Soil, 223 (n.d.) 243–252.
[190] R.A. De Sousa, N. Baccan, S. Cadore, Determination of Metals in Brazilian Coconut Water Using an Inductively Coupled Plasma Optical Emission Spectrometer, J. Braz. Chem. Soc, 16 (2005) 540–544.
[191] R.A. De Sousa, C.J.J. Silva, N. Baccan, S. Cadore, Determination of metals in bottled coconut water using an inductively coupled plasma optical emission spectrometer, J. Food Compos. Anal., 18 (2005) 399–408.
[192] A.M.N. Silva, X. Kong, M.C. Parkin, R. Cammack, R.C. Hider, Iron(iii) citrate speciation in aqueous solution, Dalt. Trans., (2009) 8616–8625.
[193] T.A. Berger, Characterization of a 2 6 microm Kinetex porous shell hydrophilic interaction liquid chromatography column in supercritical fluid chromatography with a comparison to 3 microm totally porous silica, J. Chromatogr. A, 1218 (2011) 4559–4568.
[194] I. Ali, Z.A. Al-othman, M. Al-za, Superficially porous particles columns for super fast HPLC separations, Biomed. Chromatogr., 26 (2012) 1001–1008.
[195] E. Oláh, S. Fekete, J. Fekete, K. Ganzler, Comparative study of new shell-type , sub-2 microm fully porous and monolith stationary phases , focusing on mass-transfer resistance, J. Chromatogr. A, 1217 (2010) 3642–3653.
[196] D. Garica-Gomez, E. Rodriguez-Gonzalo, R. Carabias-MArtinez, Stationary phases for separation of nucleosides and nucleotides by hydrophilic interaction liquid chromatography, Trends Anal. Chem., 47 (2013) 111–128.
[197] V.G. Mihucz, E. Tatár, B. Kmethy, G. Záray, E. Cseh, Investigation of the transported heavy metal ions in xylem sap of cucumber plants by size exclusion chromatography and atomic absorption spectrometry, J. Inorg. Biochem., 81 (2000) 81–87.

[198] Z.G. Wei, J.W.C. Wong, H.Y. Zhao, H.J. Zhang, H.X. Li, F. Hu, Separation and determination of heavy metals associated with low molecular weight chelators in xylem saps of Indian mustard (Brassica juncea) by size exclusion chromatography and atomic absorption spectrometry, Biol. Trace Elem. Res., 118 (2007) 146–158.

[199] C. Bovet, Aspects botaniques, applications et perspectives thérapeutiques de Cocos nucifera L, Nantes, 2017.

[200] A. Prades, M. Dornier, N. Diop, J.-P. Pain, Coconut water preservation and processing: a review, Fruits, 67 (2012) 157–171.

[201] A. Obike, Proximate and Trace Metal Analysis of Coconut (Cocos nucifera) Collected from Southeastern , Nigeria Proximate and Trace Metal Analysis of Coconut (Cocos nucifera) Collected from Southeastern , Nigeria, 3 (2017) 357–361.

[202] J.W.H. Yong, L. Ge, Y.F. Ng, S.N. Tan, The Chemical Composition and Biological Properties of Coconut (Cocos nucifera L) Water, Molecules, 14 (2009) 5144–5164.

[203] A. Prades, determination de la qualite de l'eau de coco en fonction du stade de maturation des noix et lors de sa stabilisation par chauffage ohmique et filtration membranaire, Montpellier II, 2011.

[204] C. Bovet, Aspects botaniques, applications et perspectives thérapeutiques de Cocos nucifera L, 2017.

[205] J.C. Jackson, A. Gordon, G. Wizzard, K. McCook, R. Rolle, Changes in chemical composition of coconut (Cocos nucifera) water during maturation of the fruit, J. Sci. Food Agric., 84 (2004) 1049–1052.

[206] T.C. Tan, L.H. Cheng, R. Bhat, G. Rusul, A.M. Easa, Effectiveness of ascorbic acid and sodium metabisulfite as anti-browning agent and antioxidant on green coconut water (Cocos nucifera) subjected to elevated thermal processing, Int. Food Res. J., 22 (2015) 631–637.

[207] G.A. Petroianu, M. Kosanovic, I. Saad Shehatta, B. Mahgoub, A. Saleh, W.H. Maleck, Green coconut water for intravenous use: Trace and minor element content, J. Trace Elem. Exp. Med., 17 (2004) 273–282.

[208] U. Santoso, K. Kubo, T. Ota, T. Tadokoro, A. Maekawa, Nutrient composition of kopyor coconuts (Cocos nucifera L), Food Chem., 57 (1996) 299–304.

[209] D. Campbell-Falck, T. Thomas, T.M. Falck, N. Tutuo, K. Clem, The intravenous use of coconut water, Am. J. Emerg. Med., 18 (2000) 108–111.

[210] I. Md Didarul, A. Rahaman, A. Afrose, Assessment of Heavy Metal Concentration in Coconut Water, Recent Res. Sci. Technol., 10 (2018) 07–10.

[211] E.M. Richter, D.P. De Jesus, R.A.A. Muñoz, C.L. Do Lago, L. Angnes, Determination of anions, cations, and sugars in coconut water by capillary electrophoresis, J. Braz. Chem. Soc., 16 (2005) 1134–1139.

[212] B.K. Uphade, S.S. Shelke, D.G. Thorat, Studies on Some Physico-Chemical Characteristics of Coconut Water Near Sugar and Chemical Factory , Kopergaon (MS), Int. J. Chem. Sci, 6 (2008) 2052–2054.

[213] R. Assa, J. Konan, N. Agbo, A. Prades, J. Nemlin, Caracteristiques physico-chimiques de l'eau des fruits de quatre cultivars de cocotier (Cocos nucifera l) en Côte d'Ivoire, Agron. Africaine, 19 (2007) 41–51.

[214] G. Chandrajith, A.C. Kannangara, K. Ranaweera, Comparative analysis of coconut water in four different maturity stages, J. Pharmacogn. Phytochem., 7 (2018) 1814–1817.

[215] A.K. Karna, A. Srinivasulu, S.P. Kumar, Review on physico chemical characters on tender nut of coconut (Cocus nucifera L), Int. J. Chem. Stud., 6 (2018) 2292–2297.

[216] A. Terdwongworakul, S. Chaiyapong, B. Jarimopas, W. Meeklangsaen, Physical properties of fresh young Thai coconut for maturity sorting, Biosyst. Eng., 103 (2009) 208–216.

[217] W. Chen, G. Zhang, W. Chen, Q. Zhong, H. Chen, Metabolomic profiling of matured coconut water during post-harvest storage revealed discrimination and distinct changes in metabolites, RSC Adv., 8 (2018) 31396–31405.

[218] W.H.O. Ernst, Bioavailability of heavy metals and decontamination of soils by plants, Appl. Geochemistry, 11 (1996) 163–167.

[219] T.O. de Araújo, L. de Freitas-Silva, B.V.N. Santana, K.N. Kuki, E.G. Pereira, A.A. Azevedo, L.C. da Silva, Tolerance to iron accumulation and its effects on mineral composition and growth of two grass species, Environ. Sci. Pollut. Res., 21 (2014) 2777–2784.

[220] B.V.N. Santana, T.O. de Araújo, G.C. Andrade, L. de Freitas-Silva, K.N. Kuki, E.G. Pereira, A.A. Azevedo, L.C. da Silva, Leaf morphoanatomy of species tolerant to excess iron and evaluation of their phytoextraction potential, Environ. Sci. Pollut. Res., 21 (2014) 2550–2562.

[221] A. Álvarez-fernández, P. Díaz-benito, A. Abadía, A. Lopez-Millan, J. Abadía, Metal species involved in long distance metal transport in plants, Front. Plant Sci., 5 (2014) 1–20.

[222] T. Oliveira, D. Araujo, M. Isaure, G. Choubassi, K. Bierla, J. Szpunar, Paspalum urvillei and Setaria parviflora , two grasses naturally adapted to extreme iron-rich environments , Plant Physiol. Biochem., (to be submitted).

7 List of figures

8 List of tables

9 Annexes

9.1 Article 1

Advances in mass spectrometry for iron speciation in plants

Trends in Analytical Chemistry

Trends in Analytical Chemistry 104 (2018) 77–86

Contents lists available at ScienceDirect

Trends in Analytical Chemistry

journal homepage: www.elsevier.com/locate/trac

Advances in mass spectrometry for iron speciation in plants

Ghaya AlChoubassi [a], Justyna Aszyk [a, b], Paulina Pisarek [a, c], Katarzyna Bierla [a], Laurent Ouerdane [a], Joanna Szpunar [a, *], Ryszard Lobinski [a, c]

[a] Institute of Analytical Sciences, IPREM, UMR 5254 CNRS-UPPA, Hélioparc, Pau, France
[b] Department of Analytical Chemistry, Faculty of Chemistry, Gdańsk University of Technology, 11/12 Narutowicza Str, Gdańsk, Poland
[c] Department of Analytical Chemistry, Warsaw University of Technology, Noakowskiego 3, 00-664, Warsaw, Poland

ARTICLE INFO

Article history:
Available online 10 November 2017

Keywords:
Iron Speciation
X ray spectroscopy
Liquid chromatography
ICP MS
Electrospray mass spectrometry
Isotope dilution

ABSTRACT

Iron is an important nutrient essential for plants and critical for human health. The state-of-the art of methods for iron speciation in cereal grains and plant fluids is critically reviewed. Particular attention is given to the latest developments in the coupling of HPLC with the parallel ICP MS and electrospray ionization (ESI) MS/MS detection, usually QTOF MS or Q-Orbitrap MS, for the identification and quantification of iron species. The coupled techniques allow the direct microanalysis of plant intracellular fluids (xylem and phloem) and complement X-ray absorption spectroscopy (XANES and EXAFS). The increasing resolution and sensitivity of electrospray mass spectrometers and emergence of software allowing extraction of iron specific data from large chromatographic data sets are responsible for the growing role of electrospray MS/MS in speciation studies. The use of stable isotopes for the probing of the reactivity and stability of endogenous metal complexes and quantitative analysis are rising in importance.

1. Introduction

Iron deficiency anemia which is a consequence of inadequate dietary intake and low bioavailability of iron affects ca. 30% of the world's population [1]. It produces serious adverse health effects with socioeconomic implications and combating it has been considered as one of the 10 major challenges faced by the mankind [1]. The core of the problem is the unfavorable iron speciation: relatively low levels of non-heme iron and high levels of dietary factors, such as e.g. phytic acid, which inhibit human iron absorption in stable food crops [2].

The challenges driving research in iron speciation in plants include the understanding of the mechanisms governing the uptake of iron from soil, its transport to aboveground plant tissues and storage, and of the mechanisms of the bioavailability of Fe from staple food, such as wheat, beans, barley, or maize [3,4]. The iron concentrations reported in studies of edible grains varied between 15 and 115 μg/g [3–7]. Higher plants have developed two distinct strategies to acquire iron, which is only slightly soluble in soil, from the rhizosphere: (i) the reduction strategy where Fe(III) is reduced to Fe(II) which can then be transported into the root epidermal cells by the divalent metal transporters and (ii) the chelation strategy where Fe(III) is complexed by soluble phytosiderophores (PS) induced upon iron deficiency and released from the root epidermis, the resulting Fe (III)-PS complexes are readily transported back into the roots [8,9]. Coumarins were recently discovered to play an important role in Fe acquisition from soil for plants [10,11]. However, the actual formation of a Fe-coumarin metal complex in root exudate seems not to have been confirmed yet. As a consequence, the direct role (by complexation) of coumarins in iron uptake [and not only by reduction of Fe(III)] cannot be proved. Chelating ability was found in an *in vitro* model study for the coumarins with 2-hydroxyl groups in ortho position, but not for those with single hydroxyl groups [12]. In a recent review the need to carry out much more work was postulated to fully understand the strong beneficial effect of coumarin secretion on Fe acquisition under alkaline conditions, both biochemically and physiologically [10].

The understanding of the iron metabolism which is critically dependent on the fine knowledge of its speciation may facilitate genetic engineering in order to increase the iron content in the required chemical form (and in a specific plant organ) in the context of human nutrition or environmental clean-up by phytoremediation [13] (*cf.* the case of the recent red mud flooding in Brazil [14]). Hyperaccumulation of iron is achieved through coordination of several processes, including enhanced metal uptake (assisted by secretion of siderophores), efficient root-to-shoot translocation and effective detoxification in leaves [15]. An additional important

* Corresponding author.
E-mail address: joanna.szpunar@univ-pau.fr (J. Szpunar).

https://doi.org/10.1016/j.trac.2017.11.006
0165-9936/

factor in the context of biofortification is the translocation of iron into (edible) grains.

Iron in plants occurs in two principal oxidation states Fe(II) and Fe(III) and in a variety of complexes of different stability. The most popular ligands complexing iron in plants are summarized in Fig. 1. The compounds of interest in speciation studies include: (i) soluble complexes with organic acids (ferric and ferrous citrates, mixed citrate-malates, aspargates), (ii) siderophores – high-affinity Fe(III) chelating compounds derived from nicotianamine: mugineic acid, 3-hydroxymugineic acid, 2′-deoxymugineic acid, avenic acid, and distichonic acid, (iii) phytate (myo-inositol-1,2,3,4,5,6-hexakis-phosphate: IP6), both soluble and insoluble, and (iv) iron-binding proteins, especially ferritin. In some cases, e.g., citrate, both (ferric and ferrous) ions are able to form complexes with the same ligand and the formation of mixed-ligand complexes (e.g., citrate-malate [16,17]) is common. Metal, including iron, species involved in long distance metal transport in plants have been reviewed [18]. A special interest was focused on ferritin due to its putative role in iron bioavailability from food plants whereas some other proteins have been identified in specific plant physiology projects [19].

Originally, iron speciation analysis was (i) limited to the discrimination of Fe(II) and Fe(III) which is readily achieved by XANES, (ii) based on the isolation of a particulate fraction, such as phytates or ferritin, for its further characterization by spectroscopic methods, and (iii) based on calculation methods determining the distribution amongst the most abundant species. The introduction of electrospray MS allowed the identification of several citrate complexes but direct ESI MS studies of plant extracts or plant fluids have been scarce [16,17,20]. The advent of HPLC with iron-specific detection, usually by ICP MS, allowed the detection of specific fractions of water soluble complexes which could be identified with more or less success by electrospray MS. A significant part of iron in plants occurs as water insoluble species and needs to be solubilized before analysis by HPLC-based techniques; it is associated with a serious risk of species loss and/or transformation.

This manuscript critically evaluates the advantages and limitations of methods of iron speciation in plants and highlights the current trends in this area. Particular attention is given to the advances in chromatography with mass spectrometric detection by ICP MS and/or high-resolution electrospray MS/MS (e.g. QTOF MS or Q-Orbitrap MS). Correct isotopic patterns can only be observed if there are no isobaric compounds co-eluting. Isobaric interferences are much more likely to occur at nominal resolution than at high resolution, and commonplace in the analysis of biological samples. This is especially critical for low concentrated iron complexes, where isobaric interferences can lead to false positive or false negative detection of Fe complexes. High resolution is critical to distinguish metal complexes from other randomly occurring organic molecules. Also – if doubts subsist because of the low intensity of signals and numerous interfering molecules or salts – high resolution spectra of molecule fragments (MS/MS) can confirm or invalidate hypotheses of the presence of the Fe complex. The high resolution MS also offers new opportunities for exploiting the potential of stable isotopes for the probing of the stability and reactivity of iron species and their quantitative determination (in the MRM or SRM mode, for Q-TOF or Q-Orbitrap mass spectrometers).

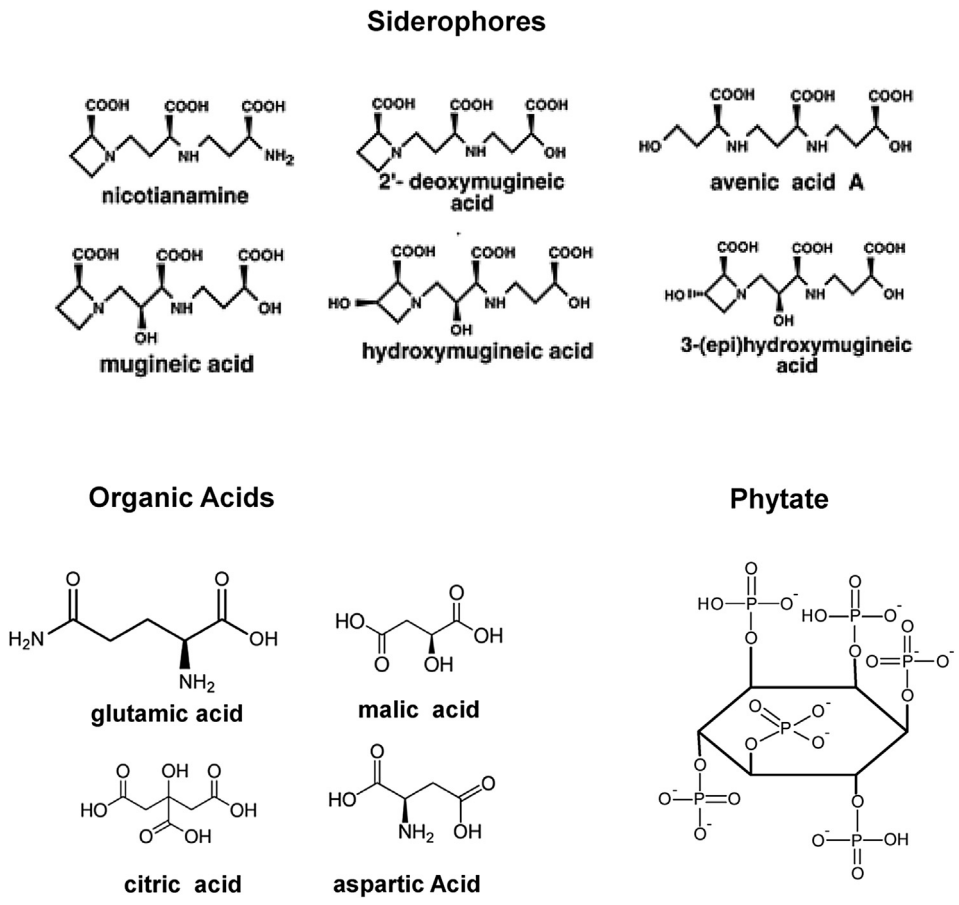

Fig. 1. Principal iron-complexing ligands in plants.

2. Direct analysis by X-ray spectroscopy

X-ray spectroscopy (XAS) provides information on the oxidation state and immediate coordination environment of iron present in the sample. The X-ray absorption near-edge structure (XANES) region of XAS spectra is sensitive to the oxidation state and coordination environment whereas the EXAFS (Extended X-ray Absorption Fine Structure) region is characteristic (coordination number and interatomic distances) of the local atomic structure surrounding an iron atom.

Edible grains (staple food) of wheat, rice, beans can be analyzed by XAS as such fixed on a holder [21] but the use of thin sections was recommended to reduce the distortion of the signal [22]. XAS has long been considered as a "direct" technique eliminating the risk of changes in speciation during sample preparation and irradiation. However, grinding and analysis of pellets was found to provoke oxidation [21]. Also, several Fe(III) complexes, e.g. succinate, nicotianamine, and α-ketoglutarate were found not to be stable in the synchrotron beam [23].

The XAS spectra (example in Fig. 2) are analyzed by linear combination fitting (LCF) using the spectra of standard compounds. This implies the need for prediction of the existence of some species and the availability of the corresponding standards. The sets of standards used in the two recent studies included (i) Fe(II) glutathione, Fe(II) sulphate, Fe(II) phytate, Fe(II) oxalate, Fe(III) phytate, Fe(III) sulphate, Fe(III) citrate, Fe(III) phosphate, and Fe_3O_4, α-FeOOH, and Fe_2O_3 [21], or (ii) citrate, α-ketoglutarate, acetate, fumarate, succinate, malate, shikimate, and nicotianamine complex [23].

XAS analysis can be used to indicate the relative amount of major species in the samples [21,23–25] with precisions below 5% for binary systems, such as e.g. Fe(II)/Fe(III) [21] or iron phytate/citrate [15]. An unmatched advantage of XAS is the consideration of insoluble Fe complexes. It turned out to be useful in the evaluation of the phytate/citrate ratio in modified and control aleurone cells of wheat grains (*Triticum aestivum* L.) [24]. The performance of XAS degrades for systems with several intervening ligands, especially at largely different concentrations. The precision of spectra is a

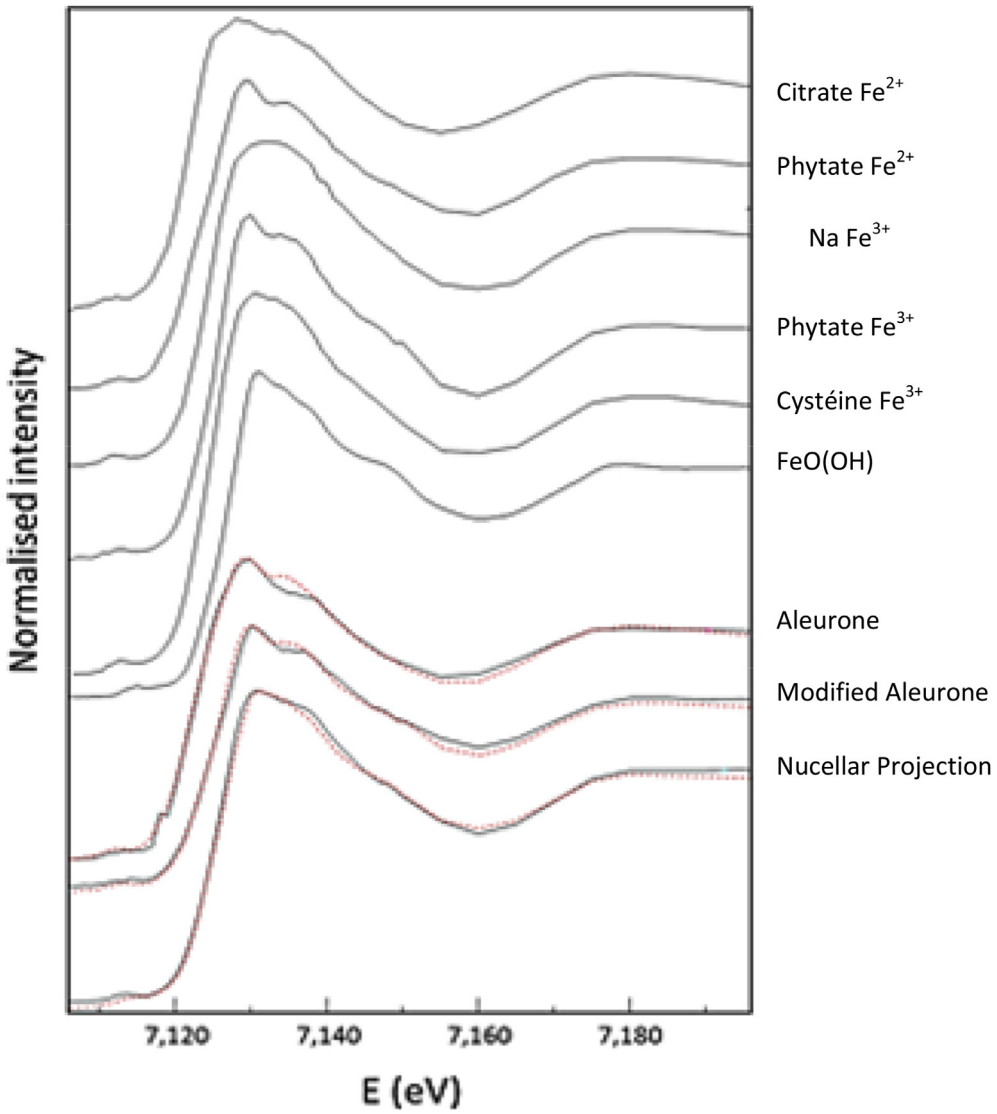

Fig. 2. Iron speciation in wheat grains (*Triticum aestivum* L.) using synchrotron XRF microscopy mapping. X-ray absorption spectra of iron complexes (standards) [citrate Fe^{2+}, phytate Fe^{2+}, nicotianamine (NA) Fe^{3+}, phytate Fe^{3+}, cysteine Fe^{3+}, FeO(OH)] and wheat grain sections. The dotted lines give the linear combination fitting results [24].

function of irradiation time which is set off by the risk of radiation damage of the analyte [23]. Also, the *a priori* knowledge of the ligands is indispensable.

XAS provided valuable hints on the oxidation state and immediate coordination region of iron, e.g. Fe-O-P-R and Fe-O-S-R [21]. Octahedral coordination by six oxygen atoms and two phosphorous atoms was observed in wheat [16,25]. Complementary information was obtained by chromatographic techniques upon extraction of water soluble species, but observed extraction yields were low [7,26]. An advantage of XAS is the possibility of speciation studies at high spatial resolution (e.g. in a leaf vein) [27].

The principal limitation of X-ray absorption techniques is the detection limit; the identification of a Fe complex requires iron concentration at the ppm levels. The evolution of XAS goes towards the use of high brilliance sources which, on one hand, decreases the detection limits down to sub-ppm levels, but, on the other hand, increases the risk of radiation damage to the analyte [23]. An analyses of xylem sap samples revealed Fe(III) to be complexed by citrate and acetate; the presence of Fe(0) in one of the samples was considered to be an artifact created by sample irradiation with high intensity synchrotron X-rays [23].

3. Liquid phase separation techniques for iron complexes in plants

The limitations of XAS (need for simple systems with a restricted number of already known ligands and relatively high iron concentrations) can be overcome by chromatography with either ICP or ESI MS detection. It is particularly true for plant sap, where the Fe concentrations in the low ppm range make speciation analysis challenging. The meaningful use of coupled techniques raises a number of questions related to sample preparation, species stability, artifact formation, separation efficiency, and column recovery and mobile phase compatibility with the detection techniques. The limitations differ for ICP MS and ESI MS which requires both techniques to be used for the internal validation of the results and elimination of analytical artefacts.

3.1. Sample preparation

Ideally, the speciation analysis should be carried out without sample preparation which favors the analysis of plant fluids, such as xylem, phloem or root exudates. The steady increase in the sensitivity of MS methods is likely to make the direct analysis of picoliter volumes of individual cells using on-chip chromatography possible in near future.

A common sampling method is cutting of the plant top with a razor blade, allowing the stumps to bleed for a few minutes, and fitting then the stem with plastic tubing for xylem sap recovery [28]. An interesting approach was the use of a brown plant hopper in a controlled environment (temperature, humidity, light exposure) conditions to suck out rice phloem sap [29]. The stylets of the insect were subsequently cut by a YAG laser and the exudated phloem sap (pH 8) was collected in microcapillary tubes [29].

The two major risks concern (i) dissociation of iron complexes and (ii) oxidation of Fe(II) to Fe(III). Drying of samples may lead to iron precipitation and destruction of complexes so lyophilisation should be avoided. Care should be taken to collect samples under N2 or Ar flushing; samples should be either analyzed promptly or frozen immediately after collection in liquid nitrogen [and kept frozen until analysis to prevent the oxidation of Fe(II)]. The use of fluorescent probes can help monitor Fe(II) concentration but they account for “free iron” or “labile iron” only and not iron-containing species [30]. The addition of isotopically enriched Fe(II) to the sample can help to follow the fate of this ion if doubts exist about its stability. However, it has to be kept in mind that molecules present in the plant matrix could lead to the oxidation of the added Fe(II) so this method seems to be more adapted to follow long term degradation during storage.

Regarding solid samples, plant leaves can be frozen in liquid N_2, homogenized in a ball mill or in a mortar, centrifuged, and filtered using a 0.22-μm filter. Grain water extracts (wholemeal wheat flour, bran, subaleurone layer, and endosperm) were obtained by incubation at 37°C for 18 h Tris-HCl with shaking, centrifugation and 0.32-μm filtration. Despite the use of fairly high temperature, the species detected do not seem to be products of enzymatic (or other) degradation of higher MW complexes. The above procedures were focused on the species which were the easiest to mobilize [3,7,26]. However, it should be kept in mind that solubilization of iron species from solid samples bears a risk of the degradation and transformation (ligand exchange).

Ideally, various sample preparations should be tested to see if consistent speciation analysis results are obtained. The sample should not be altered or mixed with anything else. However, if there is such a need, care should be taken not to add any compounds that would alter Fe speciation: pH should be kept similar to sample pH while potentially chelating molecules and excessive amount of salt or oxidizing/reducing agents should be avoided.

3.2. Coupled techniques for the analysis for Fe-compounds in plant extracts and fluids

3.2.1. Size-exclusion liquid chromatography

Size-exclusion LC allows the fractionation of iron complexes in plant fluids (xylem and phloem) [31] and plant tissue extracts [3,4,7,26] according to the molecular mass (more precisely, hydrodynamic volume) while iron or its complexes can be specifically monitored using ICP MS or ESI MS, respectively. It has been a method of choice while working with unstable metal complexes in plants as this method is often able to preserve species degraded while other separation mechanisms are used [16,32,33]. The resolution is relatively poor but a high molecular fraction at the (or close to) exclusion volume, a low molecular fraction corresponding to complexes with organic acids and siderophores and – in-between – soluble phytate fraction can be discriminated [3] (Fig. 3). Its accepted applications include (i) the determination of the apparent molecular mass of well separated compounds, such as e.g. Fe-phytate complex (12.3 kDa) [7], (ii) the isolation of iron complexes for further purification [7], and (iii) the monitoring of the reactivity of iron fractions towards specific enzymes, e.g. that of phytate-Fe complex with phytase, the enzyme responsible for successive dephosphorylation of IP_6 [7].

SEC usually requires fairly concentrated salt-rich buffers to minimize the interactions of the analytes with the stationary phase to prevent those which can lead to the dissociation of the complexes present. An interesting trend is the optimization of the choice of the stationary phase and the mobile phase conditions with dilute buffers of weak buffering capacity (*i.e.*, 10 mM ammonium acetate). At these conditions low molecular iron complexes can be separated from each other with the resolution of a single organic acid ligand, e.g. mixed maic/citric complexes [16] (Fig. 4a). Another advantage is the compatibility of such eluents with electrospray ionization allowing the on-line identification of the metal complexes [16]. The advent of more robust electrospray ionization sources and more sensitive mass spectrometers have made a successful coupling of SEC with electrospray MS possible [16]. The SEC-ESI MS coupling allowed the identification of iron nicotianamine, 2′-deoxymugineic acid and mugineic acid complexes in soybean xylem sap [31]. The Fe(III)-2′-deoxymugineic acid complex was

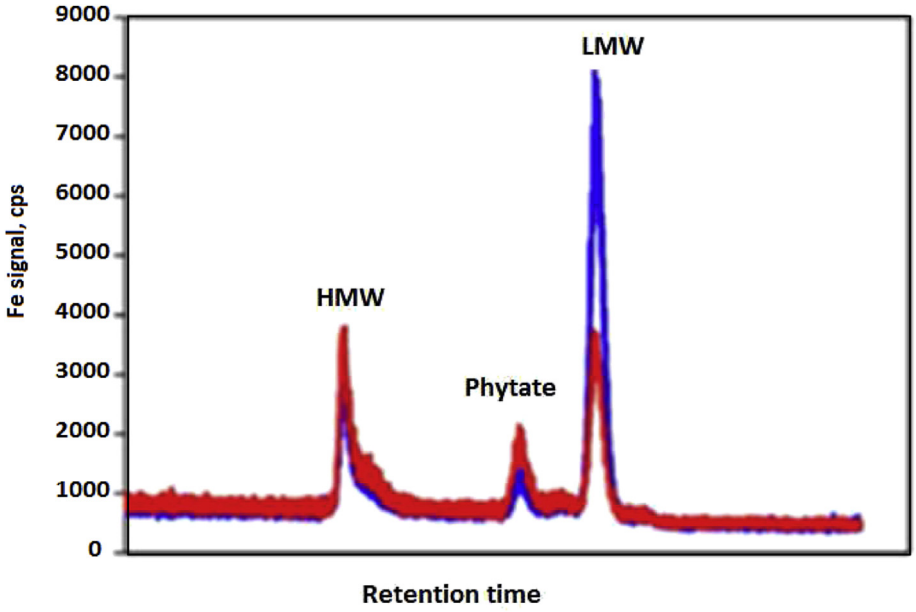

Fig. 3. Size-exclusion-ICP MS chromatograms of Fe speciation in the 50 mM Tris-HCl buffer (pH 7.5) extracts of wheat fractions (wholemeal flour, subaleurone layer, central endosperm, and core endosperm) [3] (see text for peak indentification).

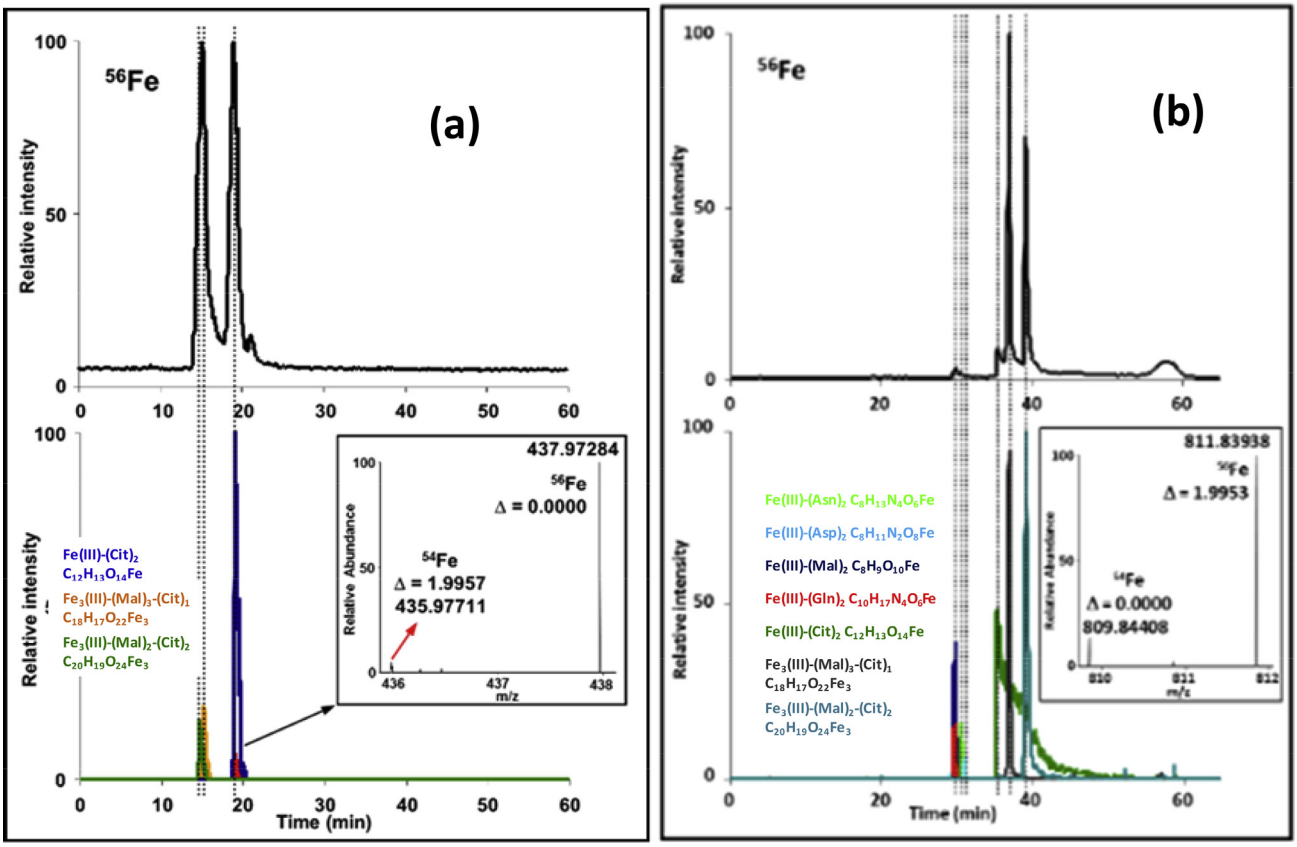

Fig. 4. Chromatograms of Fe species in pea xylem: (**a**) SEC-ICP-MS (upper part) and SEC-ESI-MS (bottom part, extracted ion chromatograms of *m/z* of: Fe(III)-$(Cit)_2$ $C_{12}H_{13}O_{14}Fe$ and mixed Fe_3(III)-$(Mal)_3$-$(Cit)_1$ $C_{18}H_{17}O_{22}Fe_3$ and Fe_3(III)-$(Mal)_2$-$(Cit)_2$ $C_{20}H_{19}O_{24}Fe_3$, (**b**) HILIC-ICP-MS (upper part) and HILIC-ESI-MS (bottom part, extracted ion chromatograms of *m/z* of Fe(III)-$(Asn)_2$ $C_8H_{13}N_4O_6Fe$, Fe(III)-$(Asp)_2$ $C_8H_{11}N_2O_8Fe$, Fe(III)-$(Mal)_2$ $C_8H_9O_{10}Fe$, Fe(III)-$(Gln)_2$ $C_{10}H_{17}N_4O_6Fe$, Fe(III)-$(Cit)_2$ $C_{12}H_{13}O_{14}Fe$ and mixed Fe_3(III)-$(Mal)_3$-$(Cit)_1$ $C_{18}H_{17}O_{22}Fe_3$, Fe_3(III)-$(Mal)_2$-$(Cit)_2$ $C_{20}H_{19}O_{24}Fe_3$. The insets depict zooms of part of mass spectra containing ions with characteristic Fe isotopic signature [16].

identified in phloem sap from rice by SEC with off-line ICP MS detection followed by ESI- time-of-flight (TOF) MS [29].

3.2.2. Hydrophilic interaction ion chromatography (HILIC)

Hydrophilic interaction chromatography (HILIC) is based on liquid-liquid partition where analytes elute in order of increasing polarity; it provides therefore an approach to efficiently separate small polar compounds on polar stationary phases [34]. Several types of stationary phases are available for HILIC separations. They differ in terms of their chemical functionalities which confer various interaction patterns and, consequently, result in very different selectivities and orders of elution [35].

The coupling of HILIC with ESI – TOF MS (canonical in metabolomics [36,37]) allowed the detection of whole range of carboxylates in the plant tissue extracts and fluids including oxalic, 2-oxoglutaric, cis-aconitic, malic, quinic, shikimic, fumaric, formic, and metaphosphoric (MPA), (succinic citric and ascorbic acids) [38]. The analysis for metal complexes is more challenging as it requires a careful optimization of the ionization mode and the separation of the metal-ligand complex from the excess of the free ligand which could interfere in the ESI process [20]. Both citrate and Fe–citrate complexes are highly polar and there is a consensus on the choice of a zwitterionic hydrophilic interaction stationary phase (ZIC-HILIC) for their separation [37,39,40]. The identification is carried out on the basis of the molecular mass and fragmentation patterns.

An important restriction in the optimization of the separation conditions is the need to maintain the original pH of the sample during chromatography in order to preserve the metal-ligand equilibria. Addition of organic solvent (usually acetonitrile or methanol) to the eluent (so to the sample) when HILIC is used can change Fe speciation because of the lower solubility of some compounds potentially associated to Fe. In particular, an addition of acetonitrile to aqueous samples leads to the precipitation of most proteins (>10 kDa). Therefore, the use of HILIC should be limited to studies of small (<10 kDa) iron complexes. Samples should be analyzed as soon as they are mixed with the solvent to limit potential loss of Fe species. To ascertain that no changes occurred, an analysis of the water extract by SEC should ideally confirm the presence of Fe complexes. The on-column precipitation should be controlled by checking the elution yield (recovery). The stability of metal-PS complexes during the HILIC separation was investigated [41]. A risk of on-column dissociation and Fe(II) oxidation was identified. It may cause column contamination, poorly reproducible retention times and lead to systematic errors in the analysis of plant samples so a column cleaning procedure using a 20 μM EDTA solution was proposed [41].

HILIC can be readily combined with ICP MS and ESI MS and several authors used both detection modes in parallel combining the iron-specific detection and the identification of the complexes present [16,17,20]. A considerable success, stimulated by an early work of Weber et al. [42], concerned the identification of iron phytosiderophores (PSs). The speciation of iron-PSs complexes is critical for understanding the biological functions of different PSs. Direct HPLC – ESI TOF-MS allowed the identification of deoxymugineic acid (DMA), mugineic acid (MA) and epihydroxymugineic acid (epi-HMA), avenic acid (AVA) and hydroxyavenic acid (HAVA), and their ferric complexes in root exudates under iron (Fe) deficiency; however no quantitative information was provided [40]. The high selectivity of a mixed-mode stationary phase allowed the baseline separation of the two Fe-MA diastereomers [39]. The limit of detection was 50 nM for Fe(III)-DMA [39].

HILIC – ESI MS (Fig. 4b) allowed the identification of a number of species with different ligands including: Fe(III)-$(Asn)_2$, Fe(III)-$(Asp)_2$, Fe(III)-$(Mal)_2$, Fe(III)-$(Gln)_2$, Fe(III)-$(Cit)_2$ and mixed Fe_3(III)-$(Mal)_3$-Cit, Fe_3(III)-$(Mal)_2$-$(Cit)_2$, Fe_3(III)-Mal-$(Cit)_3$ in pea xylem, although the presence of some of them was not confirmed by the parallel SEC-ESI MS analysis [16].

HILIC ESI MS has largely contributed to the understanding of the role of citrate [20] and citrate-malate complexes [16,17] in iron transport and metabolism. The iron citrate complex which is of high biological relevance shows relatively poor thermodynamical stability. A method to separate and identify Fe–Cit complexes was developed by analyzing Fe–Cit solutions at various Fe and Cit concentrations, Fe:Cit ratios and pH values (5.5) typical of xylem sap, using HPLC with dual ESI-TOFMS and post-column ID ICP-MS detection [20]. Among the complexes found in pea xylem [16] a special attention was paid to the mixed-ligand complexes Fe(III)$_3$-$(Cit)_{(4-x)}$-$(Mal)_x$ (with x ranging from 1 to 3). The absence of the Fe(III)$_3$-O-$(Cit)_3$ complex and Fe(III)$_3$-$(Cit)_3$ complex in the pea samples despite the presence of citric acid would confirm a higher stability for the mixed iron complexes Fe(III)$_3$-$(Cit)_{(4-x)}$-$(Mal)_x$ (x = 1 to 3) compared the 'Fe(III)$_3$-O-$(Cit)_3$' complex or Fe(III)$_3$-$(Cit)_3$ complex as it was also observed with the standard mixture [20].

Concerning Fe(II), it was found to bind at trace level citrate, malate and aspartate as Fe(III) but only Fe(II) and not Fe(III) was found to be complexed by nicotianamine [16]. The signal-to-noise ratio found in HILIC of xylem sap samples with total Fe concentrations of approximately 40 μM were 12 and 6 in HPLC–ESI-TOFMS and HPLC–ICP-MS, respectively. Therefore, in plant saps with Fe:Cit ratios favoring the formation of Fe_3Cit_3, an iron Fe concentration of approximately 25–30 μM would be needed for the Fe_3Cit_3 complex to be detected [20].

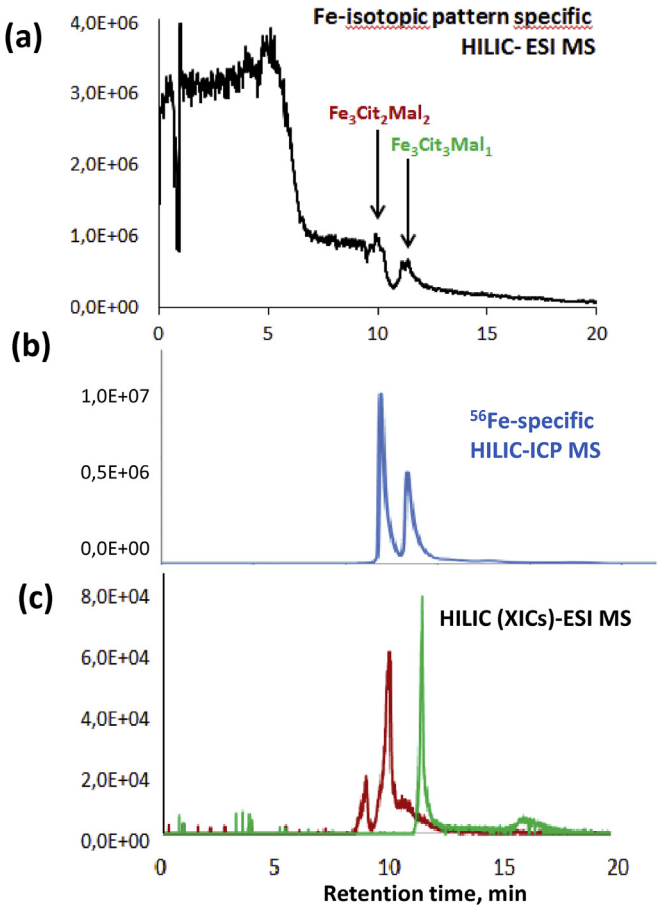

Fig. 5. A comparison of (a) the automatic data mining (Compound Discoverer™, ThermoFisher Scienfic) using two iron isotopes (^{56}Fe and ^{57}Fe), mass tolerance: 5 ppm, intensity tolerance: 20%, (b) ICP MS detection (^{56}Fe) and confirmed by (c) XICs of mixed citrate-malate iron complexes for a standard solution (100 ppb as Fe at pH 5.5, molar ratio Fe:Ma:Cit = 1:25:5).

3.2.3. Capillary zone electrophoresis (CZE)

The separation efficiency of CE measured in terms of the number of theoretical plates (50,000–100,000) exceeds by a factor of 30–50 that of HILIC, and by far more that of SEC and the analysis of nanoliter sample volumes is possible. Three phytosiderophores (mugineic acid, epi-mugineic acid and deoxymugineic acid) and their ferric model complexes were analyzed using CE-ESI MS and CE-ICP MS, the latter method was reported to be quantitative but no application to real samples was shown [43]. It has to be stated that a continuous interest and expectations raised by CZE techniques for the two decades are still largely not fulfilled, apparently because of the difficulties with the stability of metal complexes in high electric fields and because of the poor robustness of the system.

3.2.4. ICP MS vs. electrospray MS detection in chromatography

ICP MS offers the possibility of multi-element detection, including that of S and P which gives useful hints to the putative identity of the complexes present. For example, the Fe-phytate complex was tentatively identified on the basis of co-elution with phosphorous and the decrease of iron and phosphorous signals following a treatment with phytase [7]. The $Fe_4(IP_6)_{18}$ stoichiometry was proposed based on the Fe/P ratio in a further purified complex [7]. The identification in SEC based on the co-elution with other elements and on the retention time matching with standards is rather tricky as the chromatographic purity of the chromatographic signals can hardly be guaranteed.

The intensity of the iron signal is independent of the coordination environment and was considered as a measure of the quantitative distribution of iron [2]. This can be misleading for two reasons: the recovery of the individual fractions is seldom verified (ideally the fraction should be collected and re-injected) and the purity of the chromatographic purity of the peaks is poor.

The high resolution of state-of–the-art ESI MS together with high mass accuracy allow for automatic data mining in search for iron species based on its isotopic pattern and species mass defects. A good agreement was obtained for a study of standard mixture of citrate-malate iron complexes between the automatically found and ICP MS detected iron species (Fig. 5).

3.3. Validation of iron speciation data

Dynamic metal–ligand systems include inevitably labile or transient metal species and direct spectroscopic methods are ideally needed to study their equilibria. Even for relatively stable species ligand exchange reactions may occur in the presence of competing ligands and/or redox mediators. The formation of artifact Fe species which are not those actually present in the original

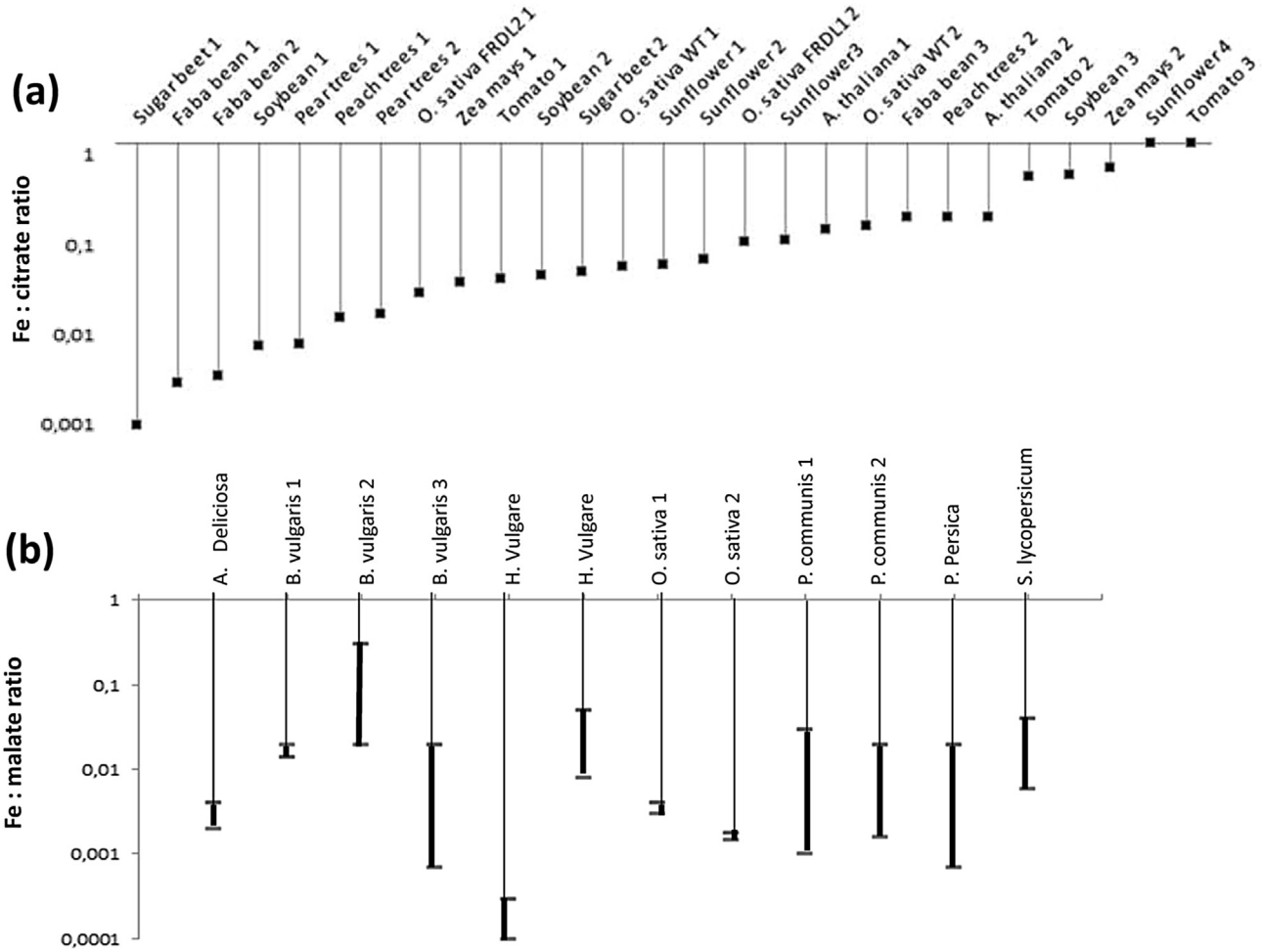

Fig. 6. Fe:citrate (a) and Fe:malate (b) ratios in plant sap samples reported in the literature (compiled from Refs. [20] and [18]).

sample may occur. Due to this specificity, the direct application of criteria for confidence levels defined and accepted in the general metabolomics community is not viable [44]. For example, for iron chelates the possibility of redox-mediated ligand exchange of the phytosiderophore 2′-deoxymugineic acid against nicotianamine [45] and direct ligand exchange of nicotianamine against citrate [46] were demonstrated.

The minimum requirements for the validation of iron-speciation data include:

(i) use of at least two different chromatographic separation mechanisms to confirm the presence of a given species. Indeed, direct large-scale detection and identification of metal complexes in plant fluids by SEC and HILIC with dual elemental and molecular mass spectrometric detection revealed the presence of a series of species in pea fluids including xylem or liquid endosperm [16]. However, out of seven iron complexes detected by HILIC-ICP/ESI MS, only three of them were confirmed to be present by a complementary SEC-ICP/ESI MS [16],

(ii) confirm the presence of ligand by on-line post column acidification at the retention time of the iron complex, different from that of the free ligand. The presence of malic and citric acids at the elution volumes of the iron complexes whereas the free citric and malic acids present in the sample eluted much later so the hypothesis of in-source formation of complexes could be discarded [16],

(iii) optimize electrospray ionization conditions for the standards complexes to avoid in-source fragmentation [20],

(iv) confirm the presence of iron in the complex detected by ESI MS by the isotopic pattern or accurate mass. The observation of the iron-characteristic isotopic pattern is difficult due to the high 15.7 intensity ratio between the first (^{56}Fe – 91.5%) and the second (^{54}Fe 5.85%) most abundant isotopes. The results obtained for natural and isotopically labeled (^{54}Fe) species were obtained in parallel in order to confirm the identity of Fe-citrate complexes [20]. ICP MS co-elution and fortification of the species isotopic pattern were proposed to as additional means of species recognition [20],

(v) confirm the identity of the molecular structures of Fe complexes by tandem MS [16]. For example, the major species identified in the tomato sap - Fe(III)$_3$-O-(Cit)$_3$ complex [20] - has the same molecular mass as the Fe(III)$_3$-(Cit)$_1$-(Mal)$_3$ one [16,17]. In the absence of MS/MS, a wrong assignment of the complex identities cannot be excluded, especially that malic acid is sometimes found in higher proportion than citrate in

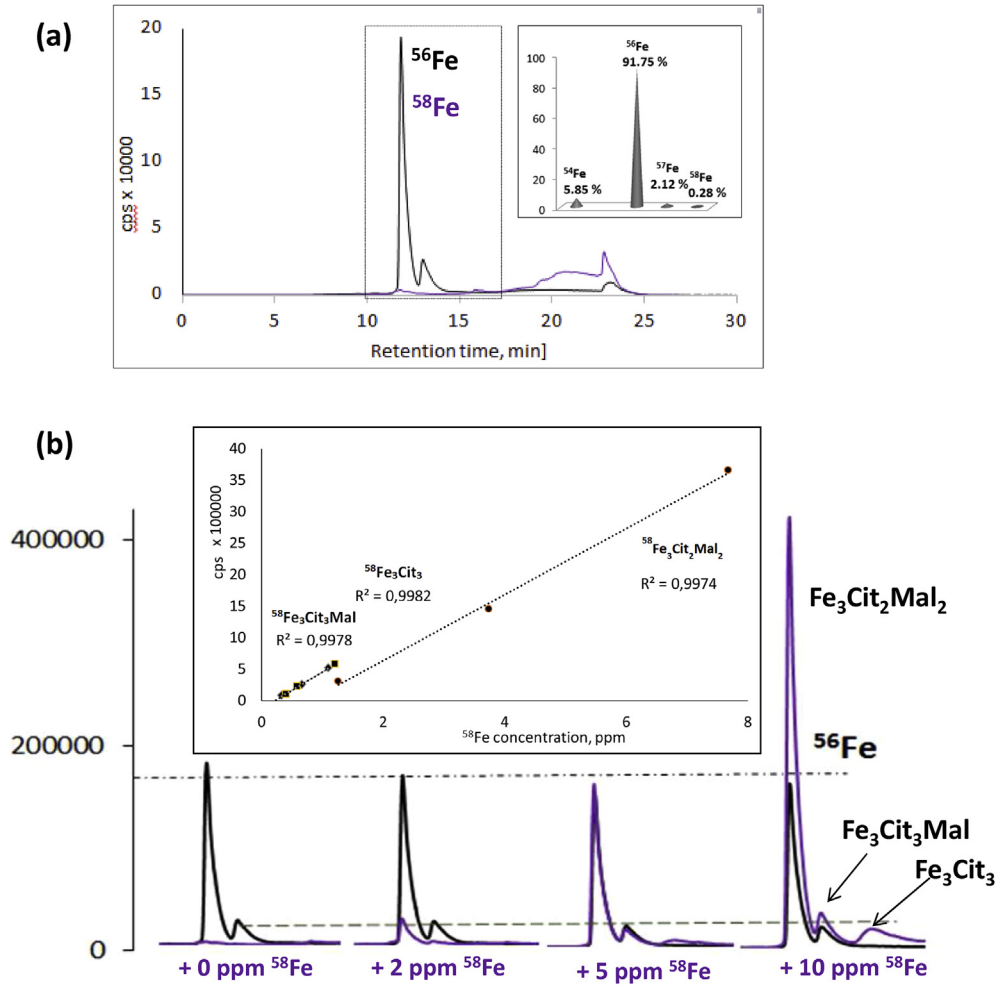

Fig. 7. Principle of the *in-situ* species-selective ID HPLC - ICP MS for speciation of low molecular Fe-species (^{56}Fe – black line, ^{58}Fe – violet line). (a) the HILIC-ICP MS chromatogram of green pea xylem (natural Fe isotopic pattern is shown in the inset), (b) the zoomed parts of chromatograms showing Fe(III)-(Cit)$_2$ and mixed Fe$_3$(III)-(Mal)$_3$-(Cit)$_1$ and Fe$_3$(III)-(Mal)$_2$-(Cit)$_2$ peaks obtained as a result of increasing additions of ionic ^{58}Fe together with a standard additions curves for individual complexes. The stability of ^{56}Fe peaks is shown by dashed lines.

plant shoots and its concentration can increase in the case of Fe deficiency [28,41,47].

3.4. Quantification techniques in Fe speciation analysis

3.4.1. Column recoveries and external calibration

The quantification of Fe complexes with organic ligands is hindered by species lability and ionization differences in ESI MS. The column recoveries are typically at the 60–70% level [16,20]. Quantification on the basis of an external calibration curve is hardly feasible. The method of standard addition of iron complexes to samples is not possible either – it leads to disturbance of complexation equilibria (e.g., addition of Fe-citrate to the mixture of citrate-malate changes the initial ratio of peaks). A broad iron peak, tentatively assigned to Fe-oxyhydroxide [20], was observed at unusually long retention time and considered as a possible artifact.

3.4.2. Pre-column species-specific and post-column species unspecific isotope dilution

Iron has 4 natural isotopes: ^{54}Fe, ^{56}Fe, ^{57}Fe and ^{58}Fe with natural relative abundance of 5.85, 91.75, 2.12 and 0.28%, respectively, which opens multiple possibilities to isotope dilution quantification.

Specific Fe-containing molecules can be quantified by isotope dilution provided that enriched iron-labeled standards are available and that iron is not exchanged with other ligands present in the sample. These prerequisites were fulfilled for ferritin, a protein considered as an important source of bioavailable iron [48,49], of which the quantification - rather than the determination of the total iron – is of interest for food chemists [50,51]. For this purpose, a recombinant [^{57}Fe]-labeled bean ferritin was produced, mixed with a sample, and purified by ion exchange chromatography [6] prior to TIMS. The concept can be potentially carried out in the on-line format as demonstrated elsewhere by anion exchange chromatography – ID ICP MS determination of iron transferrin in human serum [52].

Post-column unspecific isotopic dilution quantification was carried out by continuously adding ^{57}Fe in EDTA between the exit of the column and the ICP MS nebulizer. The HILIC-ICP-MS intensity chromatograms were converted into Fe molar flow chromatograms using the isotope pattern deconvolution (IPD) equations. Accurate isotope abundances of the isotopically enriched solutions were determined by direct ICP-MS injections and used for the calculations of eluted Fe-citrate complex in tomato plant xylem [20]. Note, that in contrast to pre-column isotope dilution, the post-column isotope dilution allows no correction for the incomplete recovery.

3.4.3. Isotope dilution HPLC-ICP MS after in-situ formation of the calibration standard

Plant fluids contain considerable excess of free ligands (citrate or malonate, Fig. 6) which opens the possibility of the *in-situ* formation of isotopically labeled species of iron as a result of the addition of ionic Fe isotope to a sample. The prerequisite is the complete reaction of the added spike which can be readily verified by HPLC-ICP MS. This method allows the correction for *on-column* dissociation or changes in speciation during chromatography. A proof-of-principle of this novel procedure (summarized in Fig. 7) has been tested for the quantification of iron citrate-malonate complexes in embryo sac liquid of *Pisum sativum*. The additions of ionic solution of ^{58}Fe resulted in the formation (violet trace in Fig. 7b) of the same (but ^{58}Fe-labeled) complexes as those present in the original sample (Fig. 7a). The originally present species are not affected by the isotope addition the original speciation of ^{56}Fe (black trace) remained unchanged despite the ^{58}Fe additions. Consequently, it was possible to establish a calibration curve to serve for the quantification (insert in Fig. 7b). A complementary model study carried out with standards showed that identical species distribution was obtained by the addition of ionic ^{58}Fe and mixing ^{56}Fe and ^{58}Fe complexes.

4. Conclusions and perspectives

Dual separation mechanisms (SEC and HILIC) HPLC with dual ICP MS and ESI MS detection offer the most accomplished, at present, tool for a comprehensive speciation of low molecular weight iron complexes in micro- or nanoliter volumes of plant fluids. The increasing sensitivity and robustness of electrospray high resolution high mass accuracy MS and the progress in software for data deconvolution for element specific analysis are responsible for the progressive replacement of ICP MS detection by ESI MS detection in chromatography for iron speciation studies. As ESI MS is a concentration specific detector, the natural trend seems to be the miniaturization of sample introduction using *on-chip* HPLC allowing the analysis of picoliter volumes of intracellular fluids. The isotopic specificity of mass spectrometric techniques spurs the use of stable iron isotopes for studies of the complex stability, exchange kinetics and the isotope dilution for quantification. In contrast to metabolites, the full characterization of iron-binding proteins seems to be a distant goal because of the lack of efficient separation techniques and by far less sensitive detection by ESI MS. There does not really seem to be really an alternative for HPLC – MS for speciation of iron at ppb concentration levels in complex samples. However, once novel species are identified, the standards can be produced and their contribution to speciation should be evaluated by X-ray absorption spectroscopy. Spectra comparisons between the sample, extracts and chromatographic fractions can allow the detection of risk of changes in speciation. The potential of X-ray absorption spectroscopy is expected to grow with the use of higher brilliance sources, larger spectrum of standards taken into account during computing and better fitting algorithms.

References

[1] World Health Organization, C.f.D.C.a, Prevention, Assessing the Iron Status of Populations, World Health Organization, Geneva, 2007.
[2] R.K. Gupta, S.S. Gangoliya, N.K. Singh, J. Food Sci. Technol. 52 (2015) 676.
[3] Y.F. Xue, T. Eagling, J. He, C.Q. Zou, S.P. McGrath, P.R. Shewry, F.J. Zhao, J. Agric. Food Chem. 62 (2014) 4738.
[4] T. Eagling, A.L. Neal, S.P. McGrath, S. Fairweather-Tait, P.R. Shewry, F.J. Zhao, J. Agric. Food Chem. 62 (2014) 708.
[5] T. Eagling, A.A. Wawer, P.R. Shewry, F.J. Zhao, S.J. Fairweather-Tait, J. Agric. Food Chem. 62 (2014) 10320.
[6] M. Hoppler, I. Egli, N. Petry, D. Gille, C. Zeder, T. Walczyk, M.W. Blair, R.F. Hurrell, J. Food Sci. 79 (2014) C1629.
[7] D.P. Persson, T.H. Hansen, K.H. Laursen, J.K. Schjoerring, S. Husted, Metallomics 1 (2009) 418.
[8] T. Kobayashi, N.K. Nishizawa, Iron Uptake, Translocation, and Regulation in Higher Plants, 2012, p. 131.
[9] J. Morrissey, M.L. Guerinot, Chem. Rev. 109 (2009) 4553.
[10] S. Clemens, M. Weber, Plant Signal Behav 11 (2016) e1114197.
[11] P. Sisó-Terraza, A. Luis-Villarroya, P. Fourcroy, J.-F. Briat, A. Abadía, F. Gaymard, J. Abadía, A. Álvarez-Fernández, Front Plant Sci 7 (2016).
[12] P. Mladenka, K. Macakova, L. Zatloukalova, Z. Rehakova, B.K. Singh, A.K. Prasad, V.S. Parmar, L. Jahodar, R. Hrdina, L. Saso, Biochimie 92 (2010) 1108.
[13] L. Guo, T.J. Cutright, Int. J. Phytoremediation 19 (2017) 254.
[14] F.R. Segura, E.A. Nunes, F.P. Paniz, A.C.C. Paulelli, G.B. Rodrigues, G.Ú.L. Braga, W. dos Reis Pedreira Filho, F. Barbosa, G. Cerchiaro, F.F. Silva, B.L. Batista, Environ. Pollut. 218 (2016) 813.
[15] F.-J. Zhao, S.P. McGrath, Curr. Opin. Plant Biol. 12 (2009) 373.
[16] P. Flis, L. Ouerdane, L. Grillet, C. Curie, S. Mari, R. Lobinski, New Phytol. 211 (2016) 1129.
[17] L. Grillet, L. Ouerdane, P. Flis, M.T.T. Hoang, M.P. Isaure, R. Lobinski, C. Curie, S. Mari, J. Biol. Chem. 289 (2014) 2515.
[18] A. Álvarez-Fernández, P. Díaz-Benito, A. Abadía, A.-F. López-Millán, J. Abadía, Front. Plant Sci. 5 (2014) 105.
[19] C. Krüger, O. Berkowitz, U.W. Stephan, R. Hell, J. Biol. Chem. 277 (2002) 25062.

[20] R. Rellán-Álvarez, J. Giner-Martínez-Sierra, J. Orduna, I. Orera, J.A. Rodríguez-Castrilln, J.I. García-Alonso, J. Abadía, A. Álvarez-Fernández, Plant Cell Physiol. 51 (2010) 31.
[21] S.P. Singh, K. Vogel-Mikuš, I. Arčon, P. Vavpetič, L. Jeromel, P. Pelicon, J. Kumar, R. Tuli, J. Exp. Bot. 64 (2013) 3249.
[22] E. Lombi, K.G. Scheckel, I.M. Kempson, Environ. Exp. Bot. 72 (2011) 3.
[23] R. Terzano, T. Mimmo, B. Vekemans, L. Vincze, G. Falkenberg, N. Tomasi, M. Schnell Ramos, R. Pinton, S. Cesco, Anal. Bioanal. Chem. 405 (2013) 5411.
[24] N. De Brier, S.V. Gomand, E. Donner, D. Paterson, E. Smolders, J.A. Delcour, E. Lombi, Plant, Cell Environ. 39 (2016) 1835.
[25] A.L. Neal, K. Geraki, S. Borg, P. Quinn, J.F. Mosselmans, H. Brinch-Pedersen, P.R. Shewry, J. Biol. Inorg. Chem. 18 (2013) 557.
[26] S. Lee, U.S. Jeon, S.J. Lee, Y.K. Kim, D.P. Persson, S. Husted, J.K. Schjorring, Y. Kakei, H. Masuda, N.K. Nishizawa, G. An, Proc. Natl. Acad. Sci. U. S. A. 106 (2009) 22014.
[27] E. Yoshimura, S. Sakaguchi, H. Nakanishi, N.K. Nishizawa, I. Nakai, S. Mori, Phytochem. Anal. 11 (2000) 160.
[28] A.F. López-Millán, F. Morales, Y. Gogorcena, A. Abadía, J. Abadía, J. Plant Physiol. 166 (2009) 375.
[29] R. Nishiyama, M. Kato, S. Nagata, S. Yanagisawa, T. Yoneyama, Plant Cell Physiol. 53 (2012) 381.
[30] T. Hirayama, H. Nagasawa, J Clin Biochem Nutr 60 (2017) 39.
[31] T. Ariga, K. Hazama, S. Yanagisawa, T. Yoneyama, Soil Sci. Plant Nutr. 60 (2014) 460.
[32] L. Ouerdane, S. Mari, P. Czernic, M. Lebrun, R. Łobiński, J. Anal. Atomic Spectrom. 21 (2006) 676.
[33] J. Szpunar, Analyst 125 (2000) 963.
[34] B. Buszewski, S. Noga, Anal. Bioanal. Chem. 402 (2012) 231.
[35] J. Köster, R. Shi, N. Von Wirén, G. Weber, J. Chromatogr. A 1218 (2011) 4934.
[36] L. Nováková, L. Havlíková, H. Vlčková, TrAC - Trends Anal. Chem. 63 (2014) 55.
[37] K. Spagou, H. Tsoukali, N. Raikos, H. Gika, I.D. Wilson, G. Theodoridis, J. Sep. Sci. 33 (2010) 716.
[38] R. Rellán-Álvarez, S. López-Gomollón, J. Abadía, A. Álvarez-Fernández, J Agric Food Chem 59 (2011) 6864.
[39] M. Dell'mour, W. Schenkeveld, E. Oburger, L. Fischer, S. Kraemer, M. Puschenreiter, M. Lämmerhofer, G. Koellensperger, S. Hann, Electrophoresis 33 (2012) 726.
[40] M. Tsednee, Y.W. Mak, Y.R. Chen, K.C. Yeh, New Phytol. 195 (2012) 951.
[41] N. Jelali, M. Wissal, M. Dell'orto, C. Abdelly, M. Gharsalli, G. Zocchi, Environ Exp Bot 68 (2010) 238.
[42] Y. Xuan, E.B. Scheuermann, A.R. Meda, H. Hayen, N. von Wirén, G. Weber, J Chromatogr A 1136 (2006) 73.
[43] M. Dell'mour, G. Koellensperger, J.P. Quirino, P.R. Haddad, C. Stanetty, E. Oburger, E. Puschenreiter, S. Hann, Electrophoresis 31 (2010) 1201.
[44] J.C. May, J.A. McLean, Advanced Multidimensional Separations in Mass Spectrometry: Navigating the Big Data Deluge, 2016, p. 387.
[45] G. Weber, N. von Wirén, H. Hayen, BioMetals 21 (2008) 503.
[46] R. Rellán-Álvarez, J. Abadía, A. Álvarez-Fernández, Rapid Commun. Mass Spectrom. 22 (2008) 1553.
[47] G. Lattanzio, S. Andaluz, A. Matros, J.J. Calvete, J. Kehr, A. Abadía, J. Abadía, A.F. López-Millán, Proteomics 13 (2013) 2283.
[48] B. Lonnerdal, Int. J. Vitam. Nutr. Res. 77 (2007) 152.
[49] C. Lv, G. Zhao, B. Lonnerdal, J. Nutr. Biochem. 26 (2015) 532.
[50] R.J. Lukac, M.R. Aluru, M.B. Reddy, J. Agric. Food Chem. 57 (2009) 2155.
[51] G. Drakakaki, S. Marcel, R.P. Glahn, E.K. Lund, S. Pariagh, R. Fischer, P. Christou, E. Stoger, Plant Mol. Biol. 59 (2006) 869.
[52] M.E. Del Castillo Busto, M. Montes-Bayón, A. Sanz-Medel, Anal. Chem. 78 (2006) 8218.

9.2 Article 2

Speciation of essential nutrient trace elements in coconut water

Food Chemistry

Speciation of essential nutrient trace elements in coconut water

Ghaya Al-Choubassi, Katarzyna Kinska*, Katarzyna Bierla, Ryszard Lobinski, Joanna Szpunar

Institute of Analytical and Physical Chemistry for the Environment and Materials (IPREM - CNRS-UPPA UMR 5254), Hélioparc, 2, av. Pr. Angot, 64053 Pau, France

Abstract

The work presents the characterization of chemical forms of Mn, Fe, Zn Ni, Mo and Cu in coconut (*Cocos Nucifera*) water. The samples from different origins (including the Ivory Coast, Costa Rica, Sri Lanka and Thailand) were examined. The developed analytical approach is based on *i*) evaluation of metals total content, *ii*) fractionation of metal species by size-exclusion chromatography and *iii)* their separation by hydrophilic interaction chromatography (HILIC), both coupled with ICP MS followed by *vi*) in parallel coupling HILIC with electrospray-Orbitrap MS for the detection and structural identification of metal complexes. The results obtained show variations in the amounts of iron, nickel, copper, zinc and manganese in coconut water, dependent of the origin of the nut; the differences observed in coconut waters from the same origin were attributed to different maturity of the nuts. The metal species identified included: $Malate_2Citrate_2Iron(III)_3$, $Glutamine_2Iron(III)$, $Malate_2Iron(III)$, Nicotianamine-Iron(II), $MalateCitrate_3Iron(III)_3$, $Aspartate_2Manganese$, Nicotianamine-Nickel, $Phenylalanine_2Nickel$, $Aspartate_2Nickel$, Nicotianamine-Copper, $Phenylalanine_2Copper$, $Phenylalanine_3Copper$.

I Introduction

Trace elements are required by the body in small quantities for normal growth, development and physiology. The metals are vital for cellular functions, enzymatic activation, gene expression and metabolism of amino acids, lipids and carbohydrates one of the most widespread dietary problems in the world is mineral deficiency. It is well accepted that the chemical form plays a major role in the bioavailability of trace elements. Low iron and zinc bioavailability from cereals is attributed to their scavenging and compellation by phytates leading to the formation of high molecular weight hardly digestible complexes. An increase in bioavailable mineral content in rice grains was achieved by enhancing nicotianamine synthase expression leading to more Fe bound to a low molecular mass, which was likely nicotianamine. The tolerance to Fe and Zn deficiencies and to excess metal (Zn, Cu, and Ni) toxicities was also observed in animals fed with genetically modified grains containing high contents of LMW metal complexes[1].

These observations have been complemented by a comparison of bioavailability of inorganic and organic metal species clearly showing higher efficiency of the latter. For example, zinc absorption from supplemental zinc citrate is comparable with that from zinc gluconate and higher than from zinc oxide[2].

Similarly, organic Cu sources have been shown to be more bioavailable than inorganic Cu sources in some animal studies but not others (Spears, 2003). Although few studies have examined supplemental Mn sources, bioavailability of Mn-methionine was found to be greater than manganese sulfate or manganese oxide in test animals [3].

As a consequence of these findings, there is a current marketing trend to offer “organic” forms of Fe, Zn, Cu and Mn as food supplements. In these products, the mineral is bound to an organic (i.e. carbon-containing) molecule, typically a carboxylic or amino acid. The popular food supplements include gluconates of iron, zinc, copper and manganese, citrates of iron and zinc, glycinates of copper, iron, zinc and manganese, iron lactate and fumarate, zinc picolinate, acetate and orotate.

Although coconut water is known for its nutritional properties[4][5], the speciation of essential trace elements in this natural drink has not been studied. Due to its nature it may be expected that most of the metals is present in the form of water soluble low molecular weight, and thus potentially easily bioavailable, species. Also, coconut water is an

interesting sample from the point of view of plant physiology as a representative example of a liquid circulating in plants. In general, the amount of such liquids as xylem sap or embryo sac liquid (liquid endosperm) can be found and sampled in low microliters range which makes the method development a difficult task. In this context, coconut (*Cocos nucifera*) water can be considered as an interesting model for method development studies of plant endosperm metallome.

The presented work investigates speciation and Fe, Ni, Zn Cu and Mn found in a number of coconut samples of different provenance. A dedicated methodology based on the use of the hyphenation of two dimensional high performance liquid chromatography (HPLC) with element (ICP MS) and molecule specific (ESI MS) detection was developed for comprehensive speciation analysis of metal complexes in coconut water. A special attention was paid to the sample preparation which is known to highly influence species stability and thus analytical results. The analytical approach presented in this work is based on *i*) determination of the metals total content, *ii*) fractionation of metal species by size-exclusion chromatography with ICP MS detection, *iii)* separation of individual species by hydrophilic interaction chromatography (HILIC) coupled with ICP MS and *iv*) in parallel coupling HILIC with electrospray-Orbitrap MS for the detection and structural identification of metal complexes.

II MATERIALS AND METHODS

II.1.Samples

Several batches of coconut water were used during this work. All of the coconut samples were acquired from different suppliers in France, Spain and Switzerland. Two of the analysed coconuts were harvested directly from a coconut tree in Thailand.

Standard reference materials: The results of the total Fe, Mn, Ni, Zn determinations were validated by the analysis of standard reference material CRM-MFD Mixed Food Diet (HPS, North Charleston, SC).

II.2. Reagents

The reagents used for digestions, dilutions and the preparation of HPLC mobile phases were: ammonium acetate (≥98% for molecular biology, Sigma-Aldrich St. Louis, USA), nitric acid (V) (70%, Fisher Chemical, Loughborough, UK), acetonitrile (≥99.9%, Sigma-Aldrich St. Louis, USA) hydrogen peroxide (30%, Sigma-Aldrich St. Louis, USA), formic acid (supplier) hydrochloric acid (37%, Fluka, Steinheim, Germany). Standard solutions (1000 ppm, supplier?) of Fe, Mn, Ni, Cu, Zn, Rh, Sc were used for the preparation of calibration curves and as internal standards (Sc and Rh).

EDTA (ethylenediaminetetraacetic acid) (Sigma-Aldrich St. Louis, USA) was used for column cleaning. Milli-Q® Type 1 Ultrapure Water Systems (Millipore, Bedford, MA) deionized water was used thoughout.

II.3. Instrumentation

MiniSpin centrifuge (Eppendorf AG, German) and DigiPrep MS system (SCP Science, Quebec, Canada) were used.

Two chromatographic systems were applied**:** Agilent 1200 Series (Tokyo, Japan) with a Superdex 75 10/300 GL SEC column (10 × 300 mm); and Dionex Ultimate 3000 RS (Thermo Scientific, UHPLC, Germany) with a Kinetex HILIC column (150 x 2.1 mm x 2.6 µm) (Phenomenex, USA) with the pre-Column Security Guard (Ultra 3/PK, 2.1 mm x 3 µm) (ULTRA, USA)**.** The ICP MS spectrometer was ICP-MS 7500 (Agilent Technologies, Tokyo, Japan) equipped with an integrated autosampler (I-AS). Electrospray ionization mass spectrometer was Q Exactive Plus (Thermo Scientific, Bremen, Germany)

III PROCEDURES

III.1. Sample Preparation

Coconut husks were opened by doing an orifice with a drilling machine perforating the fruit mesocarpe without getting to the albumen to avoid contamination or simply by removing the shell from one of three germination pores. Coconut water was manually extracted by pipette. All samples were prepared on the same day of analysis. Some part of the total volume of coconut water was ultra-centrifuged and distributed in several eppendorf tubes to be either analyzed immediately or frozen at -80°C for further analysis. Due to the possible difficulties in sample preservation [6][7], several approaches, described in the subsequent sections of this article, were applied to guarantee the optimal storage conditions.

III.2. Total metal analysis

The method used was similar to those used before by De Sousa *et al.* [7][8]. Briefly, coconut water samples were treated with mixture of nitric acid and hydrogen peroxide in ratio (3:1) and digested in DigiPrep MS system until the observation of a clear solution, typically 2.5 hours. The maximum temperature did not exceed 60°C. The digests were cooled down to the room temperature. After an appropriate dilution and the addition of internal standards (Sc and Rh) the total content of metals of interest, including Mn, Fe, Cu, Ni and Zn, was measured by inductively coupled plasma mass spectrometry; ^{54}Fe, ^{56}Fe, ^{58}Ni, ^{60}Ni, ^{62}Ni, ^{63}Cu, ^{65}Cu, ^{55}Mn, ^{64}Zn, ^{66}Zn and ^{68}Zn isotopes were monitored. The experimental parameters, such as inductively coupled plasma power, torch position, and voltage applied to extraction and focusing lenses, were optimized before each analysis. Hydrogen was used as a reaction gas to reduce spectral interferences. Standard reference materials as well as analytical blanks were run in parallel. External calibration using 5-points calibration curves for metals of interest was used. Internal standards.

Table 25. Chromatographic conditions used (Sc and Rh) were added to the blanks, calibration standards and samples.

separation mechanism	HILIC	SEC
column	Kinetex (150 x 2.1 mm x 2.6 µm)	Superdex 75 10/300 GL
guard column	Security Guard (Ultra, 3/PK 2.1 mm x 3 µm)	none
mobile phase	A: 25 mM ammonium acetate at pH=5.5; B: ACN	100 mM ammonium acetate ,pH=7.5
flow rate, mL/min	0.5	0.7
injection volume, µL	10	100
gradient elution	0-1 min 95% B ; 1-10 min 80% ; 10-13.5 min 80% B ; 13.5-17 min 60% B ; 17-21 min 60% B ; 21.01-30 min 95% B.	isocratic

Table 26. ESI MS operating conditions

ionization mode	positive	negative
resolution	140000	70000
AGC	$1e^6$	$3e^6$
max injection time, ms	500	500
capillary temperature, °C	350	280
carrier gas temperature °C	400	300
lens voltage, V	40	40
spraying voltage, kV	3.2	2.5
shielding gas flow rate, arb	60	35
carrier gas flow, arb	20	10

III.3. Metal speciation by HPLC coupled to ICP-MS and ESI-MS

The HPLC pump was coupled with ICP-MS to separate species according to either size by using a size exclusion column or hydrophobicity by using a HILIC one. The operating conditions are presented in **Table 1.** The SEC column was calibrated using a set of molecular weight standards: methylcobamine, aprotinine, cytochrome C, ribonuclease A, myoglobine, carbonic anhydrase, fetuine bovine, ovalbumine, BSA, conalbumine, ferritine, Selenomethionine, Selenocysteine. The identification of the complexes of interest formed between metals and LMW ligands was carried out by coupling a HILIC column to an electrospray ionization mass spectrometer, Q Exactive Plus (Thermo Scientific, Bremen, Germany) in a positive ionization mode. The following parameters were adjusted: capillary temperature, carrier gas temperature, shielding gas pressure and spray voltage; the typical values are given in **Table 2**. Data

processing was done using XCalibur software (Thermo Scientific, Bremen, Germany) used for the generation of theoretical masses and their comparison with the experimental ones.

IV. Results and discussion

IV.1. Total analysis of metals in coconut water samples

The initial part of the study was the determination of the total content of biologically relevant metals in fresh and pre-freezed coconut water; the results are shown in **Figure 1.** As it was described in the experimental section, part of the liquid collected from the coconut was immediately ultracentrifuged (80000xg, 30 mins, 4°C). This step made it possible to isolate the suspended fraction from the coconut water. The results obtained indicate, that in most cases, no statistically significant differences in the total content of Mn, Fe, Ni, Cu and Zn in the ultracentrifuged and non-ultracentrifuged fresh samples were found. Slightly higher concentrations were noted for non-ultracentrifuged samples, although the differences did not exceed 10%. These results were shown as histograms in (**Fig. SI**1A).

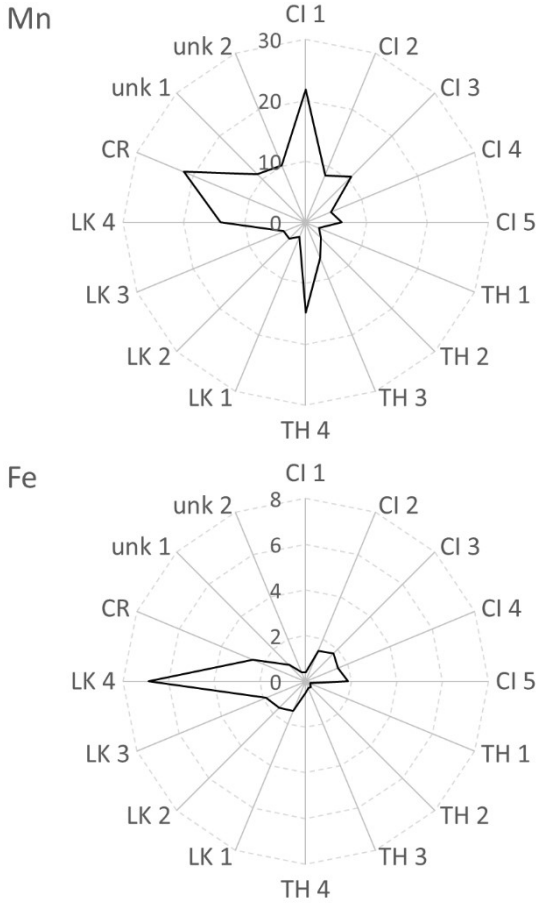

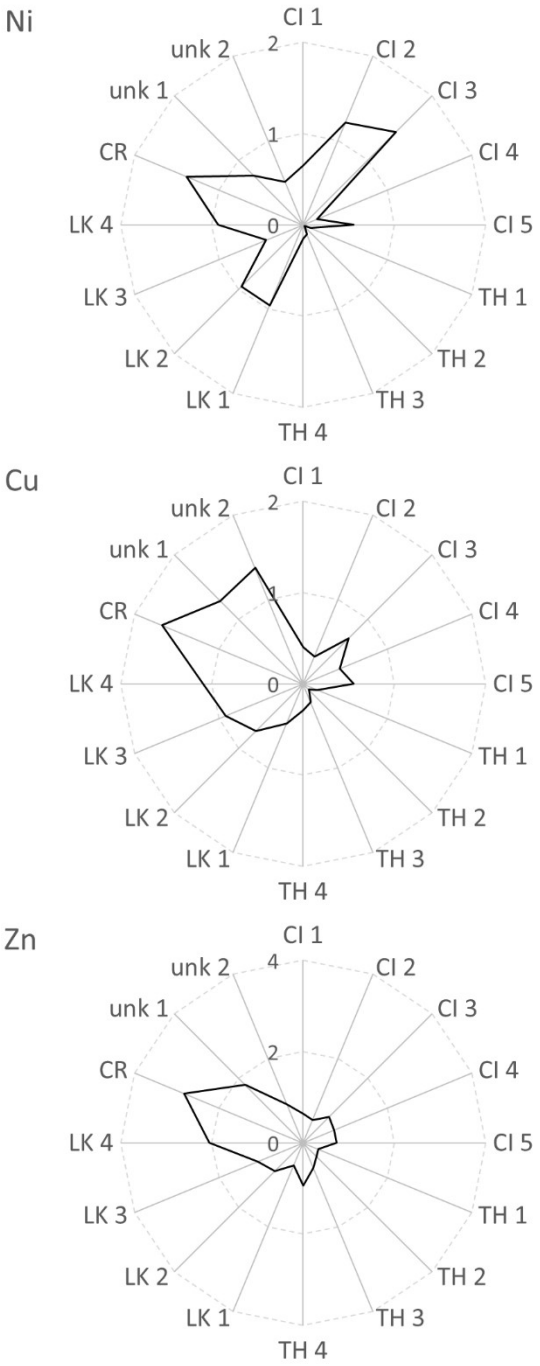

Figure 23. Spider graph of Fe, Mn, Ni, Cu and Zn in different coconut water samples. CI - Ivory Coast; TH – Thailand; LK – Sri Lanka; CR - Costa Rica; unk – unknown origin.

However, for some of samples stored at -80°C, an increase of elements content was observed after ultracentrifugation of thawed coconut water (Fig 1SIB). It might be explained by the cells explosion after freezing-defreezing step and a release of metals that may be retained inside the cells constituting suspended fraction. Therefore, in order to maintain the original speciation, ultracentrifugation was carried out for fresh samples.

As the analyzed coconuts were purchased from different providers, no information on the stage of maturity of fruits and environmental conditions of palm cultivation, which may affect the biochemical composition of coconut water, was available. The analysis of the results showed that among evaluated elements the highest contents (between 3 and 14 ppm) were found for manganese. The concentrations of Zn were in the range of 0.5-2 ppm and those of copper and nickel were between 0.3-1 ppm and 0.1-1 ppm respectively. The values corresponding to nickel, copper, zinc and iron are in the range as those reported by Midardul et al. who studied fifteen coconut water samples from Bangladesh [9]. In two of the samples tested, significantly higher concentrations of iron and zinc were also found. One of the reasons for variations in the content of elements in the analyzed matrix may be a difference in volumes of the coconut water sampled. As previously stated, the volume of liquid is dependent not only on the coconut size but also on fruit maturity. However, all the fruit analyzed were considered as mature and ready for consumption. More studies would be necessary to follow the evolution of metal contents during the fruit ripening.

IV.2. Size fractionation of metal complexes present in coconut water

The initial information on the metal complexes present in coconut water was obtained by their fractionation by size-exclusion chromatography with element selective detection by ICP MS. This technique has been extensively used for similar applications including nickel speciation in *Sebertia acuminata* [10] and metal-metallothionein complexes [11] and also for buffer exchange before and after different chromatography techniques [12]. Although, due to its poor separation efficiency, this chromatographic technique does not provide speciation data, it gives useful information about the MW of the species present. It is also able to detect most of possible species transformations related to sample pretreatment and storage. Typical SEC-ICP MS chromatograms for the metal species in coconut water are shown in **Fig. SI2A.** In general, all the chromatograms consisted of one peak with an exception of iron where two peaks representing species of different molecular weights (MW) were present. The approximate MW of the detected species corresponding to the major peak, according to the column calibration, corresponded to a few kDa. However, it has to be noted that for metal complexes a direct determination of MW on the basis of elution time from a SEC column is not possible due to secondary (except for molecular sieve) interactions of the polar compounds with the column stationary phase [12].

IV.2.1. Evaluation of changes in speciation data depending on pretreatment and storage conditions of coconut water

Coconut water remains sterile inside the cavity of the nut but once the nut is opened, its biochemical composition and physical appearance change [13]. To find optimal conditions of sample preservation before speciation analysis different storage temperatures were tested. After a week of storage at different temperatures, the samples were analyzed by SEC - ICP MS. Only slight differences in signal intensities were noted between sample stored in -80°C, +4°C and room (21°C) temperature (**Figure SI2B**). However, the intensity of signals obtained for the sample stored at room temperature was the lowest, hence, to maintain speciation, it is necessary to store samples at a low (at least 4°C) temperature.

Additionally, a hypothesis of the oxidation-related changes in speciation was checked by studying the influence of the ascorbic acid addition on SEC-ICP MS sample profiles. The most pronounced effect was observed for iron. The appearance of new signals at elution times corresponding to lower masses than the original ones was observed. This effect was observed to a much lesser extent for samples stored at +4°C, while a number of new signals for Fe were recorded at a subzero temperature, with a decrease in the intensity of peak at 22 min. The effect is related to the reducing properties of ascorbic acid and its possible redox reaction with Fe(III), even in pH 5-6, which is typical for coconut water, and formation of ferrous-ascorbate complexes [14][15][16]. It was already observed that ascorbic acid was responsible for the reduction of Fe(III) in mixed citrate-malate complexes by embryos efflux of Pisum sativum [17]. Ascorbic acid did not influence the speciation of other metals in the same degree; no significant changes were observed for ultracentrifuged samples (80000xg, 30 mins) and those analyzed directly.

An additional tests were performed to check the effect of the addition of acetonitrile (ACN), as it is present in the HILIC eluent which is used to dilute the samples before the analysis by HILIC-ICP MS

and then ESI MS. SEC-ICP MS results confirmed the removal of the high molecular weight (most probably protein-bound) iron fraction upon the addition of acetonitrile; as a result selective targeting low molecular Fe species is possible. No effect on the SEC-ICP MS profiles of other studied elements was observed (**Fig. SI2A**).

The final recommendation drawn from the above experiments was that the samples should be ultra-centrifuged and stored at -80°C. Such conditions do not affect the metals' speciation and the stability of coconut water is preserved for at least 4 months. However, if possible, it is recommended to analyze fresh samples.

IV.3. Speciation of LMW metal complexes in coconut water by HILIC-ICP MS

Hydrophilic interaction liquid chromatography (HILIC) is a method of preference for separation of LMW polar species, such as metal complexes present in the coconut water [18][19]**.** When properly optimized, it provides high resolution chromatograms with peaks corresponding to individual species [20]–[23]**.**

The chromatograms obtained for eight coconut water samples are shown in Fig. SI3. Final conditions of sample preparation and storage were applied to compare the speciation of iron, nickel, manganese and copper. All samples were opened and analyzed on the same day, after ultracentrifugation. As samples were diluted with acetonitrile-containing eluent, the soluble proteins were removed prior to analysis. All of the samples, irrespectively of the fruit origin, were characterized by similar chromatographic profiles for all elements (Figure SI3) showing three peaks corresponding to iron species, two peaks for copper and nickel and one peak for manganese. The intensities of the chromatographic peaks were in agreement with the total element concentrations of different samples with a maximum for one of the coconut waters from Sri Lanka.

HILIC-ICP MS methodology was also used to complement the investigations on sample storage conditions extensively described in the previous section. No significant changes in HILIC-ICP MS profiles were recorded for utracentrifuged (80000xg, 30 mins) and directly analyzed samples.

In order to check the reliability of the proposed procedure, the recovery of Fe, Mn, Ni, Cu and Zn from the HILIC column was tested. However, according to the results obtained, the concentration of almost all (Fe, Ni, Mn, Cu) monitored elements was higher in the efluent from chromatographic column than in the initial solution. This may be due to the carryover from metals previously retained on the column although this phenomenon was not affecting the analysis as recorded chromatograms are repeatable. No literature data discussing this phenomenon exist.

IV.4. HILIC ESI MS identification of LMW metal species in coconut water

The same chromatographic conditions were used for the coupling of HILIC to ESI MS for the identification of the Mn, Fe, Cu, Zn and Ni complexes.

The data mining consisted of three strategies: (i) checking for the presence of metal-containing species at the retention times of peaks detected by ICP MS [24]**,** (ii) targeted analysis based on the literature data and (iii) exploratory analysis based on automatic search for metal isotopic patterns (except for Mn which is monoisotopic). The molecular formulas, together with calculated and measured m/z for the identified complexes, are summarized in **Table 3** and the selected ion chromatograms together with isotopic patterns in **Fig. 2** and **3**.

The main iron containing peak was attributed to a complex of m/z 811.84, which consisting of three atoms of iron bound to two molecules of citrates and two malates. In addition; a complex of similar structure, but carrying three citrate and one malate residues (m/z 869.84) was observed. These two iron species, (Fe(III)3Cit2Mal2 and Fe(III)3Cit3Mal), were reported by Grillet et al. in a liquid endosperm of pea [17]. In the coconut water, smaller complexes formed with a single iron atom with two molecules of these ligands were found. Additionally, iron complexes with glutamine (m/z 346.06) were identified. Fe(III)-Gln2 was previously detected in xylem and ESL of pea plants [25]. Additionally, in the study of Lopez-Milan et al. on the effect of iron deficiency on the release of amino acids in the apoplastic fluid of sugar beet, it was shown that the amount of Gln doesn’t change importantly when there is Fe deficiency but it can play a role in Fe

transport [26]. Moreover, Fe(II)-NA was identified in the endosperm of coconut; this complex was identified in the ESL of pea plants by Flis et al. [25] in wheat grains by Eagling et al. and Xue et al [27][28]. Also, Tsednee *et al* reported the presence of several phytosiderephores-iron complexes, including Fe-NA, in barley [29].

The most abundant nickel complex was the one with nicotianamine (m/z 360.07) accompanied by the phenylalanine one (m/z 387.08). Similar complexes were also found for copper (m/z 365.06 and 392.08, respectively). These compounds are characteristic for xylem exudate or embryo sac liquid (known also as liquid endosperm) and were reported for *Pisum sativum* by Flis et al. [25] and by Weber et al in *Arabidopsis thaliana* in addition to Ni(II)Asp_2 [30] and in *Thlaspi caerulescens* by Mari et al [31]. To our best knowledge, no reports on Ni- phenylalanine can be found in the literature. Cu-nicotianamine was reported in chicory and tomato by Liao et al [32], in xylem and phloem saps from rice (*Oryza sativa*) [33] and in *Brassica carinata* by Irtelli *et al* [34].

Table 27. Metal complexes detected by hydrophilic interaction chromatography electrospray ionization mass spectrometry (HILIC-ESI-MS) in coconut water

Proposed structure	Molecular formula	Calcutated m/z	Measured m/z	Error m/z [ppm]
$Mal_2Cit_2Fe(III)_3$	$C_{20}H_{20}O_{24}Fe_3$	811,83873	811,83942	0.001
$Gln_2Fe(III)$	$C_{10}H_{18}O_6N_4Fe$	346,05703	346,05743	1.162
$Mal_2Fe(III)$	$C_8H_{10}O_{10}Fe$	321,96179	321,96205	0.808
NA-Fe(II)	$C_{12}H_{20}O_6N_3Fe$	358,06960	358.07022	1.721
$MalCit_3Fe(III)_3$	$C_{22}H_{22}O_{26}Fe_3$	869,84421	869,84467	0.531
Asp_2Mn	$C_8H_{13}O_8N_2Mn$	320,00469	320,00461	-0,2
NA-Ni	$C_{12}H_{20}O_6N_3Ni$	360,07001	360,06998	-0.082
Phe_2Ni	$C_{18}H_{21}O_4N_2Ni$	387,08507	387,08475	0.229
Asp_2Ni	$C_8H_{13}O_8N_2Ni$	323,00199	323,00197	-0.061
NA-Cu	$C_{12}H_{20}O_6N_3Cu$	365,06426	365,06430	0.102
Phe_2Cu	$C_{18}H_{21}O_4N_2Cu$	392,07918	392,07862	-1.440
Phe_3Cu	$C_{27}H_{32}O_6N_3Cu$	557,15816	557,15863	0.838

Mal: malate, Cit: citrate, Fe: Iron, Gln, glutamine, NA: nicotianamine, Ni: nickel, Asp: aspartate, Mn: manganese, Phe: phenylalanine, Copper.

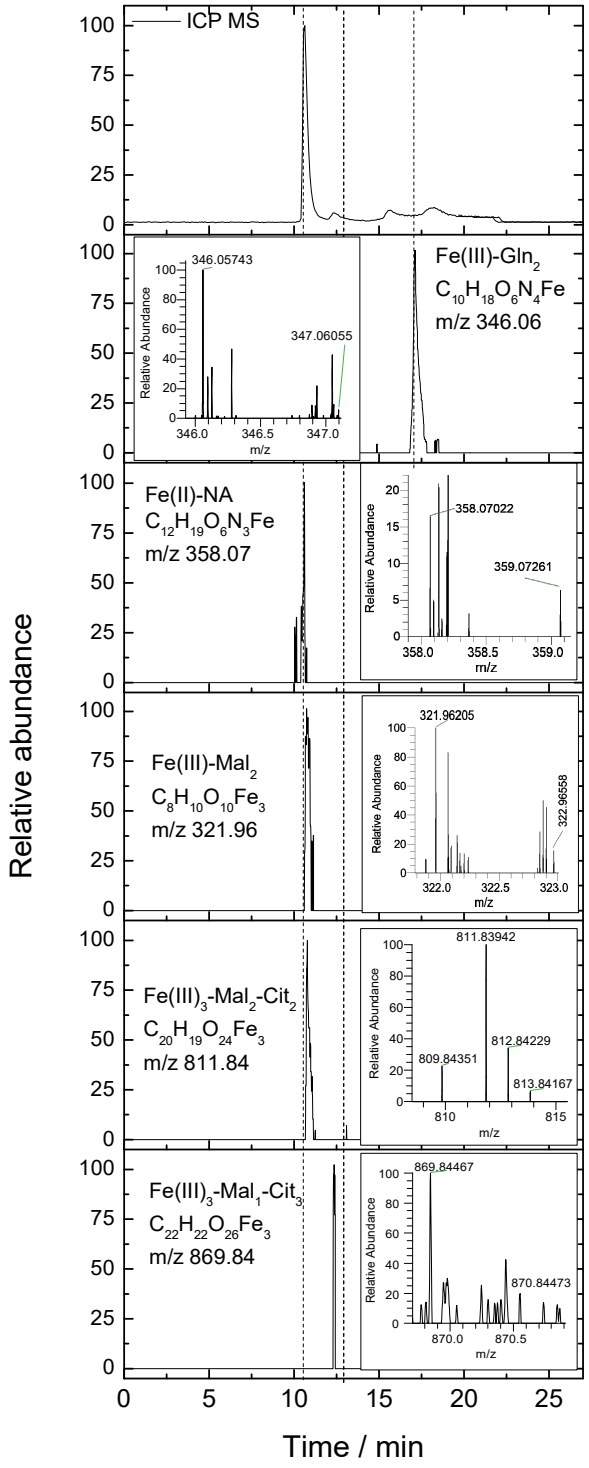
ICP MS
Fe(III)-Gln2
C10H18O6N4Fe
m/z 346.06
346.05743
347.06055
Fe(II)-NA
C12H19O6N3Fe
m/z 358.07
358.07022
359.07261
Fe(III)-Mal2
C8H10O10Fe3
m/z 321.96
321.96205
322.96558
Fe(III)3-Mal2-Cit2
C20H19O24Fe3
m/z 811.84
811.83942
809.84351
812.84229
813.84167
Fe(III)3-Mal1-Cit3
C22H22O26Fe3
m/z 869.84
869.84467
870.84473
Relative Abundance
m/z
Relative abundance
Time / min

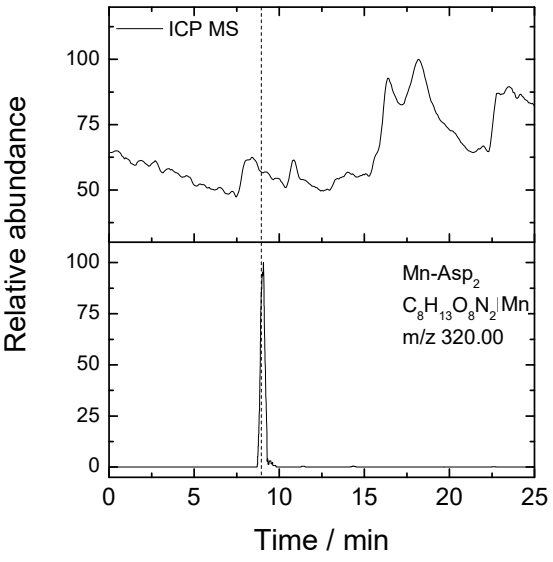
ICP MS
Mn-Asp2
C8H13O8N2Mn
m/z 320.00
Relative abundance
Time / min

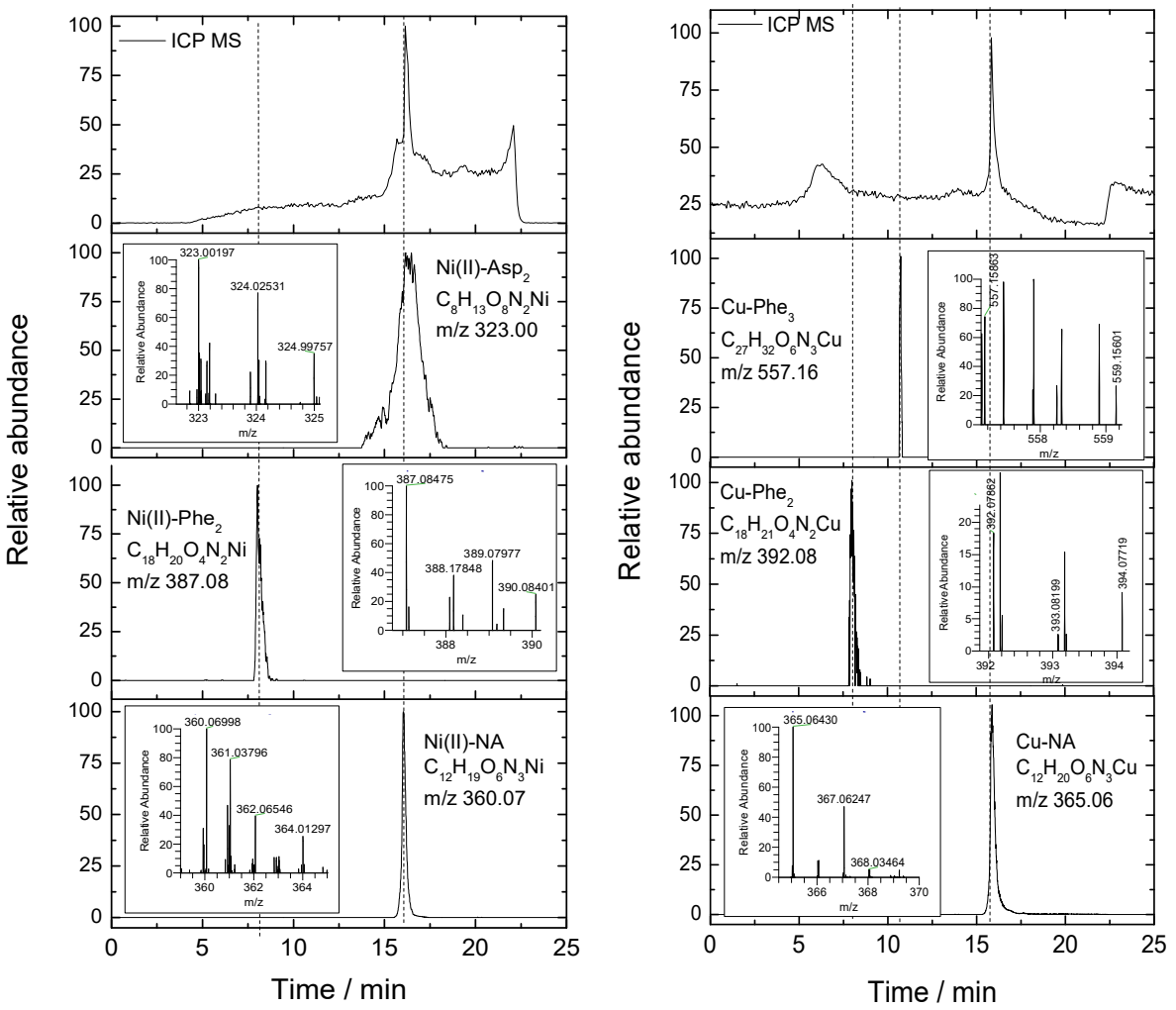

Figure 2. Identification of iron, copper, nickel and manganese species in coconut water. HILIC-ICP-MS chromatogram (top panel) and extracted ion HILIC-ESI-MS chromatograms of the species identified

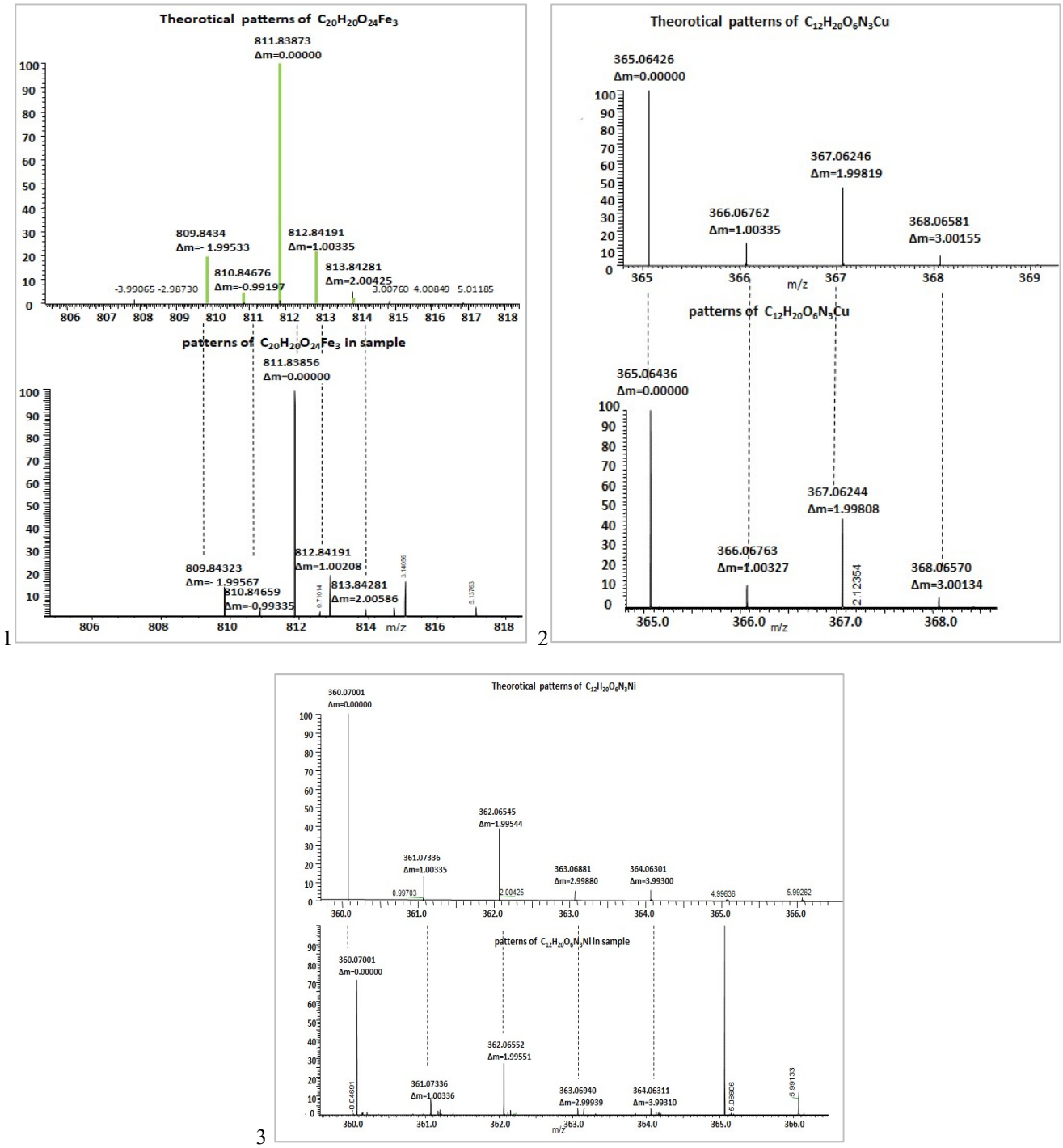

Figure 3. Comparison of experimental and theoretical isotopic patterns of selected metal complexes in coconut water: (1) $C_{20}H_{20}O_{24}Fe_3$, (2) $C_{12}H_{20}O_6N_3Cu$, (3) $C_{12}H_{20}O_6N_3Ni$.

V. Conclusions

The analytical approach presented in this work based on coupling HILIC with ICP MS electrospray-Orbitrap MS helped for the detection and structural identification of metal complexes present in coconut water after optimization of sample preparation to minimize metals losses. The results obtained showed particularly high concentration of iron, nickel, copper, zinc and manganese in coconut water, especially in samples from Ivory Coast. The HILIC-ICP MS analysis allowed detection of different metal complexes, among which $Fe_3Cit_2Mal_2$, $Fe_3Cit_3Mal_1$, Gln_2Fe, Mal_2Fe, Asp_2Mn, NACu, Asp_2Ni, Phe_2Ni and NANi, Phe_2Cu Phe_3Cu.

This work will be accomplished by a development of a method based on isotope dilution ESI MS for quantitative analysis of metals of interest in the coconut water.

Supplementary information

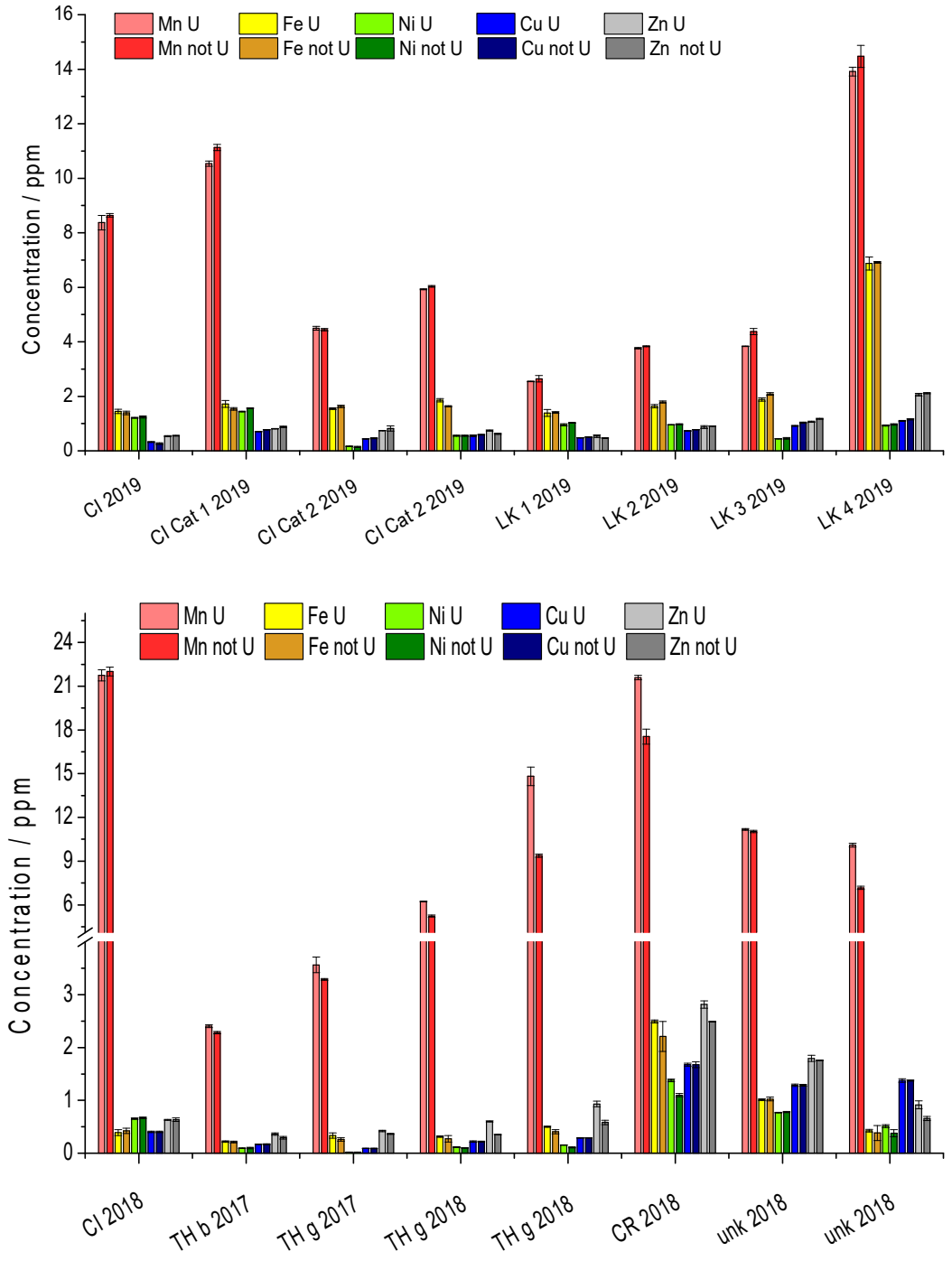

Figure SI1. Total contents of metals in samples of coconut water, centrifuged (U) and native (not U); CI – Ivory Coast; LK – Sri Lanka; TH - Thailand; CR - Costa Rica; unk – unknown origin.

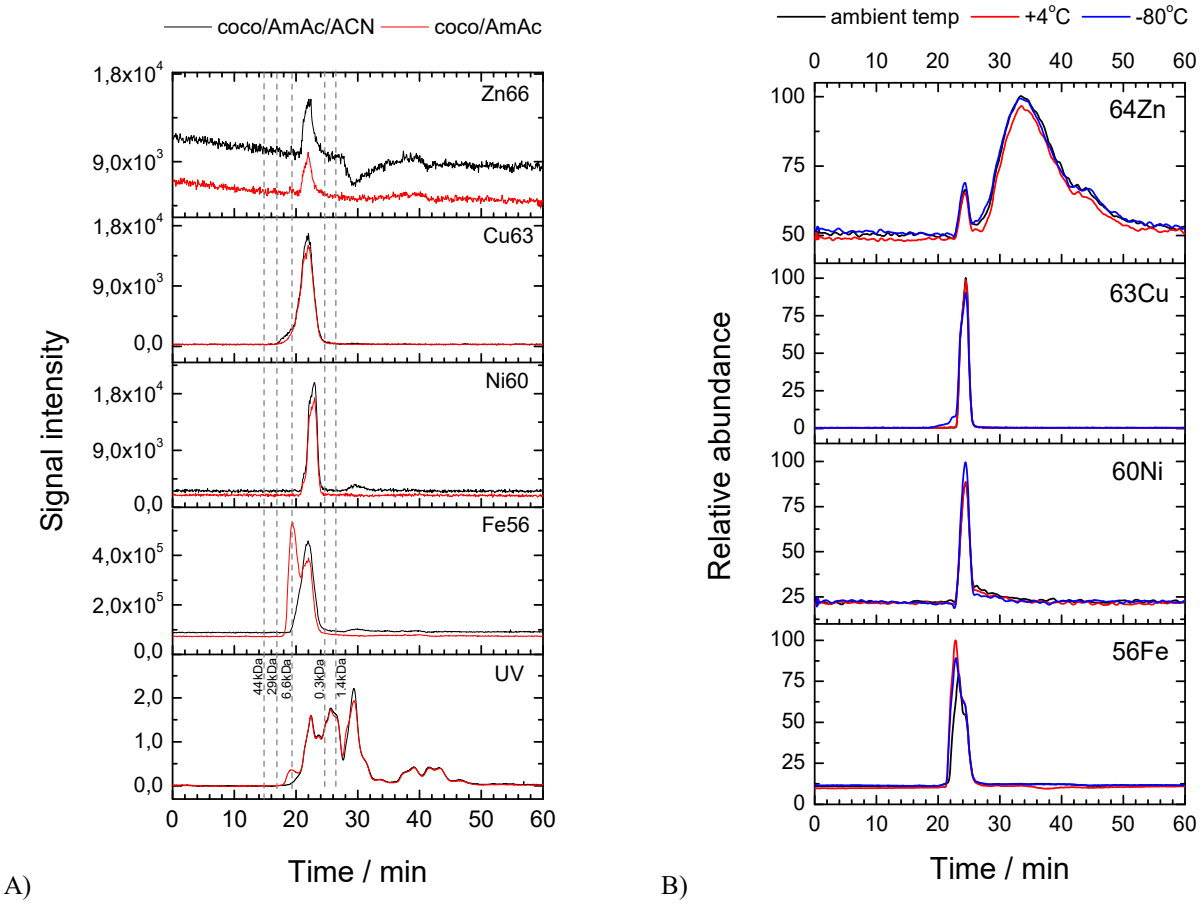

Figure SI24. SEC chromatograms of coconut water samples, with and without addition of ACN (A) and chromatograms obtained for samples stored in different temperature conditions (B). Chromatograms were obtained on SEC Superdex-75 column after injection of 100 µL of the sample and isocratic elution with ammonium acetate (pH 7.5); flow rate of 0.7 mL min-[1].

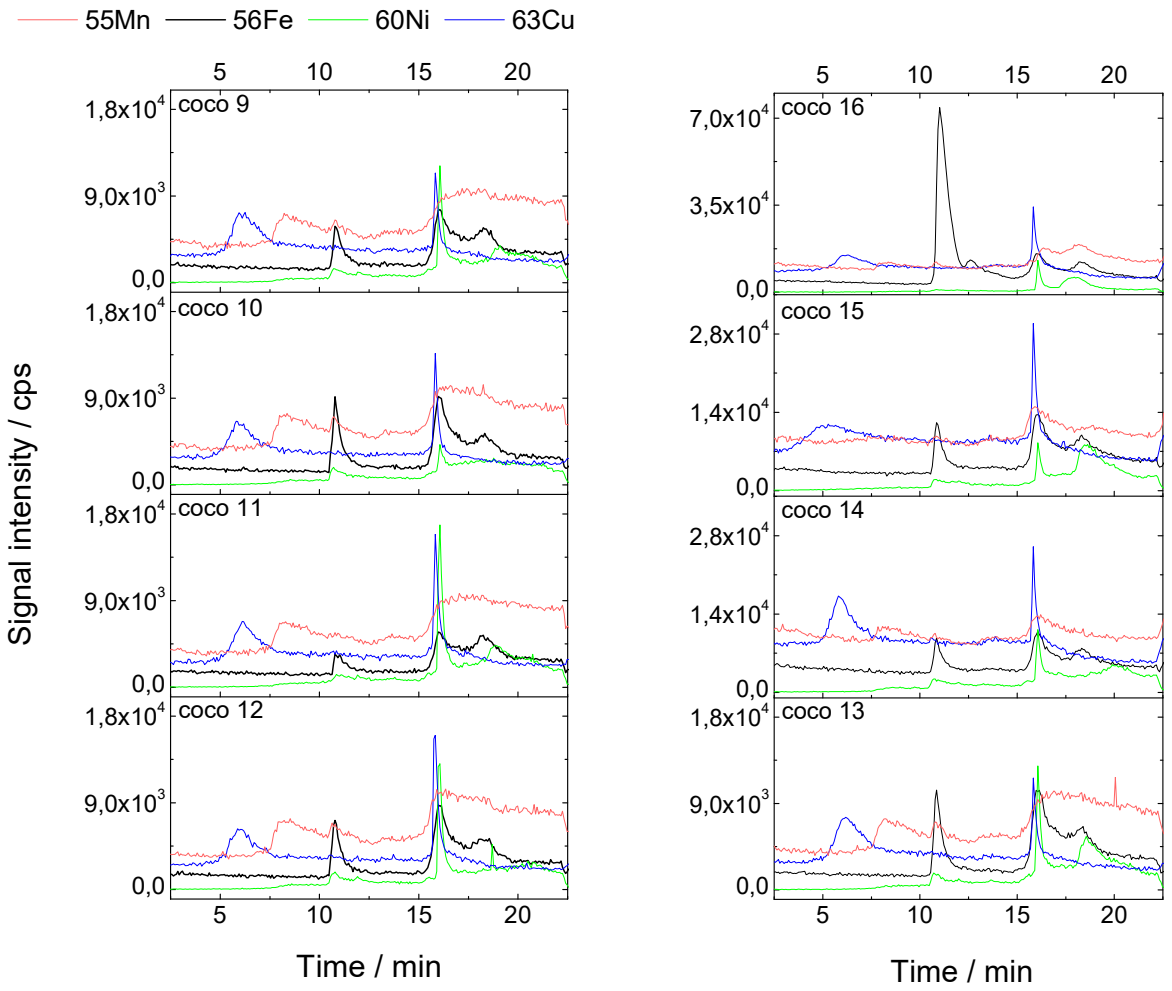

Figure SI3. HILIC chromatograms of fresh coconut water samples. Chromatograms were obtained on Phenomenex Kinetex column after injection of 10 µL of the sample and gradient elution with 5 mmol L^{-1} ammonium acetate (pH 5.5) and acetonitrile (ACN) mixtures; flow rate of 0.5 mL min^{-1}

References

[1] S. Lee et al., "Iron fortification of rice seeds through activation of the nicotianamine synthase gene," Proc. Natl. Acad. Sci. U. S. A., vol. 106, no. 51, pp. 22014–22019, 2009.

[2] R. Wegmüller, F. Tay, C. Zeder, M. Brnić, and R. F. Hurrell, "Zinc Absorption by Young Adults from Supplemental Zinc Citrate Is Comparable with That from Zinc Gluconate and Higher than from Zinc Oxide," J. Nutr., vol. 144, no. 2, pp. 132–136, 2014.

[3] P. R. Henry, C. B. Ammerman, and R. C. Littell, "Relative Bioavailability of Manganese from a Manganese-Methionine Complex and Inorganic Sources for Ruminants," J. Dairy Sci., vol. 75, pp. 3473–3478, 1992.

[4] U. Santoso, K. Kubo, T. Ota, T. Tadokoro, and A. Maekawa, "Nutrient composition of kopyor coconuts (Cocos nucifera L.)," Food Chem., vol. 57, no. 2, pp. 299–304, 1996.

[5] J. W. H. Yong, L. Ge, Y. F. Ng, and S. N. Tan, "The Chemical Composition and Biological Properties of Coconut (Cocos nucifera L.) Water," Molecules, vol. 14, pp. 5144–5164, 2009.

[6] A. Obike, "Proximate and Trace Metal Analysis of Coconut (Cocos nucifera) Collected from Southeastern , Nigeria Proximate and Trace Metal Analysis of Coconut (Cocos nucifera) Collected from Southeastern , Nigeria," vol. 3, no. March, pp. 357–361, 2017.

[7] R. A. De Sousa, N. Baccan, and S. Cadore, "Determination of Metals in Brazilian Coconut Water Using an Inductively Coupled Plasma Optical Emission Spectrometer," J. Braz. Chem. Soc, vol. 16, no. 3B, pp. 540–544, 2005.

[8] R. A. De Sousa, C. J. J. Silva, N. Baccan, and S. Cadore, "Determination of metals in bottled coconut water using an inductively coupled plasma optical emission

spectrometer," J. Food Compos. Anal., vol. 18, no. 3, pp. 399–408, 2005.

[9] I. Md Didarul, A. Rahaman, and A. Afrose, "Assessment of Heavy Metal Concentration in Coconut Water," Recent Res. Sci. Technol., vol. 10, pp. 07–10, 2018.

[10] D. Schaumlöffel, L. Ouerdane, B. Bouyssiere, and R. Łobiński, "Speciation analysis of nickel in the latex of a hyperaccumulating tree Sebertia acuminata by HPLC and CZE with ICP MS and electrospray MS-MS detection," J. Anal. At. Spectrom., vol. 18, pp. 120–127, 2003.

[11] S. Mounicou et al., "Identification of metallothionein subisoforms in HPLC using accurate mass and online sequencing by electrospray hybrid linear ion trap-orbital ion trap mass spectrometry," Anal. Chem., vol. 82, pp. 6947–6957, 2010.

[12] Harvard, "Guide to Gel Filtration," pp. 1–14.

[13] A. Prades, "DÉTERMINATION DE LA QUALITÉ DE L'EAU DE COCO EN FONCTION DU STADE DE MATURATION DES NOIX ET LORS DE SA STABILISATION PAR CHAUFFAGE OHMIQUE ET FILTRATION MEMBRANAIRE," 2011.

[14] Y. H. P. Hsieh and Y. P. Hsieh, "Kinetics of Fe(III) reduction by ascorbic acid in aqueous solutions," J. Agric. Food Chem., vol. 48, no. 5, pp. 1569–1573, 2000.

[15] S. Pervaiz, M. A. Farrukh, R. Adnan, and F. A. Qureshi, "Kinetic investigation of redox reaction between vitamin C and ferric chloride hexahydrate in acidic medium," J. Saudi Chem. Soc., vol. 16, no. 1, pp. 63–67, 2012.

[16] T. Suzuki, F. M. Clydesdale, and T. Pandolf, "Solubility of iron in model systems containing organic acids and lignin," J. Food Prot., vol. 55, no. 11, pp. 893–898, 1992.

[17] L. Grillet et al., "Ascorbate efflux as a new strategy for iron reduction and transport in plants," J. Biol. Chem., vol. 289, no. 5, pp. 2515–2525, 2014.

[18] J. Szpunar, "Bio-inorganic speciation analysis by hyphenated techniques," Analyst, vol. 125, pp. 963–988, 2000.

[19] J. Szpunar, The concept of speciation analysis and hyphenated techniques. 2003.

[20] B. Buszewski and S. Noga, "Hydrophilic interaction liquid chromatography (HILIC) — a powerful separation technique," Anal Bioanal Chem, vol. 402, pp. 231–247, 2012.

[21] L. Beuvier, "Developpement d'une methode de separation chromatographique couplee aux spectrometries de masse a source d'ionisation a source plasma a couplage inductif (ICP-MS) : application a l'analyse de speciation des lanthanides," 2015.

[22] M. Montes-Bayón, M. Sharar, and M. Corte-Rodriguez, "Trends on (elemental and molecular) mass spectrometry based strategies for speciation and metallomics," TrAC - Trends Anal. Chem., vol. 104, pp. 4–10, 2018.

[23] K. Spagou, H. Tsoukali, N. Raikos, H. Gika, I. D. Wilson, and G. Theodoridis, "Hydrophilic interaction chromatography coupled to MS for metabonomic/metabolomic studies," J. Sep. Sci., vol. 33, pp. 716–727, 2010.

[24] S. Mounicou, J. Szpunar, and R. Lobinski, "Metallomics: The concept and methodology," Chem. Soc. Rev., vol. 38, pp. 1119–1138, 2009.

[25] P. Flis, L. Ouerdane, L. Grillet, C. Curie, S. Mari, and R. Lobinski, "Inventory of metal complexes circulating in plant fluids: a reliable method based on HPLC coupled with dual elemental and high-resolution molecular mass spectrometric detection," New Phytol., vol. 211, pp. 1129–1141, 2016.

[26] A. F. Lopez-Millan, F. Morales, A. Abadia, and J. Abadia, "Effects of iron deficiency on the composition of the leaf apoplastic fluid and xylem sap in sugar beet. Implications for iron and carbon transport," Plant Physiol., vol. 124, pp. 873–884, 2000.

[27] T. Eagling, A. L. Neal, S. P. McGrath, S. Fairweather-Tait, P. R. Shewry, and F. J. Zhao, "Distribution and speciation of iron and zinc in grain of two wheat genotypes," J. Agric. Food Chem., vol. 62, pp. 708–716, 2014.

[28] Y. F. Xue et al., "Effects of nitrogen on the distribution and chemical speciation of iron and zinc in pearling fractions of wheat grain," J. Agric. Food Chem., vol. 62, pp. 4738–4746, 2014.

[29] M. Tsednee, Y. W. Mak, Y. R. Chen, and K. C. Yeh, "A sensitive LC-ESI-Q-TOF-MS method reveals novel phytosiderophores and phytosiderophore-iron complexes in barley," New Phytol., vol. 195, pp. 951–961, 2012.

[30] G. Weber, N. von Wirén, and H. Hayen, "Hydrophilic interaction chromatography of small metal species in plants using sulfobetaine- and phosphorylcholine-type zwitterionic stationary phases," J. Sep. Sci., vol. 31, pp. 1615–1622, 2008.

[31] S. Mari et al., “Root-to-shoot long-distance circulation of nicotianamine and nicotianamine-nickel chelates in the metal hyperaccumulator Thlaspi caerulescens,” J. Exp. Bot., vol. 57, no. 15, pp. 4111–4122, 2006.

[32] M. T. Liao, M. J. Hedley, D. J. Woolley, R. R. Brooks, and M. A. Nichols, “Copper uptake and translocation in chicory (Cichorium intybus L. cv Grasslands Puna) and tomato (Lycopersicon esculentum Mill. cv Rondy) plants grown in NFT system. II. The role of nicotianamine and histidine in xylem sap copper transport,” Plant Soil, vol. 223, pp. 243–252.

[33] Y. Ando, S. Nagata, S. Yanagisawa, and T. Yoneyama, “Copper in xylem and phloem saps from rice (Oryza sativa): The effect of moderate copper concentrations in the growth medium on the accumulation of five essential metals and a speciation analysis of copper-containing compounds,” Funct. Plant Biol., vol. 40, pp. 89–100, 2013.

[34] B. Irtelli, W. A. Petrucci, and F. Navari-Izzo, “Nicotianamine and histidine/proline are, respectively, the most important copper chelators in xylem sap of Brassica carinata under conditions of copper deficiency and excess,” J. Exp. Bot., vol. 60, no. 1, pp. 269–277, 2009.

9.3 Article 3

Paspalum urvillei and *Setaria parviflora*, two grasses naturally adapted to extreme iron-rich environments.

To be submitted in Plant Physiology and Biochemistry

Paspalum urvillei and *Setaria parviflora*, two grasses naturally adapted to extreme iron-rich environments.

Talita Oliveira de Araujo[a,d], Marie-Pierre Isaure[b], Ghaya Choubassi[b], Katarzyna Bierla[b], Joanna Szpunar[b], Nicolas Trcera[c], Sandrine Chay[d], Carine Alcon[d], Luzimar Campos da Silva[a], Catherine Curie[d], Stephane Mari[d]

[a]Universidade Federal de Viçosa, Laboratório de Anatomia Vegetal, Viçosa 36570-900, Brazil
[b]Université de Pau et des Pays de l'Adour, Institut des Sciences Analytiques et de Physico-Chimie pour l'Environnement et les Matériaux, Centre National de la Recherche Scientifique (UMR5254, IPREM, E2S UPPA CNRS), F-64063, Pau Cedex, France
[c]Synchrotron SOLEIL, l'Orme des Merisiers Saint Aubin BP48, 91192 Gif-sur-Yvette cedex, France

[d]BPMP, INRA, CNRS, SupAgro, Univ Montpellier, F-34060 Montpellier, France

Abstract

Paspalum urvillei and *Setaria parviflora* are two plant species naturally adapted to iron-rich environments, isolated around the decantation ponds of iron mines in Brazil. The aim of our work was to characterize how these two species cope with these extreme conditions by comparing them with related model species, *Oryza sativa* and *Setaria viridis,* that appeared to be much less tolerant to Fe excess in the growth conditions tested. Iron quantification in roots and shoots showed that both *P. urvillei* and *S. parviflora* were able to limit the amount of Fe accumulated in roots and, more importantly, to restrict the translocation of Fe to shoots, by comparison with *O. sativa* and *S. viridis* that over-accumulated Fe in shoots, leading to toxicity symptoms. To better understand the mechanisms of Fe tolerance, we then focused on specific features such as the formation of the iron plaque (IP, an iron-rich structure formed around roots), the identification of Fe forms translocated from roots to shoots and on the intracellular sites of Fe accumulation. Synchrotron micro X-ray fluorescence (µXRF) analyses showed the presence of phosphorus, calcium, silicon and sulfur on IP of *Paspalum urvillei* plants treated with Fe excess and microX-ray Absorption Near Edge Structure spectroscopy (µXANES) identified Fe(III) oxyhydroxide (ferrihydrite) as the main Fe form of IP. Moreover, Perls/DAB staining in root cross sections indicated that the IP was more developed in *P. urvillei* and *S. parviflora*, suggesting a role of this structure in the limitation of Fe uptake. Once within roots, high concentrations of Fe were localized in the cell walls and vacuoles of P. urvillei, S. parviflora and O. sativa, a mechanism that was absent in S. viridis that, instead, accumulated Fe in dot-shapped structures corresponding to ferritins. The Fe forms translocated to the shoots of S. parviflora were identified as tri-iron complexes with citrate and malate. In leaves, all species accumulated Fe in the vacuoles of bundle sheath cells and as ferritin complexes in plastids, although the Fe accumulation on chloroplasts was much more intense in O. sativa. Taken together, our results strongly suggest that Paspalum urvillei and Setaria parviflora set up mechanisms of Fe exclusion in roots and shoots to limit the toxicity induced by Fe excess.

Key words: *Paspalum urvillei*, *Setaria parviflora*, *Setaria viridis*, *Oryza sativa*, Perls-DAB method, µXRF; µXANES, iron plaque, vacuole, chloroplast, ferritin, citrate, malate.

Introduction

Iron (Fe) is an essential micronutrient that is absorbed by roots of grasses as Fe^{3+}-phytosiderophores complexes and follows the transpiration stream to the shoot along with other nutrients and minerals (Nozoye et al., 2011). Despite being required in chloroplasts and mitochondria to be used as an enzymatic cofactor in a wide range of metabolic processes (Balk and Schaedler, 2014), when in excess, ferrous ions can promote the generation of reactive oxygen species and oxidative stress (Dinakar et al., 2010). Nevertheless, some species are naturally adapted to tolerate extremely high concentrations of metals in their environment, using two distinct strategies: some species will avoid the built up of metals in the organs, particularly in

leaves, they are termed “excluders” whereas other species will promote the storage of metals in above-ground organs, these plants are known as “hyperaccumulators” (van der Ent et al., 2013). There are three criteria to classify a plant as hyperaccumulator: the shoot/root ratio of metal concentration has to be higher than 1; metal total content in the shoots divided by total metal in the medium must be greater than 1; and, metal content must be 10 – 500 times higher than found in uncontaminated plants. Threshold criteria for the concentration in foliar tissues (dry weight basis) have been defined for various elements for plants growing in their natural habitat (Redekar et al., 2015). Hyperaccumulation of Ni, Zn, Cd, As, Cu, Co, Mn, Pb, Se, Tl and rare earth elements (REE) has been reported (van der Ent et al., 2013;Reeves et al., 2018). Iron hyperaccumulation has been much less reported, probably because Fe has a low bioavailability caused by the low solubility of iron oxyhydroxides in natural environments and instead, acts as a limiting factor for plant growth. Therefore the identification of true Fe hyperaccumulators is less clearly established than for other trace elements. Nevertheless, there are some studies reporting Fe tolerance and hyperaccumulation in *Imperata cylindrica* (grass family, Poacae) from the acidic mining area of the Tinto River banks in the Iberian Pyritic Belt in Spain (Rodriguez et al., 2005;de la Fuente et al., 2017). Contrary to hyperaccumulators, true “excluder” plants have received much less attention {Bothe, 2017 #1987}.

To deal with Fe excess, plants employ mechanisms such as induction of antioxidant system (Stein et al., 2014), reorganization of the photosynthetic apparatus (Pereira et al., 2014) (Muller et al., 2015) and detoxification and / or sequestration in sites where Fe will not cause damage to cell, i.e. vacuoles and apoplastic space (Briat et al., 2010b;Zhang et al., 2012). The presence of an iron plaque (IP) can be considered as a mechanism of resistance, since it is due to Fe precipitation on the root surface, avoiding the over-accumulation of iron in leaf tissues (Green and Etherington, 1977). The IP formation occurs in roots of wetland plant where Fe is spontaneously precipitated due to oxidizing microenvironments normally created around roots of aquatic plants (Xu et al., 2009). Thus, Fe2+ is oxidized into Fe3+, which precipitates on the root surface, thereby creating a smooth regular reddish precipitate or irregular plaque coating on root surfaces (Pereira et al., 2014;Tripathi et al., 2014).

The adsorption of trace metals and nutrients is the most important characteristic of IP. A significant amount of metals bind to IP through the formation of complexes thanks to the high affinity of Fe hydroxide for different metals (Batty et al., 2000;Liu et al., 2011). Extensive efforts to understand the role of IP in metal sequestration and translocation have yielded contrasting results. Some authors agree that IP acts as a resistance barrier for metal(loids) translocation, and this barrier can function by either acting as an adsorbent of toxic elements or by simply being a physical obstacle (Pi et al., 2011;Huang et al., 2012). As an illustration, iron plaques have been demonstrated to sequester arsenic in the wetland plants *Typha latifolia* (Hansel et al., 2002;Blute et al., 2004), *Phragmites australis* (Pardo et al., 2016), *Phalaris arundinacea* (Hansel et al., 2002),and rice *Oryza sativa L* (Liu et al., 2006). Other metals such as Cu, Mn, Pb and Zn were also detected in IP from *Spartina alterniflora* (Feng et al., 2015;Xu et al., 2018) and *Phalaris arundinacea* (Hansel et al., 2001).

Alternatively, IP may act as a buffer and reservoir in nutrient uptake, particularly during the time of diminished supply of nutrients (Hu et al., 2007;Williams et al., 2014). In all cases, the nature of Fe phases in IP but also the plant species and the ionic species are likely involved in metals and metalloids uptake (Batty et al., 2000;Hansel et al., 2001;Pereira et al., 2014). Ferric iron is the predominant oxidation state of Fe on IP. Amorphous ferric oxyhydroxides, ferrihydrite, goethite (α-FeOOH), and lepidocrocite (ɤ-FeOOH) are commonly found as the main mineral phases in IP (Bacha and Hossner, 1977;Chen et al., 1980;Taylor et al., 1984;Stcyr et al., 1993;Liu et al., 2006). In highly acidic conditions, jarosite, a sulfur-rich mineral, accumulates in the IP of *Imperata cylindrical* (Rodriguez et al., 2005;Amils et al., 2007). Ferrous Fe too has been identified in IP of some species such as *Phragmites australis* (Wang and Peverly, 1996;1999). In *Phalaris arundinacea* and *Typha latifolia*, Fe(II) was detected as siderite (FeCO3) in addition to a mixture of ferryhydrite, goethite, lepidocrocite and ferric phosphate (Hansel et al., 2001;Hansel et al., 2002).

Plants which develop IP on roots are able to better survive in contaminated soils (Taylor et al., 1984) by avoiding toxic buildup of metals in their aerial parts. To understand the role of IP in Fe absorption by the root, it is essential to have a clear description of the

IP composition and of the Fe distribution strategy in roots. Chemical imaging techniques have become a key component of the toolbox to investigate metal distribution in plants. To localize Fe, histochemical staining using Perls-diaminobenzidine (DAB) has proved powerful to locate both Fe^{3+} and Fe^{2+}in plants at the cell level (Roschzttardtz et al., 2009). Since the method requires fixation and dehydration steps where loosely bound Fe species can be lost, it is useful to apply a complementary technique in which the sample preparation differs. In this context, micro X-ray fluorescence (μXRF) is of high interest due to its high sensitivity and the possibility to analyze hydrated frozen samples, which minimizes artifacts resulting from sample preparation (Sarret et al., 2013). Furthermore, μXRF can be combined with micro X-ray absorption near edge structure spectroscopy (μXANES) to probe the chemical form of metals in the same samples (Salt et al., 2002;Sarret et al., 2013;Isaure et al., 2015).

Inside the plant, Fe is translocated associated with suitable chelating molecules because of high reactivity and poor solubility {Kobayashi, 2012 #1986}. Citrate was identified as the main Fe ligand in xylem sap of tomato plants {Rellan-Alvarez, 2010 #1526}. Besides citrate, some studies have indicated malate and nicotianamine as organic molecules, which form a complex with iron {Takahashi, 2003 #748}{Grillet, 2014 #1705}. Nothing is known about the long-distance Fe transport in Fe hyperaccumulator plants, and therefore the identification, speciation and quantification of Fe transport forms in xylem sap are crucial to understand this long-distance transport. This knowledge is the basis to understand how the metal is transported across membranes and delivered to its final target.

The perennial grasses *Paspalum urvillei* Steudel and *Setaria parviflora*, native species from South America, were identified among the few species able to grow spontaneously at the margins of decantation ponds of an Fe ore pelletizing industry located in Brazil, in the Ubu district (municipality of Anchieta, state of Espìrito Santo, South-Eastern Brazil)(de Araujo et al., 2014). These ponds are supplied with water from the mining system and plumbing of the iron ore pelletizing industry, therefore creating an environment rich in iron particles. *Paspalum urvillei* and *Setaria parviflora* were further described as highly tolerant to Fe excess (de Araujo et al., 2014;Santana et al., 2014) and the formation of IP was observed around the roots (de Araujo et al., 2015).

In this study, by combining Perls/DAB histochemistry, μXRF, μXANES and chromatography coupled to mass spectrometry, we shed some light on the responses of *Paspalum urvillei* and *Setaria parviflora* to excess Fe and uncover new cellular Fe accumulation sites in response to excess.

Materials and Methods

Growth conditions and treatment application

Seeds of Paspalum urvillei Steudel (Poaceae), Setaria parviflora and Setaria viridis were grown in a glasshouse (average temperature 23°C), in three-liter plastic pots containing 0.5 l of quartz sand and 2.25 l of Humin substrate N2 Neuhaus (Klasmann-Deilmann, Bremen, Germany) irrigated with tap water for approximately 10 days. Plantlets with 3 leaves were quickly washed in tap water, rinsed and transferred to 2.4 l boxes containing Hoagland nutrient solution, at full ionic strength, with aeration every 4 hour, at pH 5.0. After that, these plants were cultivated in growth chamber with 14 hour light at 28°C and 10 hours dark at 25°C, at 80% humidity, for one week in solution containing 0.5 mM $NH_4H_2PO_4$, 3 mM KNO_3, 2 mM $Ca(NO_3)_2{\cdot}4H_2O$, 1 mM $MgSO_4{\cdot}7H_2O$, 23.13 μM H_3BO_3, 4.57 μM, $MnCl_2{\cdot}4H_2O$, 0.382 μM $ZnSO_4$ ·$7H_2O$, 0.16 μM, $CuSO_4{\cdot}5H_2O$ and 0.0695 μM MoO_3. Fe-sufficient plants were fed with 0.1 mM Fe(III)-citrate and Fe-excess plants were fed with 7 mM Fe(III)-citrate during 6 days. This solution was renewed every 3 days. Iron citrate stock solutions were prepared by mixing $FeCl_3$ with a 4-fold molar excess of citric acid and by adjusting the pH to 5.4 with KOH. For rice, seeds were germinated in water for 5 days and then transferred in hydroponic medium as described above.

Fe accumulation and localization by histochemical staining

To quantify the Fe concentration, plants were separated in leaves and roots. Roots were washed with dithionite–citrate–bicarbonate to eliminate the Fe aggregated at the root surface (Taylor and Crowder, 1983). Root and leafs samples (10–30 mg dry weight) were mineralized with a SpeedWave Two (Berghof Products, Eningen, Germany) in 1 ml of 48% HNO3 and 7.5% H_2O_2, 3 min at 100°C, 20 min at 180°C, and 10 min at 140°C. Fe concentration was determined by atomic emission spectroscopy with a Microwave Plasma Atomic Emission Spectroscope (MP-AES, Agilent), using manufacturer's standard solutions to establish calibration curves.

In order to determine the Fe location, fragments from different regions of leaf blades (basal, median and apical region) and root (meristematic, elongation and differentiation zone) were vacuum infiltrated with fixation solution containing 2% (w/v) paraformaldehyde, 1% (v/v) glutaraldehyde, 1% (w/v) caffeine in 100 mM phosphate buffer (pH 7) for 30 min and incubated for 24 h in the same solution. The fixated fragments were washed with 0.1 M phosphate buffer (pH 7.4) three times, and dehydrated in successive baths of 50%, 70%, 90%, 95%, and 100% ethanol, butanol/ethanol 1:1 (v/v), and 100% butanol. Then, the fragments were embedded in the Technovit 7100 resin (Kulzer) according to the manufacturer's instructions and thin sections (5 µm thickness) were made. Histochemical Fe staining was realized by the Perls-DAB method to highlight total iron including both ferric and ferrous species {Roschzttardtz, 2009 #1502}.

Fe staining images were captured using an Olympus BX-61 microscope (Olympus, Tokyo, Japan) equipped with Jenoptik ProgRes C5 digital camera (Jenoptik, Jena, Germany) in the PHIV (Histology and plant Cell imaging platform) imaging platform.

Elemental distribution by µXRF and Fe speciation by Fe K-edge µXANES

Fresh fragments from roots were immersed in a cryo-embedding Optimum Cutting Temperature compound (OCT, Sakura Finetek, Leiden, The Netherlands) and rapidly frozen in liquid nitrogen. They were kept at –80 °C until preparation of cryo-sections. The frozen blocks were then sectioned (25 µm thickness) in the transversal plane using a cryomicrotome just before measurements. The resulting cross-sections were deposited on Ultralene films (Spex Certiprep) and kept in liquid nitrogen until measurements.

Micro-XRF and µXANES measurements were performed on LUCIA beamline at the SOLEIL synchrotron (Saclay, France, (Vantelon et al., 2016)). The X-ray beam was monochromatized with a Si(111) double-crystal monochromator, and focused using Kirkpatrick-Baez mirrors to a spot on the sample of 3 µm x 3 µm. Measurements were carried under vacuum and at -12°C with a N2 liquid cryostat to limit beam damage and minimize metal redistribution and speciation change.

For elemental mapping, µXRF was performed on iron plaques from root sections with an incident energy of 7300 eV, a step size of 3 µm and a dwell time of 1s/pixel. Elemental fluorescence signal was recorded using a four-element silicon drift diode (SDD) detector. The fluorescence signal was then deconvoluted from fluorescence background and elemental overlapping to obtain elemental maps. Then, Fe species were studied using Fe K-edge XANES on regions of interest selected from µXRF mapping, using the same lateral resolution and in fluorescence mode. Spectra were collected in the 7050-7250 eV range, with a sampling step of 2 eV between 7050 and 7100 eV, 0.2 eV from 7100.2 to 7160 eV, and 1 eV between 7161 and 7250 eV. Three or four XANES spectra were acquired on various positions distinct from a few microns, checked for similarity, and averaged to improve the signal-to-noise ratio. Data were calibrated with metallic Fe background subtracted and normalized using a linear or two-degree polynomial function with Athena software (Ravel and Newville, 2005). Fe XANES spectra were also collected on Fe(II) and Fe(III) reference compounds prepared as pressed pellets: hematite Fe_2O_3, ferrihydrite $5Fe_2O_3.9H_2O$, goethite (FeOOH), Fe(III)phosphate $Fe_3(PO_4).2H_2O$, chromite ($FeCr_2O_4$) and siderite ($FeCO_3$). Iron plaques spectra were compared to these reference spectra and to spectra that we have previously collected (Grillet et al., 2014). A fingerprint approach was then used to fit IP spectra with Fe reference compounds. The quality of the fits was evaluated by the normalized sum-squares residuals NSS (NSS= $\Sigma[\mu_{experimental} - \mu_{fit}]^2 / \Sigma[\mu_{exp}]^2 \times 100$) in the 7090-7225 eV range. The pre-edge structures were also

examined by substracting the pre-edge background modeled by an erf function taken a few eV before and after the pre-edge.

Analysis of metal complexes using HILIC-ICP-MS

Analytical reagent grade chemicals such as acetonitrile, acetic acid, formic acid, nitric acid and ammonia were purchased from Sigma-Aldrich. Ultrapure water (18MΩ.cm) was obtained from a Milli-Q system (Millipore, Guyancourt, France). The isotopically enriched 58Fe (99.81% enrichment) was purchased from STB Isotope Germany GmbH (Hamburg, Germany).

HILIC HPLC separations were performed using a 1200 HPLC system (Agilent, Tokyo, Japan).ICP-MS detection was achieved using a model 7700 instrument (Agilent) fitted with platinum cones, 1 mm i.d. injector torch. 7.5% of oxygen was added to plasma gas to avoid carbon deposit on the cones. The HILIC ICP MS coupling was done via Scott spray chamber cooled to -5°C.

The column used for HILIC separation was a SeQuant®Zic®-cHILIC (150 x 2.1 mm, 3µm 100Å) column (Merck). Gradient elution, at a flow rate of 0.2mL min-1, was carried out using eluent A, acetonitrile, and eluent B, 25mM ammonium acetate (pH 5.5). The gradient program was: 0–1min 5% B, 1-10 min up to 20% B, 10-13.5 min 20% B, 13.5-17 min up to 40% B, 17-21 min 40% B, 21-21.01 min down to 5% B, 21.01-30 min 5% B. Samples were prepared according to protocol described in details elsewhere (AlChoubassi, Kinska). Shortly, samples were diluted with ammonium acetate, divided in aliquots of 10µL to which standard of 58Fe was added in order to create calibration curve. Later on acetonitrile was added to obtain a 1:2, sample to acetonitrile ratio, vortexed and centrifuged. A 2 µL aliquot of the supernatant was injected into the HILIC column each time.

Analysis for metal complexes using HILIC-ESI-MS

For HILIC-ESI-MS the HPLC system Ultimate 3000 UPLC pump (Dionex, Paris, France) was connected to an LTQ Orbitrap Velos mass spectrometer (Thermo Fisher Scientific, Bremen, Germany). The coupling was achieved via a heated electrospray ionization source (H-ESI II) (Thermo Fisher Scientific). The chromatographic separation conditions were as given in the previous paragraph. The ion source was operated in the positive at 3.0 kV. The vaporizer temperature of the source was set to 250°C and the capillary temperature to 350°C. In full MS mode, the resolution was set at 100 000 (FWHM at m/z 400).

Statistical analysis

The experimental design adopted was randomized with four repetitions and five or two treatments. Data were subjected to analysis of variance (ANOVA), and means were compared by Tukey test at 5 % probability, using statistical software SAEG 9.0 UFV.

Results

Analysis of Fe tolerance and accumulation

Paspalum urvillei and *Setaria parviflora* have been described as being tolerant to Fe excess (de Araujo et al., 2014). To further confirm the Fe tolerant behavior of these two species, we compared the tolerance to high concentrations of Fe-citrate of *Paspalum urvillei* and *Setaria parviflora* young plants with, respectively, rice *(Oryza sativa* cv nipponbare*)* and *Setaria viridis,* two model species used here as reference. The visual symptoms of standard and excess Fe on *Setaria parviflora* and *Setaria viridis* are illustrated in Fig. 1. Exposure to high Fe provoked the formation of brow necrotic spots in *S. viridis* leaves, whereas leaves from *S. parviflora* did not show any visible sign of toxicity. Similar symptoms were observed when comparing *Paspalum urvillei* and *Oryza sativa* (data not shown). Roots of *S. parviflora* displayed an intense brown coloration in Fe excess corresponding to the formation of the iron plaque and this phenomenon was almost absent in *S. viridis* (Fig. 1)

Figure 1: Visual symptoms of Fe toxicity on *Setaria parviflora* and *Setaria viridis* plants. Ten day-old seedlings were grown for 6 days in medium supplemented with 0.1 mM or 7 mM Fe-citrate. Bar = 1cm.

The shoot biomass of *P. urvillei* and *S. parviflora* plants was not significantly affected by an exposure to 7 mM Fe, compared to control media, whereas Fe excess provoked a two-fold reduction in biomass for *O. sativa* and *S. viridis* (Fig. 2A). This result further confirmed the Fe tolerance capacity of *P. urvillei* and *S. parviflora*. In roots, Fe excess induced a reduction of growth that was equivalent for *P. urvillei* and *O. sativa*, whereas the root biomass of both *Setaria* species was not significantly affected by the Fe treatments (Fig. 2B).

Having established that *P. urvillei* and *S. parviflora* are well-suited species to study responses to Fe excess, we then measured the Fe content in roots and shoots of plants grown on the two Fe regimes. In control condition (0.1 mM Fe-citrate) no significant difference in Fe concentration was observed in leaves of the four species (Fig. 1C). Iron excess had a moderate effect on the shoot Fe concentration of *P.* urvillei and *S. parviflora* with a 3 to 4 fold increase in Fe accumulation whereas *O. sativa* and *S. viridis* shoots accumulated massive amounts of Fe, representing ca 50-fold increase, relative to standard Fe treatment (Fig. 2C). The exposure to Fe excess induced a limited increase in Fe accumulation in roots of *P. urvillei*, *S. parviflora* and *S. viridis* whereas roots of *O. sativa* overaccumulated Fe, reaching up to 9000 ppm in response to Fe excess (Fig. 2D). From these results, we concluded that both *P.urvillei* and *S. parviflora* plants were able to tolerate high concentrations of Fe in the medium with a very moderate effect in growth that could be attributed to their capacity to restrict Fe accumulation in their organs, when compared to the less tolerant species *O. sativa* and *S. viridis*.

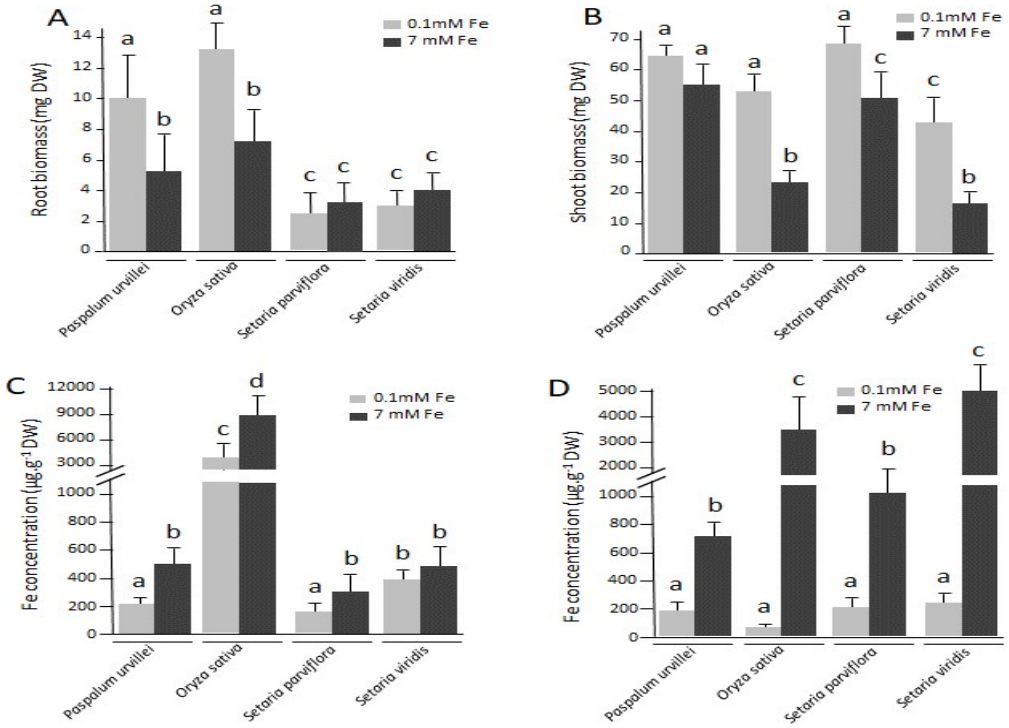

Figure 2: Biomass and Fe concentration of roots and shoots of *Paspalum urvillei*, *Oryza sativa*, *Setaria parviflora* and *Setaria viridis* plants grown in standard and excess Fe. 10 day-old seedlings were grown for 6 days in medium supplemented with 0.1 mM or 7 mM Fe-citrate. (A) root biomass, (B) shoot biomass, (C) Fe concentration on roots, (D) Fe concentration in shoots. Values are average ± SD, values followed by the same letter do not differ by Tukey's test at 5% probability.

To gain further insights in the tolerance mechanisms set up by P. urvillei and S. parviflora, we studied Fe localization in roots and shoots in control and excess conditions. In standard condition, for all species, Fe was only visible as aggregates around the roots, corresponding to the iron plaque (IP) (Fig. 3). Upon exposure to 7 mM Fe-citrate, roots of the four species displayed different behavior. Paspalum urvillei and Setaria parviflora roots had built up a significant iron plaque, compared to O. sativa and S. viridis (Fig 3, middle row). Within the root tissues of P. urvillei and S. parviflora, Fe deposits completely filled the entire volume of all cortex cells. Additionally, a strong staining was visible around the epidermal and cortical cells and this staining was attributed to the cell walls. The strong difference in Fe accumulation between epidermal-cortical cells and the central cylinder indicated that the endodermis was playing a central role in the control of Fe loading into the vascular system. To a lesser extent, rice roots also accumulated high concentrations of Fe inside cells. Strikingly, the iron staining in the central cylinder was as intense as in the cortex, suggesting that, contrarily to P. urvillei and S. parviflora, the endodermis was not such a barrier for the movement of Fe towards the conductive elements of the stele. Finally, root cells of S. viridis did not accumulate Fe in the vacuoles as the other species, instead, Fe-rich dot-shaped deposits were visible within cells. These Fe-rich structures were identical to Fe-ferritin complexes previously described in both roots and leaves of Arabidopsis thaliana plants treated with iron excess {Bournier, 2013 #2033}{Roschzttardtz, 2009 #1502}.

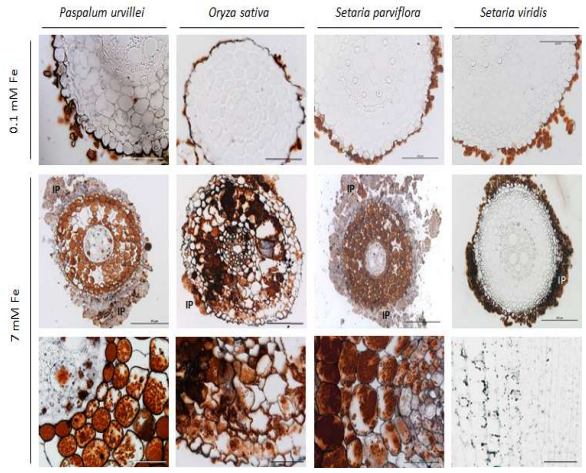

Figure 3: Fe localization in root sections of *P. urvillei, O. sativa, S. parviflora and S. viridis*. Plants were treated with 0.1 mM or 7 mM Fe-Citrate during 6 days and root samples were further fixed and embedded in resin. Sections were submitted to Perls Dab staining. IP, Iron plaque. Bar = 200 □m unless stated otherwise.

Metals distribution and speciation analyses in the iron plaque by µXRF and Fe K-edge µXANES

Micro-XRF and Fe K-edge µXANES were carried out in IP and roots of *P. urvillei* to map the distribution of Fe and other elements and determine the Fe chemical species, respectively.

Elemental maps of roots exposed to 0.1 mM Fe-citrate showed that Fe was distributed as a thin layer deposited at the surface of epidermal cells. After saturating the Fe signal to pinpoint potential lower Fe concentrations, maps showed that the metal was strictly localized in the epidermis as a thick layer but neither in cortex nor endodermis (Fig. 4A "Fe sat"). In addition to Fe, phosphorus, calcium, silicon and manganese were visualized near the epidermis as observed on the bicolor and tricolor maps (Fig. 4A). In contrast, potassium and sulfur were located within the epidermis, cortex, and vascular system but were not highly concentrated in IP.

In roots exposed to Fe excess, the layer of IP was thicker (25 µm at 7 mM Fe versus 10 µm at 0.1 mM Fe) and contained a higher amount of Fe as attested by the change in Fe scale (Fig. 4B). Interestingly, in

signal saturation conditions, we observed that Fe was strictly located in IP for the low exposure while Fe entered the root and cortex cells, and was finally retained in endodermis for the excess condition (Fig. 4B "Fe sat"). These results are in agreement with the histochemical staining showed above (Fig. 3). The amount of Ca also increased in IP while other elements remained unchanged. Co-localization of Fe with phosphorus, calcium, silicon and sulfur, indicated the presence of these elements in IP (Fig. 4).

Some biological preparations, particularly using chemical fixation and resin, can alter cellular materials and the location of key associated elements. Synchrotron µX-ray fluorescence requires no sample pretreatment, and allows non-invasive examination of Fe localization. Interestingly, Fe was visualized in tissues outside the endodermis with both Perls-DAB staining and µXRF. The endodermis cells are wrapped into a layer of suberin and sometimes lignin called the Casparian strip. This chemically modified wall controls the permeability of water and ions towards the central cylinder. In P. urvillei the casparian strip seems to act as an efficient barrier to Fe since Fe depositions were almost inexistent in the central cylinder (Fig. 4B) and the major part of Fe was found in IP.

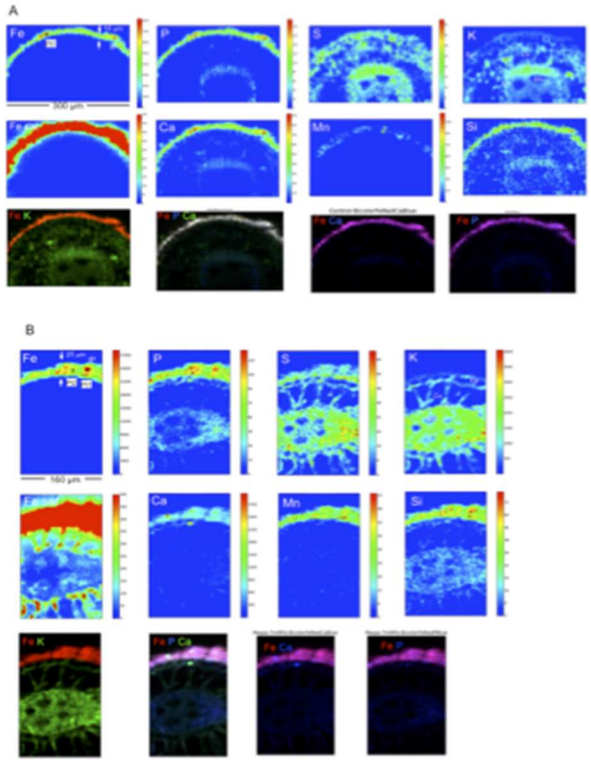

Figure 4: Elemental distribution (µXRF) on *Paspalum urvillei* roots. **A, B:** Cryo cross-sections of plants treated with 0.1 mM (A) and 7 mM Fe-Citrate (B) respectively, during 6 days and elemental distribution of iron, phosphorus, sulfur, potassium, iron saturation, calcium, manganese, and silicon. Tricolor and bicolor maps were also shown to highlight co-location. Energy = 7.3 keV, step size = 3 µm, counting rate = 1s/pixel. The crosses annotated "Pt" indicate the areas where µXANES spectra were collected in these maps.

Fe K-edge µXANES spectra were collected from µXRF maps on a number of small areas of IP containing various amounts of Fe, some of which are indicated in the map shown in Figure 4B. Those spectra were compared to Fe reference spectra (Fig. 5). IP spectra exhibited a lower K-edge in comparison to Fe(III) compounds, albeit higher than Fe(II) compounds, indicating that Fe in IP is present as a mix of oxidized and reduced forms. Examination of the pre-edge structure confirmed that both oxidation states were present in IP (Fig. 6) and the pre-edge of the control spectrum (0.1 mM Fe) was slightly shifted to lower energy values than the 7 mM Fe exposed samples, suggesting that the proportion of Fe(II) was higher for low exposure. The fingerprint approach using linear combination fitting showed that in IP formed in roots exposed to7 mM Fe, spectra were modeled by a mixture of ferrihydrite and Fe(II)-citrate ranging from 66 ± 10 to 81 ± 10 % ferrihydrite and 19 ± 10 to 38 ± 10 % Fe(II)-citrate (Fig. 7). Here Fe(II)-citrate was used as a proxy for a non crystallized form of Fe(II) since the crystallized forms siderite and chromite gave poor spectral agreement due to their well defined structure patterns. We can thus infer that Fe partially occurs as a Fe(II) form, organic or poorly crystallized in IP, in addition to ferrihydrite. In the control Fe condition, as suggested by the examination of the pre-edge, the proportion of ferrihydrite decreased (46 ± 10 %) while Fe(II) increased (51 ± 10 %).

Iron oxyhydroxides have high specific surface areas and possess -OH functional groups, which are capable of reacting with metals and other cations and anions (Kuo, 1986) It is likely that the crystalline Fe hydroxides (ferrihydrite) identified around the roots of *P. urvillei* have similar properties and immobilize and prevent the uptake of other elements. The co-localization of Fe and phosphorus on IP indicated that the plaque was probably composed of iron oxide with phosphorus adsorbed onto the surface. Phosphorus is an element easily found on the IP, since phosphate

has a high affinity to ferric hydroxides (e.g. ferrihydrite) (Voegelin et al., 2013;Senn et al., 2015). The sodium dithionite (Na2S2O4)-sodium citrate ($Na_3C_6O_7H_5$)-sodium bicarbonate ($NaHCO_3$) (DCB) mixture solution is a classical extraction reagent for IP on root surface (Lee et al., 2013). Previous results with *P. urvillei* using the extraction with DCB technique showed the presence of Fe, zinc, phosphate, and calcium in the IP (de Araujo et al., 2014). Micro-XRF mapping confirmed the occurrence of Ca and P and also revealed the presence of Mn and Si (Zn was not measured since the mapping energy was below the Zn K-absorption edge).

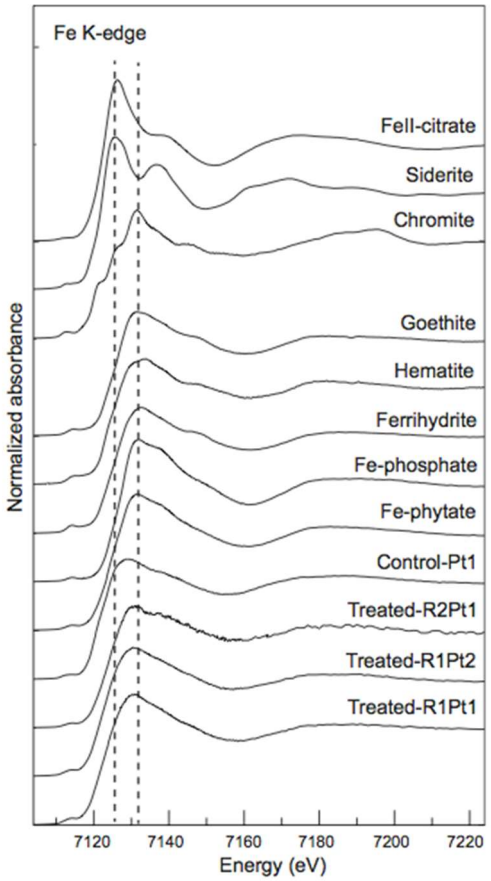

Figure 5: Fe K-edge µXANES spectra collected on iron plaque of *Paspalum urvillei* treated with 0.1 mM (Control) and 7mM (Treated) Fe-citrate compared to Fe reference spectra. Dotted lines indicate the shift between Fe(II)reference spectra and Fe(III) reference spectra.

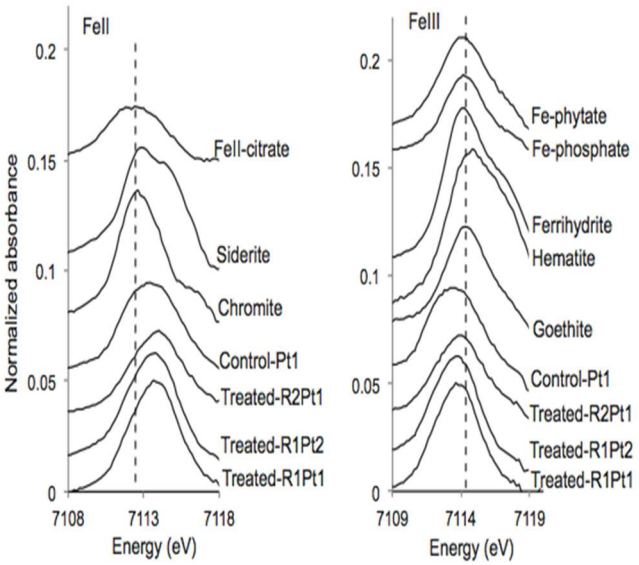

Figure 6 : Normalized pre-edge spectra (Fe K-edge) of *Paspalum urvillei* treated with 0.1 mM (Control) and 7mM (Treated) Fe-citrate compared to Fe(II) reference spectra (Left) and Fe(III) reference spectra (Right).

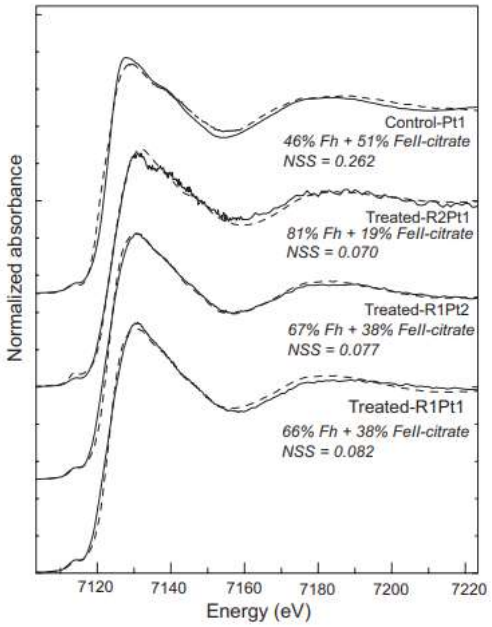

Figure 7: Linear combination fits of Fe K-edge µXANES spectra for *Paspalum urvillei* treated with 0.1 mM (Control) and 7mM (Treated) Fe-citrate. The quality of the fit is evaluated by the normalized sum-squares residuals, $NSS=\Sigma i(Xanes_{experimental}-Xanes_{fit})2 / \Sigma i(Xanes_{experimental})^2 \times 100$.

In leaves of control plants, Fe was hardly visible in tissues and cells, for all species (Fig. 8). Leaves of plants treated with Fe excess displayed high Fe accumulation, localized in different cellular compartments. The highest Fe accumulation, common to all species, corresponded the bundle

sheath cells (Fig. 8, arrows). Within these cells, Fe highly accumulated in the central vacuole. Additionally, the C4 species (*P. urvillei*, *S. parviflora* and *S. viridis*) displayed an intense Fe staining in the chloroplasts of the bundle sheath cells, contrary to rice that is a C3 species. Additionally, the Perls/DAB staining could reveal secondary sites of Fe accumulation in mesophyll cells. The chloroplasts of *P. urvillei* and *O. sativa* were strongly stained and contained Fe-rich dots (Fig. 8 arrowheads) that had been previously demonstrated to correspond to ferritin complexes (Roschzttardtz et al., 2013). In both *Setaria* species, Fe was much less visible in mesophyll cells, compared to *P. urvillei* and rice and most of the signal was located in bundle sheath cells. The Fe accumulation in these cells was nevertheless much more pronounced in *Setaria viridis*, compared to *S. parviflora*, in good agreement with the strong difference in total Fe accumulation between these two species (Fig. 2). Taken together, these results highlight the role of the bundle sheath cells in the sequestration of Fe in leaves, in response to elevated concentrations of Fe in the growth medium. Within these cells, Fe accumulated in the central vacuole for all species but also in chloroplasts for the C4 species *P. urvillei*, *S. parviflora* and *S. viridis*. The visualization of iron bound to ferritins, the expected main actor in Fe detoxification, could not be strictly correlated with the overall Fe accumulation in leaves of the four species as shown in Fig. 2, since Fe-ferritin structures were mostly visible in *P. urvillei* (low Fe) and rice (high Fe).

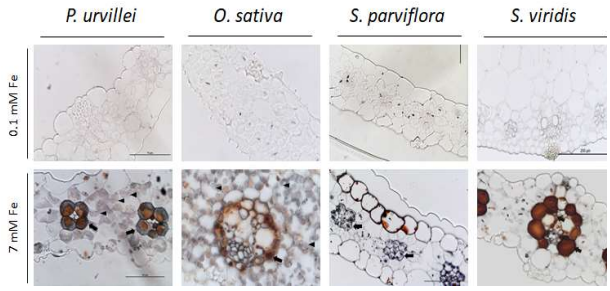

Figure 8: Fe localization in leaves of *P. urvillei, O. sativa, S. parviflora* and *S. viridis*. Plants were treated with 0.1 mM (A) or 7 mM Fe-Citrate (B-E) during 6 days and shoot samples were further fixed and embedded in resin. Sections were submitted to Perls DAB staining.

Iron speciation in the xylem sap of Setaria parviflora plants

Among the four species considered, on *Setaria parviflora* could yield sufficient amounts of xylem sap to analyze the Fe speciation. The quantification of total Fe in the xylem sap showed that high Fe concentrations in the medium tended to increase the concentration of Fe in the xylem sap (33.15ppm vs 12.6ppm) although the high variability of Fe concentration in Fe excess samples prevented to conclude statistically on such effect. Nevertheless, the speciation of Fe in the xylem sap of *Setaria parviflora* plants was analysed by means of hydrophilic interaction chromatography (HILIC) with dual detection: inductively coupled plasma mass spectrometry (ICP-MS) and electrospray ionization–Fourier-transform mass spectrometry (ESI-FTMS). The chromatographic conditions were optimized in order to ensure the best separation of the compounds, maximum recovery from the column and optimal ionisation conditions for electrospray ionisation. Additionally, the use of this separation technique requires very limited sample preparation, which helps with preservation of Fe complexes that are extremely prone to dissociation.

The analysis of samples grown in the control condition showed presence of one peak (Fig. 9a) while in the sample grown in Fe excess condition, 2 additional peaks were detected (Fig. 9b) by ICP MS. The ESI MS spectra were searched for the specific isotopic pattern (exact inter-isotopic mass differences and isotopic ratios) at the retention times corresponding to the peaks detected by HPLC ICP MS. The use of the accurate masses of the precursor ions allowed assignment of the empiric molecular formulas to compounds identified as the one containing iron, and their fragmentation led to determination of the structures for all the iron species detected. They were identified as Fe_3Cit_3 for control sample, $Fe_3Cit_2Mal_2$, and $Fe_3Cit_3Mal_1$ in case of supplemented sample.

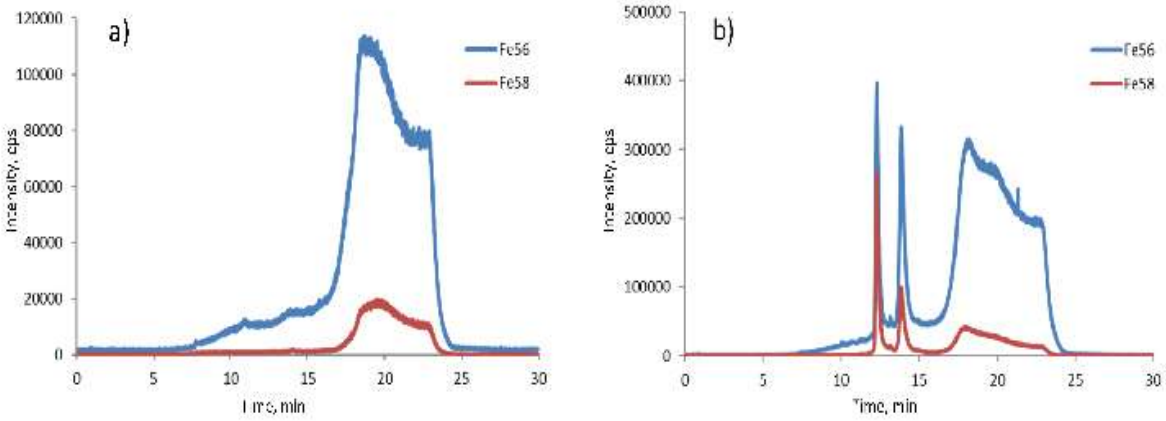

Figure 9: HILIC ICP MS chromatogram of control (A) and supplemented (B) *S. parviflora* xylem sap samples spiked with ^{58}Fe (column: Phenomenex Kinetex; gradient: 0-1 min 95% B ; 1-10 min 85% ; 10-15 min 85% B; 15-17 min 65% B; 17-25 min 65% B;25-30 min 95% B, B - ACN and A - 25mM ammonium acetate in H_2O, pH 5.5; injection: 10 µl; flow rate: 0.5 ml/min.

The determination of the concentration of ^{56}FeMalCit complexes in plant samples was performed by adding different amount of solution of ^{58}Fe in water to the plant sample. The presence of free ligands (malate and citrate) in samples allowed forming the appropriate ^{58}FeMalCit and ^{58}FeCit complexes, what was confirmed by ICP MS (Fig. 10) and ESI MS (Fig. 11).

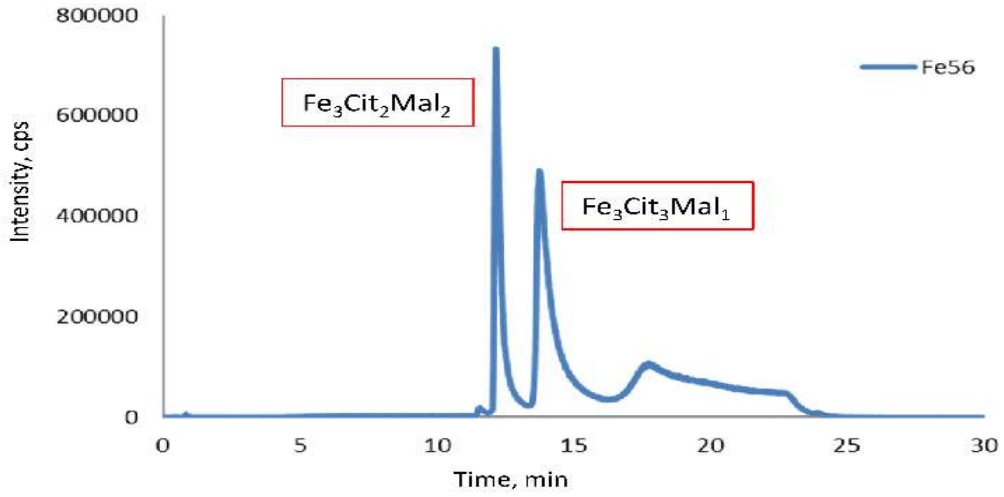

Figure 10: HILIC - ICP MS chromatogram of the standard citrate-malate iron complexes (chromatographic conditions the same as in Fig. 9).

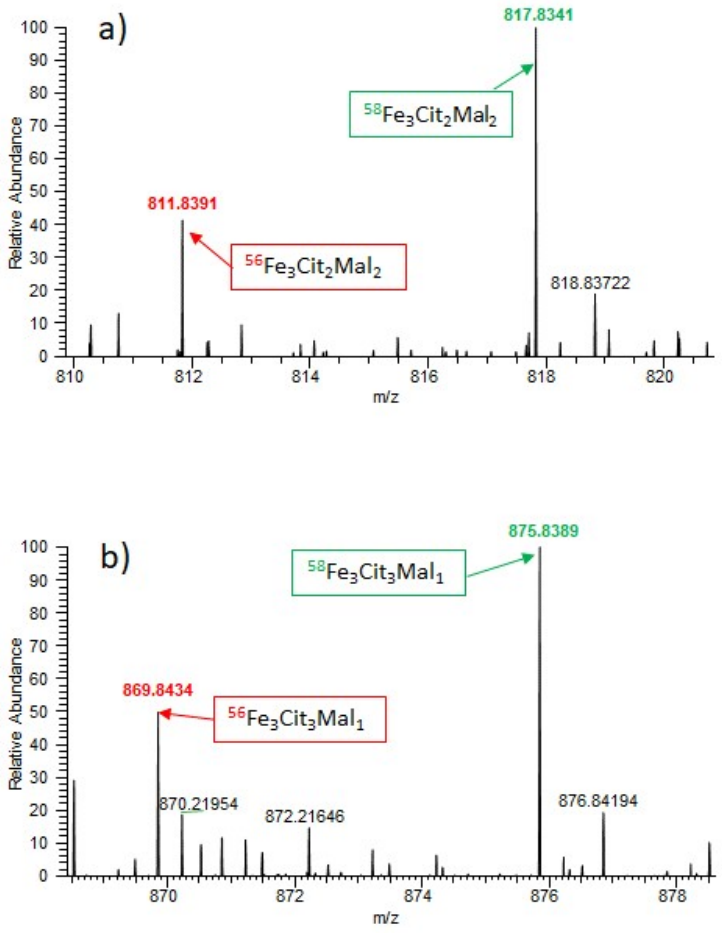

Figure 11: ESI MS spectra taken at the peak apexes at RT 12.23 min (A) and at RT 14.21 min (B) showing isotopic patterns of $Fe_3Cit_2Mal_2$ and Fe_3Cit_3Mal species respectively; mono-isotopic mass in red, mass corresponding to added isotope ^{58}Fe marked in green.

Discussion

The aim of our work was to investigate the mechanisms of Fe sequestration in plants growing in excess concentrations, using plant species naturally adapted to such conditions. Therefore, our strategy was first to verify that, in laboratory conditions, *Paspalum urvillei* and *Setaria parviflora* were also tolerant to very high Fe concentrations in the medium, by comparing them to either a model grass (rice) or a related species of the same gender (*S. viridis*), respectively. Thereafter, we have characterized the responses of young plants to short-term exposure to high Fe in the medium. Although different from the natural environment, our experimental conditions have enabled us to monitor changes in Fe distribution in both roots and shoots, to establish that P. urvillei and S. parviflora were behaving as excluders in condition of Fe excess and to identify the major sites of Fe accumulation at the tissue, cellular and subcellular levels.

In previous reports, *P. urvillei* and *S. parviflora* plants treated with high Fe-EDTA concentrations displayed higher Fe content in roots than in shoots and presented symptoms of Fe toxicity (de Araujo et al., 2014; Santana et al., 2014). In this paper, the four plant species were treated with citrate, which is another Fe chelator, with different responses. In addition to high Fe translocation rates towards shoots, *P. urvillei* and *S. parviflora* did not show any visual symptoms of toxicity by iron excess, compared to rice and *S. viridis*. Actually, it had been previously shown that depending on the culture system and the Fe source, the amount and distribution of apoplastic Fe pool was prone to be overestimated, in particular when using Fe-EDTA In this paper, the four plant species were treated with citrate, which is another Fe chelator, with different responses. In addition to high Fe translocation rates towards shoots, *P. urvillei* and

S. parviflora did not show any visual symptoms of toxicity by iron excess, compared to rice and *S. viridis*. Actually, it had been previously shown that depending on the culture system and the Fe source, the amount and distribution of apoplastic Fe pool was prone to be overestimated, in particular when using Fe-EDTA (Strasser et al., 1999; Roschzttardtz et al., 2013). The higher toxicity provoked by EDTA-based Fe complexes is most likely due to the high affinity of EDTA towards other metals present in the growth medium (logK=16.5 for Zn and logK=18.8 for Cu), with the potential risk of spontaneous formation of the corresponding Zn-EDTA and Cu-EDTA complexes, potentially leading to a "polymetallic" stress. On the contrary, citric acid is rather specific for trivalent metal ions and displays a very poor affinity for divalent metal ions compared to Fe^{3+} (logK=4.5 for Zn and 6.1 for Cu, compared to 11.85 for Fe^{3+}), which decreases the risk of polymetallic excess stress (http://www.coldcure.com/html/stability_constants.html). Therefore, the data obtained here suggested that the use of Fe-citrate as the source of iron might be a better proxy of the Fe-contaminated soil conditions encountered by *Paspalum urvillei* and *Setaria parviflora*.

The ability of *Paspalum urvillei* and *Setaria parviflora* plants to tolerate high Fe concentrations in the medium is likely to rely on several mechanisms aimed at decreasing the toxicity of this metal, by limiting the uptake at the root surface through the build-up of the iron plaque, limiting the translocation of Fe towards the shoots and by sequestering Fe in the apoplastic compartment, vacuoles, and in plastids as ferritin complexes, away from highly sensitive intracellular sites. Here we evidenced that the IP thickness increased with Fe supply, suggesting that the build-up of IP *via* the precipitation of ferrihydrite was a mechanism of Fe avoidance. Ferrihydrite is an iron mineral phase commonly identified in IP (Hansel et al., 2001; Hansel et al., 2002; Liu et al., 2006). The studies of metal speciation in the IP have revealed that actually the composition of the Fe plaque is rather heterogeneous, consisting of a mix of several minerals, including goethithe, ferrihydrite, lepidocrocite and siderite, the proportion of each mineral being tightly linked to the local environment of the roots (Snowden and Wheeler, 1995). The origin of the Fe(II) is more questioning since hydroponic cultures were done in oxic conditions where Fe was provided as ferric iron and the nature of this reduced iron could not be clearly identified. Siderite, which was suspected and identified elsewhere and likely formed by CO_2 released by the roots (Wang and Peverly, 1996; 1999; Hansel et al., 2002) was not detected here. In contrast, the Fe phase appeared to be poorly crystallized or organic. Since *P. urvillei* belongs to the grass family, Fe uptake should be achieved via Fe(III)-phytosiderophore and not by iron reduction. It is not excluded here that the root itself is able to reduce part of iron as already proposed by Wang et al (1999) (Wang and Peverly, 1999). Associated microorganisms including ferric reducing bacteria could also be involved in the Fe redox reaction at the root surface (King and Garey, 1999; Chang et al., 2014; Tian et al., 2015). The Fe(II) proportion was higher in control than in Fe excess conditions, suggesting that Fe reduction was not related to the amount of Fe in solution but rather to a limited biological process.

Since the pioneering work of Bienfait et al (Bienfait et al., 1985) on the biochemical characterization of the cell wall binding capacity towards Fe, this compartment has received little attention in the context of Fe homeostasis. Only recently, several reports have uncovered dynamic responses of cell wall components in response to Fe deficiency, including decrease in hemicellulose concentration and methylation to lower the retention of apoplastic Fe and promote its remobilization (Lei et al., 2014; Ye et al., 2015; Curie and Mari, 2017). Nevertheless, the role of the cell wall as a buffering compartment in conditions of Fe overload has been much less characterized. Here, thanks to the Perls/DAB staining procedure, it has been possible to highlight the role of the cell wall as a buffer for Fe excess in the root epidermal and cortical cells (Fig. 2). Although the chemical form of this apoplastic Fe pool remains unknown, in the Fe hyperaccumulator plant species *Imperata cylindrica*, cell wall Fe deposits were shown to correspond to jarosite, an iron and sulfur-rich mineral(Rodriguez et al., 2005;Amils et al., 2007). Although it is tempting to propose that, as for *I. cylindrica*, in cell walls of *Paspalum urvillei* and *Setaria parviflora* Fe is biomineralized as jarosite, this is very unlikely since jarosite crystals are formed only in sulfur-rich and highly acidic conditions, which was not the case for *P. urvillei or S. parviflora*. The chemical identity of this Fe pool remains thus unknown but this finding also raises the question of the specific properties and modifications of the root apoplastic compartment of this particular Fe tolerant species, as a response to Fe overload, by comparison

with the biochemical responses of the cell wall components in Fe deficiency.

Ferritin expression can be considered as the hallmark of molecular responses to Fe excess (Briat et al., 1995a; Briat et al., 1995b; Briat et al., 2010a). (Briat et al., 1995a; Briat et al., 1995b; Briat et al., 2010a). Ferritins accumulate in plastids in response to Fe excess, where they assemble in 24-mer structures that can bind up to 4500 Fe atoms. However, despite the high Fe-buffering capacity of ferritins, the exact role of these proteins in iron detoxification mechanisms remains elusive since ferritin-null mutants in the model plant *Arabidopsis thaliana* are only slightly affected by Fe excess(Ravet et al., 2008). In a previous report, we had shown that iron-ferritin complexes could be efficiently visualized by histochemical staining with the Perls/DAB procedure, as individual dots in plastids (Ravet et al., 2008; Roschzttardtz et al., 2013). Here, beside the bundle sheath cells where Fe highly accumulated in vacuoles, iron-ferritin structures could readily be detected in mesophyll cells, where they could represent an important part of Fe-rich detectable compounds accumulated (Fig. 8). Therefore, in photosynthetic tissues, ferritins seem to play an important role in buffering the excess of Fe that had been translocated from roots to leaves. However, on the basis of the intensity of the Fe staining in chloroplasts, it was not possible to correlate the total amount of Fe in shoots (Fig. 2) with the imaging of Fe (Fig. 8). It is thus difficult to use this information directly as a proxy of Fe accumulation and detoxification capacity in leaves.

In roots and bundle sheath cells of *Paspalum urvillei*, iron was massively accumulated in vacuoles. Although vacuolar storage appears as an obvious way to sequester Fe, only in few instances this mechanism has been clearly described. To date, the best example is represented by the Arabidopsis embryo, where Fe was shown to accumulate in vacuoles of a specific cell layer, the endodermis, in globoids that are phytate-rich structures(Lanquar et al., 2005;Kim et al., 2006;Ravet et al., 2008;Roschzttardtz et al., 2009). The transport of Fe in these vacuoles is mediated by the tonoplastic iron transporter VIT1 (Kim et al., 2006; Ravet et al., 2008), whereas the efflux from vacuoles that occurs during germination to remobilize the Fe atoms is catalyzed by NRAMP3 and NRAMP4 (Lanquar et al., 2005). It is therefore tempting to propose that in *P. urvillei*, VIT1 orthologs might be overexpressed in response to Fe excess, to mediate vacuolar sequestration of Fe through transport across the tonoplast. Although the chemical form of Fe that is stored in vacuoles remains uncharacterized, the granular aspect of Perls/DAB-stained Fe in *P. urvillei, O. sativa* and *S. parviflora* vacuoles was quite comparable to the vacuolar Fe oxides observed by electron microscopy in the Fe hyperaccumulator Imperata cylindrical (Raymond et al., 2003; Fuente et al., 2016) and in maize seedlings exposed to Fe2O3 nanoparticles (Li et al., 2016). Taken together, these elements of comparison tend to suggest that upon Fe overload, the strategy developed by those species would be to accumulate most of the Fe in vacuoles as ferric iron oxides.

Conclusion

We have shown that *Paspalum urvillei* and *Setaria parviflora* can tolerate high Fe concentrations in the medium through selected exclusion (IP) and detoxification (vacuole, cell wall) mechanisms leading to an excluder behavior, when compared with less tolerant species. Iron exclusion is achieved by the buildup of a barrier, the iron plaque, where Fe is immobilized as ferrihydrite. The intracellular detoxification response appears to rely mostly on the sequestration of Fe into cell walls and vacuoles. In leaves, the vacuole would represent the main intracellular site of ferric oxide buildup, strongly suggesting the high importance of vacuolar sequestration in the detoxification of excess Fe in these species.

Acknowledgments

The authors are grateful to CAPES (*Coordination of Improvement of Higher Education Personnel*) for the doctoral scholarship of T.O. Araújo and to CNPq (National Council for Scientific and Technological Development) for providing research scholarship to L.C. Silva (309170/2012-5). We also thank the Soleil Synchrotron (Gif sur Yvette, France) for the provision of beamtime on the LUCIA beamline and the French National Research Agency for the funding (projet ANR-12-BSV2-0020-01, “SUBCELIF”).

References

Amils, R., De La Fuente, V., Rodriguez, N., Zuluaga, J., Menendez, N., and Tornero, J. (2007). Composition, speciation and distribution of iron minerals in Imperata cylindrica. Plant Physiology and Biochemistry 45, 335-340.

Bacha, R.E., and Hossner, L.R. (1977). CHARACTERISTICS OF COATINGS FORMED ON RICE ROOTS AS AFFECTED BY IRON AND MANGANESE ADDITIONS. Soil Science Society of America Journal 41, 931-935.

Balk, J., and Schaedler, T.A. (2014). Iron Cofactor Assembly in Plants. Annual Review of Plant Biology, Vol 65 65, 125-+.

Batty, L.C., Baker, A.J.M., Wheeler, B.D., and Curtis, C.D. (2000). The effect of pH and plaque on the uptake of Cu and Mn in Phragmites australis (Cav.) Trin ex. Steudel. Annals of Botany 86, 647-653.

Bienfait, H.F., Briel, W.V.D., and Mesland-Mul, N.T. (1985). Free space iron pools in roots. Generation and mobilization. Plant Physiology 78, 596-600.

Blute, N.K., Brabander, D.J., Hemond, H.F., Sutton, S.R., Newville, M.G., and Rivers, M.L. (2004). Arsenic sequestration by ferric iron plaque on cattail roots. Environmental Science and Technology 38, 6074-6077.

Briat, J.F., Duc, C., Ravet, K., and Gaymard, F. (2010a). Ferritins and iron storage in plants. Biochimica Et Biophysica Acta-General Subjects 1800, 806-814.

Briat, J.F., Fobis-Loisy, I., Grignon, N., Lobréaux, S., Pascal, N., Savino, G., Thoiron, S., Von Wiren, N., and Van Wuytswinkel, O. (1995a). Cellular and molecular aspects of iron metabolism in plants. Biol. Cell 84, 69-81.

Briat, J.F., Labouré, A.M., Laulhère, A.P., A.M., L., Lobréaux, S., Pesay, H., Proudhon, D., and Wuitswinkel, O. (1995b). Molecular and cellular biology of plant ferritins. Iron Nutrition in Soils and Plants (J.Abadia, ed.), 265-276.

Briat, J.F., Ravet, K., Arnaud, N., Duc, C., Boucherez, J., Touraine, B., Cellier, F., and Gaymard, F. (2010b). New insights into ferritin synthesis and function highlight a link between iron homeostasis and oxidative stress in plants. Annals of Botany 105, 811-822.

Chang, H.S., Buettner, S.W., Seaman, J.C., Jaffé, P.R., Koster Van Groos, P.G., Li, D., Peacock, A.D., Scheckel, K.G., and Kaplan, D.I. (2014). Uranium immobilization in an iron-rich rhizosphere of a native wetland plant from the Savannah River site under reducing conditions. Environmental Science and Technology 48, 9270-9278.

Chen, C.C., Dixon, J.B., and Turner, F.T. (1980). IRON COATINGS ON RICE ROOTS - MORPHOLOGY AND MODELS OF DEVELOPMENT. Soil Science Society of America Journal 44, 1113-1119.

Curie, C., and Mari, S. (2017). New routes for plant iron mining. New Phytologist 214, 521-525.

De Araujo, T.O., De Freitas-Silva, L., Santana, B.V.N., Kuki, K.N., Pereira, E.G., Azevedo, A.A., and Da Silva, L.C. (2014). Tolerance to iron accumulation and its effects on mineral composition and growth of two grass species. Environmental Science and Pollution Research 21, 2777-2784.

De Araujo, T.O., De Freitas-Silva, L., Santana, B.V.N., Kuki, K.N., Pereira, E.G., Azevedo, A.A., and Da Silva, L.C. (2015). Morphoanatomical responses induced by excess iron in roots of two tolerant grass species. Environmental Science and Pollution Research 22, 2187-2195.

De La Fuente, V., Rufo, L., Rodríguez, N., Franco, A., and Amils, R. (2017). Comparison of iron localization in wild plants and hydroponic cultures of Imperata cylindrica (L.) P. Beauv. Plant and Soil 418, 25-35.

Dinakar, C., Abhaypratap, V., Yearla, S.R., Raghavendra, A.S., and Padmasree, K. (2010). Importance of ROS and antioxidant system during the beneficial interactions of mitochondrial metabolism with photosynthetic carbon assimilation. Planta 231, 461-474.

Feng, H., Zhang, W., Liu, W., Yu, L., Qian, Y., Wang, J., Wang, J.J., Eng, C., Liu, C.J., Jones, K.W., and Tappero, R. (2015). Synchrotron micro-scale study of trace metal transport and distribution in Spartina alterniflora root system in Yangtze River intertidal zone. Environmental Science and Pollution Research 22, 18933-18944.

Fuente, V., Rufo, L., Juarez, B.H., Menendez, N., Garcia-Hernandez, M., Salas-Colera, E., and Espinosa, A. (2016). Formation of biomineral iron oxides compounds in a Fe hyperaccumulator plant: Imperata cylindrica (L.) P. Beauv. Journal of Structural Biology 193, 23-32.

Green, M.S., and Etherington, J.R. (1977). OXIDATION OF FERROUS IRON BY RICE (ORYZA-SATIVA-L) ROOTS - MECHANISM FOR WATERLOGGING TOLERANCE. Journal of Experimental Botany 28, 678-&.

Grillet, L., Ouerdane, L., Flis, P., Hoang, M.T.T., Isaure, M.-P., Lobinski, R., Curie, C., and Mari, S. (2014). Ascorbate efflux as a new strategy for iron reduction and transport in plants. The Journal of biological chemistry 289, 2515-2525.

Hansel, C.M., Fendorf, S., Sutton, S., and Newville, M. (2001). Characterization of Fe plaque and associated metals on the roots of mine-waste impacted aquatic plants. Environmental Science & Technology 35, 3863-3868.

Hansel, C.M., La Force, M.J., Fendorf, S., and Sutton, S. (2002). Spatial and temporal association of As and Fe species on aquatic plant roots. Environmental Science and Technology 36, 1988-1994.

Hu, Z.Y., Zhu, Y.G., Li, M., Zhang, L.G., Cao, Z.H., and Smith, E.A. (2007). Sulfur (S)-induced enhancement of iron plaque formation in the rhizosphere reduces arsenic accumulation in rice (Oryza sativa L.) seedlings. Environmental Pollution 147, 387-393.

Huang, Y.C., Chen, Z., and Liu, W.J. (2012). Influence of iron plaque and cultivars on antimony uptake by and translocation in rice (Oryza sativa L.) seedlings exposed to Sb(III) or Sb(V). Plant and Soil 352, 41-49.

Isaure, M.-P., Huguet, S., Meyer, C.-L., Castillo-Michel, H., Testemale, D., Vantelon, D., Saumitou-Laprade, P., Verbruggen, N., and Sarret, G. (2015). Evidence of various mechanisms of Cd sequestration in the hyperaccumulator Arabidopsis halleri, the non-accumulator Arabidopsis lyrata, and their progenies by combined synchrotron-based techniques. Journal of Experimental Botany 66, 3201-3214.

Kim, S.A., Punshon, T., Lanzirotti, A., Li, L., Alonso, J.M., Ecker, J.R., Kaplan, J., and Guerinot, M.L. (2006). Localization of iron in Arabidopsis seed requires the vacuolar membrane transporter VIT1. Science 314, 1295-1298.

King, G.M., and Garey, M.A. (1999). Ferric iron reduction by bacteria associated with the roots of freshwater and marine macrophytes. Applied and Environmental Microbiology 65, 4393-4398.

Kuo, S. (1986). CONCURRENT SORPTION OF PHOSPHATE AND ZINC, CADMIUM, OR CALCIUM BY A HYDROUS FERRIC-OXIDE. Soil Science Society of America Journal 50, 1412-1419.

Lanquar, V., Lelievre, F., Bolte, S., Hames, C., Alcon, C., Neumann, D., Vansuyt, G., Curie, C., Schroder, A., Kramer, U., Barbier-Brygoo, H., and Thomine, S. (2005). Mobilization of vacuolar iron by AtNRAMP3 and AtNRAMP4 is essential for seed germination on low iron. Embo J 24, 4041-4051.

Le Jean, M., Schikora, A., Mari, S., Briat, J.F., and Curie, C. (2005). A loss-of-function mutation in AtYSL1 reveals its role in iron and nicotianamine seed loading. Plant J 44, 769-782.

Lee, C.H., Hsieh, Y.C., Lin, T.H., and Lee, D.Y. (2013). Iron plaque formation and its effect on arsenic uptake by different genotypes of paddy rice. Plant and Soil 363, 231-241.

Lei, G.J., Zhu, X.F., Wang, Z.W., Dong, F., Dong, N.Y., and Zheng, S.J. (2014). Abscisic acid alleviates iron deficiency by promoting root iron reutilization and transport from root to shoot in Arabidopsis. Plant Cell and Environment 37, 852-863.

Li, J.L., Hu, J., Ma, C.X., Wang, Y.Q., Wu, C., Huang, J., and Xing, B.S. (2016). Uptake, translocation and physiological effects of magnetic iron oxide (gamma-Fe2O3) nanoparticles in corn (Zea mays L.). Chemosphere 159, 326-334.

Liu, J.G., Leng, X.M., Wang, M.X., Zhu, Z.Q., and Dai, Q.H. (2011). Iron plaque formation on roots of different rice cultivars and the relation with lead uptake. Ecotoxicology and Environmental Safety 74, 1304-1309.

Liu, W.J., Zhu, Y.G., Hu, Y., Williams, P.N., Gault, A.G., Meharg, A.A., Charnock, J.M., and Smith, F.A. (2006). Arsenic sequestration in iron plaque, its accumulation and speciation in mature rice plants (Oryza Sativa L.). Environmental Science and Technology 40, 5730-5736.

Lobréaux, S., Massenet, O., and Briat, J.F. (1992). Iron induces ferritin synthesis in maize plantlets. Plant Mol. Biol. 19, 563-575.

Meguro, R., Asano, Y., Odagiri, S., Li, C., Iwatsuki, H., and Shoumura, K. (2005). The presence of ferric and ferrous iron in the nonheme iron store of resident macrophages in different tissues and organs: histochemical demonstrations by the perfusion-Perls and -Turnbull methods in the rat. Arch Histol Cytol 68, 171-183.

Muller, C., Kuki, K.N., Pinheiro, D.T., De Souza, L.R., Silva, A.I.S., Loureiro, M.E., Oliva, M.A., and Almeida, A.M. (2015). Differential physiological responses in rice upon exposure to excess distinct iron forms. Plant and Soil 391, 123-138.

Nozoye, T., Nagasaka, S., Kobayashi, T., Takahashi, M., Sato, Y., Uozumi, N., Nakanishi, H., and Nishizawa, N.K. (2011). Phytosiderophore Efflux Transporters Are Crucial for Iron Acquisition in Graminaceous Plants. Journal of Biological Chemistry 286, 5446-5454.

Pardo, T., Martínez-Fernández, D., De La Fuente, C., Clemente, R., Komárek, M., and Bernal, M.P. (2016). Maghemite nanoparticles and ferrous sulfate for the stimulation of iron plaque formation and arsenic immobilization in Phragmites australis. Environmental Pollution 219, 296-304.

Pereira, E.G., Oliva, M.A., Siqueira-Silva, A.I., Rosado-Souza, L., Pinheiro, D.T., and Almeida, A.M. (2014). TROPICAL RICE CULTIVARS FROM LOWLAND AND UPLAND CROPPING SYSTEMS DIFFER IN IRON PLAQUE FORMATION. Journal of Plant Nutrition 37, 1373-1394.

Pi, N., Tam, N.F.Y., and Wong, M.H. (2011). Formation of iron plaque on mangrove roots receiving wastewater and its role in immobilization of wastewater-borne pollutants. Marine Pollution Bulletin 63, 402-411.

Ravet, K., Touraine, B., Boucherez, J., Briat, J.F., Gaymard, F., and Cellier, F. (2008). Ferritins control

interaction between iron homeostasis and oxidative stress in Arabidopsis. Plant Journal 57, 400-412.

Ravet, K., Touraine, B., Kim, S.A., Cellier, F., Thomine, S., Guerinot, M.L., Briat, J.F., and Gaymard, F. (2009). Post-Translational Regulation of AtFER2 Ferritin in Response to Intracellular Iron Trafficking during Fruit Development in Arabidopsis. Molecular Plant 2, 1095-1106.

Raymond, K.N., Dertz, E.A., and Kim, S.S. (2003). Enterobactin: an archetype for microbial iron transport. Proc Natl Acad Sci U S A 100, 3584-3588.

Redekar, N.R., Biyashev, R.M., Jensen, R.V., Helm, R.F., Grabau, E.A., and Maroof, M.a.S. (2015). Genome-wide transcriptome analyses of developing seeds from low and normal phytic acid soybean lines. Bmc Genomics 16.

Reeves, R.D., Baker, A.J.M., Jaffré, T., Erskine, P.D., Echevarria, G., and Van Der Ent, A. (2018). A global database for plants that hyperaccumulate metal and metalloid trace elements. New Phytologist 218, 407-411.

Rodriguez, N., Menendez, N., Tornero, J., Amils, R., and De La Fuente, V. (2005). Internal iron biomineralization in Imperata cylindrica, a perennial grass: chemical composition, speciation and plant localization. New Phytologist 165, 781-789.

Roschzttardtz, H., Conejero, G., Curie, C., and Mari, S. (2009). Identification of the Endodermal Vacuole as the Iron Storage Compartment in the Arabidopsis Embryo. Plant Physiology 151, 1329-1338.

Roschzttardtz, H., Conejero, G., Divol, F., Alcon, C., Verdeil, J.-L., Curie, C., and Mari, S. (2013). New insights into Fe localization in plant tissues. Frontiers in Plant Science 4, 11.

Salt, D.E., Prince, R.C., and Pickering, I.J. (2002). Chemical speciation of accumulated metals in plants: evidence from X-ray absorption spectroscopy. Microchemical Journal 71, 255-259.

Santana, B.V.N., De Araujo, T.O., Andrade, G.C., De Freitas-Silva, L., Kuki, K.N., Pereira, E.G., Azevedo, A.A., and Da Silva, L.C. (2014). Leaf morphoanatomy of species tolerant to excess iron and evaluation of their phytoextraction potential. Environmental Science and Pollution Research 21, 2550-2562.

Sarret, G., Smits, E., Michel, H.C., Isaure, M.P., Zhao, F.J., and Tappero, R. (2013). "Use of Synchrotron-Based Techniques to Elucidate Metal Uptake and Metabolism in Plants," in Advances in Agronomy, Vol 119, ed. D.L. Sparks. (San Diego: Elsevier Academic Press Inc), 1-+.

Senn, A.C., Kaegi, R., Hug, S.J., Hering, J.G., Mangold, S., and Voegelin, A. (2015). Composition and structure of Fe(III)-precipitates formed by Fe(II) oxidation in water at near-neutral pH: Interdependent effects of phosphate, silicate and Ca. Geochimica Et Cosmochimica Acta 162, 220-246.

Snowden, R.E.D., and Wheeler, B.D. (1995). Chemical changes in selected wetland plant species with increasing Fe supply, with specific reference to root precipitates and Fe tolerance. New Phytologist 131, 503-520.

Stcyr, L., Fortin, D., and Campbell, P.G.C. (1993). MICROSCOPIC OBSERVATIONS OF THE IRON PLAQUE OF A SUBMERGED AQUATIC PLANT (VALLISNERIA-AMERICANA MICHX). Aquatic Botany 46, 155-167.

Stein, R.J., Lopes, S.I.G., and Fett, J.P. (2014). Iron toxicity in field-cultivated rice: contrasting tolerance mechanisms in distinct cultivars. Theoretical and Experimental Plant Physiology 26, 135-146.

Strasser, O., Kohl, K., and Romheld, V. (1999). Overestimation of apoplastic Fe in roots of soil grown plants. Plant and Soil 210, 179-187.

Taylor, G.J., and Crowder, A.A. (1983). USE OF THE DCB TECHNIQUE FOR EXTRACTION OF HYDROUS IRON-OXIDES FROM ROOTS OF WETLAND PLANTS. American Journal of Botany 70, 1254-1257.

Taylor, G.J., Crowder, A.A., and Rodden, R. (1984). FORMATION AND MORPHOLOGY OF AN IRON PLAQUE ON THE ROOTS OF TYPHA-LATIFOLIA L GROWN IN SOLUTION CULTURE. American Journal of Botany 71, 666-675.

Tian, C., Wang, C., Tian, Y., Wu, X., and Xiao, B. (2015). Effects of root radial oxygen loss on microbial communities involved in Fe redox cycling in wetland plant rhizosphere sediment. Fresenius Environmental Bulletin 24, 3956-3962.

Tripathi, R.D., Tripathi, P., Dwivedi, S., Kumar, A., Mishra, A., Chauhan, P.S., Norton, G.J., and Nautiyal, C.S. (2014). Roles for root iron plaque in sequestration and uptake of heavy metals and metalloids in aquatic and wetland plants. Metallomics 6, 1789-1800.

Van Der Ent, A., Baker, A.J.M., Reeves, R.D., Pollard, A.J., and Schat, H. (2013). Hyperaccumulators of metal and metalloid trace elements: Facts and fiction. Plant and Soil 362, 319-334.

Vantelon, D., Trcera, N., Roy, D., Moreno, T., Mailly, D., Guilet, S., Metchalkov, E., Delmotte, F., Lassalle, B., Lagarde, P., and Flank, A.M. (2016). The LUCIA beamline at SOLEIL. Journal of Synchrotron Radiation 23, 635-640.

Voegelin, A., Senn, A.C., Kaegi, R., Hug, S.J., and Mangold, S. (2013). Dynamic Fe-precipitate formation

induced by Fe(II) oxidation in aerated phosphate-containing water. Geochimica Et Cosmochimica Acta 117, 216-231.

Wang, T., and Peverly, J.H. (1996). Oxidation states and fractionation of plaque iron on roots of common reeds. Soil Science Society of America Journal 60, 323-329.

Wang, T., and Peverly, J.H. (1999). Iron oxidation states on root surfaces of a wetland plant (Phragmites australis). Soil Science Society of America Journal 63, 247-252.

Williams, P.N., Santner, J., Larsen, M., Lehto, N.J., Oburger, E., Wenzel, W., Glud, R.N., Davison, W., and Zhang, H. (2014). Localized Flux Maxima of Arsenic, Lead, and Iron around Root Apices in Flooded Lowland Rice. Environmental Science & Technology 48, 8498-8506.

Xu, D.F., Xu, J.M., He, Y., and Huang, P.M. (2009). Effect of Iron Plaque Formation on Phosphorus Accumulation and Availability in the Rhizosphere of Wetland Plants. Water Air and Soil Pollution 200, 79-87.

Xu, Y., Sun, X., Zhang, Q., Li, X., and Yan, Z. (2018). Iron plaque formation and heavy metal uptake in Spartina alterniflora at different tidal levels and waterlogging conditions. Ecotoxicology and Environmental Safety 153, 91-100.

Ye, Y.Q., Jin, C.W., Fan, S.K., Mao, Q.Q., Sun, C.L., Yu, Y., and Lin, X.Y. (2015). Elevation of NO production increases Fe immobilization in the Fe-deficiency roots apoplast by decreasing pectin methylation of cell wall. Scientific Reports 5, 13.

Zhang, Y., Xu, Y.H., Yi, H.Y., and Gong, J.M. (2012). Vacuolar membrane transporters OsVIT1 and OsVIT2 modulate iron translocation between flag leaves and seeds in rice. Plant Journal 72, 400-410.